isvr Institute of Sound and Vibration Research

A Receptance Based Method for the Non-linear Modelling of Squeeze Film Damped Rotor Dynamic Systems

P. Bonello, M.J. Brennan and R. Holmes

ISVR Technical Report No 292

December 2000

University of Southampton

SCIENTIFIC PUBLICATIONS BY THE ISVR

Technical Reports are published to promote timely dissemination of research results by ISVR personnel. This medium permits more detailed presentation than is usually acceptable for scientific journals. Responsibility for both the content and any opinions expressed rests entirely with the author(s).

Technical Memoranda are produced to enable the early or preliminary release of information by ISVR personnel where such release is deemed to the appropriate. Information contained in these memoranda may be incomplete, or form part of a continuing programme; this should be borne in mind when using or quoting from these documents.

Contract Reports are produced to record the results of scientific work carried out for sponsors, under contract. The ISVR treats these reports as confidential to sponsors and does not make them available for general circulation. Individual sponsors may, however, authorize subsequent release of the material.

UNIVERSITY OF SOUTHAMPTON

INSTITUTE OF SOUND AND VIBRATION RESEARCH

DYNAMICS GROUP

A Receptance Based Method for the Non-linear Modelling of Squeeze Film Damped Rotor Dynamic Systems

by

P. Bonello, M.J. Brennan and R. Holmes

ISVR Technical Report No. 292

December 2000

Authorized for issue by
Dr. M.J. Brennan
Group Chairman

ABSTRACT

A frequently encountered problem in rotor dynamics is that of an otherwise linear rotor dynamic system incorporating non-linear elements such as squeeze film dampers. Current work on such non-linear multi-degree of freedom problems has largely been centred around finite element (FE) models. The non-linear squeeze film forces are considered as external forces acting on an FE modelled linear system. Over the years, efficient frequency based linear rotor dynamic modelling techniques like the transfer matrix method and the mechanical impedance (dynamic stiffness) method have been presented to model linear rotor dynamic systems. These can be used either as alternatives to FE, or in combination with it, with certain well documented computational advantages. This report presents a general method whereby receptances, readily computed by all linear rotor dynamic modelling methods are used to solve the aforementioned non-linear problem, thereby giving the designer a flexible approach in the choice of the linear rotor dynamic modelling technique. The problem is formulated and solved in both the frequency and time domains. In the frequency domain, periodic solutions are obtained by setting up and solving the non-linear algebraic harmonic balance equations using the receptances of the linear system resulting if the non-linear forces are considered as external, along with the unbalance forces. In the time domain, the modal equations of motion at a conveniently selected location are extracted from a suitably truncated modal series expansion of the receptances of the linear undamped system resulting if the non-linear forces and certain internal linear forces are considered as external, along with the unbalance forces. These time domain equations can be used in testing for the nature of the stability of the harmonic balance solutions. The time domain equations can also be numerically integrated, if necessary. The techniques presented are applied to two common configurations incorporating one squeeze film damper. The receptances are computed by the mechanical impedance technique. Correlation between harmonic balance and time domain numerical integration solutions was found to be excellent. Very good agreement between predictions and experiment was obtained. The major conclusion drawn in this report is that harmonic balance and time domain numerical integration methods are not mutually exclusive, but complimentary, and the availability of both methods affords the designer with a flexible approach in efficiently producing reliable predictions under all operating conditions.

CONTENTS

NOMENCLATURE

a_X^s, a_Y^s	cosine coefficients in Fourier expansion of steady state displacements
A_{ij}^r	general modal constant, modal constant in x direction (kg^{-1})
A_x^s, A_y^s	cosine coefficients in squeeze film force expansions, eqs. (30)
b_X^s, b_Y^s	sine coefficients in Fourier expansion of steady state displacements
B_{ij}^r	modal constant in y direction (kg^{-1})
B_x^s, B_x^s	sine coefficients in squeeze film force expansions, eqs. (30)
c	radial clearance (m)
c_{xx}, c_{yy}	damping coefficients in squeeze film force expansions, eqs. (30)
e	journal eccentricity (m)
e_{0xJ}, e_{0yJ}	static eccentricities of J in x and y directions respectively (m)
$\mathbf{e_c}$	critical eigenvector
h	oil film thickness at position θ (m)
$h_{ij}(t)$	impulsive receptance between degrees of freedom i and j (m)
h_g	groove depth (m)
$\mathbf{I_n}$	$n \times n$ unit diagonal matrix *i.e.* with 1's on leading diagonal
k_B	stiffness of bearing housing (configuration B, chapter 7) (N/m)
k_{xx}, k_{yy}	stiffness coefficients in squeeze film force expansions, eqs. (30)
l_P	distance of point P from pivot H (m)
L	land length (m)
m	maximum number of harmonics in harmonic balance solution
m_B	bearing housing mass (configuration B, chapter 7) (kg)
m_{Jeq}	equivalent mass at SFD (configuration B, chapter 7) (kg)
M	number of terminals of linear system
$\mathbf{M}$	monodromy matrix defined in eq. (124)
n	number of squeeze film dampers
n_L	number of lands
n_s	total number of modal state variables
N	$= \Omega/\omega$, ω fundamental frequency of harmonic balance limit cycle
p	(gauge) pressure distribution in squeeze film (Pa), number of unbalances
p_c	(gauge) cavitation pressure (Pa)
p_l	(gauge) long bearing pressure distribution (Pa)
p_S	(gauge) supply pressure (Pa)
p_{sh}	(gauge) short bearing pressure distribution (Pa)
p_x^s, p_y^s	cosine coefficients in squeeze film force Fourier expansions
P_{xk}, P_{yk}	unbalance forces in x and y directions at k (N)
q	number of modes in subsystem
q_R	number of modes in rotor subsystem

q_F	number of modes in support subsystem
q_x^s, q_y^s	sine coefficients in squeeze film force Fourier expansions
Q	total number of uncoupled subsystems
Q_R, Q_T	radial and tangential squeeze film forces (N)
Q_x, Q_y	Cartesian components of squeeze film forces (N)
Q_{xo}, Q_{yo}	constant force terms in squeeze film force expansions, eqs. (30)
$\overline{Q}_x$, $\overline{Q}_y$	mean terms in squeeze film force Fourier expansions
R	bearing radius (m)
$\mathbf{R}$	general receptance matrix, eq. (18)
R_{ij}	term in $\mathbf{R}$
t	time (s)
T	period of rotation (s)
u	dynamic load parameter (configuration B, chapter 7) eq. (147)
u_J^r	perturbation in x_J^r
U_k	unbalance at k (kgm)
v_J^r	perturbation in y_J^r
W	equivalent static load on squeeze film (N)
$\mathbf{W}(\tau)$	matrix of coefficients in perturbation equations, eq. (118)
x_B, y_B	$= X_B/c$, Y_B/c
x_J, y_J	$= X_J/c$, Y_J/c
x_P, y_P	$= X_P/c$, Y_P/c
x, y	$= x_J - x_B$, $y_J - y_B$
x_P^r, y_P^r	$= X_P^r/c$, Y_P^r/c
X_B, Y_B	absolute displacements of bearing housing centre (m)
X_J, Y_J	absolute displacements of journal (m)
X, Y	relative displacements between journal and bearing housing (m)
X_0, Y_0	mean terms in Fourier expansion of steady state displacements
X_P, Y_P	displacements at P (m)
X_P^r, Y_P^r	modal displacements at P (m)
z	axial position (m)
$\mathbf{Z}$	impedance matrix
$\alpha\alpha_{ij}$, α_{ij}	direct x receptance between i and j (m/N)
$\alpha\beta_{ij}$, $\beta\alpha_{ij}$	cross-coupled receptances between i and j (m/N)
$\beta\beta_{ij}$, β_{ij}	direct y receptance between i and j (m/N)
δ_{Ns}	constant defined in eq. (36)
ε	non-dimensional eccentricity
ε_{0xJ}, ε_{0yJ}	$= e_{0xJ}/c$, e_{0yJ}/c
θ	angular position measured from maximum film thickness position (rad)
η	dynamic viscosity (Nsm^{-2})
ψ	attitude angle (rad)

ψ_i	mass normalised mode shape at degree of freedom i ($kg^{-0.5}$)
λ	end leakage factor
λ_i	Floquet multiplier
λ_c	critical Floquet multiplier
μ	general control parameter
σ	arc-length
τ	non-dimensional time ($=\Omega t$ in chapter 5, $=\omega t$ in chapter 6)
ω	general frequency, fundamental frequency of harmonic balance limit cycle (rad/s)
ω_0	lowest undamped natural frequency of linear structure (rad/s)
ω_r	natural frequency of mode r (rad/s)
ω_{xr}, ω_{yr}	natural frequencies of mode r in x, y directions (rad/s)
ω_{Rxr}, ω_{Ryr}	natural frequencies of rotor subsystem in mode r in x, y directions (rad/s)
ω_{Fxr}, ω_{Fyr}	natural frequencies of support subsystem in mode r in x, y directions (rad/s)
φ	phase angle of critical multiplier λ_c (rad)
ϕ_k	phase shift of unbalance mass at position k (rad) ($\phi_1 = 0$)
Ω	rotor rotational speed (rad/s)
Γ	period of harmonic balance limit cycle (s)
$(\ )^{\mathrm{I}}$	applied to scalar ( ): imaginary part of ( )
$(\ )^{\mathrm{R}}$	applied to scalar ( ): real part of ( )
$(\ )^{\mathrm{T}}$	applied to matrix, vector ( ): transpose of ( )
$\dot{(\ )}$	$d(\ )/dt$
$(\ )'$	$d(\ )/d\tau$

CHAPTER 1

INTRODUCTION

A frequently encountered problem in rotor dynamics is that of an otherwise linear rotor dynamic system incorporating non-linear elements such as squeeze film dampers. Current work on such non-linear multi-degree of freedom problems has largely been centred around finite element (FE) models. The non-linear squeeze film forces are considered as external forces acting on an FE modelled linear system. In [1], [2], [3] and [4] periodic solutions are obtained either by harmonic balance or the analogous trigonometric collocation method, resulting in a set of non-linear algebraic equations. A somewhat cumbersome condensation technique involving the inversion of large FE matrices is then applied to reduce the number of unknown degrees of freedom to the number of non-linear degrees of freedom. The resulting set of non-linear algebraic equations is then solved. In [5], [6] time domain numerical integration is applied to the modal equations of motion set up by computing the eigenvectors and eigenvalues of the linear undamped system.

Over the years efficient frequency based linear rotor dynamic modelling techniques like the transfer matrix method [7] and the mechanical impedance (dynamic stiffness) method [8], [9] have been presented to model linear rotor dynamic systems. These can be used either as alternatives to FE, or in combination with it, with certain well documented computational advantages [9]. The aim of this report is to present a general method whereby receptances, readily computed by all linear rotor dynamic modelling methods are used to solve the aforementioned non-linear problem, thereby giving the designer a flexible approach in the choice of the linear rotor dynamic modelling technique. The problem is formulated and solved in both the frequency and time domains. In the frequency domain, approximate periodic solutions (limit cycles) of given period are obtained by setting up and solving at each speed, the non-linear algebraic harmonic balance equations using the receptances of the linear system resulting if the non-linear forces are considered as external along with the unbalance forces. This receptance technique greatly facilitates the formulation of the harmonic balance equations since one considers the non-linear degrees of freedom exclusively, without having to perform any costly condensation. Upon solution of this set of equations the response at any arbitrary location is then readily determined, again by applying the appropriate receptances. However, difficulty is encountered when attempting to test for stability of a computed set of periodic solutions unless one can easily extract the time domain equations from the receptances. The modal equations of motion at a suitably chosen location can however be easily extracted from a suitably truncated series expansion of the receptances of the linear undamped system resulting if the non-linear forces and certain internal linear forces are considered as external, along with the unbalance forces. The nature of the stability of a set of periodic solutions over a given speed range can then be determined by computing the monodromy matrix for each solution using the highly efficient impulsive parametric excitation technique developed by Hsu and Cheng [10]. The time domain

equations can also be numerically integrated to provide a solution which will always be stable in the steady state. This is necessary when the computed periodic solutions prove to be unstable.

The techniques presented in this report are applied to two common configurations: (a) a flexible rotor incorporating a rigidly housed, highly misaligned squeeze film damper with and without retainer spring; (b) a rigid rotor on a flexibly housed squeeze film damper. In the former case the relevant receptances are computed by the mechanical impedance technique [9].

The advantages and disadvantages of the harmonic balance method and time domain numerical integration to solve the non-linear squeeze film problem are well documented [11], [12]. Time domain integration involves step-by-step numerical integration by some technique suitable for stiff differential equations [13]. A sufficient number of rotor revolutions has to be taken to eliminate the transient motion and reach steady state stable equilibrium *i.e.* for the motion to settle down to an *attractor* in state space. This attractor[1] can be either a (periodic) limit cycle, quasi periodic motion or chaotic motion. This method is inevitably time consuming. On the other hand, harmonic balance and trigonometric collocation find equilibrium periodic solutions (limit cycles) of a given assumed fundamental frequency which will be either equal to the rotational speed or some sub multiple of it. The *accuracy* of the periodic solution will depend on the number of harmonics included. Note that such *analytical* methods, presupposing periodicity of a given period will continue giving such solutions even when a bifurcation has occurred and limit cycles of such period are no longer stable[2]. Hence the *stability* of the computed limit cycle needs to be checked if it is to be accepted as physically realisable. If found to be stable, one will have homed in on it directly without having to wait for any transients to die out as in the time domain numerical integration method. However, such methods lead to a large number of non-linear algebraic equations to solve, creating convergence problems. Arc-length continuation techniques have been designed to overcome such problems, whereby a complete unbalance response curve is traced out by "climbing" along the curve, provided at least one point along the curve has already been determined [14]. In difficult cases the initial approximation to this point can be determined using time domain integration. Moreover, when the motion is aperiodic, time domain numerical integration is the only form of solution. The major conclusion drawn in this report is that harmonic balance and time domain numerical integration methods are not mutually exclusive, but complementary, and the availability of both methods affords the designer with a flexible approach in efficiently producing reliable predictions under all operating conditions.

This report is organised as follows. Following this introduction, chapter 2 continues with a summary of the models used for the *non-linear* element in the rotor dynamic system *i.e.* the squeeze film damper (SFD) (section 2.1) and a summary of the receptance formulation for the

[1] Note that step-by-step time domain numerical integration will always drive the solution towards an attractor in state space due to the local error in each time step. Points on the attractor are in a state of stable equilibrium and hence, in the steady state, despite the local errors, the computed trajectory is kept in close proximity to the exact trajectory.

[2] In such cases the limit cycle is termed a repellor in state space and points on it are in a state of unstable equilibrium since the slightest perturbation in the state variables on it would drive the motion away from the cycle. The sudden change of an attractor into a repellor as a control parameter (*e.g.* rotational speed) is changed is termed a bifurcation [14].

linear part of the system (section 2.2). In chapters 3 to 6 the receptance-based model for coupling the non-linear elements with the linear structure is developed. The model is then validated with simulations and experimental results in chapters 7 and 8. The main conclusion of this report and an outline of future research is given in chapter 9.

CHAPTER 2

SFD MODELLING AND RECEPTANCE FORMULATION

This chapter presents a summary of the models used for the *non-linear* element in the rotor dynamic system *i.e.* the squeeze film damper (SFD) (section 2.1) and a summary of the receptance formulation for the *linear* part of the system (section 2.2).

2.1 SQUEEZE FILM DAMPER MODELLING

Squeeze film dampers have been widely used in high-speed rotating machinery to attenuate vibrations, the forces transmitted to the engine frame due to rotor unbalance and to improve stability [15]. A squeeze film damper consists of an oil filled annular cavity surrounding a "squeeze ring" which is shrunk onto the outer race of a rolling element bearing mounted on the shaft. The outer race of the journal is prevented from rotating but the journal is free to orbit within the bearing housing clearance (Figures 1, 2). A soft flexible element (retainer spring) is often placed in parallel with the squeeze film to comprise a vibration isolator. By this means, the natural frequencies of the engine are artificially reduced so that they may be traversed well before normal operating speeds. The purpose of the damper is to minimise the amplitude of vibration and transmitted force as these low critical speeds are traversed. The retainer spring supports the static load on the journal and prevents the outer race of the journal from rotating. The squeeze film damper can also be used on its own, between the journal and the bearing housing, unassisted by a retainer spring. An anti-rotation pin or dog prevents rotation of the outer race of the journal in this case. The role of the damper is this case is again to reduce the vibration and transmitted force while negotiating the already existing critical speeds of the system.

Because the inner member is prevented from rotating, unlike in a journal bearing, the squeeze film itself cannot support a static load in the absence of a dynamic load. Hence, for a squeeze film damper without retainer spring the journal will roll or slide along the bearing housing inner surface until the level of the dynamic load becomes such that sufficient lift is generated in the bearing to overcome the static load. The following summary is based on a detailed presentation given in the first progress report [15].

In this work the squeeze film damper (SFD) is modelled as comprising two lands of length L separated by a deep groove of depth h_g through which oil is supplied at pressure p_S via symmetrically placed holes (Figures 1, 2). The two-land model is claimed to be valid provided the following condition is satisfied [16]:

$$\frac{c}{h_g + c} < 0.1 \tag{1}$$

This condition is satisfied for the dampers considered in this report. Referring to Figures 1 and 2, for each land the Reynolds Equation [17] can be written as

$$\frac{1}{R^2}\frac{\partial}{\partial\theta}\left\{h^3\frac{\partial p}{\partial\theta}\right\}+\frac{\partial}{\partial z}\left\{h^3\frac{\partial p}{\partial z}\right\}=12\eta c(\dot{\varepsilon}\cos\theta+\varepsilon\dot{\psi}\sin\theta) \tag{2}$$

where $h=c(1+\varepsilon\cos\theta)$ is the oil film thickness.

Equation (2) can be solved to obtain the pressure distribution $p(\theta,z)$ at any instant in time. This solution depends on whether the damper is unsealed or sealed (Figures 1(a),(b) respectively). Once $p(\theta,z)$ has been established the squeeze film forces Q_R, Q_T in the radial and tangential directions respectively (Figure 2) can be computed from the equations:

$$Q_R=-n_L R\int_{-L/2}^{L/2}\int_0^{2\pi} p_m(\theta,z)\cos\theta\ d\theta\ dz \tag{3a}$$

$$Q_T=-n_L R\int_{-L/2}^{L/2}\int_0^{2\pi} p_m(\theta,z)\sin\theta\ d\theta\ dz \tag{3b}$$

In these equations $p_m(\theta,z)$ is a pressure distribution based on $p(\theta,z)$ but modified according to assumptions made as regards the supply pressure and the extent of the effective squeeze film around the journal. These assumptions lead to different forms of $p_m(\theta,z)$ and hence different expressions for Q_R, Q_T.

2.1.1 Unsealed Damper

For an unsealed damper the *short bearing approximation* applies in which it is assumed that the pressure gradient in the circumferential (θ) direction is negligible relative to that in the axial (z) direction *i.e.*

$$\frac{\partial p}{\partial z}>>\frac{\partial p}{\partial\theta}$$

Under such conditions, integration of equation (2) yields the pressure distribution as

$$p(\theta,z)=\frac{6\eta}{c^2}\frac{\{\varepsilon\dot{\psi}\sin\theta+\dot{\varepsilon}\cos\theta\}}{\{1+\varepsilon\cos\theta\}^3}\left(z^2-\frac{L^2}{4}\right)+p_S\left(\frac{z}{L}+\frac{1}{2}\right) \tag{4}$$

Three main theories are used to determine the form of $p_m(\theta,z)$ for an unsealed damper, each leading to different expressions for the squeeze film forces Q_R, Q_T.

The 2π *film (or full film)* theory assumes that no cavitation (*i.e.* no oil film rupture) occurs. Hence, $p_m(\theta,z)$ is given simply as

$$p_m(\theta,z) = p(\theta,z) \tag{5}$$

Substitution of equation (5) into equations (3) and integration yields the full film forces as [17]:

$$Q_{R,2\pi} = n_L \frac{\eta R L^3}{c^2} \frac{\left(1+2\varepsilon^2\right)\pi}{\left(1-\varepsilon^2\right)^{\frac{5}{2}}} \dot{\varepsilon} \tag{6a}$$

$$Q_{T,2\pi} = n_L \frac{\eta R L^3}{c^2} \frac{\pi}{\left(1-\varepsilon^2\right)^{\frac{3}{2}}} \varepsilon\dot{\psi} \tag{6b}$$

The π *film (or half film)* theory assumes that (a) $p_S \approx 0$, (b) cavitation occurs at atmospheric pressure. Hence $p_m(\theta,z)$ is now given by

$$p_m(\theta,z) = \begin{matrix} p(\theta,z)\big|_{p_S=0} \\ 0 \end{matrix} \begin{matrix} , \; p(\theta,z)\big|_{p_S=0} > 0 \\ , \; p(\theta,z)\big|_{p_S=0} \le 0 \end{matrix} \tag{7}$$

From equation (4) one deduces that $p(\theta,z)\big|_{p_S=0} > 0$ from $\theta = \theta_1$ to $\theta = \theta_2 = \theta_1 + \pi$, where

$$\sin\theta_1 = \frac{\dot{\varepsilon}}{\sqrt{(\varepsilon\dot{\psi})^2 + \dot{\varepsilon}^2}}, \; \cos\theta_1 = -\frac{\varepsilon\dot{\psi}}{\sqrt{(\varepsilon\dot{\psi})^2 + \dot{\varepsilon}^2}} \tag{8}$$

Hence the use of the term π *film (or half film)*. The half film forces are [17]

$$Q_{R,\pi} = n_L \frac{\eta R L^3}{c^2} \left\{ g_1 \varepsilon\dot{\psi} + g_2 \dot{\varepsilon} \right\} \tag{9a}$$

$$Q_{T,\pi} = n_L \frac{\eta R L^3}{c^2} \left\{ g_3 \varepsilon\dot{\psi} + g_1 \dot{\varepsilon} \right\} \tag{9b}$$

where

$$g_1 = -\frac{2\varepsilon\cos^3\theta_1}{\left(1-\varepsilon^2\cos^2\theta_1\right)^2}$$

$$g_2 = \frac{\varepsilon\sin\theta_1\left\{3+\left(2-5\varepsilon^2\right)\cos^2\theta_1\right\}}{\left(1-\varepsilon^2\right)^2\left(1-\varepsilon^2\cos^2\theta_1\right)^2} + \frac{\left(1+2\varepsilon^2\right)}{\left(1-\varepsilon^2\right)^{\frac{5}{2}}}\alpha$$

$$g_3 = \frac{\varepsilon\sin\theta_1\left\{1-2\cos^2\theta_1+\varepsilon^2\cos^2\theta_1\right\}}{\left(1-\varepsilon^2\right)\left(1-\varepsilon^2\cos^2\theta_1\right)^2} + \frac{1}{\left(1-\varepsilon^2\right)^{\frac{3}{2}}}\alpha$$

$$\alpha = \frac{\pi}{2} + \arctan\left\{\frac{\varepsilon \sin\theta_1}{\left(1-\varepsilon^2\right)^{\frac{1}{2}}}\right\}$$

The full film and half film theories are classical extremes and in reality cavitation occurs at some subatmospheric pressure $p_c \leq 0$ [17]. Accordingly, the *variable film extent* theory is defined where

$$p_m(\theta,z) = \begin{matrix} p(\theta,z)\,, & p(\theta,z) > p_c \\ p_c \quad , & p(\theta,z) \leq p_c \end{matrix} \tag{10}$$

In this case the squeeze film forces will have to be determined by numerical integration. In [15], the following expressions were derived from equations (3) for an unsealed damper:

$$Q_R = Q_{R,\pi} + n_L R p_S L \sin\theta_1 - n_L R \int_{-L/2}^{L/2} \int_{\theta_2}^{\theta_2+\pi} p_m(\theta,z)\cos\theta \; d\theta \; dz \tag{11a}$$

$$Q_T = Q_{T,\pi} - n_L R p_S L \cos\theta_1 - n_L R \int_{-L/2}^{L/2} \int_{\theta_2}^{\theta_2+\pi} p_m(\theta,z)\sin\theta \; d\theta \; dz \tag{11b}$$

where $Q_{R,\pi}$, $Q_{T,\pi}$ are the half film forces given by equations (9) and $\theta_2 = \theta_1 + \pi$ with θ_1 determined by equations (8). Use of equations (11) instead of equations (3) cuts the computation time by half.

If the cavitation pressure p_c is taken as absolute zero ($-101.325\,\text{kPa}$) then the variable film extent theory is referred to as the *absolute zero cavitation theory*. In [15] it is shown that the absolute zero cavitation theory is the best theory to use in the absence of an experimentally determined value of p_c.

2.1.2 Sealed Damper

The problem of the two land sealed damper was considered in [18]. In this case the axial flow is partially restricted by the end seals. A combined pressure distribution is assumed:

$$p(\theta,z) = p_{sh}(\theta,z) + \lambda p_l(\theta)\left(\frac{1}{2} - \frac{z}{L}\right) \tag{12}$$

where $p_{sh}(\theta,z)$ is the short bearing solution, given by equation (4). $p_l(\theta)$ is the long bearing solution of the Reynold's Equation *i.e.* the solution of equation (2) when it is assumed that the pressure gradient in the axial (z) direction is negligible relative to that in the circumferential (θ) direction *i.e.*

$$\frac{\partial p}{\partial z} << \frac{\partial p}{\partial \theta}$$

λ is the empirically determined *end leakage factor*, $0 \le \lambda \le 1$. $\lambda = 0$ for full leakage (unsealed damper) and $\lambda = 1$ for zero leakage (fully sealed damper) [18]. $p_l(\theta)$ is derived in [18] as:

$$p_l(\theta) = \frac{6\eta R^2}{c^2}\left[\frac{\dot{\varepsilon}}{\varepsilon}\left\{\frac{1}{(1+\varepsilon\cos\theta)^2} - \frac{1}{(1+\varepsilon^2)^2}\right\} - 2\dot{\psi}\left(\frac{\varepsilon}{2+\varepsilon^2}\right)\frac{(2+\varepsilon\cos\theta)\sin\theta}{(1+\varepsilon\cos\theta)^2}\right] + p_0 \quad (13)$$

where

$$p_0 = p_S - \frac{\eta L^2}{c^2}\frac{\dot{\varepsilon}}{(1+\varepsilon)^3}$$

For sealed dampers the same variable film extent criterion given by equation (10) for unsealed dampers is used to compute the forces but with equation (12) being used for $p(\theta, z)$ instead of equation (4). However, the form of the pressure distribution given by equation (12) does not allow for the simplification of the numerical integration process possible for the unsealed damper, equations (11) *i.e.* the extraction of the analytical part of the forces. Hence in this case the full numerical integration over a θ interval of 2π has to be performed.

2.1.3 Computation of Squeeze Film Forces

In order to compute the squeeze film forces Q_R, Q_T by the variable film extent criterion a function was written in *MATLAB®*. This function generates a $2 \times n$ matrix of radial (row 1) and tangential (row 2) forces for time histories ε, $\dot{\varepsilon}$, ψ, $\dot{\psi}$ n points long. This means a total of $2n$ double integrations are performed. The double integration is performed using Simpson's Rule by an array scheme outlined in [19]. For an unsealed damper this function will give the integrals in equations (11), which are to be added to the analytical expressions in these equations. For the sealed damper this function gives the complete forces. With $\Delta\theta = 2\pi/52$ and $\Delta z = L/12$, force matrices with up to 50 columns could be generated in a fraction of a second to a sufficiently high accuracy on a 333 MHz Pentium II desktop computer.

2.1.4 Squeeze Film Forces in Cartesian Coordinates

Referring to Figure 2 let x_J, y_J and x_B, y_B be the non-dimensional displacements of the journal J and the bearing housing centre B respectively relative to fixed coordinates and x, y are the displacements of J relative to B. The squeeze film forces Q_x, Q_y in the x, y directions are given by

$$Q_x = -\{Q_R(\varepsilon,\psi,\dot{\varepsilon},\dot{\psi})\sin\psi + Q_T(\varepsilon,\psi,\dot{\varepsilon},\dot{\psi})\cos\psi\}$$
$$= -\frac{1}{\varepsilon}\{xQ_R(\varepsilon,\psi,\dot{\varepsilon},\dot{\psi}) - yQ_T(\varepsilon,\psi,\dot{\varepsilon},\dot{\psi})\} \quad (14a)$$

$$Q_y = Q_R(\varepsilon,\psi,\dot{\varepsilon},\dot{\psi})\cos\psi - Q_T(\varepsilon,\psi,\dot{\varepsilon},\dot{\psi})\sin\psi$$
$$= -\frac{1}{\varepsilon}\{yQ_R(\varepsilon,\psi,\dot{\varepsilon},\dot{\psi}) + xQ_T(\varepsilon,\psi,\dot{\varepsilon},\dot{\psi})\} \quad (14b)$$

where

$\varepsilon = \sqrt{(x^2+y^2)}$, $\dot{\varepsilon} = \frac{1}{\varepsilon}(x\dot{x}+y\dot{y})$, $\dot{\psi} = \frac{1}{\varepsilon^2}(x\dot{y}-y\dot{x})$

$x = x_J - x_B$, $y = y_J - y_B$

$\dot{x} = \dot{x}_J - \dot{x}_B$, $\dot{y} = \dot{y}_J - \dot{y}_B$

$x_J = X_J/c$, $y_J = Y_J/c$,.....*etc*, where X_J, Y_J,.... are the displacements.

2.2 GENERAL RECEPTANCE FORMULATION

The general receptance matrix $\mathbf{R}$ $(4M \times 4M)$ for a linear structure with M terminals is given by

$$\mathbf{u} = \mathbf{Rf} \quad (15)$$

where

$$\mathbf{u} = \left[\tilde{X}_1 \quad \tilde{\theta}_{y1} \quad \tilde{Y}_1 \quad \tilde{\theta}_{x1} \quad \cdots\cdots \quad \tilde{X}_M \quad \tilde{\theta}_{yM} \quad \tilde{Y}_M \quad \tilde{\theta}_{xM}\right]^{\mathrm{T}}$$
$$\mathbf{f} = \left[\tilde{F}_{x1} \quad \tilde{M}_{y1} \quad \tilde{F}_{y1} \quad \tilde{M}_{x1} \quad \cdots\cdots \quad \tilde{F}_{xM} \quad \tilde{M}_{yM} \quad \tilde{F}_{yM} \quad \tilde{M}_{xM}\right]^{\mathrm{T}}$$

$\tilde{X}_i$, $\tilde{\theta}_{yi}$ are the complex amplitudes of the linear, angular displacements respectively, and $\tilde{F}_{xi}$, $\tilde{M}_{yi}$ are the complex amplitudes of the force, moment respectively at terminal no. i, in the xz plane. Similarly, $\tilde{Y}_i$, $\tilde{\theta}_{xi}$ are the complex amplitudes of the linear, angular displacements respectively, and $\tilde{F}_{yi}$, $\tilde{M}_{xi}$ are the complex amplitudes of the force, moment respectively at terminal no. i, in the yz plane.

The instantaneous linear, angular displacements are given by

$$X_i(t) = \mathrm{Re}\{\tilde{X}_i e^{\mathrm{j}\omega t}\},\ \theta_{yi}(t) = \mathrm{Re}\{\tilde{\theta}_{yi} e^{\mathrm{j}\omega t}\} \ \ldots\ldots etc.$$

Similarly for the forces, moments.

The relevant terms in $\mathbf{R}$ for a linear rotor dynamic system are readily computed by a variety of methods: transfer matrix (TM), mechanical impedance method (MI), FE, or some hybrid of FE and TM or FE and MI, as extensively documented in the literature [9]. With the mechanical impedance method, the whole matrix is given by

$$\mathbf{R} = \frac{\mathbf{Z}^{-1}}{\mathrm{j}\omega} \tag{16}$$

In general $\mathbf{R}$ includes the effects of linear damping (viscous and structural) and gyroscopy and hence $\mathbf{R}$ is complex, non-symmetric and a function of angular speed Ω, as well as frequency ω *i.e.*

$$\mathbf{R} = \mathbf{R}(\omega,\Omega) = \mathbf{R}^{\mathrm{R}}(\omega,\Omega) + \mathrm{j}\mathbf{R}^{\mathrm{I}}(\omega,\Omega) \tag{17}$$

where $\mathbf{R}^{\mathrm{R}}$, $\mathbf{R}^{\mathrm{I}}$ are matrices respectively containing the real and imaginary parts of the terms in $\mathbf{R}$.

CHAPTER 3

HARMONIC BALANCE ANALYSIS

In this chapter a receptance based harmonic balance analysis technique is developed. Stability analysis of the harmonic balance solutions is deferred to chapter 6.

3.1 DEFINITION OF LINEAR SYSTEM

In this analysis the approach is to consider the non-linear squeeze film forces as external, in addition to the unbalance forces. Figure 3(a) depicts a rotor and support structure with n squeeze film dampers applied between positions Ji and Bi, $i=1\ldots n$ on the rotor and support structure respectively. The support structure is in general non-rigid and will exhibit dynamic behaviour. Ji refers to the journal centre and Bi to the bearing housing centre at squeeze film damper (SFD) no. i. In addition, p unbalance forces act at points Uk, $k=1\ldots p$ on the rotor. Ji, Bi, $i=1\ldots n$ and Uk, $k=1\ldots p$ are the terminals of the linear system for which the receptances need to be computed. Since no external moments are applied one can dispense with the moments and rotations in equation (15). Additionally, it is convenient to partition the reduced $(2M\times 2M)$ matrix as follows:

$$\mathbf{u}=\mathbf{R}\mathbf{f} \tag{18}$$

where $\mathbf{u}=\left[\tilde{X}_1 \quad \ldots \quad \tilde{X}_M \quad \tilde{Y}_1 \quad \ldots \quad \tilde{Y}_M\right]^{\mathrm{T}}$, $\mathbf{f}=\left[\tilde{F}_{x1} \quad \ldots \quad \tilde{F}_{xM} \quad \tilde{F}_{y1} \quad \ldots \quad \tilde{F}_{yM}\right]^{\mathrm{T}}$ and

$$\mathbf{R}=\begin{bmatrix}\{\alpha\alpha_{ij}\} & \{\alpha\beta_{ij}\}\\ \{\beta\alpha_{ij}\} & \{\beta\beta_{ij}\}\end{bmatrix} \tag{19}$$

The sub-matrices $\{\alpha\alpha_{ij}\}$ and $\{\beta\beta_{ij}\}$ contain the direct receptances in the x and y directions respectively and $\{\alpha\beta_{ij}\}$ and $\{\beta\alpha_{ij}\}$ contain the cross receptances:

$$\alpha\alpha_{ij}=\left.\frac{\tilde{X}_i}{\tilde{F}_{xj}}\right|_{\tilde{F}_{xq}=0,q=1\ldots M,q\neq j,\tilde{F}_{yq}=0,q=1\ldots M} \qquad \alpha\beta_{ij}=\left.\frac{\tilde{X}_i}{\tilde{F}_{yj}}\right|_{\tilde{F}_{xq}=0,q=1\ldots M,\tilde{F}_{yq}=0,q=1\ldots M,q\neq j} \tag{20a,b}$$

$$\beta\alpha_{ij}=\left.\frac{\tilde{Y}_i}{\tilde{F}_{xj}}\right|_{\tilde{F}_{xq}=0,q=1\ldots M,q\neq j,\tilde{F}_{yq}=0,q=1\ldots M} \qquad \beta\beta_{ij}=\left.\frac{\tilde{Y}_i}{\tilde{F}_{yj}}\right|_{\tilde{F}_{xq}=0,q=1\ldots M,\tilde{F}_{yq}=0,q=1\ldots M,q\neq j} \tag{20c,d}$$

Note that the number of terminals, $M = n + p$. Also, as mentioned in section 2.2, **R** includes the effects of linear damping (viscous and structural) and gyroscopy and hence **R** is complex, non-symmetric and a function of angular speed, as well as frequency.

Referring to Figure 3(b), the unbalance forces at *Uk* in the *x* and *y* directions are given by

$$\begin{aligned} P_{xk} &= U_k \Omega^2 \sin(\Omega t + \phi_k) \\ &= U_k \Omega^2 \sin\phi_k \cos\Omega t + U_k \Omega^2 \cos\phi_k \sin\Omega t \end{aligned} \tag{21a}$$

$$\begin{aligned} P_{yk} &= -U_k \Omega^2 \cos(\Omega t + \phi_k) \\ &= -U_k \Omega^2 \cos\phi_k \cos\Omega t + U_k \Omega^2 \sin\phi_k \sin\Omega t \end{aligned} \tag{21b}$$

The squeeze film forces on *Ji* in the *x* and *y* directions are given by

$$Q_{xi} = Q_{xi}(X_i, Y_i, \dot{X}_i, \dot{Y}_i) \tag{22a}$$

$$Q_{yi} = Q_{yi}(X_i, Y_i, \dot{X}_i, \dot{Y}_i) \tag{22b}$$

where $X_i = X_{Ji} - X_{Bi}$, $Y_i = Y_{Ji} - Y_{Bi}$

X_i, Y_i are the relative displacements between *Ji* and *Bi*. X_{Ji}, Y_{Ji} and X_{Bi}, Y_{Bi} are the absolute displacements of *Ji* and *Bi* respectively, both measured from the static equilibrium position of *Bi*.

Expressions for Q_{xi}, Q_{yi} were given in section 2.1. Note that the squeeze film forces on *Bi* will be $-Q_{xi}$, $-Q_{yi}$, since the inertia of the squeeze film is neglected.

3.2 REPRESENTATION OF DISPLACEMENTS AND FORCES

In harmonic balance analysis, one seeks periodic solutions of fundamental frequency ω [1]. This frequency will in general be either equal to the rotational speed Ω or some sub multiple of it:

$$\omega = \frac{\Omega}{N}, \quad N \geq 1 \tag{23}$$

The period Γ of the limit cycle to be computed is hence related to the period of rotation T by:

$$\Gamma = NT, \quad N \geq 1 \tag{24}$$

[1] Note that in this report the symbol ω is used to symbolise both a general frequency and the fundamental frequency of vibration of the harmonic balance solution. The appropriate meaning of ω will be apparent in the context.

Accordingly, the absolute displacements at SFD no. i $(i = 1...n)$ at Ji and Bi can be expressed in a Fourier series expansion:

$$X_{Ji} = X_{0Ji} + \sum_{s=1}^{m} \left(a_{XJi}^{s} \cos s\omega t + b_{XJi}^{s} \sin s\omega t \right) \tag{25a}$$

$$Y_{Ji} = Y_{0Ji} + \sum_{s=1}^{m} \left(a_{YJi}^{s} \cos s\omega t + b_{YJi}^{s} \sin s\omega t \right) \tag{25b}$$

$$X_{Bi} = X_{0Bi} + \sum_{s=1}^{m} \left(a_{XBi}^{s} \cos s\omega t + b_{XBi}^{s} \sin s\omega t \right) \tag{26a}$$

$$Y_{Bi} = Y_{0Bi} + \sum_{s=1}^{m} \left(a_{YBi}^{s} \cos s\omega t + b_{YBi}^{s} \sin s\omega t \right) \tag{26b}$$

Similarly, the relative displacements are given by

$$X_{i} = X_{0i} + \sum_{s=1}^{m} \left(a_{Xi}^{s} \cos s\omega t + b_{Xi}^{s} \sin s\omega t \right) \tag{27a}$$

$$Y_{i} = Y_{0i} + \sum_{s=1}^{m} \left(a_{Yi}^{s} \cos s\omega t + b_{Yi}^{s} \sin s\omega t \right) \tag{27b}$$

where

$X_{0i} = X_{0Ji} - X_{0Bi}$, $a_{Xi}^{s} = a_{XJi}^{s} - a_{XBi}^{s}$, $b_{Xi}^{s} = b_{XJi}^{s} - b_{XBi}^{s}$
$Y_{0i} = Y_{0Ji} - Y_{0Bi}$, $a_{Yi}^{s} = a_{YJi}^{s} - a_{YBi}^{s}$, $b_{Yi}^{s} = b_{YJi}^{s} - b_{YBi}^{s}$.

Because the squeeze film forces Q_{xi}, Q_{yi} are functions of the relative displacements and velocities, they will also be periodic with fundamental frequency ω and can be expressed in a Fourier series expansion:

$$Q_{xi} = \overline{Q}_{xi} + \sum_{s=1}^{m} \left(p_{xi}^{s} \cos s\omega t + q_{xi}^{s} \sin s\omega t \right) \tag{28a}$$

$$Q_{yi} = \overline{Q}_{yi} + \sum_{s=1}^{m} \left(p_{yi}^{s} \cos s\omega t + q_{yi}^{s} \sin s\omega t \right) \tag{28b}$$

where

$$\begin{aligned} \overline{Q}_{xi} &= \frac{1}{\Gamma} \int_{0}^{\Gamma} Q_{xi}\, dt \\ p_{xi}^{s} &= \frac{2}{\Gamma} \int_{0}^{\Gamma} Q_{xi} \cos s\omega t\, dt \\ q_{xi}^{s} &= \frac{2}{\Gamma} \int_{0}^{\Gamma} Q_{xi} \sin s\omega t\, dt \end{aligned} \tag{29a}$$

$$\overline{Q}_{yi} = \frac{1}{\Gamma}\int_0^{\Gamma} Q_{yi}\, dt$$

$$p_{yi}^s = \frac{2}{\Gamma}\int_0^{\Gamma} Q_{yi}\cos s\omega t\, dt$$

$$q_{yi}^r = \frac{2}{\Gamma}\int_0^{\Gamma} Q_{yi}\sin s\omega t\, dt \qquad (29b)$$

In the solution of the harmonic balance equations is convenient to express the periodic squeeze film forces as follows [11]

$$Q_{xi} = Q_{x0i} + k_{xxi}X_i + c_{xxi}\dot{X}_i + \sum_{s=1}^{m}\left(A_{xi}^s\cos s\omega t + B_{xi}^s\sin s\omega t\right) \qquad (30a)$$

$$Q_{yi} = Q_{y0i} + k_{yyi}X_i + c_{yyi}\dot{X}_i + \sum_{s=1}^{m}\left(A_{yi}^s\cos s\omega t + B_{yi}^s\sin s\omega t\right) \qquad (30b)$$

where

$$A_{xi}^s,\ B_{xi}^s,\ A_{yi}^s,\ B_{yi}^s = 0 \text{ for } s = N \qquad (31)$$

i.e. the constants A_{xi}^s, B_{xi}^s, A_{yi}^s, B_{yi}^s *are non-zero for the non-synchronous harmonics and zero for the synchronous harmonic* (see equation (23)). Hence $2m+1$ coefficients in each of the equations (30) need to be determined. Substituting for X_i and its time derivative from equation (27a) into equation (30a):

$$Q_{xi} = Q_{x0i} + k_{xxi}X_{0i} + k_{xxi}\sum_{s=1}^{m}\left(a_{Xi}^s\cos s\omega t + b_{Xi}^s\sin s\omega t\right) + c_{xxi}\sum_{s=1}^{m}\left(-s\omega a_{Xi}^s\sin s\omega t + s\omega b_{Xi}^s\cos s\omega t\right)$$
$$+\sum_{s=1}^{m}\left(A_{xi}^s\cos s\omega t + B_{xi}^s\sin s\omega t\right) \qquad (32)$$

Equating the constant terms and cosine and sine coefficients on the right hand side of equation (30a) and equation (32) gives

$$\overline{Q}_{xi} = Q_{x0i} + k_{xxi}X_{0i}$$

$$p_{xi}^s = k_{xxi}a_{Xi}^s + s\omega c_{xxi}b_{Xi}^s + A_{xi}^s$$

$$q_{xi}^s = -s\omega c_{xxi}a_{Xi}^s + k_{xxi}b_{Xi}^s + B_{xi}^s$$

for $s = 1\ldots m$. (33a)

These equations can be written in matrix form:

$$\begin{bmatrix} \overline{Q}_{xi} \\ p_{xi}^1 \\ q_{xi}^1 \\ p_{xi}^2 \\ q_{xi}^2 \\ \vdots \\ p_{xi}^m \\ q_{xi}^m \end{bmatrix} = \begin{bmatrix} 1 & X_{0i} & 0 & \cdots & \cdots & \cdots & \cdots & \cdots & 0 \\ 0 & a_{Xi}^1 & \omega b_{Xi}^1 & 1 & 0 & \cdots & \cdots & \cdots & \vdots \\ \vdots & b_{Xi}^1 & -\omega a_{Xi}^1 & 0 & 1 & \ddots & \cdots & \cdots & \vdots \\ \vdots & \vdots & \vdots & \vdots & \ddots & \ddots & \ddots & \cdots & \vdots \\ \vdots & \vdots & \vdots & \vdots & \cdots & \ddots & \ddots & \ddots & \vdots \\ \vdots & a_{Xi}^m & m\omega b_{Xi}^m & \vdots & \cdots & \cdots & \ddots & 1 & 0 \\ 0 & b_{Xi}^m & -m\omega a_{Xi}^m & 0 & \cdots & \cdots & \cdots & 0 & 1 \end{bmatrix} \begin{bmatrix} Q_{x0i} \\ k_{xxi} \\ c_{xxi} \\ A_{xi}^1 \\ B_{xi}^1 \\ \vdots \\ A_{xi}^m \\ B_{xi}^m \end{bmatrix} \tag{34a}$$

or,

$$\mathbf{q_x} = \mathbf{G_x r_x}$$

$\mathbf{q_x}$ is $(2m+1)\times 1$, $\mathbf{G_x}$ is $(2m+1)\times(2m+3)$ and

$$\mathbf{r_x}\{(2m+3)\times 1\} = \begin{bmatrix} \mathbf{k_x} \\ \mathbf{a_x} \end{bmatrix}$$

where $\mathbf{k_x} = [Q_{x0i} \quad k_{xxi} \quad c_{xxi}]^T$ and $\mathbf{a_x} = [A_{xi}^1 \quad B_{xi}^1 \quad \cdots \quad \cdots \quad A_{xi}^m \quad B_{xi}^m]^T$.

Noting that A_{xi}^N, $B_{xi}^N = 0$ (equation (31)), the following algorithm is applied to compute $\mathbf{r_x}$:

-delete from $\mathbf{G_x}$ the $2(N+1)th$ and $\{2(2N+1)+1\}th$ columns to obtain the $(2m+1)\times(2m+1)$ matrix $\mathbf{G_{xred}}$

-compute $\mathbf{r_{xred}}$

where $$\mathbf{r_{xred}} = \mathbf{G_{xred}^{-1} q_x}$$

and $$\mathbf{r_{xred}} = \begin{bmatrix} \mathbf{k_x} \\ \mathbf{a_{xred}} \end{bmatrix}$$

$\mathbf{a_{xred}}$ is $\mathbf{a_x}$ but with the Nth and $(N+1)th$ columns omitted.

-recover $\mathbf{a}$ by setting up $2m\times 1$ vector with its Nth and $(N+1)th$ rows equal to zero and the elements in the remaining rows taken from $\mathbf{a_{xred}}$.

A similar process is applied for the determination of $\mathbf{k_y} = [Q_{y0i} \quad k_{yyi} \quad c_{yyi}]^T$ and $\mathbf{a_y} = [A_{yi}^1 \quad B_{yi}^1 \quad \cdots \quad \cdots \quad A_{yi}^m \quad B_{yi}^m]^T$ where one starts from the equations:

$$\overline{Q}_{yi} = Q_{y0i} + k_{yyi} Y_{0i}$$

$$p^s_{yi} = k_{yyi} a^s_{Yi} + s\omega c_{yyi} b^s_{Yi} + A^s_{yi}$$

$$q^s_{yi} = -s\omega c_{yyi} a^s_{Yi} + k_{yyi} b^s_{Yi} + B^s_{yi}$$

for $s = 1 \ldots m$, (33b)

or, in matrix form:

$$\begin{bmatrix} \overline{Q}_{yi} \\ p^1_{yi} \\ q^1_{yi} \\ p^2_{yi} \\ q^2_{yi} \\ \vdots \\ p^m_{yi} \\ q^m_{yi} \end{bmatrix} = \begin{bmatrix} 1 & Y_{0i} & 0 & \cdots & \cdots & \cdots & \cdots & \cdots & 0 \\ 0 & a^1_{Yi} & \omega b^1_{Yi} & 1 & 0 & \cdots & \cdots & \cdots & \vdots \\ \vdots & b^1_{Yi} & -\omega a^1_{Yi} & 0 & 1 & \ddots & \cdots & \cdots & \vdots \\ \vdots & \vdots & \vdots & \vdots & \ddots & \ddots & \ddots & \cdots & \vdots \\ \vdots & \vdots & \vdots & \vdots & \cdots & \ddots & \ddots & \ddots & \vdots \\ \vdots & a^m_{Yi} & m\omega b^m_{Yi} & \vdots & \cdots & \cdots & \ddots & 1 & 0 \\ 0 & b^m_{Yi} & -m\omega a^m_{Yi} & 0 & \cdots & \cdots & \cdots & 0 & 1 \end{bmatrix} \begin{bmatrix} Q_{y0i} \\ k_{yyi} \\ c_{yyi} \\ A^1_{yi} \\ B^1_{yi} \\ \vdots \\ A^m_{yi} \\ B^m_{yi} \end{bmatrix} \quad (34b)$$

The notation used in equations (30), also used elsewhere *e.g.* [11], is unfortunate in that it can *mislead* one into thinking that cross-coupling effects were neglected. This is absolutely not the case. The expressions for the SFD forces in equations (30) are merely an alternative *mathematical* way of expressing the SFD forces in equations (28), as seen from equations (34a,b). The form for the SFD forces in equations (30) is used since it is found to enhance convergence of the iterative solution of the harmonic balance equations (derived in section 3.3).

The unbalance forces in equation (21) can be conveniently written in a form similar to that of the squeeze film force Fourier expansion (28) by writing

$$P_{xk} = \sum_{s=1}^{m} \delta_{Ns} \left\{ \left(U_k \Omega^2 \sin\phi_k \right) \cos s\omega t + \left(U_k \Omega^2 \cos\phi_k \right) \sin s\omega t \right\} \quad (35a)$$

$$P_{yk} = \sum_{s=1}^{m} \delta_{Ns} \left\{ -\left(U_k \Omega^2 \cos\phi_k \right) \cos s\omega t + \left(U_k \Omega^2 \sin\phi_k \right) \sin s\omega t \right\} \quad (35b)$$

where the constant δ_{Ns} is defined by

$$\delta_{Ns} = \begin{cases} 0 & s \neq N \\ 1 & s = N \end{cases} \quad (36)$$

i.e. δ_{Ns} *is non-zero only for the synchronous harmonic component* (see equation (23))

3.3 HARMONIC BALANCE EQUATIONS

Prior to setting up the harmonic balance equations, a rudimentary pattern is illustrated which will be used as a "template" for the actual equations. Let $X(t)$ be the response at a point i on a linear structure due to a harmonic force $F(t)$ at frequency $s\omega$ at point j. Let r be the receptance connecting $X(t)$ with $F(t)$. The superscripts R, I applied to a scalar complex number denote respectively the real and imaginary parts of that number.

$$X(t)=\mathrm{Re}\left\{\tilde{X}e^{\mathrm{j}s\omega t}\right\}=\mathrm{Re}\left\{\left(\tilde{X}^{\mathrm{R}}+\mathrm{j}\tilde{X}^{\mathrm{I}}\right)e^{\mathrm{j}s\omega t}\right\}=\tilde{X}^{\mathrm{R}}\cos s\omega t-\tilde{X}^{\mathrm{I}}\sin s\omega t=X_c\cos s\omega t+X_s\sin s\omega t$$

$$F(t)=\mathrm{Re}\left\{\tilde{F}e^{\mathrm{j}s\omega t}\right\}=\mathrm{Re}\left\{\left(\tilde{F}^{\mathrm{R}}+\mathrm{j}\tilde{F}^{\mathrm{I}}\right)e^{\mathrm{j}s\omega t}\right\}=\tilde{F}^{\mathrm{R}}\cos s\omega t-\tilde{F}^{\mathrm{I}}\sin s\omega t=F_c\cos s\omega t+F_s\sin s\omega t$$

$$\tilde{X}=r\tilde{F}=\left(r^{\mathrm{R}}+\mathrm{j}r^{\mathrm{I}}\right)\left(\tilde{F}^{\mathrm{R}}+\mathrm{j}\tilde{F}^{\mathrm{I}}\right)=\left(r^{\mathrm{R}}\tilde{F}^{\mathrm{R}}-r^{\mathrm{I}}\tilde{F}^{\mathrm{I}}\right)+\mathrm{j}\left(r^{\mathrm{R}}\tilde{F}^{\mathrm{I}}+r^{\mathrm{I}}\tilde{F}^{\mathrm{R}}\right)$$

Hence,

$$\tilde{X}^{\mathrm{R}}=r^{\mathrm{R}}\tilde{F}^{\mathrm{R}}-r^{\mathrm{I}}\tilde{F}^{\mathrm{I}}$$
$$\tilde{X}^{\mathrm{I}}=r^{\mathrm{R}}\tilde{F}^{\mathrm{I}}+r^{\mathrm{I}}\tilde{F}^{\mathrm{R}}$$

or,

$$X_c=r^{\mathrm{R}}F_c+r^{\mathrm{I}}F_s \tag{37a}$$
$$X_s=r^{\mathrm{R}}F_s-r^{\mathrm{I}}F_c \tag{37b}$$

The pair of equations (37) is applied to the cosine and sine components of the harmonic $s\omega$ of each force to obtain the cosine and sine components of the elemental response due to each force in that harmonic $s\omega$. Linearity of the structure enables one to add up these cosine and sine components of the elemental responses to obtain respectively the cosine and sine components of the full response in harmonic $s\omega$.

Let e_{0xJi} and e_{0yJi} be the static eccentricities of Ji from Bi in the x and y directions respectively. These are determined either by measurement or by the solution of the static problem. Considering the squeeze film forces in equations (28), the unbalance forces in equations (35), and applying equations (37) one can write the following.

For each Ji in the x direction:

$$X_{0Ji}-e_{0xJi}=\sum_{j=1}^{n}\left[\alpha\alpha_{JiJj}(0)-\alpha\alpha_{JiBj}(0)\right]Q_{xj}+\sum_{j=1}^{n}\left[\alpha\beta_{JiJj}(0)-\alpha\beta_{JiBj}(0)\right]Q_{yj}\ ^{1} \tag{38a}$$

[1] All zero frequency receptances are real.

$$a^s_{XJi} = \sum_{j=1}^{n}\left[\alpha\alpha^{\mathrm{R}}_{JiJj}(s\omega) - \alpha\alpha^{\mathrm{R}}_{JiBj}(s\omega)\right]p^s_{xj} + \delta_{Ns}\sum_{k=1}^{p}\alpha\alpha^{\mathrm{R}}_{JiUk}(s\omega)U_k\Omega^2\sin\phi_k$$

$$+ \sum_{j=1}^{n}\left[\alpha\alpha^{\mathrm{I}}_{JiJj}(s\omega) - \alpha\alpha^{\mathrm{I}}_{JiBj}(s\omega)\right]q^s_{xj} + \delta_{Ns}\sum_{k=1}^{p}\alpha\alpha^{\mathrm{I}}_{JiUk}(s\omega)U_k\Omega^2\cos\phi_k$$

$$+ \sum_{j=1}^{n}\left[\alpha\beta^{\mathrm{R}}_{JiJj}(s\omega) - \alpha\beta^{\mathrm{R}}_{JiBj}(s\omega)\right]p^s_{yj} + \delta_{Ns}\sum_{k=1}^{p} -\alpha\beta^{\mathrm{R}}_{JiUk}(s\omega)U_k\Omega^2\cos\phi_k$$

$$+ \sum_{j=1}^{n}\left[\alpha\beta^{\mathrm{I}}_{JiJj}(s\omega) - \alpha\beta^{\mathrm{I}}_{JiBj}(s\omega)\right]q^s_{yj} + \delta_{Ns}\sum_{k=1}^{p}\alpha\beta^{\mathrm{I}}_{JiUk}(s\omega)U_k\Omega^2\sin\phi_k \qquad (38b)$$

$$b^s_{XJi} = \sum_{j=1}^{n}\left[\alpha\alpha^{\mathrm{R}}_{JiJj}(s\omega) - \alpha\alpha^{\mathrm{R}}_{JiBj}(s\omega)\right]q^s_{xj} + \delta_{Ns}\sum_{k=1}^{p}\alpha\alpha^{\mathrm{R}}_{JiUk}(s\omega)U_k\Omega^2\cos\phi_k$$

$$- \sum_{j=1}^{n}\left[\alpha\alpha^{\mathrm{I}}_{JiJj}(s\omega) - \alpha\alpha^{\mathrm{I}}_{JiBj}(s\omega)\right]p^s_{xj} - \delta_{Ns}\sum_{k=1}^{p}\alpha\alpha^{\mathrm{I}}_{JiUk}(s\omega)U_k\Omega^2\sin\phi_k$$

$$+ \sum_{j=1}^{n}\left[\alpha\beta^{\mathrm{R}}_{JiJj}(s\omega) - \alpha\beta^{\mathrm{R}}_{JiBj}(s\omega)\right]q^s_{yj} + \delta_{Ns}\sum_{k=1}^{p}\alpha\beta^{\mathrm{R}}_{JiUk}(s\omega)U_k\Omega^2\sin\phi_k$$

$$- \sum_{j=1}^{n}\left[\alpha\beta^{\mathrm{I}}_{JiJj}(s\omega) - \alpha\beta^{\mathrm{I}}_{JiBj}(s\omega)\right]p^s_{yj} - \delta_{Ns}\sum_{k=1}^{p} -\alpha\beta^{\mathrm{I}}_{JiUk}(s\omega)U_k\Omega^2\cos\phi_k \qquad (38c)$$

for $s = 1\ldots m$.

For each *Bi* in the *x* direction:

$$X_{0Bi} = \sum_{j=1}^{n}\left[\alpha\alpha_{BiJj}(0) - \alpha\alpha_{BiBj}(0)\right]\overline{Q}_{xj} + \sum_{j=1}^{n}\left[\alpha\beta_{BiJj}(0) - \alpha\beta_{BiBj}(0)\right]\overline{Q}_{yj} \qquad (39a)$$

$$a^s_{XBi} = \sum_{j=1}^{n}\left[\alpha\alpha^{\mathrm{R}}_{BiJj}(s\omega) - \alpha\alpha^{\mathrm{R}}_{BiBj}(s\omega)\right]p^s_{xj} + \delta_{Ns}\sum_{k=1}^{p}\alpha\alpha^{\mathrm{R}}_{BiUk}(s\omega)U_k\Omega^2\sin\phi_k$$

$$+ \sum_{j=1}^{n}\left[\alpha\alpha^{\mathrm{I}}_{BiJj}(s\omega) - \alpha\alpha^{\mathrm{I}}_{BiBj}(s\omega)\right]q^s_{xj} + \delta_{Ns}\sum_{k=1}^{p}\alpha\alpha^{\mathrm{I}}_{BiUk}(s\omega)U_k\Omega^2\cos\phi_k$$

$$+ \sum_{j=1}^{n}\left[\alpha\beta^{\mathrm{R}}_{BiJj}(s\omega) - \alpha\beta^{\mathrm{R}}_{BiBj}(s\omega)\right]p^s_{yj} + \delta_{Ns}\sum_{k=1}^{p} -\alpha\beta^{\mathrm{R}}_{BiUk}(s\omega)U_k\Omega^2\cos\phi_k$$

$$+ \sum_{j=1}^{n}\left[\alpha\beta^{\mathrm{I}}_{BiJj}(s\omega) - \alpha\beta^{\mathrm{I}}_{BiBj}(s\omega)\right]q^s_{yj} + \delta_{Ns}\sum_{k=1}^{p}\alpha\beta^{\mathrm{I}}_{BiUk}(s\omega)U_k\Omega^2\sin\phi_k \qquad (39b)$$

$$b^s_{XBi} = \sum_{j=1}^{n}\left[\alpha\alpha^{\mathrm{R}}_{BiJj}(s\omega) - \alpha\alpha^{\mathrm{R}}_{BiBj}(s\omega)\right]q^s_{xj} + \delta_{Ns}\sum_{k=1}^{p}\alpha\alpha^{\mathrm{R}}_{BiUk}(s\omega)U_k\Omega^2\cos\phi_k$$

$$-\sum_{j=1}^{n}\left[\alpha\alpha^{\mathrm{I}}_{BiJj}(s\omega) - \alpha\alpha^{\mathrm{I}}_{BiBj}(s\omega)\right]p^s_{xj} - \delta_{Ns}\sum_{k=1}^{p}\alpha\alpha^{\mathrm{I}}_{BiUk}(s\omega)U_k\Omega^2\sin\phi_k$$

$$+\sum_{j=1}^{n}\left[\alpha\beta^{\mathrm{R}}_{BiJj}(s\omega) - \alpha\beta^{\mathrm{R}}_{BiBj}(s\omega)\right]q^s_{yj} + \delta_{Ns}\sum_{k=1}^{p}\alpha\beta^{\mathrm{R}}_{BiUk}(s\omega)U_k\Omega^2\sin\phi_k$$

$$-\sum_{j=1}^{n}\left[\alpha\beta^{\mathrm{I}}_{BiJj}(s\omega) - \alpha\beta^{\mathrm{I}}_{BiBj}(s\omega)\right]p^s_{yj} - \delta_{Ns}\sum_{k=1}^{p} -\alpha\beta^{\mathrm{I}}_{BiUk}(s\omega)U_k\Omega^2\cos\phi_k \qquad (39c)$$

for $s = 1\ldots m$.

For each *Ji* in the *y* direction:

$$Y_{0Ji} - e_{0\,yJi} = \sum_{j=1}^{n}\left[\beta\beta_{JiJj}(0) - \beta\beta_{JiBj}(0)\right]\overline{Q}_{yj} + \sum_{j=1}^{n}\left[\beta\alpha_{JiJj}(0) - \beta\alpha_{JiBj}(0)\right]\overline{Q}_{xj} \qquad (40a)$$

$$a^s_{YJi} = \sum_{j=1}^{n}\left[\beta\beta^{\mathrm{R}}_{JiJj}(s\omega) - \beta\beta^{\mathrm{R}}_{JiBj}(s\omega)\right]p^s_{yj} + \delta_{Ns}\sum_{k=1}^{p} -\beta\beta^{\mathrm{R}}_{JiUk}(s\omega)U_k\Omega^2\cos\phi_k$$

$$+\sum_{j=1}^{n}\left[\beta\beta^{\mathrm{I}}_{JiJj}(s\omega) - \beta\beta^{\mathrm{I}}_{JiBj}(s\omega)\right]q^s_{yj} + \delta_{Ns}\sum_{k=1}^{p}\beta\beta^{\mathrm{I}}_{JiUk}(s\omega)U_k\Omega^2\sin\phi_k$$

$$+\sum_{j=1}^{n}\left[\beta\alpha^{\mathrm{R}}_{JiJj}(s\omega) - \beta\alpha^{\mathrm{R}}_{JiBj}(s\omega)\right]p^s_{xj} + \delta_{Ns}\sum_{k=1}^{p}\beta\alpha^{\mathrm{R}}_{JiUk}(s\omega)U_k\Omega^2\sin\phi_k$$

$$+\sum_{j=1}^{n}\left[\beta\alpha^{\mathrm{I}}_{JiJj}(s\omega) - \beta\alpha^{\mathrm{I}}_{JiBj}(s\omega)\right]q^s_{xj} + \delta_{Ns}\sum_{k=1}^{p}\beta\alpha^{\mathrm{I}}_{JiUk}(s\omega)U_k\Omega^2\cos\phi_k \qquad (40b)$$

$$b^s_{YJi} = \sum_{j=1}^{n}\left[\beta\beta^{\mathrm{R}}_{JiJj}(s\omega) - \beta\beta^{\mathrm{R}}_{JiBj}(s\omega)\right]q^s_{yj} + \delta_{Ns}\sum_{k=1}^{p}\beta\beta^{\mathrm{R}}_{JiUk}(s\omega)U_k\Omega^2\sin\phi_k$$

$$-\sum_{j=1}^{n}\left[\beta\beta^{\mathrm{I}}_{JiJj}(s\omega) - \beta\beta^{\mathrm{I}}_{JiBj}(s\omega)\right]p^s_{yj} - \delta_{Ns}\sum_{k=1}^{p} -\beta\beta^{\mathrm{I}}_{JiUk}(s\omega)U_k\Omega^2\cos\phi_k$$

$$+\sum_{j=1}^{n}\left[\beta\alpha^{\mathrm{R}}_{JiJj}(s\omega) - \beta\alpha^{\mathrm{R}}_{JiBj}(s\omega)\right]q^s_{xj} + \delta_{Ns}\sum_{k=1}^{p}\beta\alpha^{\mathrm{R}}_{JiUk}(s\omega)U_k\Omega^2\cos\phi_k$$

$$-\sum_{j=1}^{n}\left[\beta\alpha^{\mathrm{I}}_{JiJj}(s\omega) - \beta\alpha^{\mathrm{I}}_{JiBj}(s\omega)\right]p^s_{xj} - \delta_{Ns}\sum_{k=1}^{p}\beta\alpha^{\mathrm{I}}_{JiUk}(s\omega)U_k\Omega^2\sin\phi_k \qquad (40c)$$

for $s = 1 \ldots m$.

For each Bi in the y direction:

$$Y_{0Bi} = \sum_{j=1}^{n} \left[\beta\beta_{BiJj}(0) - \beta\beta_{BiBj}(0)\right]\overline{Q}_{yj} + \sum_{j=1}^{n} \left[\beta\alpha_{BiJj}(0) - \beta\alpha_{BiBj}(0)\right]\overline{Q}_{xj} \tag{41a}$$

$$\begin{aligned} a^{s}_{YBi} = & \sum_{j=1}^{n} \left[\beta\beta^{\mathrm{R}}_{BiJj}(s\omega) - \beta\beta^{\mathrm{R}}_{BiBj}(s\omega)\right]p^{s}_{yj} + \delta_{Ns} \sum_{k=1}^{p} - \beta\beta^{\mathrm{R}}_{BiUk}(s\omega) U_k \Omega^2 \cos\phi_k \\ & + \sum_{j=1}^{n} \left[\beta\beta^{\mathrm{I}}_{BiJj}(s\omega) - \beta\beta^{\mathrm{I}}_{BiBj}(s\omega)\right]q^{s}_{yj} + \delta_{Ns} \sum_{k=1}^{p} \beta\beta^{\mathrm{I}}_{BiUk}(s\omega) U_k \Omega^2 \sin\phi_k \\ & + \sum_{j=1}^{n} \left[\beta\alpha^{\mathrm{R}}_{BiJj}(s\omega) - \beta\alpha^{\mathrm{R}}_{BiBj}(s\omega)\right]p^{s}_{xj} + \delta_{Ns} \sum_{k=1}^{p} \beta\alpha^{\mathrm{R}}_{BiUk}(s\omega) U_k \Omega^2 \sin\phi_k \\ & + \sum_{j=1}^{n} \left[\beta\alpha^{\mathrm{I}}_{BiJj}(s\omega) - \beta\alpha^{\mathrm{I}}_{BiBj}(s\omega)\right]q^{s}_{xj} + \delta_{Ns} \sum_{k=1}^{p} \beta\alpha^{\mathrm{I}}_{BiUk}(s\omega) U_k \Omega^2 \cos\phi_k \end{aligned} \tag{41b}$$

$$\begin{aligned} b^{s}_{YBi} = & \sum_{j=1}^{n} \left[\beta\beta^{\mathrm{R}}_{BiJj}(s\omega) - \beta\beta^{\mathrm{R}}_{BiBj}(s\omega)\right]q^{s}_{yj} + \delta_{Ns} \sum_{k=1}^{p} \beta\beta^{\mathrm{R}}_{BiUk}(s\omega) U_k \Omega^2 \sin\phi_k \\ & - \sum_{j=1}^{n} \left[\beta\beta^{\mathrm{I}}_{BiJj}(s\omega) - \beta\beta^{\mathrm{I}}_{BiBj}(s\omega)\right]p^{s}_{yj} - \delta_{Ns} \sum_{k=1}^{p} - \beta\beta^{\mathrm{I}}_{BiUk}(s\omega) U_k \Omega^2 \cos\phi_k \\ & + \sum_{j=1}^{n} \left[\beta\alpha^{\mathrm{R}}_{BiJj}(s\omega) - \beta\alpha^{\mathrm{R}}_{BiBj}(s\omega)\right]q^{s}_{xj} + \delta_{Ns} \sum_{k=1}^{p} \beta\alpha^{\mathrm{R}}_{BiUk}(s\omega) U_k \Omega^2 \cos\phi_k \\ & - \sum_{j=1}^{n} \left[\beta\alpha^{\mathrm{I}}_{BiJj}(s\omega) - \beta\alpha^{\mathrm{I}}_{BiBj}(s\omega)\right]p^{s}_{xj} - \delta_{Ns} \sum_{k=1}^{p} \beta\alpha^{\mathrm{I}}_{BiUk}(s\omega) U_k \Omega^2 \sin\phi_k \end{aligned} \tag{41c}$$

for $s = 1 \ldots m$.

Substituting for $\overline{Q}_{xj}$, p^{s}_{xj}, q^{s}_{xj}, $\overline{Q}_{yj}$, p^{s}_{yj}, q^{s}_{yj} from equations (33a,b) in the above equations (38)-(41) (see Appendix A), one arrives at the following system of equations:

$$\left\{\begin{bmatrix} \mathbf{M}_{xx} & \mathbf{M}_{xy} \\ \mathbf{M}_{yx} & \mathbf{M}_{yy} \end{bmatrix} - \mathbf{I}_{4n(2m+1)}\right\}\begin{bmatrix} \mathbf{v}_x \\ \mathbf{v}_y \end{bmatrix} = \begin{bmatrix} \mathbf{f}_{xx} + \mathbf{f}_{xy} \\ \mathbf{f}_{yx} + \mathbf{f}_{yy} \end{bmatrix} \tag{42}$$

where:

$$\mathbf{v_x} = \begin{bmatrix} \mathbf{v_{xJ}} \\ \mathbf{v_{xB}} \end{bmatrix},\ \mathbf{v_{xJ}} = \begin{bmatrix} \mathbf{v_{xJ1}} \\ \vdots \\ \mathbf{v_{xJn}} \end{bmatrix}, \mathbf{v_{xB}} = \begin{bmatrix} \mathbf{v_{xB1}} \\ \vdots \\ \mathbf{v_{xBn}} \end{bmatrix}$$

$$\mathbf{v_{xJi}} = \begin{bmatrix} X_{0Ji} & a^1_{XJi} & b^1_{XJi} & \cdots & a^m_{XJi} & b^m_{XJi} \end{bmatrix}^{\mathbf{T}},\ i = 1 \ldots n$$

$$\mathbf{v_{xBi}} = \begin{bmatrix} X_{0Bi} & a^1_{XBi} & b^1_{XBi} & \cdots & a^m_{XBi} & b^m_{XBi} \end{bmatrix}^{\mathbf{T}},\ i = 1 \ldots n$$

$$\mathbf{v_y} = \begin{bmatrix} \mathbf{v_{yJ}} \\ \mathbf{v_{yB}} \end{bmatrix},\ \mathbf{v_{yJ}} = \begin{bmatrix} \mathbf{v_{yJ1}} \\ \vdots \\ \mathbf{v_{yJn}} \end{bmatrix}, \mathbf{v_{yB}} = \begin{bmatrix} \mathbf{v_{yB1}} \\ \vdots \\ \mathbf{v_{yBn}} \end{bmatrix}$$

$$\mathbf{v_{yJi}} = \begin{bmatrix} Y_{0Ji} & a^1_{YJi} & b^1_{YJi} & \cdots & a^m_{YJi} & b^m_{YJi} \end{bmatrix}^{\mathbf{T}},\ i = 1 \ldots n$$

$$\mathbf{v_{yBi}} = \begin{bmatrix} Y_{0Bi} & a^1_{YBi} & b^1_{YBi} & \cdots & a^m_{YBi} & b^m_{YBi} \end{bmatrix}^{\mathbf{T}},\ i = 1 \ldots n$$

The matrices $\mathbf{M_{xx}}$, $\mathbf{M_{xy}}$, $\mathbf{M_{yx}}$, $\mathbf{M_{yy}}$ and the column vectors $\mathbf{f_{xx}}$, $\mathbf{f_{xy}}$, $\mathbf{f_{yx}}$, $\mathbf{f_{yy}}$ are given in the Appendix A, equations (A6)-(A25). It suffices to say that:
$\mathbf{M_{xx}}$, $\mathbf{M_{yx}}$ are square matrices of order $2n(2m+1)$ both containing the coefficients k_{xxj}, c_{xxj}, and, respectively, the receptances $\alpha\alpha(s\omega)$, $\beta\alpha(s\omega)$;
$\mathbf{M_{xy}}$, $\mathbf{M_{yy}}$ are square matrices of order $2n(2m+1)$ both containing the coefficients k_{yyj}, c_{yyj}, and, respectively, the receptances $\alpha\beta(s\omega)$, $\beta\beta(s\omega)$;
$\mathbf{f_{xx}}$, $\mathbf{f_{yx}}$ are column vectors of order $2n(2m+1)\times 1$ both containing the coefficients Q_{xoj}, A^s_{xj}, B^s_{xj} and, respectively, the receptances $\alpha\alpha(s\omega)$, $\beta\alpha(s\omega)$;
$\mathbf{f_{xy}}$, $\mathbf{f_{yy}}$ are square matrices of order $2n(2m+1)\times 1$ both containing the coefficients Q_{yoj}, A^s_{yj}, B^s_{yj} and, respectively, the receptances $\alpha\beta(s\omega)$, $\beta\beta(s\omega)$

..... where $j = 1 \ldots n$ and $s = 0 \ldots m$.

Hence the terms in $\mathbf{M_{xx}}$, $\mathbf{M_{xy}}$, $\mathbf{M_{yx}}$, $\mathbf{M_{yy}}$, $\mathbf{f_{xx}}$, $\mathbf{f_{xy}}$, $\mathbf{f_{yx}}$, $\mathbf{f_{yy}}$ are non-linear functions of the elements in $\mathbf{v_x}$, $\mathbf{v_y}$, from equations (33), (29), (22), (14), (3).

Note that if cross-coupling (mostly due to gyroscopic effects) in the linear system is neglected *i.e.* $\{\alpha\beta_{ij}\}, \{\beta\alpha_{ij}\} = \mathbf{0}$ in eq., then $\mathbf{M_{xy}}$, $\mathbf{M_{yx}}$, $\mathbf{f_{xy}}$, $\mathbf{f_{yx}} = \mathbf{0}$ and the system of equations reads:

$$\left\{ \begin{bmatrix} \mathbf{M_{xx}} & \mathbf{0} \\ \mathbf{0} & \mathbf{M_{yy}} \end{bmatrix} - \mathbf{I}_{4n(2m+1)} \right\} \begin{bmatrix} \mathbf{v_x} \\ \mathbf{v_y} \end{bmatrix} = \begin{bmatrix} \mathbf{f_{xx}} \\ \mathbf{f_{yy}} \end{bmatrix}$$

or

$$\left\{\mathbf{M}_{xx}-\mathbf{I}_{2n(2m+1)}\right\}\mathbf{v}_x=\mathbf{f}_{xx} \tag{43a}$$

$$\left\{\mathbf{M}_{yy}-\mathbf{I}_{2n(2m+1)}\right\}\mathbf{v}_y=\mathbf{f}_{yy} \tag{43b}$$

However the two resulting systems in the x and y directions will still be coupled since the coefficients in $\mathbf{M}_{xx}$, $\mathbf{f}_{xx}$ are derived from $Q_{xj}=Q_{xj}\left(X_j,Y_j,\dot{X}_j,\dot{Y}_j\right)$ and the coefficients in $\mathbf{M}_{yy}$, $\mathbf{f}_{yy}$ are derived from $Q_{yj}=Q_{yj}\left(X_j,Y_j,\dot{X}_j,\dot{Y}_j\right)$. Hence, the system of equations (42) or (43) will always represent a system of $4n(2m+1)$ coupled non-linear algebraic equations in $4n(2m+1)$ unknowns contained in $\mathbf{v}_x$, $\mathbf{v}_y$.

The system of equations (42) is then expressed as

$$\mathbf{f}(\mathbf{v})=0 \tag{44}$$

where

$$\mathbf{v}=\begin{bmatrix}\mathbf{v}_x\\ \mathbf{v}_y\end{bmatrix} \tag{45a}$$

and $\mathbf{f}(\mathbf{v})$ is a non-linear vector function of $\mathbf{v}$:

$$\mathbf{f}(\mathbf{v})=\left\{\begin{bmatrix}\mathbf{M}_{xx} & \mathbf{M}_{xy}\\ \mathbf{M}_{yx} & \mathbf{M}_{yy}\end{bmatrix}-\mathbf{I}_{4n(2m+1)}\right\}\begin{bmatrix}\mathbf{v}_x\\ \mathbf{v}_y\end{bmatrix}-\begin{bmatrix}\mathbf{f}_{xx}+\mathbf{f}_{xy}\\ \mathbf{f}_{yx}+\mathbf{f}_{yy}\end{bmatrix} \tag{45b}$$

and solved by any iterative solver suitable for systems of non-linear algebraic equations. This is explained in the following section 3.4.

Note that the number of unknowns is $4n(2m+1)$ *i.e.* $(2m+1)\times$*number of non-linear degrees of freedom*[1]. This number is the same as for other alternative methods used to solve this class of non-linear problem by harmonic balance [1], [2].

[1] Associated with each squeeze film i, $i=1\ldots n$, there are 4 degrees of freedom: $X_{Ji}, Y_{Ji}, X_{Bi}, Y_{Bi}$.

3.4 SOLUTION OF THE HARMONIC BALANCE EQUATIONS

For any assumed $\mathbf{v}$ the non-linear vector function $\mathbf{f}(\mathbf{v})$, given by equation (45b) can be evaluated as follows:

(a) From the elements in $\mathbf{v}$ construct the time histories over one period Γ of the relative displacements X_i, Y_i and the relative velocities $\dot{X}_i$, $\dot{Y}_i$ at each squeeze film from equations (27).

(b) Construct the time history over Γ of each squeeze film force pair $Q_{xi}(X_i, Y_i, \dot{X}_i, \dot{Y}_i)$, $Q_{yi}(X_i, Y_i, \dot{X}_i, \dot{Y}_i)$ from equations (14) and one of equations (6), (9), (11) or (3), depending on the choice of cavitation model and end sealing conditions.

(c) Using equations (29) compute the Fourier coefficients $\overline{Q}_{xj}$, p^s_{xj}, q^s_{xj}, $\overline{Q}_{yj}$, p^s_{yj}, q^s_{yj} ($s = 1 \ldots m$), for each squeeze film.

(d) For each squeeze film determine the terms Q_{xoi}, c_{xxi}, k_{xxi}, A^s_{xi}, B^s_{xi}, Q_{yoi}, c_{yyi}, k_{yyi}, A^s_{yi}, B^s_{yi} ($s = 1 \ldots m$), from equations (34a,b).

(e) Compute the matrices in equation (45b) from equations (A6)-(A25) in Appendix A.

Hence, the equation (44) can be solved by some iterative procedure for a given value μ_i of a particular control parameter μ. The result obtained can then be used to obtain an initial approximation to the solution for the next value μ_{i+1} of the control parameter μ. Hence a continuation process [14] is set up. If the rotational speed Ω is used as the control parameter then the system of equations to be solved for each Ω_i is equation (44):

$$\mathbf{f}(\mathbf{v}) = \mathbf{0}$$

Use of the rotational speed Ω as control parameter of the continuation process results in failure at multiple solutions [14] *i.e.* when more than one solution is possible for a given speed (*e.g.* bistable regions in the unbalance response due to spring hardening or softening effects of the SFD). In order to overcome this, arc-length continuation [14] is employed. The control parameter is changed from Ω to an "arc-length" σ. The rotational speed Ω now becomes an unknown, $\Omega = \Omega(\sigma)$ and an extra equation needs to be added to the system (44). Suppose that $\mathbf{v}$ and Ω are required for $\sigma = \sigma_i$ *i.e.* $\mathbf{v}_i$, Ω_i are required. Suppose that $\mathbf{v}_{i-1}$, Ω_{i-1}, corresponding to $\sigma = \sigma_{i-1}$ are known. Then the equation that defines σ in the interval $\sigma_{i-1} \le \sigma \le \sigma_i$ is [14]:

$$(\sigma - \sigma_{i-1})^2 = \frac{1}{c^2}\|\mathbf{v} - \mathbf{v}_{i-1}\| + \left(\frac{\Omega}{\omega_0} - \frac{\Omega_{i-1}}{\omega_0}\right)^2, \quad \sigma_{i-1} \le \sigma \le \sigma_i \qquad (46)$$

where $\|\mathbf{a}\|$ is defined thus: if vector $\mathbf{a} = [a_1 \quad \cdots \quad a_n]^T$, then $\|\mathbf{a}\| = a_1^2 + \ldots + a_n^2$.

c is the radial clearance of any one of the dampers and ω_0 is the lowest natural frequency of the undamped linear system. Note that c and ω_0 are merely introduced to non-dimensionalise the

right hand side of equation (46) in order to work with a non-dimensional arc-length σ. The system of equations to be solved for each given value of σ, σ_i is

$$\begin{cases} \mathbf{f}(\Omega, \mathbf{v}) = \mathbf{0} \\ p(\Omega, \mathbf{v}) = 0 \end{cases} \tag{47}$$

where $\mathbf{f}(\Omega, \mathbf{v}) = \mathbf{f}(\mathbf{v})$ in equation (45b) and, from equation (46):

$$p(\Omega, \mathbf{v}) = \frac{1}{c^2}\|\mathbf{v} - \mathbf{v}_{i-1}\| + \left(\frac{\Omega}{\omega_0} - \frac{\Omega_{i-1}}{\omega_0}\right)^2 - (\sigma - \sigma_{i-1})^2 \tag{48}$$

The vector of unknowns is now augmented to

$$\mathbf{w} = \begin{bmatrix} \mathbf{v} \\ \Omega \end{bmatrix} \tag{49a}$$

and the system of equations (47) can be expressed as

$$\mathbf{g}(\mathbf{w}) = \mathbf{0} \tag{50}$$

where

$$\mathbf{g}(\mathbf{w}) = \begin{bmatrix} \mathbf{f}(\Omega, \mathbf{v}) \\ p(\Omega, \mathbf{v}) \end{bmatrix} \tag{49b}$$

A given value of σ will correspond to just one solution $\mathbf{w}$. Hence the problem of multiple solutions does not arise when σ is used as control parameter. As σ is increased the continuation process "climbs" along the unbalance response curve[1] in one direction with ease, no matter how intricate the curve may be. The unbalance response curve is traced out in all its detail using arc-length continuation (in contrast to the poor performance of rotational speed control parameter in bistable regions).

Equations (44) or (50) are solved for a given value of the control parameter by a predictor-corrector iterative process [14]. The process used in this research is summarised below. It refers to the solution of the general system

$$\mathbf{h}(\mathbf{x}) = \mathbf{0} \tag{51}$$

[1] By "unbalance response curve" is meant a curve showing the variation of one element of $\mathbf{v}$ (*e.g.* mean y displacement at a squeeze film) or some combination of certain elements in $\mathbf{v}$ (*e.g.* peak to peak amplitude at a squeeze film) with the rotational speed Ω.

with control parameter μ. If $\mu = \Omega$, then $\mathbf{h}$ is $\mathbf{f}$ and $\mathbf{x}$ is $\mathbf{v}$ *i.e.* we have equation (44). If $\mu = \sigma$, then $\mathbf{h}$ is $\mathbf{g}$ and $\mathbf{x}$ is $\mathbf{w}$ *i.e.* we have equation (50). The iterative scheme was implemented on *MATLAB*® (Version 5).

3.4.1 Iterative Scheme

To find the solution $\mathbf{x}_i$ for $\mu = \mu_i$: let $\mathbf{x}_i^j$ be the jth iterate for $\mathbf{x}_i$.

A. PREDICTOR STEP

If $\mu = \Omega$ (*i.e.* rotational speed control parameter)

$$\mathbf{x}_i^0 = \mathbf{x}_{i-1}$$

If $\mu = \sigma$ (*i.e.* arc length control parameter), linear interpolation [14] is used:

$$\mathbf{x}_i^0 = \mathbf{x}_{i-1} + \left(\frac{\sigma_i - \sigma_{i-1}}{\sigma_{i-1} - \sigma_{i-2}} \right) (\mathbf{x}_{i-1} - \mathbf{x}_{i-2})$$

B. CORRECTOR STEP

B1. Compute the Jacobian matrix of $\mathbf{h}(\mathbf{x})$ at $\mathbf{x} = \mathbf{x}_i^0$:

$$\mathbf{J}_i^0 = \left. \frac{\partial \mathbf{h}(\mathbf{x})}{\partial \mathbf{x}} \right|_{\mathbf{x}=\mathbf{x}_i^0}$$

B2. Apply the damped Newton-Raphson Method [20]:

$$\mathbf{x}_i^{j+1} = \mathbf{x}_i^j - \gamma \mathbf{H}_i^j \mathbf{h}_i^j$$

where $\mathbf{h}_i^j = \mathbf{h}(\mathbf{x}_i^j)$, $\mathbf{H}_i^j = (\mathbf{J}_i^j)^{-1}$, $\gamma \leq 1$ is the damping factor

B3. Increase j by 1.

While $|\mathbf{x}_i^j - \mathbf{x}_i^{j-1}| \leq tol$ do steps B4-B6:

B4. Update $\mathbf{H}_i^j$ using Broyden's Method [20]

$$\mathbf{H}_i^j = \mathbf{H}_i^{j-1} - \frac{(\mathbf{H}_i^{j-1}\mathbf{y} - \mathbf{q})\mathbf{q}^T \mathbf{H}_i^{j-1}}{\mathbf{q}^T \mathbf{H}_i^{j-1} \mathbf{y}}$$

where $\mathbf{q} = \mathbf{x}_i^j - \mathbf{x}_i^{j-1}$, $\mathbf{y} = \mathbf{h}_i^j - \mathbf{h}_i^{j-1}$

B5. Compute $\mathbf{x}_i^{j+1}$ using damped Newton –Raphson Method, step B2

B6. Increase j by 1.

While $\left(\left|\mathbf{x}_i^j - \mathbf{x}_i^{j-1}\right| \le eps\right)$ OR $\left(\left|\mathbf{h}_i^j\right| \le eps\right)$ do steps B7-B9:

B7. Update $\mathbf{H}_i^j$ using step B4.

B8. Compute $\mathbf{x}_i^{j+1}$ using undamped Newton-Raphson Method: step B2 with $\gamma = 1$

B9. Increase j by 1.

B.10. $\mathbf{x}_i^j = \mathbf{x}_i$.

In step B1 the Jacobian matrix was evaluated using the *MATLAB®* function *numjac.m©* [21]. For steps B2 and B5 the damping factor $\gamma = 0.1$. For steps B4-B6 $tol = 10^{-8}$. In steps B7-B9, $eps = 2\times10^{-16}$, the smallest number registered in *MATLAB®*.

To start the arc-length continuation process, two previous solutions $\mathbf{x}_{i-2}$, $\mathbf{x}_{i-1}$ are required. Hence to compute the "points" $\mathbf{x}_1$, $\mathbf{x}_2$,..... on an unbalance response the following procedure was followed:
a). Compute $\mathbf{x}_1$ and $\mathbf{x}_2$ with control parameter $\mu = \Omega$.
b). Compute the remaining solutions $\mathbf{x}_3$, $\mathbf{x}_4$,..... with control parameter $\mu = \sigma$.

The starting estimate for the first solution $\mathbf{x}_1$, *i.e.* $\mathbf{x}_1^0$ in predictor step, is found as follows:
a). In the case of a rotor fully supported on retainer springs, since one starts the solution at a low speed, the mean displacements will be approximately equal to the known static displacements. The amplitudes of vibration are taken as zero.
b). In all other cases, assumptions for $\mathbf{x}_1^0$ usually fail, especially with a large number of unknowns. In such a case $\mathbf{x}_1^0$ is obtained from a time domain numerical integration solution (chapter 4), for the first speed.

In the arc-length continuation process, the arc-length length increment used in this research was around 0.1. Occasionally this value had to be reduced. In the simulations carried out (chapters 7, 8) the arc-length continuation method proved its effectiveness in dealing with multiple solutions.

3.5 RESPONSE AT A GENERAL POSITION

Once the harmonic balance equations (44), have been solved then the vibration at a general position P can be computed. The displacements X_P, Y_P at P, measured from its static equilibrium position will be given by:

$$X_P = X_{0P} + \sum_{s=1}^{m} \left(a_{XP}^s \cos s\omega t + b_{XP}^s \sin s\omega t \right) \tag{52a}$$

$$Y_P = Y_{0P} + \sum_{s=1}^{m} \left(a_{YP}^s \cos s\omega t + b_{YP}^s \sin s\omega t \right) \tag{52b}$$

Having determined the elements in the vector $\mathbf{v}$ in equation (44) *i.e.* the vector of unknown harmonic components at the squeeze films, the Fourier components of the squeeze film forces $\overline{Q}_{xi}$, p_{xi}^s, q_{xi}^s, $\overline{Q}_{yi}$, p_{yi}^s, q_{yi}^s $(s = 1 \ldots m)$ can be determined as in steps (a) to (c) of the first paragraph of section 3.4. The terms in equations (52) are then obtained by applying the same principle used to derive the harmonic balance equations, equations (38)-(41).

$$X_{0P} = \sum_{j=1}^{n} \left[\alpha\alpha_{PJj}(0) - \alpha\alpha_{PBj}(0) \right] \overline{Q}_{xj} + \sum_{j=1}^{n} \left[\alpha\beta_{PJj}(0) - \alpha\beta_{PBj}(0) \right] \overline{Q}_{yj} \tag{53a}$$

$$\begin{aligned}
a_{XP}^s = & \sum_{j=1}^{n} \left[\alpha\alpha_{PJj}^{\mathrm{R}}(s\omega) - \alpha\alpha_{PBj}^{\mathrm{R}}(s\omega) \right] p_{xj}^s + \delta_{Ns} \sum_{k=1}^{p} \alpha\alpha_{PUk}^{\mathrm{R}}(s\omega) U_k \Omega^2 \sin\phi_k \\
& + \sum_{j=1}^{n} \left[\alpha\alpha_{PJj}^{\mathrm{I}}(s\omega) - \alpha\alpha_{PBj}^{\mathrm{I}}(s\omega) \right] q_{xj}^s + \delta_{Ns} \sum_{k=1}^{p} \alpha\alpha_{PUk}^{\mathrm{I}}(s\omega) U_k \Omega^2 \cos\phi_k \\
& + \sum_{j=1}^{n} \left[\alpha\beta_{PJj}^{\mathrm{R}}(s\omega) - \alpha\beta_{PBj}^{\mathrm{R}}(s\omega) \right] p_{yj}^s + \delta_{Ns} \sum_{k=1}^{p} -\alpha\beta_{PUk}^{\mathrm{R}}(s\omega) U_k \Omega^2 \cos\phi_k \\
& + \sum_{j=1}^{n} \left[\alpha\beta_{PJj}^{\mathrm{I}}(s\omega) - \alpha\beta_{PBj}^{\mathrm{I}}(s\omega) \right] q_{yj}^s + \delta_{Ns} \sum_{k=1}^{p} \alpha\beta_{PUk}^{\mathrm{I}}(s\omega) U_k \Omega^2 \sin\phi_k
\end{aligned} \tag{53b}$$

$$\begin{aligned}
b_{XP}^s = & \sum_{j=1}^{n} \left[\alpha\alpha_{PJj}^{\mathrm{R}}(s\omega) - \alpha\alpha_{PBj}^{\mathrm{R}}(s\omega) \right] q_{xj}^s + \delta_{Ns} \sum_{k=1}^{p} \alpha\alpha_{PUk}^{\mathrm{R}}(s\omega) U_k \Omega^2 \cos\phi_k \\
& - \sum_{j=1}^{n} \left[\alpha\alpha_{PJj}^{\mathrm{I}}(s\omega) - \alpha\alpha_{PBj}^{\mathrm{I}}(s\omega) \right] p_{xj}^s - \delta_{Ns} \sum_{k=1}^{p} \alpha\alpha_{PUk}^{\mathrm{I}}(s\omega) U_k \Omega^2 \sin\phi_k \\
& + \sum_{j=1}^{n} \left[\alpha\beta_{PJj}^{\mathrm{R}}(s\omega) - \alpha\beta_{PBj}^{\mathrm{R}}(s\omega) \right] q_{yj}^s + \delta_{Ns} \sum_{k=1}^{p} \alpha\beta_{PUk}^{\mathrm{R}}(s\omega) U_k \Omega^2 \sin\phi_k \\
& - \sum_{j=1}^{n} \left[\alpha\beta_{PJj}^{\mathrm{I}}(s\omega) - \alpha\beta_{PBj}^{\mathrm{I}}(s\omega) \right] p_{yj}^s - \delta_{Ns} \sum_{k=1}^{p} -\alpha\beta_{PUk}^{\mathrm{I}}(s\omega) U_k \Omega^2 \cos\phi_k
\end{aligned} \tag{53c}$$

for $s = 1 \ldots m$.

Similarly for the y direction.

3.6 LIMITATIONS OF THE HARMONIC BALANCE EQUATIONS

The equations (38)-(41) are completely general except for the "mean equations" (38a)-(41a). These pre-assume that the linear structure on which the non-linear forces and unbalances act is not capable of rigid body motion[1]. If the structure is capable of rigid body motion it is termed degenerate [22] and one or more of the receptances, $\alpha\alpha_{JiJj}(0)$, $\beta\beta_{JiJj}(0) \rightarrow \infty$. Note that this usually restricted to the receptances at the rotor and not at the support structure. Hence it is equations (38a), (40a) that are generally subject to this limitation. A typical case where this occurs is a rotor that is coupled to the support structure only through squeeze films, without retainer springs, as in Figure 4. In this case the linear system consists of two uncoupled subsystems, rotor and foundation, with the former capable of rigid body motion for which the mean equations (38a), (40a) do not apply and need alteration. Hence, for any receptance $\alpha\alpha_{JiJj}(0), \beta\beta_{JiJj}(0) \rightarrow \infty$ the element in the first row, first column of the matrices $\left\{\mathbf{M}^{\mathbf{R}}_{\mathbf{xxJij}}\right\}$, $\left\{\mathbf{M}^{\mathbf{R}}_{\mathbf{yyJij}}\right\}$ (see Appendix A, equations (A14a), (A15a)) and the first element in $\mathbf{f}^{\mathbf{R}}_{\mathbf{xxJi}}$, $\mathbf{f}^{\mathbf{R}}_{\mathbf{yyJi}}$ (see Appendix A, equations (A24a), (A25a)) need amendment. This alteration shall be done for the specific cases considered in chapter 5. The principle used is that all the zero frequency forces acting on the degenerate rotor subsystem, comprising the mean oil forces $\overline{Q}_{xi}$, $\overline{Q}_{yi}$, and any static load (e.g. gravity, for the y direction) must be in equilibrium, since, for periodic vibration, there is no mean (zero frequency) acceleration anywhere (easily seen by differentiating twice any of equations (25), (26)). Hence the mean equations (38a), (40a), are replaced by equilibrium equations. A general method to cater for such situations in the case of many squeeze films ($n \geq 3$) is the object of current research and shall not be reported on at this stage[2].

---

[1] In FE terms this means that the stiffness matrix $\mathbf{K}$ is not singular *i.e.* $|\mathbf{K}| \neq 0$, $\mathbf{K}$ is positive definite [23]. If $\mathbf{K}$ is singular then it will be positive semi-definite, and one or more of the eigenvalues dynamic system will be zero, enabling rigid body motion.

[2] In such situations, involving positive semi-definite rotor subsystems, the case $n \geq 3$ involves the solution of a "statically indeterminate" problem within the dynamic equations.

CHAPTER 4

TIME DOMAIN ANALYSIS

In this chapter, a receptance based time domain analysis method is developed.

4.1 DEFINITION OF LINEAR SYSTEM

In this analysis, the "linear system" is defined in a slightly different fashion to that used in harmonic balance analysis. *All* damping forces at the supports, linear as well as non-linear, and gyroscopic moments, if significant, are considered as external, along with the unbalance forces. Suppose the resulting undamped linear system consists of Q uncoupled subsystems. For example if the xz plane is uncoupled from the yz plane then one has two uncoupled subsystems and $Q=2$. If, in addition, the rotor is uncoupled from the support structure (*e.g.* Figure 4) then one has a total of $Q=4$ uncoupled subsystems (rotor in xz, yz planes, support in xz, yz planes). The receptance matrix $\mathbf{R}(\omega)$ for each such subsystem is real and symmetric and any term $R_{ij}(\omega)$ can be expanded as a modal series [24]:

$$R_{ij}(\omega)=\sum_{r=1}^{\infty}\frac{A_{ij}^{r}}{\omega_r^2-\omega^2} \tag{54}$$

where ω_r is the undamped natural frequency of the subsystem in mode r and A_{ij}^{r} is the corresponding modal constant which is given by [24]:

$$A_{ij}^{r}=\psi_i^{r}\psi_j^{r} \tag{55}$$

ψ_i^{r}, ψ_j^{r} are the values of the mass normalised mode shape of mode r evaluated at degrees of freedom i and j respectively.

In practice, over a given frequency range, the series (54) can be truncated after a finite number of modes q:

$$R_{ij}(\omega)\approx\sum_{r=1}^{q}\frac{A_{ij}^{r}}{\omega_r^2-\omega^2} \tag{56}$$

Note that by considering any gyroscopic moments as external one not only removes asymmetry in the complete system receptance matrix and uncouples the xz and yz planes[1] but removes the

[1] Provided no cross-coupled stiffness terms are present in the linear system.

rotational speed dependency of the system receptance matrix. Hence, the sub-system receptance matrices will be real, symmetric and independent of rotational speed.

4.2 COMPUTATION OF TERMS IN SERIES EXPANSION

The undamped natural frequencies ω_r are easily determined by applying to each subsystem any linear frequency based rotor dynamic modelling technique e.g. transfer matrix, mechanical impedance (MI). In particular, with MI the ω_r's are found by locating the zeros of $|\mathbf{Z}(\omega)|$ where $\mathbf{Z}(\omega)$ is the impedance matrix of the subsystem (see equation (16)) *i.e.* by solving

$$|\mathbf{Z}(\omega)| = 0 \tag{57}$$

This equation is effectively solved for any chosen number of zeros within a specified frequency range using Muller's algorithm [25].

Once the ω_r's, $r = 1 \ldots q$ have been determined, the corresponding modal constants A_{ij}^r, $r = 1 \ldots q$ of a receptance term $R_{ij}(\omega)$ are very easily determined by computing $R_{ij}(\omega)$ for p selected frequencies $\omega_{sel\ i}$, $i = 1 \ldots p$ within the chosen frequency range and performing a modal fit [24] by solving the equations:

$$\begin{bmatrix} R_{ij}(\omega_{sel\ 1}) \\ \vdots \\ \vdots \\ R_{ij}(\omega_{sel\ p}) \end{bmatrix} = \begin{bmatrix} \frac{1}{\omega_1^2 - \omega_{sel\ 1}} & \cdots & \frac{1}{\omega_q^2 - \omega_{sel\ 1}} \\ \vdots & \cdots & \vdots \\ \vdots & \cdots & \vdots \\ \frac{1}{\omega_1^2 - \omega_{sel\ p}} & \cdots & \frac{1}{\omega_q^2 - \omega_{sel\ p}} \end{bmatrix} \begin{bmatrix} A_{ij}^1 \\ \vdots \\ A_{ij}^q \end{bmatrix} \tag{58}$$

or

$$\underset{(p\times 1)}{\mathbf{r}} = \underset{(p\times q)}{\mathbf{M}} \underset{(q\times 1)}{\mathbf{a}}$$

Now $p \geq q$. If $p = q$ *i.e. as many points are taken as modes*, then

$$\mathbf{a} = \mathbf{M}^{-1}\mathbf{r} \tag{59}$$

If $p > q$ *i.e. more points are taken than the number of unknown modal constants*

$$\mathbf{a} = \mathbf{M}^{\perp}\mathbf{r} \tag{60}$$

where $\mathbf{M}^{\perp}$ is the *pseudo- inverse* of **M,** given by [24]:

$$\mathbf{M}^{\perp} = \left\{\mathbf{M}^{\mathrm{T}}\mathbf{M}\right\}^{-1}\mathbf{M}^{\mathrm{T}} \tag{61}$$

Note that for the cases considered in section 5.1.1 $p = q$ where the number of modes in each subsystem was $q = 4$. This was found to give highly accurate results. Note also that prior to performing a modal decomposition of the receptance $R_{ij}(\omega)$ over a given frequency range it is wise to check if any of the resonances ω_r of the subsystem is missing, *e.g.* by plotting it $R_{ij}(\omega)$ out over that range, or, much quicker, by checking if $R_{ij}(\omega)$ changes sign in passing through each ω_r. If a resonance is found to be missing then corresponding modal constant is zero[1] and should be omitted from the series expansion (56) prior to performing the fit *i.e.* the appropriate row and column should be deleted from **r, M** and **a** in equation (58), prior to inversion.

4.3 DERIVATION OF EQUATIONS

For clarity general equations are presented for both the following conditions satisfied:

1). The *xz* and *yz* planes are uncoupled in the linear undamped system. Hence $Q = 2$ uncoupled subsystems (in the *xz* and *yz* planes) are considered which means that two uncoupled $2M \times 2M$ [2] receptance matrices $\mathbf{R}_{\mathbf{xz}}$, $\mathbf{R}_{\mathbf{yz}}$ are used where

$$\mathbf{u}_{\mathbf{xz}} = \mathbf{R}_{\mathbf{xz}}\mathbf{f}_{\mathbf{xz}},\ \mathbf{u}_{\mathbf{xz}} = \left[\tilde{X}_1 \quad \tilde{\theta}_{y1} \quad \cdots \quad \tilde{X}_M \quad \tilde{\theta}_{yM}\right],\ \mathbf{f}_{\mathbf{xz}} = \left[\tilde{F}_{x1} \quad \tilde{M}_{y1} \quad \cdots \quad \tilde{F}_{xM} \quad \tilde{M}_{yM}\right] \tag{62a}$$

$$\mathbf{u}_{\mathbf{yz}} = \mathbf{R}_{\mathbf{yz}}\mathbf{f}_{\mathbf{yz}},\ \mathbf{u}_{\mathbf{yz}} = \left[\tilde{Y}_1 \quad \tilde{\theta}_{x1} \quad \cdots \quad \tilde{Y}_M \quad \tilde{\theta}_{xM}\right],\ \mathbf{f}_{\mathbf{yz}} = \left[\tilde{F}_{y1} \quad \tilde{M}_{x1} \quad \cdots \quad \tilde{F}_{yM} \quad \tilde{M}_{xM}\right] \tag{62b}$$

2). Additionally, the "external" gyroscopic moments are negligible. Hence, the moments and rotations can be dropped from equations (62) and one works with the reduced $M \times M$ receptance matrices in the *x* and *y* directions $\{\alpha_{ij}\}$, $\{\beta_{ij}\}$:

$$\mathbf{u}_{\mathbf{x}} = \{\alpha_{ij}\}\mathbf{f}_{\mathbf{x}},\ \mathbf{u}_{\mathbf{x}} = \left[\tilde{X}_1 \quad \cdots \quad \tilde{X}_M\right],\ \mathbf{f}_{\mathbf{x}} = \left[\tilde{F}_{x1} \quad \cdots \quad \tilde{F}_{xM}\right] \tag{63a}$$

$$\mathbf{u}_{\mathbf{y}} = \{\beta_{ij}\}\mathbf{f}_{\mathbf{y}},\ \mathbf{u}_{\mathbf{y}} = \left[\tilde{Y}_1 \quad \cdots \quad \tilde{Y}_M\right],\ \mathbf{f}_{\mathbf{y}} = \left[\tilde{F}_{y1} \quad \cdots \quad \tilde{F}_{yM}\right] \tag{63b}$$

The schematic diagram in Figure 3(a) is used to describe such a system. However, the damper symbol now denotes a general damper, linear, as well as non-linear, as do the symbols Q_{xi}, Q_{yi} $i = 1 \ldots n$ for the damping forces. The symbols P_{xk}, P_{yk}, $k = 1 \ldots p$, are used for the unbalance forces (equations (21)). As in section 3.1, $X_{Bi}(t)$, $Y_{Bi}(t)$ are defined as the displacements of *Bi* from its static equilibrium position. $X_{Ji}(t)$, $Y_{Ji}(t)$ are defined the displacements of *Ji* from the static equilibrium position of *Bi*. e_{0xi}, e_{0yi} denote the static

[1] If moments and rotations are not considered in the receptance matrix (as in equations (63)) this means that point *i* and/or point *j* is a node in the *r*th mode, from equation (55).
[2] *M* is the number of terminals (nodes) of the subsystem.

displacements of *Ji* from *Bi*. Hence, the *dynamic* displacements of *Ji i.e.* the displacements of *Ji* from *its own* equilibrium position are given by $X_{Ji}(t)-e_{0xi}$, $Y_{Ji}(t)-e_{0yi}$.

Considering the x response at a particular journal *Ja*, the general frequency domain equation can be written as:

$$\begin{aligned}\Im\{X_{Ja}(t)-e_{0xa}\}=&\{\alpha_{JaJ1}(\omega)-\alpha_{JaB1}(\omega)\}\Im\{Q_{x1}(t)\}+.....+\{\alpha_{JaJn}(\omega)-\alpha_{JaBn}(\omega)\}\Im\{Q_{xn}(t)\}\\&+\alpha_{JaU1}(\omega)\Im\{P_{x1}(t)\}+.....+\alpha_{JaUp}(\omega)\Im\{P_{xp}(t)\}\end{aligned}\tag{64}$$

where $\Im\{f(t)\}$ denotes the Fourier transform of $f(t)$.

Hence, transforming into the time domain:

$$\begin{aligned}X_{Ja}(t)-e_{0xa}=&\{h_{JaJ1}(t)-h_{JaB1}(t)\}*Q_{x1}(t)+.....+\{h_{JaJn}(t)-h_{JaBn}(t)\}*Q_{xn}(t)\\&+h_{JaU1}(t)*P_{x1}(t)+.....+h_{JaUp}(t)*P_{xp}(t)\end{aligned}\tag{65}$$

where '$*$' denotes the convolution operation and $h_{ij}(t)$ is the *impulsive receptance* [26] between i and j, defined as

$$h_{ij}(t)=\Im^{-1}\{\alpha_{ij}(\omega)\}\tag{66}$$

Now $\alpha_{ij}(\omega)=\sum_{r=1}^{q}\frac{A_{ij}^{r}}{\omega_{xr}^2-\omega^2}$ (equation (56))

Hence, by applying the inverse Fourier transform to each term in the series of equation (56) gives

$$h_{ij}(t)=\sum_{r=1}^{q}\frac{A_{ij}^{r}}{\omega_{xr}}\sin\omega_{xr}t\tag{67}$$

Note that $\frac{1}{\omega_{xr}}\sin\omega_{xr}t$ is the impulse response function of a single degree of freedom of unit mass and natural frequency ω_{xr}. Hence substitution of $h_{ij}(t)$ as given by equation (67) into equation (65) shows that the dynamic response $X_{Ja}(t)-e_{0xa}$ is the sum of the modal responses $X_{Ja}^{r}(t)$ of undamped single degree of freedom systems of unit mass, natural frequency ω_r each subjected to modal forces $\left(A_{JaJj}^{r}-A_{JaBj}^{r}\right)Q_{xj}$, $A_{JaUk}^{r}P_{xk}$. Hence one can write:

$$\ddot{X}_{Ja}^{r}+\omega_{xr}^2X_{Ja}^{r}=\sum_{j=1}^{n}\left(A_{JaJj}^{r}-A_{JaBj}^{r}\right)Q_{xj}\left(X_j,Y_j,\dot{X}_j,\dot{Y}_j\right)+\sum_{k=1}^{p}A_{JaUk}^{r}P_{xk}(t)\tag{68a}$$

for $r=1\ldots q$, where $X_{Ja}=e_{oxa}+\sum_{r=1}^{q}X_{Ja}^{r}$.

Similarly, for the y direction

$$\ddot{Y}_{Ja}^{r}+\omega_{yr}^{2}Y_{Ja}^{r}=\sum_{j=1}^{n}\left(B_{JaJj}^{r}-B_{JaBj}^{r}\right)Q_{yj}\left(X_{j},Y_{j},\dot{X}_{j},\dot{Y}_{j}\right)+\sum_{k=1}^{p}B_{JaUk}^{r}P_{yk}(t) \tag{68b}$$

for $r=1\ldots q$, where $Y_{Ja}=e_{oya}+\sum_{r=1}^{q}Y_{Ja}^{r}$.

For equation (68b) the required modal constants B_{ij}^{r} are obtained by decomposing the corresponding receptances:

$$\beta_{ij}(\omega)=\sum_{r=1}^{q}\frac{B_{ij}^{r}}{\omega_{yr}^{r}-\omega^{2}} \tag{69}$$

The next step is to bring each relative displacement X_j, Y_j $j=1\ldots n$ in terms of the modal displacements X_{Ja}^{r}, Y_{Ja}^{r}. Consider the x response at a general position P. The modal equations can be written as

$$\ddot{X}_{P}^{r}+\omega_{xr}^{2}X_{P}^{r}=\sum_{j=1}^{n}\left(A_{PJj}^{r}-A_{PBj}^{r}\right)Q_{xj}\left(X_{j},Y_{j},\dot{X}_{j},\dot{Y}_{j}\right)+\sum_{k=1}^{p}A_{PUk}^{r}P_{xk}(t) \tag{70}$$

where the dynamic response at P is $\sum_{r=1}^{q}X_{P}^{r}$.

Now from equation (55), it is evident that the following relationship between modal constants applies:

$$A_{ij}^{r}=\frac{A_{ia}^{r}A_{aj}^{r}}{A_{aa}^{r}} \tag{71}$$

This means that

$$A_{PJj}^{r}=\frac{A_{PJa}^{r}}{A_{JaJa}^{r}}A_{JaJj}^{r},\quad A_{PBj}^{r}=\frac{A_{PJa}^{r}}{A_{JaJa}^{r}}A_{JaBj}^{r},\quad A_{PUk}^{r}=\frac{A_{PJa}^{r}}{A_{JaJa}^{r}}A_{JaUk}^{r}$$

This means that the right hand side of equation (70) can be obtained by multiplying both sides of equation (68a) by A_{PJa}^{r}/A_{JaJa}^{r}. Hence it follows that

$$X_P^r = \frac{A_{PJa}^r}{A_{JaJa}^r} X_{Ja}^r \tag{72a}$$

Similarly,

$$Y_P^r = \frac{B_{PJa}^r}{B_{JaJa}^r} Y_{Ja}^r \tag{72b}$$

Therefore,

$$X_{Jj} = e_{oxj} + \sum_{r=1}^{q} X_{Jj}^r = e_{0xj} + \sum_{r=1}^{q} \frac{A_{JjJa}^r}{A_{JaJa}^r} X_{Ja}^r \tag{73}$$

and

$$X_{Bj} = \sum_{r=1}^{q} X_{Bj}^r = \sum_{r=1}^{q} \frac{A_{BjJa}^r}{A_{JaJa}^r} X_{Ja}^r \tag{74}$$

Hence,

$$X_j = X_{Jj} - X_{Bj} = e_{0xj} + \sum_{r=1}^{q} \left(\frac{A_{JjJa}^r}{A_{JaJa}^r} - \frac{A_{BjJa}^r}{A_{JaJa}^r} \right) X_{Ja}^r \tag{75a}$$

Similarly,

$$Y_j = e_{0yj} + \sum_{r=1}^{q} \left(\frac{B_{JjJa}^r}{B_{JaJa}^r} - \frac{B_{BjJa}^r}{B_{JaJa}^r} \right) Y_{Ja}^r \tag{75b}$$

Hence, finally, equations (68) are brought entirely in terms of X_{Ja}^r, Y_{Ja}^r. These are represented below:

$$\ddot{X}_{Ja}^r + \omega_{xr}^2 X_{Ja}^r = \sum_{j=1}^{n} \left(A_{JaJj}^r - A_{JaBj}^r \right) Q_{xj}\left(X_j, Y_j, \dot{X}_j, \dot{Y}_j \right) + \sum_{k=1}^{p} A_{JaUk}^r P_{xk}(t) \tag{76a}$$

$$\ddot{Y}_{Ja}^r + \omega_{yr}^2 Y_{Ja}^r = \sum_{j=1}^{n} \left(B_{JaJj}^r - B_{JaBj}^r \right) Q_{yj}\left(X_j, Y_j, \dot{X}_j, \dot{Y}_j \right) + \sum_{k=1}^{p} B_{JaUk}^r P_{yk}(t) \tag{76b}$$

for $r = 1 \ldots q$, where

$$X_j = e_{0xj} + \sum_{r=1}^{q} \left(\frac{A_{JjJa}^r}{A_{JaJa}^r} - \frac{A_{BjJa}^r}{A_{JaJa}^r} \right) X_{Ja}^r,\ Y_j = e_{0yj} + \sum_{r=1}^{q} \left(\frac{B_{JjJa}^r}{B_{JaJa}^r} - \frac{B_{BjJa}^r}{B_{JaJa}^r} \right) Y_{Ja}^r$$

$$\dot{X}_j = \sum_{r=1}^{q} \left(\frac{A_{JjJa}^r}{A_{JaJa}^r} - \frac{A_{BjJa}^r}{A_{JaJa}^r} \right) \dot{X}_{Ja}^r,\ \dot{Y}_j = \sum_{r=1}^{q} \left(\frac{B_{JjJa}^r}{B_{JaJa}^r} - \frac{B_{BjJa}^r}{B_{JaJa}^r} \right) \dot{Y}_{Ja}^r.$$

Q_{xj}, Q_{yj} are given by the appropriate expressions in section 2.1 for squeeze film dampers. For any linear damper they are given simply as $C_{xj}\dot{X}_j$, $C_{yj}\dot{Y}_j$ where C_{xj}, C_{yj} are the viscous damping coefficients. The unbalance forces $P_{xk}(t)$, $P_{yk}(t)$ are given by equations (21).

This set of $2q$ coupled[1] non-linear second order differential equations can be solved numerically by any technique suitable for stiff differential equations (see section 4.4). Once solved, the response at each squeeze film i, $i=1\ldots n$, is given by equations (73), (74):

$$X_{Ji}=e_{0xi}+\sum_{r=1}^{q}\frac{A^r_{JiJa}}{A^r_{JaJa}}X^r_{Ja},\ Y_{Ji}=e_{0yi}+\sum_{r=1}^{q}\frac{B^r_{JiJa}}{B^r_{JaJa}}Y^r_{Ja} \tag{73a,b}$$

$$X_{Bi}=\sum_{r=1}^{q}\frac{A^r_{BiJa}}{A^r_{JaJa}}X^r_{Ja},\ Y_{Bi}=\sum_{r=1}^{q}\frac{B^r_{BiJa}}{B^r_{JaJa}}Y^r_{Ja} \tag{74a,b}$$

The dynamic response of any other position P is obtained from equations (72)

$$X_P=\sum_{r=1}^{q}\frac{A^r_{PJa}}{A^r_{JaJa}}X^r_{Ja},\ Y_P=\sum_{r=1}^{q}\frac{B^r_{PJa}}{B^r_{JaJa}}Y^r_{Ja} \tag{77a,b}$$

Note that the chosen location Ja for the solution of the modal equations is arbitrary. In fact, it need not be a squeeze film journal at all and can be any point A on the structure. Hence the subscript Ja can be replaced by A in all the above equations. What is important is that A or Ja is not a node for some mode b within $r=1\ldots q$. This will make A^r_{JaJa} (or A^r_{AA}) $=0$ for $r=b$ in the denominator of all equations (72)-(75).

The general number n_{eq} of second order modal equations of motion for Q subsystems is given by

$$n_{eq}=Q\sum(\text{number of modes taken for each subsystem}) \tag{78}$$

Furthermore, if gyroscopic effects were to be taken into account, they are treated in a similar manner to the squeeze film forces. The appropriate rotational receptances contained in the matrices $\mathbf{R_{xz}}$, $\mathbf{R_{yz}}$ in equations (62) have to be decomposed. The gyroscopic moments G_{yD}, G_{xD} at a disc D of polar moment of inertia I_P in the xz, yz planes are given respectively by

$$G_{yD}=-I_P\Omega\theta_{xD} \tag{79a}$$

$$G_{xD}=I_P\Omega\theta_{yD} \tag{79b}$$

The rotations θ_{yD}, θ_{xD} in the xz, yz planes are then brought in terms of X^r_{Ja}, Y^r_{Ja} as for the relative displacements X_j, Y_j at the squeeze films in equation (75), using the relation (55).

[1] Through the squeeze film forces.

4.4 SOLUTION OF MODAL EQUATIONS OF MOTION

Defining

$$\mathbf{s} = \begin{bmatrix} t & X_{Ja}^1 & Y_{Ja}^1 & \cdots & X_{Ja}^q & Y_{Ja}^q & \dot{X}_{Ja}^1 & \dot{Y}_{Ja}^1 & \cdots & \dot{X}_{Ja}^q & \dot{Y}_{Ja}^q \end{bmatrix}^T$$

the system of $2q$ non-linear second order differential equations (76) can be written in standard form, as a system of $4q+1$ first order differential equations:

$$\dot{\mathbf{s}} = \mathbf{f}(\mathbf{s}) \tag{80}$$

The system given by equation (80) is then integrated numerically. Note that even for the simplest of problems involving squeeze films, problems of stiffness arise [15], [13]. A "stiff" system is one that requires ever decreasing time step sizes to maintain the local integration error within the desired tolerance. This makes Runge-Kutta methods unsuitable. A fast integration method (FIM) [13] was implemented successfully in [15] and can be used to solve the above systems. Moreover, *MATLAB®* (Version 5) has a function *ODE23S©* [21] that is specially designed to solve stiff systems. It works on roughly similar principles as the fast integration method, involving the computation of the Jacobian matrix at each time step. It was found to take roughly the same time as FIM to integrate over a given number of revolutions. Most of the time domain simulations presented in this report used this function. A factor which aggravates stiffness is the number of equations to be solved, determined by the number of modes q taken in the receptance decomposition. According to Petyt [23], the larger the system to be solved, the smaller the time step size required for a given tolerance. Hence the number of modes taken, q has to be carefully considered. This should be the minimum number to ensure a decent fit over a carefully chosen frequency range. The quality of fit is checked by plotting out the approximate receptance reconstructed from q modes, equation (56), and the exact receptance over the chosen frequency range. Because the problem is non-linear, the chosen frequency range has to cover a minimum number of harmonics of the top rotational speed.

Note that in harmonic balance analysis the number of non-linear algebraic equations to be solved increases directly with the number of non-linear elements (see end of section 3.3). On the other hand in time domain analysis the number of non-linear differential equations to be solved, given by (78) is independent of the number of non-linear elements. Hence, for problems involving several dampers, when harmonic balance is prone to convergence problems, time domain analysis provides a useful backup. Note finally that in the harmonic balance analysis, one works with *exact* receptances (covering the infinite modal series) but with responses having a finite number of harmonics. In the time domain analysis, approximate receptances (covering a finite modal series) are used but the computed response has an infinite frequency spectrum. It should be noted however that that part of the spectrum outside the fitting frequency range should be not be considered and should be negligible for a good fit.

CHAPTER 5

APPLICATION TO SPECIFIC CONFIGURATIONS

In this chapter the frequency and time domain equations presented in chapters 3, 4 are applied to two configurations A, B, each incorporating one squeeze film.

5.1 DESCRIPTION OF CONFIGURATIONS

In both configurations A, B gyroscopic effects are neglected and the squeeze film is taken to be the only source of damping. Hence the "linear system" as used in the harmonic balance analysis context (section 3.1) will be identical to that used in the time domain analysis context (section 4.1). This means that the receptances will be real and obey the reciprocity principle for both types of analysis. There is also no *x-y* cross-coupling.

5.1.1 Configuration A: flexible shaft in rigidly housed SFD

In configuration A, a flexible shaft is supported by a self-aligning bearing H at one end and by a rigidly housed squeeze film damper at J (Figure 5). An unbalance disc is carried on the overhung portion at U. The self-aligning bearing H is modelled as a fixed pivot. A retainer spring can be optionally placed in parallel with the squeeze film, leading to two alternative schematic configurations: A1 (with retainer spring, Figure 5(a)) and A2 (without retainer spring, Figure 5(b)). As illustrated in Figure 5(a), in configuration A1 the retainer spring is not grounded at the rigid bearing housing B but at a different location F. This permits the static eccentricities (misalignments) ε_{0xJ}, ε_{0yJ} $(=e_{0xJ}/c,\ e_{0yJ}/c,\ c=\text{radial clearance of damper})$ of the journal from the bearing housing to be altered by moving the bearing housing horizontally and vertically respectively. In this work $\varepsilon_{0xJ}=0$ and only ε_{0yJ} is varied. The equations that describe configuration A1 apply both for the retainer spring fully supporting the static load, $\varepsilon_{0yJ}>-1$, and for the retainer spring partially supporting the static load, $\varepsilon_{0yJ}\le -1$[1].

5.1.2 Configuration B: flexible shaft in flexibly housed, unsupported SFD

Configuration B is illustrated schematically in Figure 6. A rotor is supported by a self-aligning bearing at one end H and by a flexibly housed squeeze film damper at J. No retainer spring is placed in parallel with the damper. Instead the damper is in series with the flexibility of the bearing housing B. The self-aligning bearing H is again modelled as a fixed pivot. This configuration was studied experimentally and analytically by Dogan [27] for low speeds (rigid

[1] Note that ε_{0xJ}, ε_{0yJ} refer to the static displacements of J from B with the full static load taken by the retainer spring. With J resting at the bottom of the clearance circle, this static position lies at some point outside the clearance circle ($\varepsilon_{0yJ}<-1$).

rotor). It has been recently studied experimentally by Levesley *et al* [28] for high speeds (flexible rotor). Note that in the linear system, the rotor is uncoupled from the bearing housing. The absolute displacements of J and B are measured from the static equilibrium position of B *prior* to loading it with the static load from the rotor.

For both configurations A2 and B it is assumed that the distributed static load can be replaced by a concentrated load at J equal to W, the equivalent static load at the squeeze film, given by:

$$W = \frac{\sum M_x}{l_J} \tag{81}$$

where $\sum M_x$= sum of anti-clockwise moments of gravity forces about H and l_J = distance of SFD from pivot H.

5.2 HARMONIC BALANCE EQUATIONS

In this section the symbol ω refers to the fundamental frequency of the limit cycle.

5.2.1 Configuration A (Figure 5)

For configuration A, equations (42), with $n=1$ (number of squeeze films), $p=1$ (number of unbalance forces), rigid bearing housing ($\mathbf{v}_{xB}, \mathbf{v}_{yB} = \mathbf{0}$), no x-y cross-coupling ($\{\alpha\beta_{ij}\}$, $\{\beta\alpha_{ij}\} = \mathbf{0}$) collapse to:

$$\left\{\begin{bmatrix}\mathbf{M}_x & \mathbf{0}\\ \mathbf{0} & \mathbf{M}_y\end{bmatrix} - \mathbf{I}_{2(2m+1)}\right\}\begin{bmatrix}\mathbf{v}_x\\ \mathbf{v}_y\end{bmatrix} = \begin{bmatrix}\mathbf{f}_x\\ \mathbf{f}_y\end{bmatrix} \tag{82}$$

where

$$\mathbf{v}_x = \begin{bmatrix}X_{0J} & a^1_{XJ} & b^1_{XJ} & \cdots & a^m_{XJ} & b^m_{XJ}\end{bmatrix}^T$$
$$\mathbf{v}_y = \begin{bmatrix}Y_{0J} & a^1_{YJ} & b^1_{YJ} & \cdots & a^m_{YJ} & b^m_{YJ}\end{bmatrix}^T$$

For configuration A1 (retainer spring in place) (Figure 5(a)):

From equations (A6), (A9), (A10a), (A13a), (A14a), (A15a), Appendix A, for real receptances ($\{\alpha\alpha^I_{ij}\}$, $\{\beta\beta^I_{ij}\} = \mathbf{0}$)

$$\mathbf{M_x} = \begin{bmatrix} k_{xx}\alpha_{JJ}(0) & & & & & \\ & k_{xx}\alpha_{JJ}(\omega) & \omega c_{xx}\alpha_{JJ}(\omega) & & & \\ & -\omega c_{xx}\alpha_{JJ}(\omega) & k_{xx}\alpha_{JJ}(\omega) & & & \\ & & & \ddots & & \\ & & & & k_{xx}\alpha_{JJ}(m\omega) & m\omega c_{xx}\alpha_{JJ}(m\omega) \\ & & & & -m\omega c_{xx}\alpha_{JJ}(m\omega) & k_{xx}\alpha_{JJ}(m\omega) \end{bmatrix} \tag{83a}$$

$$\mathbf{M_y} = \begin{bmatrix} k_{yy}\beta_{JJ}(0) & & & & & \\ & k_{yy}\beta_{JJ}(\omega) & \omega c_{yy}\beta_{JJ}(\omega) & & & \\ & -\omega c_{yy}\beta_{JJ}(\omega) & k_{yy}\beta_{JJ}(\omega) & & & \\ & & & \ddots & & \\ & & & & k_{yy}\beta_{JJ}(m\omega) & m\omega c_{yy}\beta_{JJ}(m\omega) \\ & & & & -m\omega c_{yy}\beta_{JJ}(m\omega) & k_{yy}\beta_{JJ}(m\omega) \end{bmatrix} \tag{83b}$$

From equations (A16), (A19), (A20a), (A23a), (A24a), (A25a) in Appendix A

$$\mathbf{f_x} = -\begin{bmatrix} e_{0xJ} + \alpha_{JJ}(0)Q_{x0} \\ \alpha_{JJ}(\omega)A_x^1 \\ \alpha_{JJ}(\omega)B_x^1 + \delta_{N1}\alpha_{JU}(\omega)U\Omega^2 \\ \vdots \\ \vdots \\ \alpha_{JJ}(m\omega)A_x^m \\ \alpha_{JJ}(m\omega)B_x^m + \delta_{Nm}\alpha_{JU}(m\omega)U\Omega^2 \end{bmatrix}, \quad \mathbf{f_y} = -\begin{bmatrix} e_{0yJ} + \beta_{JJ}(0)Q_{y0} \\ \beta_{JJ}(\omega)A_y^1 - \delta_{N1}\beta_{JU}(\omega)U\Omega^2 \\ \beta_{JJ}(\omega)B_y^1 \\ \vdots \\ \vdots \\ \beta_{JJ}(m\omega)A_y^m - \delta_{Nm}\beta_{JU}(m\omega)U\Omega^2 \\ \beta_{JJ}(m\omega)B_y^m \end{bmatrix} \tag{84a,b}$$

The phase angle ϕ of the unbalance is taken as zero. Also, recall that δ_{Ns} $(s = 1 \ldots m)$ is non-zero only for the synchronous harmonic ($s = N$, where the fundamental frequency of vibration $\omega = \Omega/N$). On the other hand, the constants A_x^s, B_x^s, A_y^s, B_y^s will be zero for the synchronous harmonic, $s = N$). The receptances α_{ij}, β_{ij} in the x and y directions respectively are for a beam pinned at H and sprung at J. $\alpha_{ij} = \beta_{ij}$ if retainer spring is isotropic.

The mean and harmonic components of the dynamic response X_P, Y_P at a general position P (equations (52)) are given by equations (53) which reduce to

$$X_{0P} = \alpha_{PJ}(0)\overline{Q}_x \tag{85a}$$
$$a^s_{XP} = \alpha_{PJ}(s\omega)p^s_x \tag{86a}$$
$$b^s_{XP} = \alpha_{PJ}(s\omega)q^s_x + \delta_{Ns}\alpha_{PU}(s\omega)U\Omega^2 \tag{87a}$$

$$Y_{0P} = \beta_{PJ}(0)\overline{Q}_y \tag{85b}$$
$$a^s_{YP} = \beta_{PJ}(s\omega)p^s_y - \delta_{Ns}\beta_{PU}(s\omega)U\Omega^2 \tag{86b}$$
$$b^s_{YP} = \beta_{PJ}(s\omega)q^s_y \tag{87b}$$

For configuration A2 (no retainer spring) (Figure 5(b))**:**

The linear system now consists of a pinned-free beam, which is degenerate. The linear system is capable of rigid body motion: rotation about H. Hence $\alpha_{JJ}(0) \to \infty$. Hence, as explained in section 3.6, the zero frequency equations need modification. This means that the element in the first row, first column of $\mathbf{M_x}$, $\mathbf{M_y}$ as given by equations (83a,b) and the first element in $\mathbf{f_x}$, $\mathbf{f_y}$ as given by equations (84a,b), need alteration. As explained in section 3.6, the zero frequency equations become equilibrium equations. Recall the Fourier expansion for the squeeze film forces, equation (28):

$$Q_x = \overline{Q}_x + \sum_{s=1}^{m}\left(p^s_x \cos s\omega t + q^s_x \sin s\omega t\right)$$
$$Q_y = \overline{Q}_y + \sum_{s=1}^{m}\left(p^s_y \cos s\omega t + q^s_y \sin s\omega t\right)$$

Using the principle of equilibrium at zero frequency and taking moments about H:

$$\overline{Q}_x = 0 \tag{88a}$$
$$\overline{Q}_y = W \tag{88b}$$

Now, from equations (33a,b)

$$\overline{Q}_x = Q_{x0} + k_{xx}X_0$$
$$\overline{Q}_y = Q_{y0} + k_{yy}Y_0$$

Hence, equations (88) become:

$$k_{xx}X_0 = -Q_{x0} \tag{89a}$$
$$k_{yy}Y_0 = -Q_{y0} + W \tag{89b}$$

Equations (89) are now the zero frequency equations and the specified elements in $\mathbf{M_x}$, $\mathbf{M_y}$, $\mathbf{f_x}$, $\mathbf{f_y}$ can now be amended. Hence the matrices and vectors $\mathbf{M_x}$, $\mathbf{M_y}$, $\mathbf{f_x}$, $\mathbf{f_y}$ in equation (82) are now given by:

$$\mathbf{M_x} = \begin{bmatrix} k_{xx}+1 & & & & & \\ & k_{xx}\alpha_{JJ}(\omega) & \omega c_{xx}\alpha_{JJ}(\omega) & & & \\ & -\omega c_{xx}\alpha_{JJ}(\omega) & k_{xx}\alpha_{JJ}(\omega) & & & \\ & & & \ddots & & \\ & & & & \ddots & \\ & & & & k_{xx}\alpha_{JJ}(m\omega) & m\omega c_{xx}\alpha_{JJ}(m\omega) \\ & & & & -m\omega c_{xx}\alpha_{JJ}(m\omega) & k_{xx}\alpha_{JJ}(m\omega) \end{bmatrix} \tag{90a}$$

$$\mathbf{M_y} = \begin{bmatrix} k_{yy}+1 & & & & & \\ & k_{yy}\beta_{JJ}(\omega) & \omega c_{yy}\beta_{JJ}(\omega) & & & \\ & -\omega c_{yy}\beta_{JJ}(\omega) & k_{yy}\beta_{JJ}(\omega) & & & \\ & & & \ddots & & \\ & & & & \ddots & \\ & & & & k_{yy}\beta_{JJ}(m\omega) & m\omega c_{yy}\beta_{JJ}(m\omega) \\ & & & & -m\omega c_{yy}\beta_{JJ}(m\omega) & k_{yy}\beta_{JJ}(m\omega) \end{bmatrix} \tag{90b}$$

$$\mathbf{f_x} = -\begin{bmatrix} Q_{x0} \\ \alpha_{JJ}(\omega)A_x^1 \\ \alpha_{JJ}(\omega)B_x^1 + \delta_{N1}\alpha_{JU}(\omega)U\Omega^2 \\ \vdots \\ \vdots \\ \alpha_{JJ}(m\omega)A_x^m \\ \alpha_{JJ}(m\omega)B_x^m + \delta_{Nm}\alpha_{JU}(m\omega)U\Omega^2 \end{bmatrix}, \quad \mathbf{f_y} = -\begin{bmatrix} Q_{y0} - W \\ \beta_{JJ}(\omega)A_y^1 - \delta_{N1}\beta_{JU}(\omega)U\Omega^2 \\ \beta_{JJ}(\omega)B_y^1 \\ \vdots \\ \vdots \\ \beta_{JJ}(m\omega)A_y^m - \delta_{Nm}\beta_{JU}(m\omega)U\Omega^2 \\ \beta_{JJ}(m\omega)B_y^m \end{bmatrix} \tag{91a,b}$$

The receptances α_{ij}, β_{ij} in the x and y directions respectively now refer to a pinned-free beam. $\alpha_{ij} = \beta_{ij}$.

The harmonic components of the response X_P, Y_P at a general position P are given by equations (86a,b), (87a,b). However, the mean components, given by equations (85a,b), need modification.

Since the distributed static load has been replaced by a concentrated load at J, the zero frequency forces acting on the rotor produce no deformation of the rotor. Hence

$$X_{0P} = \frac{l_P}{l_J} X_{0J}, \; Y_{0P} = \frac{l_P}{l_J} Y_{0J} \tag{92a,b}$$

where l_J is the distance of P from the pivot H. Hence, X_P, Y_P are measured from the line joining H to the bearing centre.

5.2.2 Configuration B (Figure 6)

For configuration B, equations (42), for $n=1$ (number of squeeze films), $p=1$ (number of unbalance forces), flexible bearing housings, no x-y cross-coupling ($\{\alpha\beta_{ij}\}$, $\{\beta\alpha_{ij}\}=\mathbf{0}$), are of the form:

$$\left\{\begin{bmatrix}\mathbf{M_x} & \mathbf{0}\\ \mathbf{0} & \mathbf{M_y}\end{bmatrix} - \mathbf{I}_{4(2m+1)}\right\}\begin{bmatrix}\mathbf{v_x}\\ \mathbf{v_y}\end{bmatrix} = \begin{bmatrix}\mathbf{f_x}\\ \mathbf{f_y}\end{bmatrix} \tag{93}$$

where:

$$\mathbf{v_x} = \begin{bmatrix}\mathbf{v_{xJ}}\\ \mathbf{v_{xB}}\end{bmatrix}, \; \mathbf{v_y} = \begin{bmatrix}\mathbf{v_{yJ}}\\ \mathbf{v_{yB}}\end{bmatrix}$$

$$\mathbf{v_{xJ}} = \begin{bmatrix}X_{0J} & a^1_{XJ} & b^1_{XJ} & \cdots & a^m_{XJ} & b^m_{XJ}\end{bmatrix}^T, \; \mathbf{v_{xB}} = \begin{bmatrix}X_{0B} & a^1_{XB} & b^1_{XB} & \cdots & a^m_{XB} & b^m_{XB}\end{bmatrix}^T$$
$$\mathbf{v_{yJ}} = \begin{bmatrix}Y_{0J} & a^1_{YJ} & b^1_{YJ} & \cdots & a^m_{YJ} & b^m_{YJ}\end{bmatrix}^T, \; \mathbf{v_{yB}} = \begin{bmatrix}Y_{0B} & a^1_{YB} & b^1_{YB} & \cdots & a^m_{YB} & b^m_{YB}\end{bmatrix}^T$$

From equations (A6), (A9):

$$\mathbf{M_x} = \begin{bmatrix}\mathbf{M_{xJ}} & -\mathbf{M_{xJ}}\\ \mathbf{M_{xB}} & -\mathbf{M_{xB}}\end{bmatrix}, \; \mathbf{M_y} = \begin{bmatrix}\mathbf{M_{yJ}} & -\mathbf{M_{yJ}}\\ \mathbf{M_{yB}} & -\mathbf{M_{yB}}\end{bmatrix}$$

From equations (A16), (A19):

$$\mathbf{f_x} = \begin{bmatrix}\mathbf{f_{xJ}}\\ \mathbf{f_{xB}}\end{bmatrix}, \; \mathbf{f_y} = \begin{bmatrix}\mathbf{f_{yJ}}\\ \mathbf{f_{yB}}\end{bmatrix}$$

$\mathbf{M_{xJ}}$, $\mathbf{M_{xB}}$, $\mathbf{M_{yJ}}$, $\mathbf{M_{yB}}$, $\mathbf{f_{xJ}}$, $\mathbf{f_{xB}}$, $\mathbf{f_{yJ}}$, $\mathbf{f_{xB}}$ are nominally respectively given by equations (A14a), (A14b), (A15a), (A15b), (A24a), (A24b), (A25a), (A25b) in Appendix A, but taking note that the receptances are real ($\{\alpha\alpha^1_{ij}\}$, $\{\beta\beta^1_{ij}\}=\mathbf{0}$) and that the receptances connecting J and B and

those connecting U and B are zero (due to the uncoupling of the rotor and foundation subsystems in the linear system). Since the rotor subsystem is degenerate, $\mathbf{M_{xJ}}$, $\mathbf{M_{yJ}}$, $\mathbf{f_{xJ}}$, $\mathbf{f_{yJ}}$ need correction. Since the rotor subsystem is the same configuration as A2 then $\mathbf{M_{xJ}}$, $\mathbf{M_{yJ}}$, $\mathbf{f_{xJ}}$, $\mathbf{f_{yJ}}$ are given by equations (90a,b), (91a,b). Hence....

$$\mathbf{M_{xJ}} = \begin{bmatrix} k_{xx}+1 & & & & & \\ & k_{xx}\alpha_{JJ}(\omega) & \omega c_{xx}\alpha_{JJ}(\omega) & & & \\ & -\omega c_{xx}\alpha_{JJ}(\omega) & k_{xx}\alpha_{JJ}(\omega) & & & \\ & & & \ddots & & \\ & & & & k_{xx}\alpha_{JJ}(m\omega) & m\omega c_{xx}\alpha_{JJ}(m\omega) \\ & & & & -m\omega c_{xx}\alpha_{JJ}(m\omega) & k_{xx}\alpha_{JJ}(m\omega) \end{bmatrix} \tag{94a}$$

$$\mathbf{M_{yJ}} = \begin{bmatrix} k_{yy}+1 & & & & & \\ & k_{yy}\beta_{JJ}(\omega) & \omega c_{yy}\beta_{JJ}(\omega) & & & \\ & -\omega c_{yy}\beta_{JJ}(\omega) & k_{yy}\beta_{JJ}(\omega) & & & \\ & & & \ddots & & \\ & & & & k_{yy}\beta_{JJ}(m\omega) & m\omega c_{yy}\beta_{JJ}(m\omega) \\ & & & & -m\omega c_{yy}\beta_{JJ}(m\omega) & k_{yy}\beta_{JJ}(m\omega) \end{bmatrix} \tag{94b}$$

$$\mathbf{f_{xJ}} = -\begin{bmatrix} Q_{x0} \\ \alpha_{JJ}(\omega)A_x^1 \\ \alpha_{JJ}(\omega)B_x^1 + \delta_{N1}\alpha_{JU}(\omega)U\Omega^2 \\ \vdots \\ \vdots \\ \alpha_{JJ}(m\omega)A_x^m \\ \alpha_{JJ}(m\omega)B_x^m + \delta_{N1}\alpha_{JU}(m\omega)U\Omega^2 \end{bmatrix}, \quad \mathbf{f_{yJ}} = -\begin{bmatrix} Q_{y0} - W \\ \beta_{JJ}(\omega)A_y^1 - \delta_{N1}\beta_{JU}(\omega)U\Omega^2 \\ \beta_{JJ}(\omega)B_y^1 \\ \vdots \\ \vdots \\ \beta_{JJ}(m\omega)A_y^m - \delta_{Nm}\beta_{JU}(m\omega)U\Omega^2 \\ \beta_{JJ}(m\omega)B_y^m \end{bmatrix} \tag{95a,b}$$

From equations (A14b), (A15b) in Appendix A

$$\mathbf{M_{xB}} = -\begin{bmatrix} k_{xx}\alpha_{BB}(0) & & & & & \\ & k_{xx}\alpha_{BB}(\omega) & \omega c_{xx}\alpha_{BB}(\omega) & & & \\ & -\omega c_{xx}\alpha_{BB}(\omega) & k_{xx}\alpha_{BB}(\omega) & & & \\ & & & \ddots & & \\ & & & & k_{xx}\alpha_{BB}(m\omega) & m\omega c_{xx}\alpha_{BB}(m\omega) \\ & & & & -m\omega c_{xx}\alpha_{BB}(m\omega) & k_{xx}\alpha_{BB}(m\omega) \end{bmatrix} \tag{96a}$$

$$\mathbf{M_{yB}} = \begin{bmatrix} k_{yy}\beta_{BB}(0) & & & & & \\ & k_{yy}\beta_{BB}(\omega) & \omega c_{yy}\beta_{BB}(\omega) & & & \\ & -\omega c_{yy}\beta_{BB}(\omega) & k_{yy}\beta_{BB}(\omega) & & & \\ & & & \ddots & & \\ & & & & k_{yy}\beta_{BB}(m\omega) & m\omega c_{yy}\beta_{BB}(m\omega) \\ & & & & -m\omega c_{yy}\beta_{BB}(m\omega) & k_{yy}\beta_{BB}(m\omega) \end{bmatrix} \tag{96b}$$

From equations (A24b), (A25b) in Appendix A

$$\mathbf{f_{xB}} = \begin{bmatrix} \alpha_{BB}(0)Q_{x0} \\ \alpha_{BB}(\omega)A_x^1 \\ \alpha_{BB}(\omega)B_x^1 \\ \vdots \\ \vdots \\ \alpha_{BB}(m\omega)A_x^m \\ \alpha_{BB}(m\omega)B_x^m \end{bmatrix}, \quad \mathbf{f_{yB}} = \begin{bmatrix} \beta_{BB}(0)Q_{y0} \\ \beta_{BB}(\omega)A_y^1 \\ \beta_{BB}(\omega)B_y^1 \\ \vdots \\ \vdots \\ \beta_{BB}(m\omega)A_y^m \\ \beta_{BB}(m\omega)B_y^m \end{bmatrix} \tag{97a,b}$$

The response at a general position P on the rotor, X_P, Y_P, is given by equations (86a,b), (87a,b) for the harmonic components and equations (92a,b) for the mean components. X_P, Y_P are measured from the line joining H to the static equilibrium position of the bearing centre prior to loading it with *W*.

5.3 TIME DOMAIN EQUATIONS

These equations are presented in terms of the non-dimensional variables

$$\tau = \Omega t\,,\ x_J^r = X_J^r/c\,,\ x_B^r = X_B^r/c\,,\ y_J^r = Y_J^r/c\,,\ y_B^r = Y_B^r/c\,,\ d(\ )/d\tau = (\ )'$$

In this section the symbol ω refers to a general frequency.

5.3.1 Configuration A (Figure 5)

In this configuration $Q = 2$ subsystems are considered: rotor in xz and yz planes. Hence for both configurations A1 and A2 the equations are obtained from equations (76) but with the addition of the static load W for A2.

For configuration A1 (retainer spring) (Figure 5(a)):

$$x_J''^r + \frac{\omega_{xr}^2}{\Omega^2} x_J^r = \frac{1}{c\Omega^2} A_{JJ}^r Q_x(x, y, x', y') + \frac{1}{c} A_{JU}^r U \sin\tau \tag{98a}$$

$$y_J''^r + \frac{\omega_{yr}^2}{\Omega^2} y_J^r = \frac{1}{c\Omega^2} B_{JJ}^r Q_y(x, y, x', y') - \frac{1}{c} B_{JU}^r U \cos\tau\,, \quad r = 1 \ldots q \tag{98b}$$

$$x = x_J = \varepsilon_{0x} + \sum_{r=1}^{q} x_J^r\,,\ y = y_J = \varepsilon_{0y} + \sum_{r=1}^{q} y_J^r\,,\ x' = \sum_{r=1}^{q} x_J'^r\,,\ y' = \sum_{r=1}^{q} y_J'^r \tag{99a,b,c,d}$$

The *dynamic* response of any point P on the rotor (*i.e.* displacement of P from its own equilibrium position) is given by:

$$x_P = \sum_{r=1}^{q} \frac{A_{PJ}^r}{A_{JJ}^r} x_J^r\,, \qquad y_P = \sum_{r=1}^{q} \frac{B_{PJ}^r}{B_{JJ}^r} y_J^r \tag{100a,b}$$

For configuration A2 (no retainer spring) (Figure 5(b)):

$$x_J''^r + \frac{\omega_{xr}^2}{\Omega^2} x_J^r = \frac{1}{c\Omega^2} A_{JJ}^r Q_x(x, y, x', y') + \frac{1}{c} A_{JU}^r U \sin\tau \tag{101a}$$

$$y_J''^r + \frac{\omega_{yr}^2}{\Omega^2} y_J^r = \frac{1}{c\Omega^2} B_{JJ}^r \{Q_y(x, y, x', y') - W\} - \frac{1}{c} B_{JU}^r U \cos\tau\,, \quad r = 1 \ldots q \tag{101b}$$

$$x = x_J = \sum_{r=1}^{q} x_J^r\,,\ y = y_J = \sum_{r=1}^{q} y_J^r\,,\ x' = x_J' = \sum_{r=1}^{q} x_J'^r\,,\ y' = y_J' = \sum_{r=1}^{q} y_J'^r \tag{102a,b,c,d}$$

The response of any point P on the rotor is given by:

$$x_P = \sum_{r=1}^{q} \frac{A_{PJ}^r}{A_{JJ}^r} x_J^r, \quad y_P = \sum_{r=1}^{q} \frac{B_{PJ}^r}{B_{JJ}^r} y_J^r \tag{103a,b}$$

The required modal constants are given by decomposing the corresponding receptances as in section 4.2:

$$\alpha_{ij}(\omega) = \sum_{r=1}^{q} \frac{A_{ij}^r}{\omega_{xr}^2 - \omega^2}, \quad \beta_{ij}(\omega) = \sum_{r=1}^{q} \frac{B_{ij}^r}{\omega_{yr}^2 - \omega^2} \tag{104a,b}$$

Note that for case A2 $\alpha_{ij}(\omega) = \beta_{ij}(\omega)$ hence $\omega_{xr} = \omega_{yr}$ and $A_{ij}^r = B_{ij}^r$. This will also be the case for A1 if the retainer spring is isotropic. Note also, in the case A2, ω_{x1}, $\omega_{y1} = 0$ since the first mode is rigid body rotation about the pivot H. Hence, for $r = 1$, equations (101a,b) are the rigid body equations with $1/A_{JJ}^1$ and $1/A_{JU}^1$ being respectively equal to the equivalent rigid body mass at J and the equivalent rigid body mass at U referred to J. For this reason, the response at any arbitrary position P, given by equations (103a,b), is measured from the line joining H to the bearing housing centre, as for the harmonic balance equations (92a,b).

5.3.2 Configuration B (Figure 6)

In configuration B $Q = 4$ uncoupled subsystems are considered: rotor in *xz* and *yz* planes and support in *xz* and *yz* planes. q_R modes are taken for the rotor subsystem in both the *xz* and *yz* planes. q_F modes are taken for the support subsystem in both the *xz* and *yz* planes. If the support is modelled as a mass on a spring, $q_F = 1$. Accordingly, the equations are

$$x_J^{\prime\prime r} + \frac{\omega_{Rxr}^2}{\Omega^2} x_J^r = \frac{1}{c\Omega^2} A_{JJ}^r Q_x(x, y, x', y') + \frac{1}{c} A_{JU}^r U \sin\tau \tag{105a}$$

$$y_J^{\prime\prime r} + \frac{\omega_{Ryr}^2}{\Omega^2} y_J^r = \frac{1}{c\Omega^2} B_{JJ}^r \{Q_y(x, y, x', y') - W\} - \frac{1}{c} B_{JU}^r U \cos\tau, \quad r = 1 \ldots q_R \tag{105b}$$

$$x_B^{\prime\prime s} + \frac{\omega_{Fxs}^2}{\Omega^2} x_B^s = -\frac{1}{c\Omega^2} A_{BB}^s Q_x(x, y, x', y') \tag{105c}$$

$$y_B^{\prime\prime s} + \frac{\omega_{Fys}^2}{\Omega^2} y_B^s = -\frac{1}{c\Omega^2} B_{BB}^s Q_y(x, y, x', y'), \quad s = 1 \ldots q_F \tag{105d}$$

$$x_J = \sum_{r=1}^{q_R} x_J^r \quad y_J = \sum_{r=1}^{q_R} y_J^r \quad x_B = \sum_{s=1}^{q_F} x_B^s \quad y_B = \sum_{s=1}^{q_F} y_B^s \tag{106a,b,c,d}$$

$$x_J' = \sum_{r=1}^{q_R} x_J^{\prime r} \quad y_J' = \sum_{r=1}^{q_R} y_J^{\prime r} \quad x_B' = \sum_{s=1}^{q_F} x_B^{\prime s} \quad y_B' = \sum_{s=1}^{q_F} y_B^{\prime s} \tag{106e,f,g,h}$$

$$x = x_J - x_B, \quad y = y_J - y_B, \quad x' = x_J' - x_B', \quad y' = y_J' - y_B' \tag{106i,j,k,l}$$

For points i, j on the rotor the required modal constants are determined from the modal decomposition of the corresponding receptances:

$$\alpha_{ij}(\omega)=\sum_{r=1}^{q_R}\frac{A_{ij}^r}{\omega_{Rxr}^2-\omega^2},\quad \beta_{ij}(\omega)=\sum_{r=1}^{q_R}\frac{B_{ij}^r}{\omega_{Ryr}^2-\omega^2} \tag{107a,b}$$

For the bearing housing only

$$\alpha_{BB}(\omega)=\sum_{s=1}^{q_F}\frac{A_{BB}^s}{\omega_{Fxs}^2-\omega^2},\quad \beta_{BB}(\omega)=\sum_{s=1}^{q_F}\frac{B_{ij}^s}{\omega_{Fys}^2-\omega^2} \tag{108a,b}$$

Note that for the rotor $\alpha_{ij}(\omega)=\beta_{ij}(\omega)$ hence $\omega_{Rxr}=\omega_{Ryr}$ and $A_{ij}^r=B_{ij}^r$. This will also be true for the bearing housing if the support stiffness is isotropic. The response x_P, y_P at a general position P on the rotor is given by equation (103a,b). x_P, y_P are measured from the line joining H to the static equilibrium position of B prior to loading it with the rotor.

5.4 SOLUTION OF EQUATIONS

The harmonic balance equations were solved according to the iterative scheme in section 3.4.1.

For the time domain equations, each of the three sets (98), (101), (105) was expressed as

$$\mathbf{s}'=\mathbf{f}(\mathbf{s}) \tag{109}$$

and solved as explained in section 4.4. For equations (98) or equations (101) (configuration A)

$$\mathbf{s}=\begin{bmatrix}\tau & x_J^1 & y_J^1 & \dots & x_J^q & y_J^q & x_J'^1 & y_J'^1 & \dots & x_J'^q & y_J'^q\end{bmatrix}^T$$

For equations (105) (configuration B)

$$\mathbf{s}=\begin{bmatrix}\tau & x_J^1 & y_J^1 & \dots & x_J^{q_R} & y_J^{q_R} & x_B^1 & y_B^1 & \dots & x_B^{q_F} & y_B^{q_F} \\ & x_J'^1 & y_J'^1 & \dots & x_J'^{q_R} & y_J'^{q_R} & x_B'^1 & y_B'^1 & \dots & x_B'^{q_F} & y_B'^{q_F}\end{bmatrix}^T.$$

The tolerance on the magnitude of the local integration error in $\mathbf{s}$ was 0.1% of the element of smallest magnitude in $\mathbf{s}$.

Software was developed in *MATLAB*® (Version 5) to solve the equations presented in this chapter.

CHAPTER 6

STABILITY OF HARMONIC BALANCE SOLUTIONS

Having established both the harmonic balance and time domain equations for a squeeze film damped rotor dynamic system one can address the issue of stability of the computed harmonic balance solutions. As explained in the Introduction, chapter 1, these solutions are periodic, equilibrium solutions *i.e.* limit cycles in state space, which can be either stable (attractors) or unstable (repellors), depending on the operating conditions. Limit cycles that are repellors are in unstable equilibrium and hence unattainable in practice due to inevitable minor fluctuations in the operating conditions. Hence, any harmonic balance solution technique must be accompanied by some technique to check for stability in order to determine which solutions are reliable predictions. Additionally, the stability test method should be as efficient as possible in order not to detract from the computational efficiency gained in using the harmonic balance method. Two main methods I, II are applied in this report to test for stability of a limit cycle. Both methods assume that the computed limit cycle is a reasonably accurate approximation to the exact limit cycle.

6.1 METHOD I – Direct integration from equilibrium initial conditions

This is the most basic method. One takes the state variables of any one point on the computed limit cycle and uses them as initial conditions in the solution of the time domain equations. The time domain equations are then integrated with these initial conditions over a limit number of rotor revolutions (say 10). If the computed trajectory remains on the limit cycle then that cycle is is stable (attractor). If it diverges from it, it is unstable (repellor). In the latter case, continuation of the solution for a further number of revolutions will reveal to what attractor the trajectory will settle down to[1].

One has to remember however that the time domain equations are formulated in terms of *modal* state variables x_J^r, y_J^r, $x_J'^r$, $y_J'^r$ in equations (98). The harmonic balance solutions on the other hand give the actual *full* state variables x_J, y_J, x_J', y_J' (equations (99), $= X_J/c$, Y_J/c, $\dot{X}_J/(\Omega c)$, $\dot{Y}_J/(\Omega c)$ in equations (82)). Hence, in order to extract the initial conditions to the time domain equations from an instantaneous point on the limit cycle one has to perform a modal decomposition of the harmonic balance solution. This is done as follows. Consider configuration A. Suppose one wishes to decompose the state variables of the harmonic balance

[1] *Theoretically*, a trajectory starting exactly on an unstable limit cycle should remain on it. The divergence from a repellor occurs primarily because of the local error, *however small*, in each integration step. Two additional reasons are the fact that the computed limit cycle is itself approximate (finite number of harmonics), as are the time domain equations integrated (finite number of modes).

solution at $\tau = 0$, $x_J(0)$, $y_J(0)$, $x'_J(0)$, $y'_J(0)$ into the corresponding modal state variables $x^r_J(0)$, $y^r_J(0)$, $x'^r_J(0)$, $y'^r_J(0)$, $r = 1...q$. Take q points on the rotor P1.....Pq. Determine the harmonic balance displacements and velocities at Pi, $X_{Pi}(0)$, $Y_{Pi}(0)$, $\dot{X}_{Pi}(0)$, $\dot{Y}_{Pi}(0)$, $i = 1...q$, from equations (52), (85)-(87). Then

$$x_{Pi}(0) = \frac{X_{Pi}(0)}{c},\ y_{Pi}(0) = \frac{Y_{Pi}(0)}{c},\ x'_{Pi}(0) = \frac{\dot{X}_{Pi}(0)}{\Omega c},\ y'_{Pi}(0) = \frac{\dot{Y}_{Pi}(0)}{\Omega c} \qquad \text{(110a,b,c,d)}$$

But, from equations (100a,b)

$$x_{Pi}(0) = \sum_{r=1}^{q} \frac{A^r_{PiJ}}{A^r_{JJ}} x^r_J(0)$$

$$y_{Pi}(0) = \sum_{r=1}^{q} \frac{B^r_{PiJ}}{B^r_{JJ}} y^r_J(0)$$

$$x'_{Pi}(0) = \sum_{r=1}^{q} \frac{A^r_{PiJ}}{A^r_{JJ}} x'^r_J(0)$$

$$y'_{Pi}(0) = \sum_{r=1}^{q} \frac{B^r_{PiJ}}{B^r_{JJ}} y'^r_J(0)$$

Hence,

$$\begin{bmatrix} x_{P1}(0) \\ \vdots \\ x_{Pq}(0) \end{bmatrix} = \begin{bmatrix} A^1_{P1J}/A^1_{JJ} & \cdots & A^q_{P1J}/A^q_{JJ} \\ \vdots & \vdots & \vdots \\ A^1_{PqJ}/A^1_{JJ} & \cdots & A^q_{PqJ}/A^q_{JJ} \end{bmatrix} \begin{bmatrix} x^1_J(0) \\ \vdots \\ x^q_J(0) \end{bmatrix} \qquad \text{(111a)}$$

$$\begin{bmatrix} y_{P1}(0) \\ \vdots \\ y_{Pq}(0) \end{bmatrix} = \begin{bmatrix} B^1_{P1J}/B^1_{JJ} & \cdots & B^q_{P1J}/B^q_{JJ} \\ \vdots & \vdots & \vdots \\ B^1_{PqJ}/B^1_{JJ} & \cdots & B^q_{PqJ}/B^q_{JJ} \end{bmatrix} \begin{bmatrix} y^1_J(0) \\ \vdots \\ y^q_J(0) \end{bmatrix} \qquad \text{(111b)}$$

$$\begin{bmatrix} x'_{P1}(0) \\ \vdots \\ x'_{Pq}(0) \end{bmatrix} = \begin{bmatrix} A^1_{P1J}/A^1_{JJ} & \cdots & A^q_{P1J}/A^q_{JJ} \\ \vdots & \vdots & \vdots \\ A^1_{PqJ}/A^1_{JJ} & \cdots & A^q_{PqJ}/A^q_{JJ} \end{bmatrix} \begin{bmatrix} x'^1_J(0) \\ \vdots \\ x'^q_J(0) \end{bmatrix} \qquad \text{(111c)}$$

$$\begin{bmatrix} y'_{P1}(0) \\ \vdots \\ y'_{Pq}(0) \end{bmatrix} = \begin{bmatrix} B^1_{P1J}/B^1_{JJ} & \cdots & B^q_{P1J}/B^q_{JJ} \\ \vdots & \vdots & \vdots \\ B^1_{PqJ}/B^1_{JJ} & \cdots & B^q_{PqJ}/B^q_{JJ} \end{bmatrix} \begin{bmatrix} y'^1_J(0) \\ \vdots \\ y'^q_J(0) \end{bmatrix} \qquad \text{(111d)}$$

The modal constants A^r_{PiJ}, B^r_{PiJ}, $r=1...q$, are computed as in section 4.2. The modal state variables of J at $\tau=0$, (to be referred to as the initial modal state variables) are then obtained by solving each of the above four systems of equations (111a,b,c,d). The initial conditions state vector $\mathbf{s}_0$ is hence obtained:

$$\mathbf{s}_0=\begin{bmatrix}0 & x_J^1(0) & y_J^1(0) & \dots & x_J^q(0) & y_J^q(0) & x_J'^1(0) & y_J'^1(0) & \dots & x_J'^q(0) & y_J'^q(0)\end{bmatrix}^{\mathrm{T}} \qquad (112)$$

Experience gained from the simulations presented later in this report has shown that the *conditioning* of the matrices in equations (111) strongly affects the accuracy of the computed initial modal state variables. The reason for this is that equations (111) are approximations since the infinite modal series is truncated after q modes. If the points Pi are close together then the matrices in equations (111) are close to singular. Hence the error due to the modal truncation is grossly amplified upon inversion. Therefore, the following steps are taken to minimise this effect:

(a) The points Pi should be as far apart as possible: divide the span of the rotor into q segments and take points Pi joining these segments.

(b) Use more modes q in equations (111) than are actually used when solving the differential equations (98). This makes equations (111) more accurate and hence less adversely affected by any ill conditioning of the matrices in these equations. The extra initial state variables generated upon solution of equations (111) are then dropped when forming the initial conditions state vector $\mathbf{s}_0$, equation (112). Steps (a) and (b) proved highly effective in the simulations carried out.

6.2 METHOD II: using Floquet Theory

In this method, one considers small perturbations of the modal state variables about the limit cycle. For this analysis, the system of equations (109) in the time domain is written as:

$$\mathbf{s}'=\mathbf{f}(\tau,\mathbf{s}) \qquad (113)$$

where $\mathbf{s}$ is now the vector of modal state variables only, *excluding* τ (previously the first element in $\mathbf{s}$. Also, for convenience, τ is defined as $\tau=\omega t$ where ω is the fundamental frequency of the limit cycle, rather than $\tau=\Omega t$ ($\Omega=$rotational speed), as previous. Let $\mathbf{s}_\mathbf{E}=\mathbf{s}_\mathbf{E}(\tau)$ be the equilibrium state vector *i.e.* the vector of modal state variables at a general point on the limit cycle (harmonic balance solution). Hence $\mathbf{s}_\mathbf{E}$ is a periodic function of τ with period 2π. Note that in Method I $\mathbf{s}_\mathbf{E}(0)$ was computed to use as initial conditions for the time domain equations (98). Now

$$\mathbf{s}_\mathbf{E}'=\mathbf{f}(\tau,\mathbf{s}_\mathbf{E}) \qquad (114)$$

$$\therefore\ \mathbf{s}'-\mathbf{s}_\mathbf{E}'=\mathbf{f}(\tau,\mathbf{s})-\mathbf{f}(\tau,\mathbf{s}_\mathbf{E}) \qquad (115)$$

Define $\mathbf{u} = \mathbf{s} - \mathbf{s}_E$ = vector of perturbations in the modal state variables. For *small* perturbations about the limit cycle one can write

$$\mathbf{u}' \approx \left.\frac{\partial \mathbf{f}}{\partial \mathbf{s}}\right|_{\mathbf{s}=\mathbf{s}_E} \mathbf{u} \tag{116}$$

where, in the above equation (116), $\mathbf{f}(\tau,\mathbf{s})$ has been expanded as a Taylor series about $\mathbf{s} = \mathbf{s}_E$:

$$\mathbf{f}(\tau,\mathbf{s}) = \mathbf{f}(\tau,\mathbf{s}_E) + \left.\frac{\partial \mathbf{f}}{\partial \mathbf{s}}\right|_{\mathbf{s}=\mathbf{s}_E} (\mathbf{s}-\mathbf{s}_E) + \ldots \tag{117}$$

Equation (116) is written as

$$\mathbf{u}' = \mathbf{W}(\tau)\mathbf{u} \tag{118}$$

where

$$\mathbf{W}(\tau) = \left.\frac{\partial \mathbf{f}}{\partial \mathbf{s}}\right|_{\mathbf{s}=\mathbf{s}_E} \tag{119}$$

$\mathbf{W}(\tau)$ is an $n_s \times n_s$ matrix of partial derivatives where n_s is the number of modal state variables. Since these partial derivatives are evaluated at $\mathbf{s}_E(\tau)$ which is periodic with period 2π then $\mathbf{W}(\tau)$ will also be periodic with period 2π:

$$\mathbf{W}(\tau) = \mathbf{W}(\tau + k2\pi), \; k = 1,2,\ldots \tag{120}$$

Hence equation (118) is a system of ordinary linear homogeneous differential equations with periodically varying coefficients. The study of the stability of the limit cycle has hence been reduced to the study of the stability of such a system of equations. Such a study is referred to as Floquet Theory and can be found in any standard text book on ordinary linear differential equations *e.g.* [14], [29], [30], [31]. The matrix $\mathbf{W}(\tau)$ for the specific configurations A, B will be presented in section 6.2.3. In the following section the fundamentals of Floquet Theory are presented.

6.2.1 Fundamentals of Floquet Theory

The system of equations (118) will have n_s linearly independent solutions $\mathbf{u}_1(\tau),\ldots\ldots,\mathbf{u}_{n_s}(\tau)$. These can be collected into a *fundamental matrix* $\mathbf{U}(\tau)$:

$$\mathbf{U}(\tau) = \left[\mathbf{u}_1(\tau) \;\; \ldots \;\; \mathbf{u}_{n_s}(\tau)\right] \tag{121}$$

Hence, $\mathbf{U}(\tau)$ is *a* solution of the *matrix* differential equation

$$\mathbf{U}' = \mathbf{W}(\tau)\mathbf{U} \tag{122}$$

If, in addition, $\mathbf{u_1}(0)=[1 \;\; 0 \;\; \cdots \;\; 0]^T$, $\mathbf{u_2}(0)=[0 \;\; 1 \;\; \cdots \;\; 0]^T$, ..., $\mathbf{u}_{n_s}(0)=[0 \;\; \cdots \;\; 0 \;\; 1]^T$, then $\mathbf{U}(\tau)$ is referred to as the *principal fundamental matrix* $\mathbf{U_P}(\tau)$. Hence $\mathbf{U_P}(\tau)$ is the unique solution of the initial value problem

$$\mathbf{U}' = \mathbf{W}(\tau)\mathbf{U}, \;\; \mathbf{U}(0)=\mathbf{I}_{n_s} \tag{123}$$

In general neither $\mathbf{U}(\tau)$ nor $\mathbf{U_P}(\tau)$ are periodic. The *monodromy matrix* $\mathbf{M}$ is defined as

$$\mathbf{M} = \mathbf{U_P}(2\pi) \tag{124}$$

It can be shown [30] that the *discrete* general solution of equation (118) is of the form

$$\mathbf{u}(k2\pi)=\sum_{i=1}^{n_s}\lambda_i^k c_i \mathbf{e}_i, \quad k=0,1,2,\ldots \tag{125}$$

where λ_i, $i=1\ldots n_s$ is an eigenvalue of $\mathbf{M}$, $\mathbf{e_i}$ the corresponding eigenvector and c_i an arbitrary constant. Note that equation (125) gives the perturbation vector $\mathbf{u}$ sampled at intervals of 2π, which is the period of the limit cycle. Any two rows in $\mathbf{u}(k2\pi)$ can be plotted against each other for $k=0,1,2,\ldots$. The resulting plot of sampled points (or *return points*) is a Poincare map. The eigenvalues of $\mathbf{M}$ are referred to as the characteristic or Floquet multipliers. From equation (125), these govern the stability of the perturbation vector $\mathbf{u}(\tau)$ and the evolution of the sampling points on the Poincare map. For stability

$$|\lambda_i| < 1, \text{ for } i=1\ldots n_s, \tag{126}$$

i.e. each λ_i must lie within a unit circle. If $|\lambda_i| > 1$ for one or more values of i then the motion is unstable and the sampled points diverge. Moreover, in such a case, one can determine the stable type of motion the perturbed trajectory *tends* to by examining λ_c, the critical multiplier, responsible for the instability. It is important to note in what follows that since all the information is obtained from equation (118), which is valid only in the immediate vicinity of the limit cycle one can only ascertain the *tendency* to a certain type of motion. Suppose that $\mathbf{u}(0)\approx\mathbf{0}$ *i.e.* the first sampled point on the Poincare map is very close to the unstable equilibrium position (0,0), representing the limit cycle.

(a) λ_c **real and positive** ($\rightarrow$ jump, same period bifurcation [31], [3]):

From equation (125)

$$\mathbf{u}(k2\pi) \approx \lambda_c^k c_c \mathbf{e}_c \tag{127}$$

Since λ_c is real, consecutive sampled points on a Poincare map will lie approximately on a straight line of direction determined by the eigenvector $\mathbf{e}_c$. Since $\lambda_c > 0$ they will lie on the same side of the unstable equilibrium point (0,0) but at increasing distances from it. Hence, in this case the motion of the perturbed trajectory tends to a limit cycle of the same period. The perturbed trajectory will settle down to such motion if such a stable limit cycle exists, in which case the points will congregate at a single point at one end of the line.

(b) λ_c real and negative ($\rightarrow$ period doubling bifurcation [31], [3]):

Equation (127) still applies and consecutive sampled points on a Poincare map will approximately lie on a straight line of direction determined by $\mathbf{e}_c$. However since the critical multiplier $\lambda_c < 0$, consecutive sampling points flip on either side of the unstable equilibrium point (0,0), at increasing distances from it. Hence, the perturbed trajectory tends to a limit cycle of period twice the unstable limit cycle. The perturbed trajectory will settle down to such a motion if such a stable limit cycle exists, in which case the points eventually congregate at two points at each end of the line on either side of the unstable equilibrium point. Hence, a period doubling bifurcation is termed a "flip" bifurcation.

(c) λ_c complex ($\rightarrow$ quasi-periodicity, secondary Hopf bifurcation [31], [3], [12], [14]):

In this case two complex conjugate multipliers λ_c, λ_c^* cross the unit circle simultaneously. From equation (125)

$$\mathbf{u}(k2\pi) \approx \lambda_c^k c_1 \mathbf{e}_c + (\lambda_c^*)^k c_2 \mathbf{e}_c^*$$

Now $\lambda_c = |\lambda_c| e^{j\varphi}$, $\therefore\ \lambda_c^k = |\lambda_c|^k e^{jk\varphi} = |\lambda_c|^k \{\cos k\varphi + j \sin k\varphi\}$

Hence,

$$\mathbf{u}(k2\pi) \approx |\lambda_c|^k \{\mathbf{d}_1 \cos k\varphi + \mathbf{d}_2 \sin k\varphi\} \tag{128}$$

Equation (128) plotted on a Poincare plane gives one or more (depending on φ) spirals emanating from the unstable equilibrium point (0,0). As an example, the two rows of $\mathbf{u}(k2\pi)$, $k = 0,1,2,\ldots$ are plotted against each other for $|\lambda_c| = 1.1$, $\mathbf{d}_1 = [0.2 \quad 0.4]^T$, $\mathbf{d}_2 = [0.4 \quad 0.2]^T$. A single spiral for consecutive return points is obtained for $\varphi = 0.3491$ (Figure 7(a)). For $\varphi = 3.4907$, *alternate* return points (circles and squares in Figure 7(b)) form two spirals. For $\varphi = 4.6432$ the return points form 4 spirals, Figure 7(c). If a stable quasi-periodic attractor exists in the vicinity of the unstable limit cycle, the return points will diverge from the unstable

equilibrium point along one or more spirals and settle down into a "drift ring" of points surrounding the unstable equilibrium point [14], [12]. The bifurcation of a limit cycle into quasi-periodic motion is referred to as a *secondary Hopf bifurcation*[1]. Quasi-periodic motion is characterised by a frequency that is irrationally related to the fundamental frequency of the limit cycle (= sampling frequency). Hence the points never quite coincide with each other, forming a "drift ring". In exceptional circumstances the two frequencies are rationally related, in which case "phase locking" is said to occur and the drift ring degenerates into a finite number of points [31].

To summarise, in order to test for stability of a limit cycle by Floquet Theory one needs to determine the perturbation matrix $\mathbf{W}(\tau)$ and the associated monodromy matrix **M**, and examine the eigenvalues of **M**.

6.2.2 Computation of monodromy matrix

The monodromy matrix **M** can be computed by two alternative methods, designated in this report as Methods IIa and IIb.

Method IIa – direct from the definition of **M** in equation (124).

This involves solving the perturbation equations (118) numerically (by fast integration [13], or Runge-Kutta,.....*etc*) n_s times over the interval $\tau = 0$ to $\tau = 2\pi$, with the initial conditions $\mathbf{u}_1(0) = [1 \quad 0 \quad \cdots \quad 0]^T$, $\mathbf{u}_2(0) = [0 \quad 1 \quad \cdots \quad 0]^T$, ..., $\mathbf{u}_{n_s}(0) = [0 \quad \cdots \quad 0 \quad 1]^T$ respectively. **M** is then given by

$$\mathbf{M} = \left[\mathbf{u}_1(2\pi) \quad \ldots \quad \mathbf{u}_{n_s}(2\pi)\right] \tag{129}$$

where $\mathbf{u}_1(\tau)\ldots\mathbf{u}_{n_s}(\tau)$ are the solutions obtained. Needless to say, this is extremely time consuming, even more so since this has to be performed for each limit cycle in a complete set computed by the harmonic balance method (*i.e.* the unbalance response). In this research this process was found to run into several hours. Hence, such a method would eradicate all the computational efficiency gained using the harmonic balance method. In fact, Method I (section 6.1) is much faster than this method (IIa). Notwithstanding its gross inefficiency, this method has been used in the literature to test for the stability of harmonic balance solutions *e.g.* Hahn *et al* [1], July 1994 and Chu *et al* [32], 1998. Not surprisingly, in the cited references only a few solutions were tested from a complete unbalance response.

---

[1] A (primary) Hopf bifurcation occurs when a limit cycle (*i.e.* periodic oscillation) is born from an unstable constant solution (unstable equilibrium point in *state space*). On a *phase plane* the limit cycle surrounds this unstable equilibrium point. Analogously, on a *Poincare map* the stable drift ring of sampled points of the stable quasi-periodic attractor surrounds the unstable equilibrium sample point of the unstable limit cycle. Hence the term *secondary Hopf bifurcation* [14].

Method IIb – using impulsive parametric excitation theory.

Hsu [33], [10] in 1972 developed a very fast approximate method for computing the monodromy matrix. This method was implemented by Zhao *et al* [3], April 1994 (*i.e.* before [1] and [32], where the slow Method IIa was used). In this technique the periodic interval $[0,2\pi]$ of the periodic matrix function $\mathbf{W}(\tau)$ is divided into K equal segments $\Delta\tau$. Let τ_k, $k=1\ldots K$, be the value of τ at the midpoint each segment. $\mathbf{W}(\tau)$ is replaced over $[0,2\pi]$ by a series of impulses of strength $\mathbf{W}_k\Delta\tau$ [10] where

$$\mathbf{W}_k = \mathbf{W}(\tau_k) \tag{130}$$

It can be shown [33], that

$$\mathbf{M} \approx e^{\mathbf{W}_K\Delta\tau}e^{\mathbf{W}_{K-1}\Delta\tau}\ldots e^{\mathbf{W}_2\Delta\tau}e^{\mathbf{W}_1\Delta\tau} \tag{131}$$

The above product converges to the exact matrix $\mathbf{M}$ as $K\to\infty$. However, in the simulations presented in this report, $K=200$ gave highly accurate results. In this research the matrix exponentials in the product in equation (131) were computed using the *MATLAB®* function *expm3.m©* [21]. Such a function computes the matrix exponential via the eigenvalues and eigenvectors of the exponent. Hence it is extremely rapid (around a fraction of a second in this work). In this work it is shown that the application of Method IIb cuts down the time to compute the stability along an entire unbalance response curve from several hours (Method IIa) down to a few minutes, with negligible loss of accuracy.

6.2.3 Derivation of $\mathbf{W}(\tau)$ for configurations A, B

Configuration A (Figure 5):

Consider configuration A1. Equations (98) are rewritten in terms of the redefined variable $\tau=\omega t$ where ω is the fundamental frequency of the limit cycle:

$$x_J^{''r}+\frac{\omega_{xr}^2}{\omega^2}x_J^r=\frac{1}{c\omega^2}A_{JJ}^rQ_x(x,y,x',y')+\frac{1}{c}A_{JU}^rUN^2\sin(N\tau) \tag{132a}$$

$$y_J^{''r}+\frac{\omega_{yr}^2}{\omega^2}y_J^r=\frac{1}{c\omega^2}B_{JJ}^rQ_y(x,y,x',y')-\frac{1}{c}B_{JU}^rUN^2\cos(N\tau) \tag{132b}$$

Let x_{JE}^r, y_{JE}^r, $x_{JE}^{'r}$, $y_{JE}^{'r}$ be the equilibrium modal state variables (modal state variables on the limit cycle) and u_J^r, v_J^r, $u_J^{'r}$, $v_J^{'r}$ the respective perturbations *i.e.*

$$x_J^r=x_{JE}^r+u_J^r,\ y_J^r=y_{JE}^r+v_J^r,\ x_J^{'r}=x_{JE}^{'r}+u_J^{'r},\ y_J^{'r}=y_{JE}^{'r}+v_J^{'r} \tag{133a,b,c,d}$$

Consider equation (132a):

$$x''^{r}_{JE}+\frac{\omega^2_{xr}}{\omega^2}x^r_{JE}=\frac{1}{c\omega^2}A^r_{JJ}Q_x(x_E,y_E,x'_E,y'_E)+\frac{1}{c}A^r_{JU}UN^2\sin(N\tau) \tag{134}$$

Subtracting equation (134) from equation (132a) gives:

$$\begin{aligned}u''^{r}_{J}+\frac{\omega^2_{xr}}{\omega^2}u^r_J&=\frac{1}{c\omega^2}A^r_{JJ}[Q_x(x,y,x',y')-Q_x(x_E,y_E,x'_E,y'_E)]\\&\approx\frac{1}{c\omega^2}A^r_{JJ}\left[\frac{\partial Q_x}{\partial x}(x-x_E)+\frac{\partial Q_x}{\partial y}(y-y_E)+\frac{\partial Q_x}{\partial x'}(x'-x'_E)+\frac{\partial Q_x}{\partial y'}(y'-y'_E)\right]\end{aligned} \tag{135}$$

where the right hand side of the above equation has been expanded in a Taylor series about the equilibrium state and truncated beyond the linear terms. Now, from equations (99)

$$x_E=x_{JE}=\varepsilon_{0x}+\sum_{r=1}^{q}x^r_{JE},\quad y_E=y_{JE}=\varepsilon_{0y}+\sum_{r=1}^{q}y^r_{JE}, \tag{136a,b}$$

$$x'_E=x'_{JE}=\sum_{r=1}^{q}x'^{r}_{JE},\quad y'_E=y'_{JE}=\sum_{r=1}^{q}y'^{r}_{JE} \tag{136c,d}$$

From equations (133a,b,c,d)

$$x=x_J=\varepsilon_{0x}+\sum_{r=1}^{q}\left(x^r_{JE}+u^r_J\right),\quad y=y_J=\varepsilon_{0y}+\sum_{r=1}^{q}\left(y^r_{JE}+v^r_J\right), \tag{137a,b}$$

$$x'=x'_J=\sum_{r=1}^{q}\left(x'^{r}_{JE}+u'^{r}_J\right),\quad y'=y'_J=\sum_{r=1}^{q}\left(y'^{r}_{JE}+v'^{r}_J\right) \tag{137c,d}$$

Hence, substituting for $x-x_E$, $y-y_E$, $x'-x'_E$, $y'-y'_E$ from equations (136), (137) into equation (135):

$$u''^{r}_{J}+\frac{\omega^2_{xr}}{\omega^2}u^r_J=\frac{1}{c\omega^2}A^r_{JJ}\left[\frac{\partial Q_x}{\partial x}\sum_{h=1}^{q}u^h_J+\frac{\partial Q_x}{\partial y}\sum_{h=1}^{q}v^h_J+\frac{\partial Q_x}{\partial x'}\sum_{h=1}^{q}u'^{h}_J+\frac{\partial Q_x}{\partial y'}\sum_{h=1}^{q}v'^{h}_J\right] \tag{138a}$$

Similarly, for the y direction

$$v''^{r}_{J}+\frac{\omega^2_{yr}}{\omega^2}v^r_J=\frac{1}{c\omega^2}B^r_{JJ}\left[\frac{\partial Q_y}{\partial x}\sum_{h=1}^{q}u^h_J+\frac{\partial Q_y}{\partial y}\sum_{h=1}^{q}v^h_J+\frac{\partial Q_y}{\partial x'}\sum_{h=1}^{q}u'^{h}_J+\frac{\partial Q_y}{\partial y'}\sum_{h=1}^{q}v'^{h}_J\right] \tag{138b}$$

The partial derivatives in equations (138) are evaluated at the equilibrium state variables $x_E(\tau)$, $y_E(\tau)$, $x'_E(\tau)$, $y'_E(\tau)$ and hence they are periodic functions of τ, period 2π.

Defining

$$\mathbf{u}=\left[u^1_J\quad v^1_J\quad\ldots\quad u^q_J\quad v^q_J\quad u'^1_J\quad v'^1_J\quad\ldots\quad u'^q_J\quad v'^q_J\right]^{\mathrm{T}}$$

Equations are written in the form (118), where

$$\mathbf{W}(\tau)=\begin{bmatrix}\mathbf{0} & \mathbf{I}_{2q}\\ \mathbf{W}_1(\tau)-\mathbf{D} & \mathbf{W}_2(\tau)\end{bmatrix} \tag{139}$$

$$\mathbf{W}_1(\tau)=\frac{1}{c\omega^2}\begin{bmatrix} A_{JJ}^1\frac{\partial Q_x}{\partial x} & A_{JJ}^1\frac{\partial Q_x}{\partial y} & \cdots & \cdots & A_{JJ}^1\frac{\partial Q_x}{\partial x} & A_{JJ}^1\frac{\partial Q_x}{\partial y}\\ B_{JJ}^1\frac{\partial Q_y}{\partial x} & B_{JJ}^1\frac{\partial Q_y}{\partial y} & \cdots & \cdots & B_{JJ}^1\frac{\partial Q_y}{\partial x} & B_{JJ}^1\frac{\partial Q_y}{\partial y}\\ \vdots & & & & \vdots & \vdots\\ \vdots & & & & \vdots & \vdots\\ A_{JJ}^q\frac{\partial Q_x}{\partial x} & A_{JJ}^q\frac{\partial Q_x}{\partial y} & \cdots & \cdots & A_{JJ}^q\frac{\partial Q_x}{\partial x} & A_{JJ}^q\frac{\partial Q_x}{\partial y}\\ B_{JJ}^q\frac{\partial Q_y}{\partial x} & B_{JJ}^q\frac{\partial Q_y}{\partial y} & \cdots & \cdots & B_{JJ}^q\frac{\partial Q_y}{\partial x} & B_{JJ}^q\frac{\partial Q_y}{\partial y}\end{bmatrix} \tag{140}$$

$$\mathbf{D}=\frac{1}{\omega^2}\mathbf{diag}\begin{pmatrix}\omega_{x1}^2 & \omega_{y1}^2 & \cdots & \cdots & \omega_{xq}^2 & \omega_{yq}^2\end{pmatrix} \tag{141}$$

$$\mathbf{W}_2(\tau)=\frac{1}{c\omega^2}\begin{bmatrix} A_{JJ}^1\frac{\partial Q_x}{\partial x'} & A_{JJ}^1\frac{\partial Q_x}{\partial y'} & \cdots & \cdots & A_{JJ}^1\frac{\partial Q_x}{\partial x'} & A_{JJ}^1\frac{\partial Q_x}{\partial y'}\\ B_{JJ}^1\frac{\partial Q_y}{\partial x'} & B_{JJ}^1\frac{\partial Q_y}{\partial y'} & \cdots & \cdots & B_{JJ}^1\frac{\partial Q_y}{\partial x'} & B_{JJ}^1\frac{\partial Q_y}{\partial y'}\\ \vdots & \vdots & & & \vdots & \vdots\\ \vdots & \vdots & & & \vdots & \vdots\\ A_{JJ}^q\frac{\partial Q_x}{\partial x'} & A_{JJ}^q\frac{\partial Q_x}{\partial y'} & \cdots & \cdots & A_{JJ}^q\frac{\partial Q_x}{\partial x'} & A_{JJ}^q\frac{\partial Q_x}{\partial y'}\\ B_{JJ}^q\frac{\partial Q_y}{\partial x'} & B_{JJ}^q\frac{\partial Q_y}{\partial y'} & \cdots & \cdots & B_{JJ}^q\frac{\partial Q_y}{\partial x'} & B_{JJ}^q\frac{\partial Q_y}{\partial y'}\end{bmatrix} \tag{142}$$

For configuration A2 the matrix $\mathbf{W}(\tau)$ remains unchanged from that in equations (139)-(142).

Configuration B (Figure 6)**:**

Equations (105) are rewritten in terms of $\tau=\omega t$ and a process similar to the above is applied. The perturbation vector in equation (118) is now

$$\mathbf{u}=\begin{bmatrix} u_J^1 & v_J^1 & \cdots & u_J^{q_R} & v_J^{q_R} & u_B^1 & v_B^1 & \cdots & u_B^{q_F} & v_B^{q_F} \\ u_J'^1 & v_J'^1 & \cdots & u_J'^{q_R} & v_J'^{q_R} & u_B'^1 & v_B'^1 & \cdots & u_B'^{q_F} & v_B'^{q_F} \end{bmatrix}^{\mathrm{T}}$$

and $\mathbf{W}(\tau)$ is given by

$$\mathbf{W}(\tau)=\begin{bmatrix} \mathbf{0} & \mathbf{I}_{2(q_R+q_F)} \\ \mathbf{W}_1(\tau)-\mathbf{D} & \mathbf{W}_2(\tau) \end{bmatrix} \tag{143}$$

$$\mathbf{W}_1(\tau)=$$

$$\frac{1}{c\omega^2}\begin{bmatrix} A_{JJ}^1\frac{\partial Q_x}{\partial x} & A_{JJ}^1\frac{\partial Q_x}{\partial y} & \cdots & A_{JJ}^1\frac{\partial Q_x}{\partial x} & A_{JJ}^1\frac{\partial Q_x}{\partial y} & -A_{JJ}^1\frac{\partial Q_x}{\partial x} & -A_{JJ}^1\frac{\partial Q_x}{\partial y} & \cdots & -A_{JJ}^1\frac{\partial Q_x}{\partial x} & -A_{JJ}^1\frac{\partial Q_x}{\partial y} \\ B_{JJ}^1\frac{\partial Q_y}{\partial x} & B_{JJ}^1\frac{\partial Q_y}{\partial y} & \cdots & B_{JJ}^1\frac{\partial Q_y}{\partial x} & B_{JJ}^1\frac{\partial Q_y}{\partial y} & -B_{JJ}^1\frac{\partial Q_y}{\partial x} & -B_{JJ}^1\frac{\partial Q_y}{\partial y} & \cdots & -B_{JJ}^1\frac{\partial Q_y}{\partial x} & -B_{JJ}^1\frac{\partial Q_y}{\partial y} \\ \vdots & \vdots & & \vdots & \vdots & \vdots & \vdots & & \vdots & \vdots \\ A_{JJ}^{q_R}\frac{\partial Q_x}{\partial x} & A_{JJ}^{q_R}\frac{\partial Q_x}{\partial y} & & A_{JJ}^{q_R}\frac{\partial Q_x}{\partial x} & A_{JJ}^{q_R}\frac{\partial Q_x}{\partial y} & -A_{JJ}^{q_R}\frac{\partial Q_x}{\partial x} & -A_{JJ}^{q_R}\frac{\partial Q_x}{\partial y} & \cdots & -A_{JJ}^{q_R}\frac{\partial Q_x}{\partial x} & -A_{JJ}^{q_R}\frac{\partial Q_x}{\partial y} \\ B_{JJ}^{q_R}\frac{\partial Q_y}{\partial x} & B_{JJ}^{q_R}\frac{\partial Q_y}{\partial y} & & B_{JJ}^{q_R}\frac{\partial Q_y}{\partial x} & B_{JJ}^{q_R}\frac{\partial Q_y}{\partial y} & -A_{JJ}^{q_R}\frac{\partial Q_y}{\partial x} & -A_{JJ}^{q_R}\frac{\partial Q_y}{\partial y} & \cdots & -A_{JJ}^{q_R}\frac{\partial Q_y}{\partial x} & -A_{JJ}^{q_R}\frac{\partial Q_y}{\partial y} \\ -A_{BB}^1\frac{\partial Q_x}{\partial x} & -A_{BB}^1\frac{\partial Q_x}{\partial y} & \cdots & -A_{BB}^1\frac{\partial Q_x}{\partial x} & -A_{BB}^1\frac{\partial Q_x}{\partial y} & A_{BB}^1\frac{\partial Q_x}{\partial x} & A_{BB}^1\frac{\partial Q_x}{\partial y} & \cdots & A_{BB}^1\frac{\partial Q_x}{\partial x} & A_{BB}^1\frac{\partial Q_x}{\partial y} \\ -B_{BB}^1\frac{\partial Q_y}{\partial x} & -B_{BB}^1\frac{\partial Q_y}{\partial y} & \cdots & -B_{BB}^1\frac{\partial Q_y}{\partial x} & -B_{BB}^1\frac{\partial Q_y}{\partial y} & B_{BB}^1\frac{\partial Q_y}{\partial x} & B_{BB}^1\frac{\partial Q_y}{\partial y} & \cdots & B_{BB}^1\frac{\partial Q_y}{\partial x} & B_{BB}^1\frac{\partial Q_y}{\partial y} \\ \vdots & \vdots & & \vdots & \vdots & \vdots & \vdots & & \vdots & \vdots \\ -A_{BB}^{q_F}\frac{\partial Q_x}{\partial x} & -A_{BB}^{q_F}\frac{\partial Q_x}{\partial y} & \cdots & -A_{BB}^{q_F}\frac{\partial Q_x}{\partial x} & -A_{BB}^{q_F}\frac{\partial Q_x}{\partial y} & A_{BB}^{q_F}\frac{\partial Q_x}{\partial x} & A_{BB}^{q_F}\frac{\partial Q_x}{\partial y} & \cdots & A_{BB}^{q_F}\frac{\partial Q_x}{\partial x} & A_{BB}^{q_F}\frac{\partial Q_x}{\partial y} \\ -B_{BB}^{q_F}\frac{\partial Q_y}{\partial x} & -B_{BB}^{q_F}\frac{\partial Q_y}{\partial y} & \cdots & -B_{BB}^{q_F}\frac{\partial Q_y}{\partial x} & -B_{BB}^{q_F}\frac{\partial Q_y}{\partial y} & B_{BB}^{q_F}\frac{\partial Q_y}{\partial x} & B_{BB}^{q_F}\frac{\partial Q_y}{\partial y} & \cdots & B_{BB}^{q_F}\frac{\partial Q_y}{\partial x} & B_{BB}^{q_F}\frac{\partial Q_y}{\partial y} \end{bmatrix} \tag{144}$$

$$\mathbf{D}=\frac{1}{\omega^2}\mathbf{diag}\begin{pmatrix}\omega_{Rx1}^2 & \omega_{Ry1}^2 & \cdots & \omega_{Rxq_R}^2 & \omega_{Ryq_R}^2 & \omega_{Fx1}^2 & \omega_{Fy1}^2 & \cdots & \omega_{Fxq_F}^2 & \omega_{Fyq_F}^2\end{pmatrix} \tag{145}$$

$$\mathbf{W}_2(\tau)=$$

$$\frac{1}{c\omega^2}\begin{bmatrix}
A^1_{JJ}\frac{\partial Q_x}{\partial x'} & A^1_{JJ}\frac{\partial Q_x}{\partial y'} & \cdots & A^1_{JJ}\frac{\partial Q_x}{\partial x'} & A^1_{JJ}\frac{\partial Q_x}{\partial y'} & -A^1_{JJ}\frac{\partial Q_x}{\partial x'} & -A^1_{JJ}\frac{\partial Q_x}{\partial y'} & \cdots & -A^1_{JJ}\frac{\partial Q_x}{\partial x'} & -A^1_{JJ}\frac{\partial Q_x}{\partial y'} \\
B^1_{JJ}\frac{\partial Q_y}{\partial x'} & B^1_{JJ}\frac{\partial Q_y}{\partial y'} & \cdots & B^1_{JJ}\frac{\partial Q_y}{\partial x'} & B^1_{JJ}\frac{\partial Q_y}{\partial y'} & -B^1_{JJ}\frac{\partial Q_y}{\partial x'} & -B^1_{JJ}\frac{\partial Q_y}{\partial y'} & \cdots & -B^1_{JJ}\frac{\partial Q_y}{\partial x'} & -B^1_{JJ}\frac{\partial Q_y}{\partial y'} \\
\vdots & \vdots & & \vdots & \vdots & \vdots & \vdots & & \vdots & \vdots \\
A^{q_R}_{JJ}\frac{\partial Q_x}{\partial x'} & A^{q_R}_{JJ}\frac{\partial Q_x}{\partial y'} & & A^{q_R}_{JJ}\frac{\partial Q_x}{\partial x'} & A^{q_R}_{JJ}\frac{\partial Q_x}{\partial y'} & -A^{q_R}_{JJ}\frac{\partial Q_x}{\partial x'} & -A^{q_R}_{JJ}\frac{\partial Q_x}{\partial y'} & \cdots & -A^{q_R}_{JJ}\frac{\partial Q_x}{\partial x'} & -A^{q_R}_{JJ}\frac{\partial Q_x}{\partial y'} \\
B^{q_R}_{JJ}\frac{\partial Q_y}{\partial x'} & B^{q_R}_{JJ}\frac{\partial Q_y}{\partial y'} & & B^{q_R}_{JJ}\frac{\partial Q_y}{\partial x'} & B^{q_R}_{JJ}\frac{\partial Q_y}{\partial y'} & -A^{q_R}_{JJ}\frac{\partial Q_y}{\partial x'} & -A^{q_R}_{JJ}\frac{\partial Q_y}{\partial y'} & \cdots & -A^{q_R}_{JJ}\frac{\partial Q_y}{\partial x'} & -A^{q_R}_{JJ}\frac{\partial Q_y}{\partial y'} \\
-A^1_{BB}\frac{\partial Q_x}{\partial x'} & -A^1_{BB}\frac{\partial Q_x}{\partial y'} & \cdots & -A^1_{BB}\frac{\partial Q_x}{\partial x'} & -A^1_{BB}\frac{\partial Q_x}{\partial y'} & A^1_{BB}\frac{\partial Q_x}{\partial x'} & A^1_{BB}\frac{\partial Q_x}{\partial y'} & \cdots & A^1_{BB}\frac{\partial Q_x}{\partial x'} & A^1_{BB}\frac{\partial Q_x}{\partial y'} \\
-B^1_{BB}\frac{\partial Q_y}{\partial x'} & -B^1_{BB}\frac{\partial Q_y}{\partial y'} & \cdots & -B^1_{BB}\frac{\partial Q_y}{\partial x'} & -B^1_{BB}\frac{\partial Q_y}{\partial y'} & B^1_{BB}\frac{\partial Q_y}{\partial x'} & B^1_{BB}\frac{\partial Q_y}{\partial y'} & \cdots & B^1_{BB}\frac{\partial Q_y}{\partial x'} & B^1_{BB}\frac{\partial Q_y}{\partial y'} \\
\vdots & \vdots & & \vdots & \vdots & \vdots & \vdots & & \vdots & \vdots \\
-A^{q_F}_{BB}\frac{\partial Q_x}{\partial x'} & -A^{q_F}_{BB}\frac{\partial Q_x}{\partial y'} & \cdots & -A^{q_F}_{BB}\frac{\partial Q_x}{\partial x'} & -A^{q_F}_{BB}\frac{\partial Q_x}{\partial y'} & A^{q_F}_{BB}\frac{\partial Q_x}{\partial x'} & A^{q_F}_{BB}\frac{\partial Q_x}{\partial y'} & \cdots & A^{q_F}_{BB}\frac{\partial Q_x}{\partial x'} & A^{q_F}_{BB}\frac{\partial Q_x}{\partial y'} \\
-B^{q_F}_{BB}\frac{\partial Q_y}{\partial x'} & -B^{q_F}_{BB}\frac{\partial Q_y}{\partial y'} & \cdots & -B^{q_F}_{BB}\frac{\partial Q_y}{\partial x'} & -B^{q_F}_{BB}\frac{\partial Q_y}{\partial y'} & B^{q_F}_{BB}\frac{\partial Q_y}{\partial x'} & B^{q_F}_{BB}\frac{\partial Q_y}{\partial y'} & \cdots & B^{q_F}_{BB}\frac{\partial Q_y}{\partial x'} & B^{q_F}_{BB}\frac{\partial Q_y}{\partial y'}
\end{bmatrix} \tag{146}$$

6.3 SUMMARY

Three methods for testing the stability have been presented in this chapter: Method I, based on direct integration of the time domain equations and Methods IIa,b based on the computation of the monodromy matrix. Method IIa is not practicable. The best approach, adopted in the simulations in this research is to derive the stability curve[1] for a given unbalance response using the fast Method IIb and then perform confirmatory spot checks at salient points using Method I. All three methods assume that the computed limit cycle is a reasonably accurate approximation to the exact limit cycle. Hence sufficient harmonics need to be included in the harmonic balance solution. Also, an adequate number of modes need to be included in the time domain equations (for Method I) and the perturbation equations (Methods II). Since Methods I and IIa involve numerical integration of differential equations the number of modes has to be limited to avoid problems of stiffness. On the other hand, in the approximate Method IIb, more modes can taken and despite the increased size of the matrices in the exponents in the product in equation (130) the speed of computation is only moderately affected (chapter 8).

Software was developed in *MATLAB*® (Version 5) to perform the stability analysis according to the methods developed in this chapter. The partial derivatives contained in $\mathbf{W}(\tau)$, equations (139)-(142) and (143)-(146), were evaluated numerically from the relevant squeeze film force expressions presented in section 2.1.

[1] *i.e.* curve showing the variation of the leading multiplier (*i.e.* multiplier with greatest magnitude) with rotational speed.

CHAPTER 7

ANALYSIS: CONFIGURATION B

In this chapter an analysis of configuration B (Figure 6) is presented. The analysis is restricted to a rigid rotor.

7.1 SIMULATION

For this analysis it is assumed that the rotor in Figure 6 is rigid and the bearing housing is modelled as a mass on a spring. This is done to compare directly with time domain simulations done in [27], [34] and harmonic balance (HB) and time domain (TD) simulations already done in [15], but which did not employ the receptance formulation. This assumption did not in any way simplify the harmonic balance equations. Receptances for a flexible shaft were simply replaced by receptances for a rigid shaft. However, the time domain and stability equations were considerably simplified since, in equations (105), (106) and (143)–(146) the number of modes of the rotor subsystem in both the *xz* and *yz* planes, $q_R = 1$, and the number of modes of the support subsystem, in both the *xz* and *yz* planes, $q_F = 1$. The numerical integration of the simplified form of equations of motion (105) had already been performed by a fast integration method in the first report [15].

In [34] and [15], the rigid body model used was as shown in Figure 8 where m_{eq} is the equivalent mass at the squeeze film. Also, the unbalance U was expressed in [34] as

$$U = m_{eq} u \tag{147}$$

where u was defined as the non-dimensional *dynamic load parameter*. Hence, in order to make direct comparison with [34], [15] the receptances $\alpha_{JJ} (= \beta_{JJ})$, $\alpha_{JU} (= \beta_{JU})$, $\alpha_{BB} (= \beta_{BB})$ used were

$$\alpha_{JJ} = \alpha_{JU} = -\frac{1}{\omega^2 m_{eq}} \tag{148}$$

$$\alpha_{BB} = \frac{1}{k_B - \omega^2 m_B} \tag{149}$$

where $m_{eq} = 24.5\,\text{kg}$, $m_B = 3.5\,\text{kg}$, $k_B = 6.21\,\text{MN/m}$ [34]. The equivalent static load at J, $W = 294\,\text{N}$. The first undamped natural frequency ω_0, of the system with the squeeze film damper (SFD) *shimmed out* was 75 Hz (corresponding to a critical speed of 4500 rpm). The SFD parameters were as in Table 1.

Bearing radius R	68.216 mm
Land length L	9 mm
Radial clearance c	0.216 mm

Table 1: ***SFD geometric parameters (configuration B).***

The oil viscosity $\eta = 21\text{cP} = 0.021\text{Nsm}^{-2}$. The SFD considered was unsealed and a two land model (section 2.1) was used, as in [34]. In [34] the variable film theory (section 2.1.1) was used with an experimentally determined cavitation pressure p_c. In the present work the variable film theory was also used but the cavitation pressure p_c was fixed at –101.325 kPa (*i.e.* absolute zero cavitation). The supply pressure p_S was 34.5 kPa [34].

The arc-length continuation technique was used in the HB solution. All simulations were done for a dynamic load parameter $u = 0.229$, as in [34]. All results presented in the following section refer to the *relative displacement* of the journal J from the bearing housing B.

7.2 RESULTS AND DISCUSSION

Figures 9(a1),(a2) show the variation of the predicted non-dimensional half peak to peak x, y relative displacements with rotational speed. Figures 9(b1),(b2) show the variation of the non-dimensional mean x, y relative displacements with rotational speed. These were predicted using HB with $N = 1$, (*i.e.* fundamental period Γ of limit cycle =period of rotation T, equations (23), (24)) and number of harmonics $m = 5$. Another way of expressing the unbalance response was through harmonic ellipses [3]. From equations (27), the s^{th} harmonic components of the relative displacement in the x and y directions are given by

$$ {}^{s}X(t) = a_X^s \cos s\omega t + b_X^s \sin s\omega t \qquad (150a) $$

$$ {}^{s}Y(t) = a_Y^s \cos s\omega t + b_Y^s \sin s\omega t \qquad (150b) $$

This pair of orthogonal harmonic components forms an ellipse ("harmonic ellipse"). Figure 10(a),(b),(c) show the variation of the semi-major axes of the first three predicted harmonic ellipses with rotational speed.

Figure 11 shows the variation of the rotational speed with the arc-length control parameter σ. From Figures 9-11 it is evident that multiple solutions exist within the speed range 3020 rpm to 3383 rpm. This is especially evident from Figure 11 where, in the range 3020 rpm to 3383 rpm, a given rotational speed corresponds to three different values of σ. The y displacements in Figure 9(a2),(b2) and the harmonic ellipses in Figure 10 reveal a spring *softening* characteristic in the *series* combination considered (*i.e.* SFD in series with bearing housing flexibility). This contrasts with the spring *hardening* characteristic observed in *parallel* combinations (*i.e.* SFD in parallel with retainer spring in rigid bearing housing) [35].

The stability of the computed HB $N=1$, $m=5$ [1] solutions was checked using Floquet Theory (Method II, section 6.2). The monodromy matrix was computed using both the long method (Method IIa) and the fast, approximate method (Method IIb, with $K=200$ in equation (131)). The results are presented in Figures 12(a),(b),(c) which respectively show the variation of the magnitude, real part and imaginary part of the leading multiplier with rotational speed by both Methods IIa, IIb. For Method IIa (section 6.2.2), the fourth-order Runge-Kutta method was used. The results are seen to be virtually identical. Method IIb was found to cut down the computation time from 8 hours (Method IIa) to less that 8 minutes (Method IIb) with negligible loss of accuracy. Hence Method IIa is seen to be useless. It is of the author's opinion that the use of this method in [1], [32] was totally unwarranted.

The stability data as presented in Figure 12 were not found to be easy to interpret, for this problem. Hence, a facility was included in the software to indicate the stability of each HB solution, based on the value of the associated leading Floquet multiplier, directly on the unbalance response curves in Figures 9-11 according to the notation in Table 2.

notation	state of stability
'o'	stable
'+'	unstable, same period instability (section 6.2.1)
' '	unstable, period doubling instability (section 6.2.1)
'*'	unstable, quasi-periodic instability (section 6.2.1)

Table 2: ***Indicators for state of stability of HB solutions in Figures 9-11***

The stability results computed by Floquet Theory were then examined by Method I at the salient points of Figures 9-11. As explained in section 6.1, Method I involved performing a TD integration solution using initial conditions computed from the HB solution. Since a rigid body model was used there was no need to perform a modal decomposition of the HB solution. Consider any convenient figure from Figures 9-11 (*e.g.* Figure 10(a)).

Section A-B (see Figure 10(a)): Along this branch all HB $N=1$ solutions are stable. In Figure 13, the TD solution for point B (3383 rpm) continues to follow the HB computed limit cycle, indicating that it is an attractor.

Section C-D (see Figure 10(a)): Along this branch the HB $N=1$ solutions are unstable (repellors). Trajectories starting close to such limit cycles tend to be repelled to the stable limit cycles of the same period residing on branch A-B. This is illustrated in Figure 14, which refers to point D (3076 rpm).

[1] Note that the value of m merely controls the *accuracy* of the computed limit cycle. Stability analysis naturally assumes that the HB computed limit cycle is fairly accurate.

Section E-E′ (point E′ excluded) (see Figure 10(a)): The HB $N=1$ solutions along this short section are unstable. Trajectories starting close to such limit cycles *initially* tend to flip about the unstable $N=1$ limit cycle, indicating a tendency to double the period. However, no stable $N=2$ limit cycle exists in the vicinity, the flip effect dies out and the trajectory eventually collapses to a stable $N=1$ limit cycle along branch A-B, as in Figure 14. This misleading effect is a direct consequence of the fact that Floquet Theory strictly applies to the immediate vicinity of the limit cycle being tested for stability. Strictly speaking it can only state for certain whether the cycle is stable or not. This is dealt with more fully in section 8.4.2 (Figure 49).

Section E′-F (see Figure 10(a)): Period doubling actually cuts in at E′ rather than E. Along this section, HB $N=1$ solutions are unstable. Trajectories starting close to such limit cycles will be repelled to stable $N=2$ limit cycles as shown in Figure 15, which refers to point E′ (3243 rpm). In Figure 15(d), the return points flip on either side of the first (unstable equilibrium point E on this figure) and eventually congregate at positions A, B. A set of $N=2$ limit cycles along branch E-F on Figure 10(a) was computed using HB, $N=2$, $m=10$. Figure 16(a) shows the variation of the semi-major axis of the first harmonic ellipse (*i.e.* the $\Omega/2$ subharmonic component, Ω being the rotational speed (rad/s)). Hence this curve shows the variation of the strength of the subharmonic component along branch E-F of Figure 10(a) (*which itself refers to* $N=1$ *limit cycles*). An unstable $N=2$ limit cycle at point M (3080 rpm) of Figure 16(a) is shown in Figure 16(b1). This is very similar to the unstable $N=1$ limit cycle at point D (3076 rpm) of Figure 10(a), shown in Figure 14(a). Two stable $N=2$ limit cycles are possible at point F (4277 rpm) of Figure 10(a). These are shown in Figures 16(b2),(b3) and correspond respectively to points O and P of Figure 16(a). As one moves along the curve in Figure 16(a), the two loops of the $N=2$ limit cycles first diverge from each other and then start merging into one another until subharmonic activity dies out.

G (4431 rpm) (see Figure 10(a)): At this point the $N=1$ limit cycle is stable. This is verified in Figure 17.

Section H-I (see Figure 10(a)): Along this short section the HB $N=1$ solutions are unstable, exhibiting a quasi-periodic instability. This is verified in Figure 18, which refers to point H (4655 rpm). As shown in the Poinare Map in Figure 18(d) the return points spiral out from the first (unstable equilibrium point E on this figure) along two spirals and eventually settle down on a drift ring surrounding E.

Section J-K (see Figure 10(a)): Along this section the HB $N=1$ solutions are unstable, exhibiting a period-doubling instability. This is verified in Figure 19, which refers to point J (5149 rpm). As shown in the Poincare Map in Figure 19(d) the return points flip on either side of the unstable equilibrium point E, neatly along a straight line and congregate at A and B.

L- (see Figure 10(a)): Beyond point L the HB $N=1$ limit cycles are stable as verified in Figure 20, which refers to point L (5961 rpm).

Some experimental results obtained from [27] (or [34]) are reproduced in Figure 21. These show that a jump up in the relative displacement does occur as the speed is increased and that the jump is followed by period doubling. Period doubling around the first undamped[1] critical speed ω_0 in a series combination was also experimentally verified in [36] with a test rig of similar configuration and dimensions. Its occurrence in the region of ω_0 was also explained by elementary reasoning in [35], [36].

It has to be mentioned that in [27], [34], dynamic pressures below absolute zero were measured. These appeared as tension spikes, followed by instantaneous recovery to absolute zero in the measured pressure pulse. This means that the oil temporarily withstood tension before rupturing (cavitating). Such a phenomenon was also observed in [17], where a list of references on studies about instantaneous tension in oil is given. In the simulations made in [27], [34], the best value for cavitation pressure p_c was found to be an average between the measured tension spike minimum and absolute zero. However, in this report the spring softening and period doubling effects were still *predicted* using a fixed cavitation pressure of absolute zero.

7.3 CONCLUSION

In this chapter the stability and bifurcation response of an SFD in series with bearing housing flexibility around the first undamped critical speed was studied using a realistic predictive model for the SFD based on absolute zero cavitation. The study was confined to a rigid rotor. The system dynamics were found to be particularly rich, exhibiting a jump, period doubling bifurcations and a secondary Hopf bifurcation (quasi-periodicity). The series combination was found to exhibit a spring softening characteristic in contrast to the spring hardening characteristic observed in parallel combinations. The predicted jump-up in relative displacement and period doubling agreed with experimental observations.

[1] SFD shimmed out.

CHAPTER 8

ANALYSIS: CONFIGURATION A

In this chapter a quantitative and qualitative analysis of a test rig that can be modified to configurations A1 or A2 (Figure 5) is presented. Simulations from harmonic balance and time domain analyses are compared with each other and with experimental data from the test rig.

8.1 DESCRIPTION OF TEST RIG

The test rig (see Figure 22) used is housed in the Mechanical Engineering laboratories of the University of Southampton. Experimental work has been previously carried out on this rig and is described in [16]. Referring to Figure 22, a motor driven pulley (1) drives the mild steel stepped shaft (4) through a flexible coupling (2). The shaft has two self-aligning ball bearings (3), (6). The one on the left hand end (3) is rigidly housed. A ring (the *squeeze ring*) is shrunk onto the outer race of the ball bearing on the right hand end (6). The complete assembly (forming the *journal*, J) is free to move within the clearance of the rigidly supported bearing housing B (7). Oil is pumped into this clearance via three equi-spaced holes in B around a central circumferential groove to provide the squeeze film damping. The damper is unsealed (as in Figure 1(a)). A disc (8) is carried on the overhung portion at U to which unbalance masses can be attached.

In configuration A1, four flexible bars (5), forming a squirrel cage, connect the squeeze ring assembly J to the rigid frame (9) at F. Hence, these bars (forming the *retainer spring*) are in parallel with the squeeze film. However, since they are grounded at F, one can vary the static misalignments ε_{0xJ}, ε_{0yJ} of J by moving the bearing housing B (as mentioned in section 5.1.1). The retainer spring fully or partially supports the static load (see section 5.1.1). The spring also prevents the outer race of the journal J (*i.e.* the squeeze ring) from rotating. In configuration A2 the bars (5) are removed and the journal J rests on the bottom of the clearance in the static condition. Also, an anti-rotation bolt is used to prevent the squeeze ring from rotating with the shaft, as explained in [16]. For configuration A2, the equivalent static load to be borne by the squeeze film was computed as 151 N.

Safety regulations did not allow the rotational speed to exceed 100 rev/s (6000 rpm). Simulations revealed that the effect of the stiffness of the ball bearing (3) (typically of the order of 10^{10} N/m) had virtually no effect on the dynamics of the rig over a frequency range covering at least five times the top rotational speed of 100 rev/s. Hence (3) corresponds to the fixed pivot H in Figure 5. On the other hand, J will be a rigid mass attached to the shaft. The first two *undamped* natural frequencies of the rig in configuration A1 (*i.e.* pinned at H, sprung at J) were computed as 14 Hz and 40 Hz by the mechanical impedance technique. With the squeeze film damper shimmed out

(*i.e.* with shaft pinned at both H and J) the first two undamped natural frequencies were computed as 31 Hz and 91 Hz.

Vibration in the x and y directions was monitored at three locations: the squeeze film position J, the disc position U and the mid-shaft position M. The latter position is roughly the mid-point of the 50 mm diameter portion of the shaft. The x, y vibrations at the three positions J, U and M (Figure 22) were measured by three pairs of orthogonal displacement transducers. The support bracket for each transducer was of stiff aluminium construction and fixed to the rigid frame of the rig (9). The rigidity of these support brackets over the operational speed range was verified in [16].

The parameters of the squeeze film damper (SFD) are given in Table 3 [16].

Bearing radius R	50.022 mm
Land length L	9.72 mm
Radial clearance c	0.132 mm

Table 3: ***SFD geometric parameters (configuration A).***

The experimental results presented for configurations A1 and A2 came from different sources. For A1 the experimental work was conducted by the author of this report. For A2, the experimental data were obtained from [16]. In [16] the groove depth h_g was 1.82 mm. Since then the groove has been deepened to 5.25 mm. Hence, for the SFD in configuration A2 the ratio on the left hand side of the inequality (1), section 2.1, was 0.07 (< 0.1). For the SFD in configuration A1 the ratio was equal to 0.02 (< 0.1). In both cases the rato satisfies the inequality (1). Hence the two land model (section 2.1) for the squeeze film was assumed to be applicable to both SFDs used. Evidently, it was much more accurate for the SFD used in A1.

The oil used in the SFD was calibration fluid C Shell with viscosity of 0.006 Nsm^{-2} at 21°C. The viscosity changes mostly between 20°C-25°C when it is reduced to 0.005 Nsm^{-2} [16]. The viscosity at the average operational temperature was taken as 0.0045 Nsm^{-2}, as in [16]. This value was used in all simulations. Hence no measurements were carried out before the oil temperature reached 25°C. The oil temperature was measured at the oil-collecting tray, directly below the SFD.

8.2 SIMULATIONS

8.2.1 Configuration A1

For configuration A1 two static misalignment conditions were considered: $\varepsilon_{0yJ} = -0.6, -0.8$. In both conditions $\varepsilon_{0xJ} = 0$. For each misalignment condition, the responses for two different

unbalances at U were computed : $U = 2.59\times10^{-4}$ kgm and $U = 5.10\times10^{-4}$ kgm. The simulations carried out were as follows:

(a) Solution of the harmonic balance equations (82) with $N = 1$ (*i.e.* fundamental period Γ = period of rotation T, equations (23), (24)) and $m = 5$ harmonics for the speed range 10-100 rev/s using arc-length continuation.
(b) Stability analysis of the response computed in (a), using the fast Method IIb with $K = 200$ (section 6.2.2, equation (131)).
(c) Confirmation of the stability results obtained in (b) at selected speeds by using Method I (section 6.1, equations (110)-(112), (98)). Poincare maps were used where appropriate.

The simulations were performed using two different cavitation models for the SFD (section 2.1): full film theory (*i.e.* no cavitation), and absolute zero cavitation theory (*i.e.* variable film theory with the cavitation pressure p_c set to absolute zero, -101.325 kPa). The supply pressure p_S was 1 bar. These two theories where used to investigate the influence of cavitation in the SFD on the predicted dynamic behaviour.

The receptances of the shaft supported by the spring (5) (Figure 22) were computed using the mechanical impedance technique [9]. As explained in [9] the shaft element impedance matrices incorporate both distributed stiffness and distributed inertia effects and are exact, regardless of the element size, so long as the element is uniform. Shear deformation was taken into account. Since gyroscopic effects were neglected in all equations in chapter 6, rotatory inertia (transverse and polar moment of inertia) was neglected for both the shaft elements and the attachments. The model input into the *MATLAB*® mechanical impedance program *REC.m* is described in Table 4.

station / element	**No. /** No.	diameter (mm)	length (m)	**attached mass (kg)**	**attached stiffness (kN/m)**	**fixed pivot?**
station	**1**			**0.15176**		
element	1	16.000	0.0200			
station	**2**			**0.06922**		
element	2	25.405	0.0290			
station	**3**					**yes**
element	3	25.405	0.0440			
station	**4**					
element	4	50.000	0.7150			
station	**5**					
element	5	25.405	0.2620			
station	**6**			**1.35667**	**123.4**	
element	6	25.405	0.0130			
station	**7**					
element	7	25.385	0.2093			
station	**8**			**6.40390**		
element	8	25.385	0.0127			
station	**9**					

Table 4: ***Summary of input into mechanical impedance program.***
(Data in bold type refers to the stations, data in light type refers to the elements).

As can be seen from Table 4 the model has 8 elements and hence, 9 stations, of which station 3 (H) is a fixed pivot and station 6 (J) is sprung. The small mass of the coupling hub at the left hand end of the shaft in Figure 22 was lumped at stations 1 and 2. The squeeze ring assembly mass was lumped at station 6 and the disc mass at station 8. It was naturally assumed that the left hand end of the shaft was free of any shear force and bending moment (flexible coupling).

For the time domain and stability analyses the appropriate receptances were decomposed as in section 4.2. The first five undamped natural frequencies $\omega_{xr} = \omega_{yr} = \omega_r$, $r = 1 \ldots 5$ were computed as explained in section 4.2 and are given in Table 5.

mode no. r	$f_r = \omega_r/(2\pi)$ (Hz)	A^r_{JJ} ($\times 10^{-3}$kg^{-1})	A^r_{JU} ($\times 10^{-3}$kg^{-1})
1	13.7	54.235	77.803
2	40.4	38.334	-34.209
3	173.9	251.196	-38.783
4	334.7	104.839	-13.606
5	749.1	19.513	0.207

Table 5: ***Undamped modal parameters of linear system (A1)***

The modal constants A^r_{ij} $(= B^r_{ij})$, $r = 1...5$ of the appropriate receptances α_{ij} $(= \beta_{ij})$ were computed according to the procedure described in section 4.2. Table 5 gives the modal constants A^r_{JJ}, A^r_{JU}, $r = 1...5$. The fitting frequency range was 0-500 Hz. This range hence covered 5 harmonics of the top rotational speed of 100 rev/s. When integrating the time domain equations (98) the number of modes used was reduced to 4 *i.e.* A^5_{ij} $(= B^5_{ij})$ was not used. This was done to avoid problems of stiffness (section 4.4). The accuracy of this simplification was ascertained *a priori* from Figures 23. These figures respectively give the point receptance α_{JJ} and the transfer receptance α_{JU}. In each figure the solid line gives the exact receptance and the dashed line gives the approximate receptance reconstructed from 4 modes (*i.e.* using the first 4 terms in the series in equation (54)). Satisfactory agreement is guaranteed up to 500 Hz.

In simulations (c), when generating the initial modal state variables from the modal decomposition of the harmonic balance solution, it was considered prudent to retain the fifth mode. This is due to reasons given in section 6.1, relating to the conditioning of the matrices in equations (111). As explained in this section, the additional initial modal state variables generated were then dropped when forming the initial conditions vector $\mathbf{s_0}$ (equation (112)). In the simulations (b), where Method IIb was used, the addition of the fifth mode, despite increasing the size of the matrices $\mathbf{W_k}$ in the exponents of the product (131), hardly affected the speed of computation. However, its inclusion hardly influenced the accuracy of the results.

8.2.2 Configuration A2

For configuration A2 only one unbalance $U = 5.10 \times 10^{-4}$kgm was considered. The absolute zero theory was used as the cavitation model since the full film theory gives no lift for the case of no retainer spring [17]. Moreover, the half film theory (section 2.1.1) overestimates the vibration [17]. The supply pressure p_S was 1.2 bar. Simulations (a) to (c) in section 8.2.1 were performed on equations (82), (101). In addition, the time domain equations (101) were integrated over 120 revolutions for each speed in the range 24-100 rev/s, steps of 2 rev/s. A waterfall diagram was constructed from the fast fourier transforms (FFTs) of the last 0.5s of each solution. The

frequency resolution was hence 2 Hz, as that used in the measurements [16]. Analysing the last 0.5s of each solution also meant that the number of revolutions neglected was *at least* 70 (at 100 rev/s). This was considered sufficient to eliminate the transient vibration. The initial conditions for a given speed were obtained from the final conditions of the previous speed. For the first speed the initial conditions vector $\mathbf{s}_0$ was given by

$$\begin{aligned}\mathbf{s}_0 &= \left[0 \quad x_J^1(0) \quad y_J^1(0) \quad \cdots \quad x_J^4(0) \quad y_J^4(0) \quad x_J'^1(0) \quad y_J'^1(0) \quad \cdots \quad x_J'^4(0) \quad y_J'^4(0)\right]^T \\ &= \left[0 \quad 0 \quad -0.99 \quad 0 \quad \cdots \quad 0\right]^T,\end{aligned}$$

which corresponds to the shaft lying at the bottom of the clearance circle. For speeds lower than 24 rev/s no lift was obtained due to the low oil viscosity.

For the receptance computation, the input into the mechanical impedance program *Rec.m* was identical to that in Table 4 except that no spring was included at station 6 (J). As for A1, the receptance decomposition for the time domain and stability analysis was done over 5 modes for a frequency range of 0-500 Hz. Table 6 gives the first five undamped natural frequencies and the modal constants A_{JJ}^r, A_{JU}^r, $r = 1 \ldots 5$.

mode no. r	$f_r = \omega_r/(2\pi)$ (Hz)	A_{JJ}^r ($\times 10^{-3}\text{kg}^{-1}$)	A_{JU}^r ($\times 10^{-3}\text{kg}^{-1}$)
1	0	66.771	81.309
2	39.0	31.507	-36.914
3	171.6	248.118	-39.777
4	334.2	102.339	-13.415
5	749.0	19.438	0.207

Table 6: ***Undamped modal parameters of linear system (A2)***

When integrating the time domain equations only 4 modes were used, as for A1. The accuracy of this simplification was ascertained *a priori* from Figures 24, which respectively give the point receptance α_{JJ} and the transfer receptance α_{JU}. In each figure the solid line gives the exact receptance and the dashed line gives the approximate receptance reconstructed from 4 modes (*i.e.* using the first 4 terms in the series in equation (54)). Satisfactory agreement is again guaranteed up to 500 Hz. As for A1, the fifth mode was retained in the modal decomposition of the harmonic balance solution in simulation (c) (section 8.2.1). It was also retained for simulation (b).

8.3 EXPERIMENTAL WORK

8.3.1 Configuration A1

In this work the displacement transducers at positions J and U were *Bently Nevada 3300XL®* (eddy current probes). The transducers at M were *Hypertone®* (capacitance probes). Details on the calibration of the probes is given in Appendix B.

Referring to Figure 22, the static eccentricities (misalignments) of the journal J from the bearing housing B were adjusted by loosening the screws bolting B to the frame at G. A small clearance in the screw holes through B allowed its position to be adjusted prior to retightening. The adjustment of the eccentricity was complicated by the initial bend in the shaft which meant that the static misalignment varied as the shaft was turned. A dial test indicator with its stem pressed against the shaft close to the SFD position revealed that as the shaft was rotated slowly, the run-out at the SFD position was around 0.0425mm in the vertical direction. This run-out corresponded to around 30% of the radial clearance of the damper. The run-out was significantly lower in the horizontal direction, suggesting that gravity effects aggravated the run-out. Hence, as the shaft was rotated manually, J traced out an elliptical orbit within the clearance with its major axis approximately vertical. Efforts were made to centre this orbit at the desired static eccentricities (*i.e.* $\varepsilon_{0xJ}, \varepsilon_{0yJ} = 0.0, -0.6$ in one case, and $\varepsilon_{0xJ}, \varepsilon_{0yJ} = 0.0, -0.8$ in the other). Hence, the eccentricity was adjusted in the vertical and horizontal directions for four angular positions (0°, 90°, 180°, 270°) of the shaft. The angular position 0° corresponds to the "high spot" on the shaft at the SFD position. For each direction x, y the average eccentricity for the four angular positions was brought as close as possible to the desired eccentricity in that direction. The static misalignment was rechecked after each experiment when the rig was hot. Details are found in Appendix B.

For each misalignment condition, the unbalance response was measured for $U = 2.59 \times 10^{-4}$ kgm and for $U = 5.10 \times 10^{-4}$ kgm. Vibration data (time histories) were obtained from all six transducers for each speed in the range 10-100 rev/s, in steps of 2 rev/s. An eight channel *HP3566A® Analyzer* coupled with a personal computer (pc) was used to capture the time histories. The time capture length was 0.5s with a sampling rate of 4096/s. Hence the frequency spectrum of the data was 0-1.6 kHz with frequency resolution of 2 Hz. This resolution was generally considered adequate since a 2 rev/s step was the smallest attainable with the speed controller. However, the data length was increased to 2s at those speeds where a more detailed frequency spectrum was required. The data were converted to *MATLAB®* data format using the *sdftoml©* data conversion program and analysed in *MATLAB®* were peak-to-peak amplitudes and the frequency spectrum for each speed could be computed. Unlike [16], the *HP3566A® Analyzer* was set to measure the "dc" component of the vibration. The procedure followed is explained in Appendix B.

As in [16], cavitation effects were monitored by observing closely the oil just as it came out of the annular clearance. Cavitation was characterised by tiny pin-hole bubbles in the oil. This was observed over certain speed ranges. Table 7 below summarises the four experiments conducted and the speed ranges where cavitation was observed.

ε_{0xJ}	ε_{0yJ}	U ($\times 10^{-4}$ kgm)	p_S (bar)	start temperature (°C)	finish temperature (°C)	cavitation speed range (rev/s)
0.0	-0.6	2.59	1	32	36	-
0.0	-0.6	5.10	1	25	33	30-34
0.0	-0.8	2.59	1	25	33	30-36, 86-92
0.0	-0.8	5.10	1	25	33	30-36, 80-100

Table 7: ***Summary of experimental conditions***

It is important to note that the cavitation speed ranges in Table 7 tend to agree with those obtained Burghardt [16] who worked with static eccentricities $\varepsilon_{0yJ} = -0.4, -0.8$ and a supply pressure 1.2 bar.

In these experiments no attempt was made to compensate for the effect of the residual unbalance on the measurements.

8.3.2 Configuration A2

The experimental work for this configuration is explained in [16]. It suffices to say here that as in the previous section, vibration data (time histories) were obtained from all six transducers for each speed in the range 8-100 rev/s, in steps of 2 rev/s, using the *HP3566A® Analyzer* and pc. However, the *HP3566A® Analyzer* was set to measure only the alternating ("ac") component of the vibration only. The time capture length was 0.5s and the sampling rate was 2048/s. Hence the frequency spectrum of the data was 0-800 Hz, resolution 2 Hz. The data was processed in *MATLAB®* as explained in the previous section.

8.4 RESULTS AND DISCUSSION

8.4.1 Configuration A1

Half peak to peak unbalance response

In Figures 25-28 the experimentally determined unbalance response (half peak to peak amplitude) in the x and y directions at the locations J, U, M is compared with the HB, $N=1$, $m=5$ prediction. Figures 25, 26 both refer to a static eccentricity $\varepsilon_{0yJ} = -0.6$ and to unbalances $U = 2.59\times10^{-4}$ kgm and $U = 5.1\times10^{-4}$ kgm respectively. Figures 27, 28 both refer to a static eccentricity $\varepsilon_{0yJ} = -0.8$ and to unbalances $U = 2.59\times10^{-4}$ kgm and $U = 5.1\times10^{-4}$ kgm respectively. In all measured and predicted responses an anti-resonance speed of around 52 rev/s is evident. This corresponds to the anti-resonance in the transfer receptance α_{JU} (52 Hz) in Figure 23(b).

In Figure 25 ($\varepsilon_{0yJ} = -0.6, U = 2.59\times10^{-4}$ kgm) it is seen that the full film theory works reasonably well and it was not felt necessary to redo the simulation with absolute zero cavitation theory. This agrees with experimental observation of no cavitation (Table 5). The discrepancies at the mid-shaft position M are attributed to the effects of residual unbalance and the lower sensitivity of the probes used at M (~2 V/mm) when compared to those at J and U (~8 V/mm). In the x direction (where the SFD is centralised) two maxima are observed in both measurement and prediction at the SFD (J) and disc (U). These are quite close to the undamped natural frequencies of configuration A1 (pinned-sprung shaft), 14 rev/s, 40 rev/s (Table 5). In the y direction (where the SFD is offset) the first maximum is not present while the second one occurs at a lower speed (around 32 rev/s). Hence the behaviour in the y direction is more akin to the pin-pin configuration (first natural frequency 31 Hz, see section 8.1, end of third paragraph).

The weakness of the full film theory becomes apparent at the higher unbalance of $U = 5.1\times10^{-4}$ kgm (Figure 26) around 30-34 rev/s, which is the zone of maximum amplitude. Outside this region predictions from both full film and absolute zero cavitation theories give identical results. This suggests that cavitation occurs only around 30-34 rev/s, as observed in experiment (Table 5). The full film theory predicts extremely high vibration at around 30-34 rev/s at positions other than the SFD (*i.e.* at U and M) which were (fortunately) not verified in practice. It is important to note that the arc-length continuation technique revealed this effect in all its detail since the process "climbs" along the unbalance response curve, as explained in section 3.4. If rotational speed were used as control parameter the high amplitude effect would have appeared less stark since the process would have "cut across" the zone 30-34 rev/s in the horizontal direction.

The failure of the full film theory becomes even starker at a higher eccentricity $\varepsilon_{0yJ} = -0.8$ (Figures 27, 28). Discrepancies between the full film and absolute zero cavitation theories emerge not just in the 30-36 rev/s zone, but, for the y direction especially, in the 80-100 rev/s zone (Figures 27(b),(d),(f) and Figures 28(b),(d),(f)). This suggests that cavitation also occurs in the range 80-100 rev/s, which agrees with experimental observation (Table 5).

From the full film unbalance response predictions in Figures 26-28 it is evident that as the y static eccentricity and unbalance is increased an uncavitated SFD causes the rotor to behave in certain speed ranges as though it were pinned at the SFD journal J. This tendency is especially strong in the y direction at the higher static eccentricity of -0.8. The critical speeds tend to ~32 rev/s for $\varepsilon_{0yJ} = -0.6$, $U = 5.1\times10^{-4}$ kgm and to ~31 rev/s, ~91 rev/s for $\varepsilon_{0yJ} = -0.8$. Cavitation in the SFD around these speeds eliminates the pinning effect at J and maintains the vibration at acceptable limits at all positions along the rotor. In the case of $\varepsilon_{0yJ} = -0.8$, cavitation completely attenuates the second pin-pin critical speed of 91 rev/s (Figures 27(b),(d),(f) and Figures 28(b),(d),(f)) both in the predictions and the measurements. The vibration attenuation at these speeds is a direct result of the lift produced by the cavitation effect. It is well known that cavitation results in lift of the journal [15], [17]. Figure 29 compares the mean y displacements

(lifts) for $\varepsilon_{0yJ} = -0.6$, $U = 5.1\times10^{-4}$ kgm predicted with the full film and absolute zero theories. Figures 30(a),(b) compare the lifts predicted with both theories for $\varepsilon_{0yJ} = -0.8$ and $U = 2.59\times10^{-4}$ kgm, $U = 5.1\times10^{-4}$ kgm respectively. In these figures it is evident that cavitation lifts the journal roughly within the speed ranges in Table 5. Elsewhere there is no lift from the static position, as for the full film prediction. In the range 30-34 rev/s the predicted amplitude of vibration at the SFD is high by both theories. However, since there is no lift in the full film prediction, the minimum oil film thickness at the base of the clearance is extremely small, due to the static offset in the y direction. This results in excessive damping forces, effectively causing instantaneous pinning of the shaft at J, and consequently excessive vibration at all other positions (like U and M). On the other hand, the lift produced by cavitation counters the static eccentricity and hence results in a larger minimum oil film thickness. Hence the lift eliminates this instantaneous pinning effect at J, keeping the amplitudes at all other locations low.

Orbital Motion

In Figures 31, 32, 33 the orbital motion in the resonance region (26-38 rev/s) is presented for $\varepsilon_{0yJ} = -0.6$, $U = 2.59\times10^{-4}$ kgm (Figure 31), $\varepsilon_{0yJ} = -0.6$, $U = 5.1\times10^{-4}$ kgm (Figure 32) and $\varepsilon_{0yJ} = -0.8$, $U = 5.1\times10^{-4}$ kgm (Figure 33). The predictions are HB, $N = 1$, $m = 5$ with the appropriate cavitation model (*i.e.* full film in Figure 31, absolute zero cavitation in Figures 32, 33). Overall, it is seen that the orbital motion was reasonably well predicted. In particular one notes the following.

(a) The reasonable agreement of the predicted and measured SFD orbits in size, shape and orientation.
(b) The elliptical shape of the disc orbits in both measurement and predictions. Note that the glitches caused by the lack of roundness of the disc periphery where the displacement was measured resulted in spiky and jagged orbits at U.
(c) The change in orientation of both the SFD and disc orbits as the range 26-38 rev/s was traversed.
(d) The kinks in both measured and predicted orbits at mid-shaft M (Figures 31(c3), 32(a3),(b3), 33(b3),(c3). These kinks disappeared at 38 rev/s in both measured and predicted orbits (Figure 31(d3), 32(f3), 33(f3)).

Aperiodic motion was measured for $\varepsilon_{0yJ} = -0.6$, $U = 5.1\times10^{-4}$ kgm in the range 32-34 rev/s (Figures 32(c),(d)) and for $\varepsilon_{0yJ} = -0.8$, $U = 5.1\times10^{-4}$ kgm in the wider range 30-36 rev/s (Figures 33(c),(d),(e)). Aperiodic motion was also measured for $\varepsilon_{0yJ} = -0.8$, $U = 2.59\times10^{-4}$ kgm, but only at one speed (30 rev/s). Naturally, the harmonic balance method could not predict such motion. However, as seen from Figures 32(c1),(d1) and 33(c1),(d1),(e1) the HB computed SFD orbit fitted nicely around the outer loop of the measured SFD orbit. Hence the peak to peak vibrations were still adequately predicted with HB in this speed range. Also, as seen from

Figures 32(b1), 33(b1) the SFD orbits were over predicted. This suggests that cavitation actually started at a slightly higher speed than predicted.

In order to explain the measured aperiodic motion, the stability of the HB $N=1$ solutions needed to be examined.

Stability of HB solutions

Figure 34(a),(b) shows the results of the fast stability check (Method IIb) made on the HB, $N=1$, $m=5$ solutions for $\varepsilon_{0yJ}=-0.6$, $U=2.59\times10^{-4}$kgm (*full film*) and $U=5.1\times10^{-4}$kgm (*absolute zero cavitation*). All solutions were found to be stable. This was confirmed by spot checks made using Method I at selected speeds. Two results of such a check are presented in Figures 36 and 37. In Figure 36 the HB ($N=1$, $m=5$) and time domain (TD) orbits at 32 rev/s are compared for $\varepsilon_{0yJ}=-0.6$, $U=2.59\times10^{-4}$kgm, full film theory. The initial conditions for the TD solution were obtained by doing a modal decomposition of the HB solution. As can be seen, the TD orbit remains on the HB orbit after 10 shaft revolutions, indicating that the HB computed limit cycle is indeed an attractor. In Figure 37 the same is performed on the orbit at 90 rev/s for $\varepsilon_{0yJ}=-0.6$, $U=5.1\times10^{-4}$kgm, absolute zero theory. As can be seen, the HB orbit is an attractor. The slight initial perturbations in the disc (U) and mid-shaft (M) responses, Figure 37(b),(c) are due to slight errors in the initial modal state variables computed by the modal decomposition technique. This example at 90 rev/s is included to demonstrate that the TD method with number of modes $q=4$ is accurate even at such high speeds (as ascertained previously from Figures 23).

Figure 35 shows the results of the fast stability check (Method IIb) made on the HB solutions ($N=1$, $m=5$) for $\varepsilon_{0yJ}=-0.8$. Figure 35(a) refers to the unbalance $U=2.59\times10^{-4}$kgm, absolute zero cavitation. All solutions were found to be stable. Figure 35(b1) refers to the unbalance $U=5.1\times10^{-4}$kgm, absolute zero cavitation. It is evident that in the rotational speed region 32-35 rev/s the HB $N=1$ solutions are unstable. From Figure 35(b2) it is seen that the leading multiplier in this region is complex. This indicates that the motion in the region 32-35 rev/s tends to quasi-periodicity. This was then verified by Method I. Three speeds were considered: 30, 34, 38 rev/s. The first and last (30, 38 rev/s) are outside the instability zone and the middle (34 rev/s) within it. Figure 38 refers to 30 rev/s. In Figures 38(a1)-(a3) the TD solution over 10 revolutions with initial conditions derived from the HB solution is overlaid on the HB solution. The small initial perturbations were due to slight errors in the initial modal state variables. In fact, Figures 38(b1)-(b3) show the TD solution over a further 5 revolutions: the perturbations have disappeared and the TD solution remains closely matched to the HB solution, indicating that the HB computed $N=1$ limit cycle at 30 rev/s is an attractor. The same applies to Figure 39, which refers to speed 38 rev/s. The HB computed $N=1$ limit cycle at 38 rev/s is an attractor. Figure 40 refers to the speed 34 rev/s. As can be seen, the $N=1$ limit cycle is a

repellor[1]. The TD solution in Figure 40 is over 80 shaft revolutions. The TD solution was continued over a further 80 revolutions and a Poincare map constructed for the complete motion (160 revolutions) (see Figure 41). As can be seen from Figure 41, the return points (*i.e.* sampled points) spiral out from the first (point E, on unstable limit cycle) along 4 spirals and settle down on a drift ring around the unstable equilibrium point E. This confirms that the 32-35 rev/s zone is indeed a quasi-periodic zone, as indicated by the fast Method IIb (Figure 35(b1), (b2)). In Figure 42 the TD predicted steady state quasi-periodic motion at 34 rev/s (last 80 revolutions out of 160) is compared with the corresponding measurement. The time capture data length for this speed was increased from 0.5s to 2s. As can be seen from Figures 42(a1), (b1) both measured and predicted SFD orbits consist of two sets of "opposing" loops interwoven into one another, although in the predicted orbit they are more densely interwoven. The similarity between prediction and measurement is more striking for the disc position U (Figures 42(a2), (b2)) and the mid-shaft position M (Figures 42(a3), (b3)). The frequency spectra for measurement and prediction at the SFD at 34 rev/s are shown in Figure 43. The frequency resolution is 0.5 Hz. Subsynchronous activity is evident in both measurement and prediction. A strong 9 Hz component was predicted in both x and y directions. This 9 Hz component was measured only in the y direction (Figure 43(b2)). Additional frequency components were measured at 13 Hz and 21 Hz. The 21 Hz component is the difference between the 34 Hz and 13 Hz components. The 13 Hz component was not predicted. A fairly strong 25 Hz component was predicted in the y direction. This is the difference between the 34 Hz component and the 9 Hz component. The predicted second order subharmonic (17 Hz) was negligible. The measured one was more significant. This explains why the two sets of opposing loops in the measured SFD orbit (Figure 42 (b1)) are not densely woven into each other. Both measured and predicted spectra show some frequency components between the 34 Hz and 68 Hz components. The predicted 43 Hz component is the sum of the 9 Hz and 34 Hz component.

The questions remain as to why the measured aperiodic motion in Figure 32(c),(d) for $\varepsilon_{0yJ} = -0.6$, $U = 5.1\times10^{-4}$ kgm was not predicted (Figure 34(b)) and why the predicted aperiodic region for $\varepsilon_{0yJ} = -0.8$, $U = 5.1\times10^{-4}$ kgm (*i.e.* 32-35 rev/s) was not as wide as measured (30-36 rev/s). If one compares Figures 34(b) and 35(b1), it is seen that for given unbalance, the effect of increasing static misalignment is to shift the stability curve upward and its peak (around 34 rev/s) further into the unstable quasi-periodic zone. Now, as mentioned previously, the run-out of the shaft at the SFD in the vertical direction results in a variable static misalignment. The values for ε_{0yJ} used in the simulations are based on averages (see Tables B1, B2, Appendix B). For the ideal condition $\varepsilon_{0yJ} = -0.6$ the static misalignment can be as high as -0.8 at $\theta = 180°$ in Tables B1(a2),(b2). This explains the measurement of aperiodic motion in the region 32-34 rev/s for $\varepsilon_{0yJ} = -0.6$, $U = 5.1\times10^{-4}$ kgm. For the ideal condition $\varepsilon_{0yJ} = -0.8$ the static misalignment can be as high as –1.0 at $\theta = 180°$ in Tables B2(a2),(b2). This explains why the measured region of aperiodic motion for $\varepsilon_{0yJ} = -0.8$, $U = 5.1\times10^{-4}$ kgm was wider than predicted. The variable static eccentricity may also have introduced a chaotic element into the

[1] The limit cycle is indicated in ***** in Figure 40 to increase visibility.

motion which may explain why the measured SFD orbit in Figure 42(b1) was not as "neat" at the predicted SFD orbit in Figure 42(a1). This chaotic element may also explain the "fuzziness" in the measured frequency spectra, Figure 43(b1),(b2), which is a characteristic of chaotic motion [12]. Preliminary processing of data acquired with $\varepsilon_{0yJ} < -1.0$ (*i.e.* retainer spring supporting only part of the static load in the static condition) gave neater aperiodic SFD orbits in the region 30-36 rev/s, with less fuzzy spectra, possibly due to an invariant static misalignment.

It should be mentioned that it does not seem possible to construct Poincare maps from measurements. The reason for this is that the rotational speed can never be determined exactly. If the measured motion is T periodic (T = the rotational period), small errors in the rotational speed (=sampling frequency of map) will cause a cumulative drift in the return points, which should otherwise all coincide. Hence T periodic motion would appear aperiodic, over several revolutions. This means that any measured aperiodic motion cannot be identified as being either quasi-periodic or chaotic motion using the Poincare map as was done on the predicted aperiodic motion in Figure 41.

8.4.2 Configuration A2

Measured *vs.* HB predicted unbalance response

Figure 44 shows the experimentally determined unbalance response (half peak-to-peak) compared with the HB prediction for $N=1$, $m=5$, absolute zero cavitation. The following observations can be made.

(a) At the SFD and in the y direction especially, there is hardly any vibration except in the regions around 31 rev/s and 90 rev/s. These correspond to the first two undamped natural frequencies of the pinned-pinned shaft (31 Hz, 91 Hz).
(b) Around the first critical speed (31 rev/s) the predicted motion is very complicated with multiple solutions. The arc-length continuation technique was the only method of solution.
(c) The SFD vibration around the second critical speed (~90 rev/s) is grossly under-predicted by the HB $N=1$, $m=5$ method.
(d) The recorded values for half peak-to-peak amplitude at the SFD in the y direction around the first two critical speed regions were actually greater than the radial clearance. It was reported in [16] that the shaft shook violently in these regions and the anti-rotation bolt (preventing the squeeze ring from rotating) was not very effective. Since the probes measured the displacement of the squeeze ring, its rotation was probably responsible for this discrepancy.

From Figure 45 it is predicted that the journal J lifts only around 30 rev/s and 90 rev/s. At other speeds it rests at the base of the clearance. This matches with observations made in [16], although the HB predicted lift around 90 rev/s was much smaller than observed.

Stability and orbital motion

Figure 46 presents the results of the fast stability check (Method IIb) on the HB $N=1$, $m=5$ solutions. As can be seen, the HB solutions outside the critical speed regions are on the threshold of stability. Around the first critical speed (30-31 rev/s) a multiplicity of solutions exists, some of which are stable, some unstable. Beyond 82 rev/s all the HB computed $N=1$ limit cycles are clearly unstable. This explains why the SFD vibration and lift beyond ~80 rev/s were grossly under-predicted by HB, $N=1$. The results in Figure 46 were next confirmed at the salient points using Method I.

In Figure 47 an HB $N=1$ limit cycle at 31 rev/s found to be stable by the fast Method IIb is checked by Method I. For accuracy, the number of harmonics m is increased from 5 to 8. Figure 47(a) shows the time domain integration solution ($q=4$) over 20 revolutions with initial conditions derived from the HB solution. Considerable *initial* perturbations are obtained. These are not attributed to instability of the orbit but to errors in the initial modal state variables computed by the modal decomposition technique. These perturbations virtually disappear over a further 5 revolutions, Figure 47(b1)-(b3), and the TD trajectory follows the HB computed $N=1$ limit cycle, proving that it is indeed an attractor. As can be seen from Figure 47(b1) the inaccuracy of the $N=1$, $m=8$ solution (evident along the upper part of the orbit) was responsible for the errors in the initial modal state variables and hence the initial ruffling of the TD trajectory in Figure 47(a). The stable HB orbits at 31 rev/s were found to fit very closely around the measured orbits *for 30 rev/s* (see Figure 48(a1),(a2)). Note that the resolution of the speed controller was not better than 2 rev/s and the tachometer measured speed to the nearest 1 rev/s. Figures 48(b1),(b2) and 48(c1),(c2) show predictions and measurements at 32 rev/s and 36 rev/s respectively. Only the disc and mid-shaft orbits are shown since the SFD measurements were spoilt by the rotation of the squeeze ring. For direct comparison with the ("ac") measurements, the "dc" component of the HB predictions was removed. Not that the kinks at the upper part of the measured mid-shaft orbits in Figure 48(a2),(b2) were predicted by the HB method.

As mentioned earlier, the HB $N=1$ solutions are clearly unstable for the range 82-100 rev/s. Figure 46(b2) indicates that the instability is of the quasi-periodic type (critical multiplier complex). However, a small region AB (85-87 rev/s) exists where the critical multiplier is real and negative, indicating a period doubling instability (see Figure 46(b2)). This phenomenon is investigated in Figure 49 where the stability of the SFD limit cycle at 86 rev/s computed by HB, $N=1$, $m=5$ is investigated by Method I. Figure 49(a) shows the evolution of the TD solution with initial conditions derived from the HB solution, over 20 shaft revolutions. As can be seen, the trajectory flips neatly on either side of the unstable HB computed limit cycle. This also shows up in the Poincare map of the first 20 revolutions (Figure 49(b)): consecutive return points, enclosed in circles and squares respectively, flip on either side of the first (unstable equilibrium point E). This indicates that the critical multiplier is indeed real and negative. However, a stable $N=2$ limit cycle does not exist in the vicinity of the unstable $N=1$ limit cycle, the flip effect dies out and the trajectory evolves as shown in Figure 49(c), over a further 80 revolutions. This

example highlights the fact that while the leading Floquet multiplier can definitely indicate instability, it can only indicate the potential to a certain type of stable motion in the vicinity of an unstable limit cycle.

The stable orbital motion beyond 82 rev/s is next considered. The predictions were obtained by computing the time domain response over the range 24-100 rev/s as explained in the beginning of section 8.2.2 (page 69).

Figure 50 refers to the orbital motion at the SFD at 84 rev/s. Figure 50(a) shows the prediction (last 80 revolutions out of 180). Figure 50(b) shows the corresponding Poincare map. Figure 50(c) shows the measured SFD orbit (alternating "ac" component only) over 0.5s. Note that rotation of the squeeze ring caused the measured peak-to-peak vibration to appear larger than the diametral clearance. However, the measured orbit still bears a striking resemblance to the predicted orbit in Figure 50(a). Both orbits consist of two sets of opposing loops (like butterfly wings), with a concentration of trajectories at the lower right hand part of the orbit. Figure 51 shows the frequency spectra of the predicted (steady state) and measured SFD orbit over 0.5s. The frequency resolution is hence 2 Hz for both predicted and measured spectra. Strong subsynchronous components that loosely approximate to one-third and two-thirds subharmonic components appear in both measurement (32, 52 Hz respectively) and prediction (30, 54 Hz respectively). Additional minor subsynchronous components are also evident in both measurement (22, 62 Hz) and prediction (24, 60 Hz). From Figure 51 it is seen that most of the non-synchronous components are reasonably well predicted. In order to classify the type of *predicted* aperiodic motion at 84 rev/s, the TD solution was continued from that shown in Figure 50(a) over a further 160 revolutions. The results are shown in Figure 52. Figures 50(a),(b) are reproduced in Figures 52(a1),(a2) for comparison. Figures 52(b1),(b2) show the motion over a further 160 revolutions. The forms of both orbit and Poincare map are repeatable. This indicates that the aperiodic motion is probably a complex form of quasi-periodic motion rather than chaotic motion. However, a formal test for chaos using the Lyapunov exponent [31] was not performed to confirm this. Notice that the Poincare map (Figure 52(a2) or (b2)) is roughly triangular in shape, reflecting the presence of the strong approximate one-third subharmonic.

The type of aperiodic motion shown in Figure 50 was found to be prevalent over the range 82-100 rev/s in both measurements and prediction. However, for the predicted motion only, over a narrow range 85-87 rev/s, the aperiodic motion locks into $3T$-periodic motion *i.e.* limit cycles with $N = 3$ ("phase locking", page 54). The steady state periodic solution at 86 rev/s, computed by time domain integration, was used to provide an initial approximation to the harmonic balance continuation process with $N = 3$ and $m = 20$. A branch of stable $N = 3$ limit cycles was hence computed in the range 85-87 rev/s. Figure 53 shows the stability check by Method I of the HB $N = 3$, $m = 20$ orbits at 86 rev/s. The TD ($q = 4$) integration solution with initial conditions derived from the HB solution is shown in Figures 53(a1)-(a3) for the first 10 revolutions. The steady state TD solution is shown in Figures 53(b1)-(b3). The HB computed $N = 3$ limit cycle is an attractor. This example of $3T$ periodic motion at 86 rev/s highlights the accuracy of using $q = 4$ modes in the TD solution even when many harmonics of the fundamental frequency are

significant. In fact, the highest significant harmonic in the HB solution is $20\times86/3=573$ Hz *i.e.* beyond the fitting frequency range of 0-500 Hz in Figure 24. Figure 54(b) shows the Poincare map of the steady state TD solution over 30 shaft revolutions. The triangular form in the Poincare maps of Figures 52(a2),(b2) has degenerated into three fixed points at the corners, among which the 31 return points are distributed. Phase locking is an exceptional case, occurring when the lowest frequency component becomes an exact rational multiple of the synchronous component. It was not verified in the measurement at 86 rev/s (Figure 54(c)), which remained similar to the orbits in Figure 50(a),(c). Figure 55 compares the measured and predicted frequency spectra of the SFD orbit at 86 rev/s. For the prediction (Figure 55(a1),(a2)) the frequency resolution was refined to 1 Hz. For the measurement (Figure 55(b1),(b2)) it was 2 Hz. As can be seen, the additional minor subsynchronous components of ~22, 62 Hz that were predicted and measured at 84 rev/s (Figure 51) have disappeared from the prediction (Figure 55(a1),(a2)), which contains only exact harmonics of the fundamental frequency of $86/3\approx28.67$ Hz. The extra frequency components remain in the measurement, however (Figure 55(b1),(b2)).

From this section it is concluded that the phenomenon of subharmonic resonance occurs in the region 82-100 rev/s, which also contains the second pin-pin critical speed (91 rev/s). Subharmonic resonance is caused in this case by the rotational speed being close to 3 times the first pin-pin critical speed of 31 rev/s.

Measured *vs.* TD predicted unbalance response

Figure 56 compares the measured half peak-to-peak vibration with that predicted by TD integration in the range 24-100 rev/s. As explained in section 8.2.2, the integration was carried out over 120 shaft revolutions at each speed (steps of 2 rev/s) and only the last 0.5s of data was considered. This was more than adequate to eliminate the transients at all speeds except at 30 rev/s where the disc and mid-shaft predictions are much higher than measured due to the transients. The TD predicted response in Figure 56 shows a general improvement over the HB $N=1$ response in Figure 44. However, the y vibration at the disc and mid-shaft positions was over-predicted beyond about 82 rev/s (Figures 56(d),(f)), despite the fact that the transients were completely eliminated from the TD solution.

Figures 57-59 show the predicted and measured waterfall diagrams at the three positions J, U, M. Good agreement between prediction and measurement is evident. Subsynchronous activity beyond 82 rev/s is especially strong at the SFD in the y direction, Figures 57(a2),(b2), with components approximately one-third and two-thirds of the rotational speed. At the disc position (Figure 58) the synchronous component is the only significant component, although a one-third subharmonic makes an appearance around the second critical speed (~90 rev/s). The mid-shaft vibration, Figure 59, is richer in harmonics and subharmonics. The measured subsynchronous components at the disc and mid-shaft positions in the y direction are much weaker than those predicted. This may help to explain why the HB $N=1$ predictions at the disc and mid-shaft

positions beyond 80 rev/s are not that bad, despite the fact that the $N=1$ limit cycles become unstable (Figures 44(c)-(f)).

8.5 CONCLUSIONS

For configuration A1 the following conclusions were reached.

- The full film theory worked well at low static eccentricity and low unbalance. As the unbalance and/or static eccentricity was increased, absolute zero cavitation theory had to be used. Cavitation effects were experimentally observed in those speed ranges where divergences between the two cavitation models appeared.
- The lift at the SFD journal caused by cavitation kept the vibration at other locations low as the first critical speed was traversed.
- The model managed to predict aperiodic behaviour measured in the critical speed region of 30-36 rev/s at a static eccentricity of -0.8, and unbalance of 5.1×10^{-4} kgm. The aperiodic motion predicted was of the quasi-periodic type. The variation of the static misalignment due to the vertical run-out of the shaft and the consequent use of a conservative average value for ε_{0yJ} in the prediction was the reason for not predicting aperiodic motion measured at $\varepsilon_{0yJ}=-0.6$ and $U=5.1\times10^{-4}$ kgm.

For configuration A2, the shaft behaved like a pin-pin beam and the single SFD provided little benefit. The shaft hardly lifted except around the two critical speeds. It was evident that the low viscosity oil was not suitable for this configuration (*i.e.* single unsupported SFD). The model managed to predict strong subsynchronous activity around the second pin-pin critical speed of ~90 rev/s. Subharmonic resonance in this region was caused by the rotational speed being close to three times the first pin-pin critical speed of 31 rev/s.

CHAPTER 9

CONCLUSION AND FUTURE RESEARCH

In this report a comprehensive receptance based method for the non-linear modelling of squeeze film damped rotor dynamic systems has been presented. This method encompassed harmonic balance analysis, stability analysis, and time domain integration analysis. In chapter 3 a general method for harmonic balance (HB) analysis using exact receptances was developed. In chapter 4 a general method for time domain (TD) analysis based on the approximate modal decomposition of the receptances was presented. The equations developed in chapters 3 and 4 were then applied to specific configurations A, B involving one squeeze film damper (SFD), in chapter 5. Configuration A comprised a flexible shaft in a rigidly housed SFD either with parallel retainer spring (A1) or without parallel retainer spring (A2). Configuration B was similar to A2 but with the bearing housing flexible. In chapter 6 two general methods for the stability analysis of limit cycles computed by HB were presented with reference to the specific configurations A, B. Method I involved time domain integration over a limited number of cycles using initial conditions determined from a modal decomposition of the HB solution. Method II was based on Floquet Theory and entailed the computation of the monodromy matrix. This matrix could be computed in two alternative ways: either straight from its definition (Method IIa), or approximately, using impulsive parametric excitation theory (Method IIb). Method IIa was seen to be useless, despite being used in the literature. A quantitative and qualitative analysis of configurations B and A was presented in chapters 7 and 8 respectively. Analysis on configuration B was restricted to a rigid rotor. The reader is referred to the specific conclusions reached, summarised at the end of these chapters. The approach adopted to analyse these problems was as follows.

(a) Perform the HB $N = 1$ solution with a suitable number of harmonics m, using arc-length continuation.
(b) Derive the stability characteristic of the HB computed unbalance response using the fast Method IIb.
(c) Confirm the stability results obtained in (b) at the salient points of the unbalance response using Method I.
(d) Perform TD integration, as required, in those speed ranges where instability of the HB $N = 1$ solutions is detected.

Simulations showed excellent correlation between all the various analytical techniques developed. This in itself validated the soundness of the receptance model. Additionally, the model was experimentally validated.

The major conclusion drawn is that the use of a comprehensive receptance based model, encompassing both time and frequency based methods, allows fast, reliable predictions under all

operating conditions. Moreover, use of the receptance formulation allows a wide choice of linear rotor dynamic modelling techniques (*e.g.* finite element (FE), mechanical impedance (MI), transfer matrix (TM), hybrids FE/TM, FE/MI) for efficient receptance computation.

The next phase of the research will involve the following tasks.

- Processing of data already acquired for configuration A1 with partially supported journal (*i.e.* $\varepsilon_{0yJ} < -1$). Experimental results for this condition have revealed "neater" quasi-periodic orbits in the region 30-36 rev/s than those obtained for $\varepsilon_{0yJ} = -0.8$. This was attributed to the invariant static misalignment condition.
- Further tests on configuration A2 with more suitable, thicker oil.
- Extension of the simulations of configuration B to cover the flexible rotor. Experimental validation of these simulations would involve collaboration with M. Levesley of the University of Leeds, who has already carried out such experimental work in [28].
- Possible application of the model to a test rig with two flexibly house squeeze film dampers and experimental validation. The test rig (to be designated "configuration C") was described in the first report [15] and is still under construction.
- As for the model itself, the only area still to be developed is the problem of degenerate rotor subsystems with number of squeeze films $n \geq 3$ (see end of section 3.6).

REFERENCES

1. E. J. HAHN, P. Y. P. CHEN 1994 *ASME Journal of Tribology* **116**, 499-507. Harmonic Balance Analysis of General Squeeze Film Damped Multidegree-of-Freedom Rotor Bearing Systems.

2. T. -N. SHIAU, A. -N. JEAN 1990 *ASME Journal of Vibration and Acoustics* **112**, 501-507. Prediction of Periodic Response of Flexible Mechanical Systems With Non-Linear Characteristics.

3. J. Y. ZHAO, I. W. LINNETT, L. J. McLEAN 1994 *ASME Journal of Tribology* **116**, 361-368. Stability and Bifurcation of Unbalanced Response of a Squeeze Film Damped Flexible Rotor.

4. C. NATARAJ, H. D. NELSON 1989 *ASME Journal of Vibration, Acoustics, Stress, and Reliability in Design* **111**, 187-193. Periodic Solutions in Rotor Dynamic Systems With Nonlinear Supports: A General Approach.

5. K. H. BECKER, E. STEINHARDT 1990 *J. M. Montalvao e Silva and F. A. Pina da Silva (eds.), Vibration and Wear in High Speed Rotating Machinery*, 263-277. A General Method for Rotordynamic Analysis.

6. R. W. ARMENTROUT, E. J. GUNTER 1999 *SPIE Proceedings* **3727(1)**, 290-296. Transient Modal Analysis of Nonlinear Rotor-Bearing Systems.

7. H. D. NELSON 1998 *JSME International Journal Series C* **41**, No. 1, 1-11. Rotordynamic Modelling and Analysis Procedures: A Review.

8. N. F. REIGER, C. B. THOMAS and W. W. WALTER 1976 *Vibrations in Rotating Machinery, IMechE Conference Publications 1976-9,* **C187/76**, 187-193. Dynamic Stiffness Matrix Approach for Rotor-Bearing Analysis.

9. P. BONELLO 1998 *M.Sc. Thesis, University of Southampton.* Predicting the Vibration Response of a Multi-Span Coupled Rotor-Bearing-Foundation System by the Mechanical Impedance Technique.

10. C. S. HSU, W. -H.. CHENG 1973 *ASME Journal of Applied Mechanics* March 1973, 78-86. Applications of the Theory of Impulsive Parametric Excitation and New Treatments of General Parametric Excitation Problems.

11. M. C. LEVESLEY, R. HOLMES 1994 *Proceedings of the Institution of Mechanical Engineers* **208**, 41-51. The Efficient Computation of the Vibration Response of an Aero-Engine Rotor-Damper Assembly.

12. J. Y. ZHAO, E. J. HAHN 1993 *Proceedings of the Institution of Mechanical Engineers* **207**, 383-392. Subharmonic, Quasi-Periodic and Chaotic Motions of a Rigid Rotor Supported by an Eccentric Squeeze Film Damper.

13. A. H. CRAVEN, R. HOLMES 1972 *International Journal for Numerical Methods in Engineering* **5**, 17-24. The Vibration of Engine Crankshafts - A Fast Numerical Solution.

14. R. SEYDEL 1988 *From Equilibrium to Chaos: Practical Bifurcation and Stability Analysis.* Elsevier Science.

15. P. BONELLO 2000 *ISVR Technical Memorandum No. 857, University of Southampton* December 2000. Modelling the Non-Linear Dynamics of An Aero-Engine Low Pressure Rotor Mounted on Squeeze Film Bearings.

16. M. BURGHARDT 1998 *M.Sc. Thesis, University of Southampton.* An Investigation of The Squeeze Film Damping of A Super-Critical Rotor.

17. B. HUMES, R. HOLMES 1978 *Journal of Mechanical Engineering Science* **20**, No.5, 283-289. The Role of Subatmospheric Film Pressures in the Vibration Performance of Squeeze-Film Bearings.

18. M. M. DEDE, M. DOGAN, R. HOLMES 1985 ASME *Journal of Tribology* **107**, 411-418. The Damping Capacity of a Sealed Squeeze Film Bearing.

19. C. F. GERALD 1980 *Applied Numerical Analysis.* Second Edition, Addison-Wesley Publishing Company.

20. G. DAHLQUIST 1974 *Numerical Methods.* Prentice-Hall.

21. THE MATHWORKS INC. 1999 *MATLAB® Version 5 User's Guide.* Prentice-Hall.

22. S. S. RAO 1995 *Mechanical Vibrations.* Addison-Wesley Publishing Company.

23. M. PETYT 1998 *Introduction to finite element vibration analysis*, p.448. Cambridge University Press.

24. D. J. EWINS 1984 *Modal Testing: Theory and Practice.* Research Student Press.

25. S. D. CONTE, C. DE BOOR 1972 *Elementary Numerical Analysis: An Algorithmic Approach.* McGraw-Hill Book Company.

26. R. E. D. BISHOP, D. C. JOHNSON 1960 *The Mechanics of Vibration.* Cambridge University Press.

27. M. DOGAN 1983 *Ph.D. Thesis, University of Sussex.* Investigation of an Aero-Engine Squeeze-Film Damper.

28. M. C. LEVESLEY, R. HOLMES *Vibrations in Rotating Machinery, IMechE Conference Transactions 2000-6,* **C576/104.** Influence of Various Parameters on The Non-Linear Behaviour of A Flexible Shaft Incorporating An Uncentralized Squeeze Film Damper.

29. R. GRIMSHAW 1990 *Nonlinear Ordinary Differential Equations.* Blackwell Scientific Publications.

30. G. IOOS, D. D. JOSEPH 1980 *Elementary Stability and Bifurcation Theory.* Springer-Verlag.

31. R.C. HILBORN 1994 *Chaos and Nonlinear Dynamics.* Oxford University Press.

32. F. CHU, Z. ZHANG 1998 *Journal of Sound and Vibration* **210**(1), 1-18. Bifurcation and Chaos in A Rub-Impact Jeffcott Rotor System

33. C. S. HSU 1972 *ASME Journal of Applied Mechanics* June 1972, 551-558. Impulsive Parametric Excitation: Theory.

34. R. HOLMES, M. DOGAN 1982 *Proceedings of the Institution of Mechanical Engineers* **24 No 3**, 129-137. Investigation of A Rotor Bearing Assembly Incorporating A Squeeze-Film Damper Bearing.

35. R. HOLMES, S. BOX 1992 *Machine Vibration* **1**, 71-79. On the Use of Squeeze-Film Dampers in Rotor Support Structures.

36. R. HOLMES, M. M. DEDE 1989 *Proceedings of the Institution of Mechanical Engineers* **203**, 25-34. Non-Linear Phenomena in Aero-Engine Rotor Vibration.

FIGURES

(a)

(b)

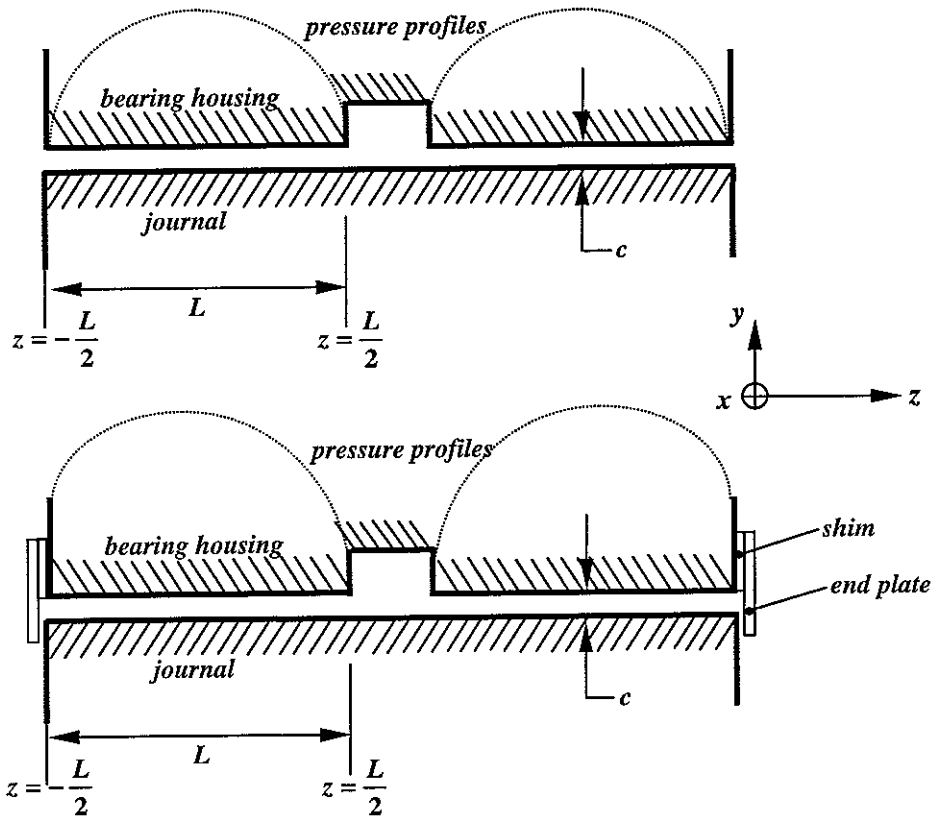

Figure 1: *Schematic axial cross-section of* (a) *unsealed damper* (b) *sealed damper*

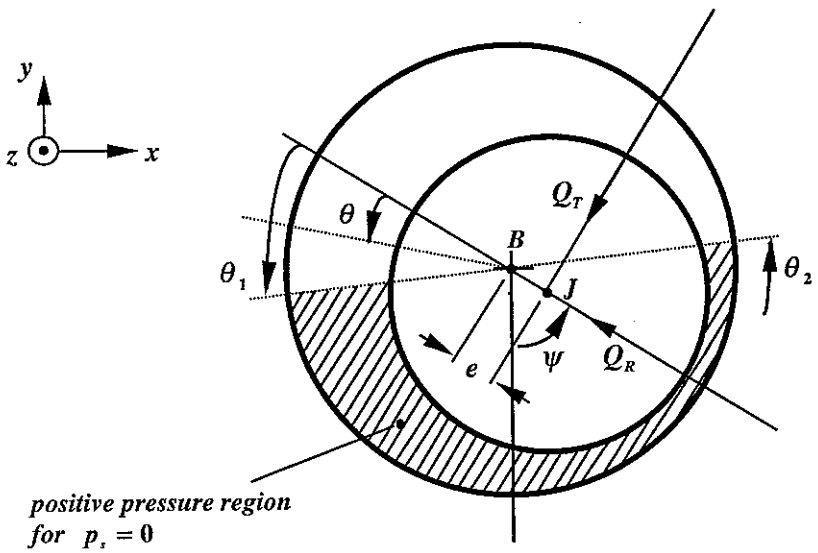

Figure 2: *Schematic cross-section of squeeze film damper in x-y plane*

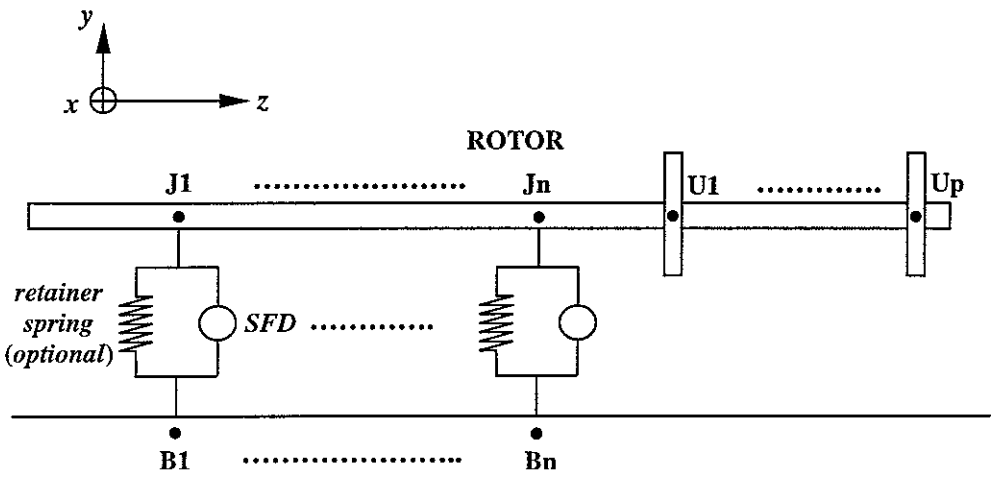

(a)

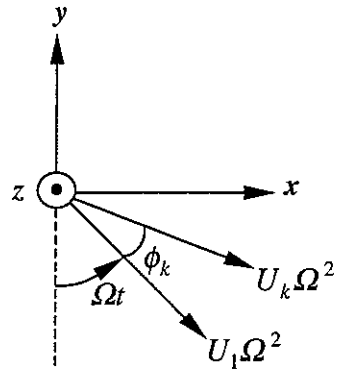

(b)

Figure 3: (a) *General representation of linear system* (b) *Rotating unbalance forces*

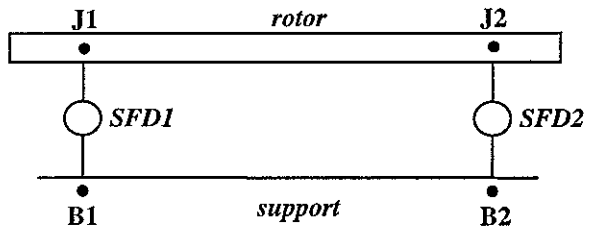

Figure 4: *Example of a degenerate system*

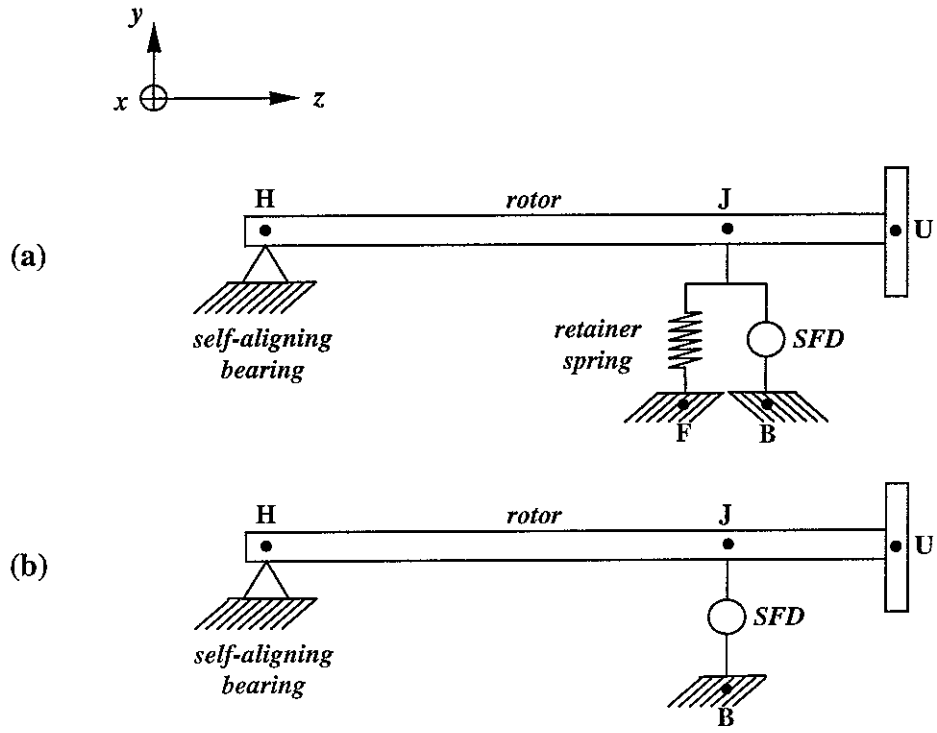

Figure 5: *Configuration A*: (a) *configuration A1* (b) *configuration A2*

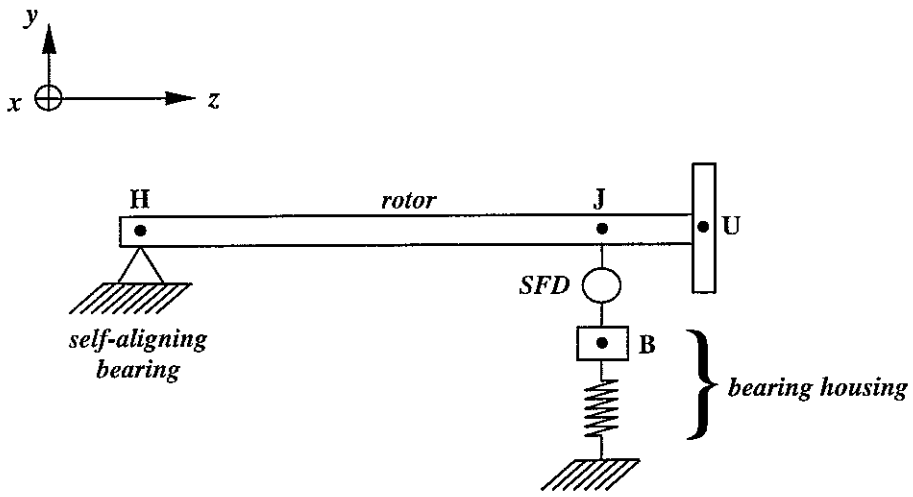

Figure 6: *Configuration B*

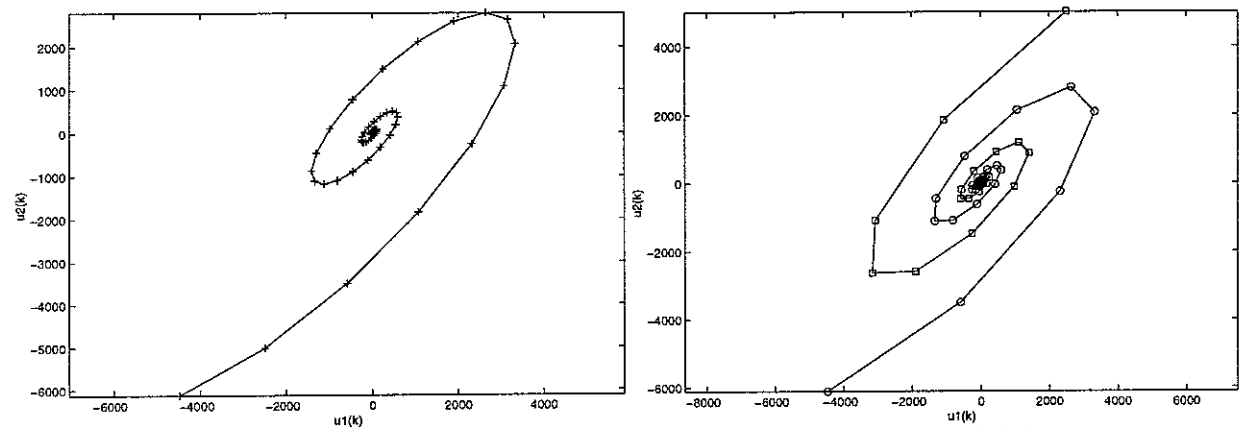

(a) $\varphi = 0.3491$ (b) $\varphi = 3.4907$

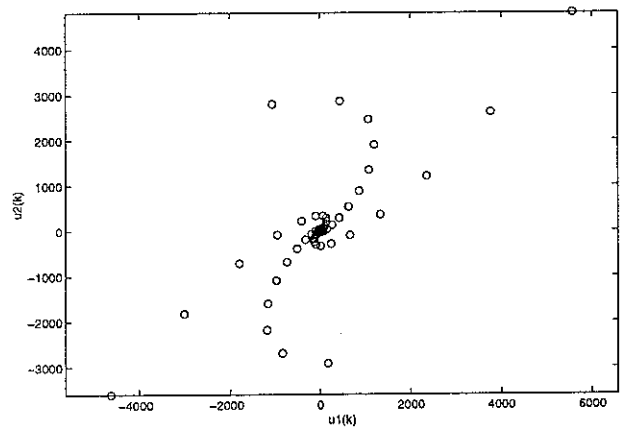

(c) $\varphi = 4.6432$

Figure 7: *Spiral behaviour of sampled points for λ_c complex.*
(φ is the phase of λ_c, in rad).

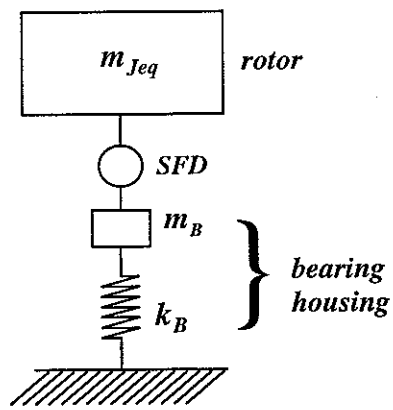

Figure 8: *Equivalent rigid body model for configuration B used in [27], [34].*

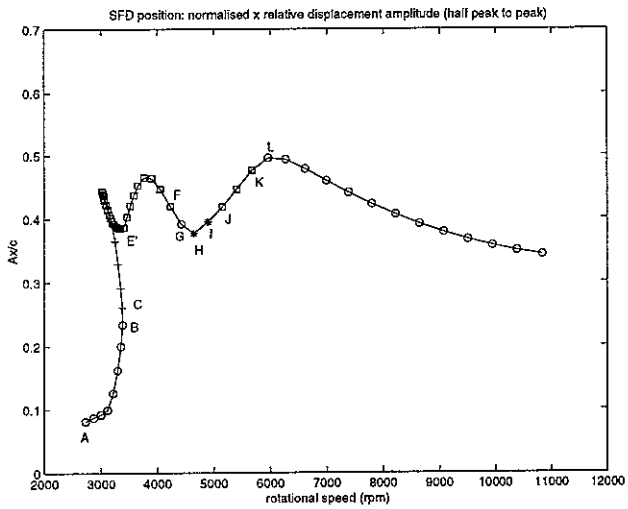

(a1) *x direction, half peak to peak*

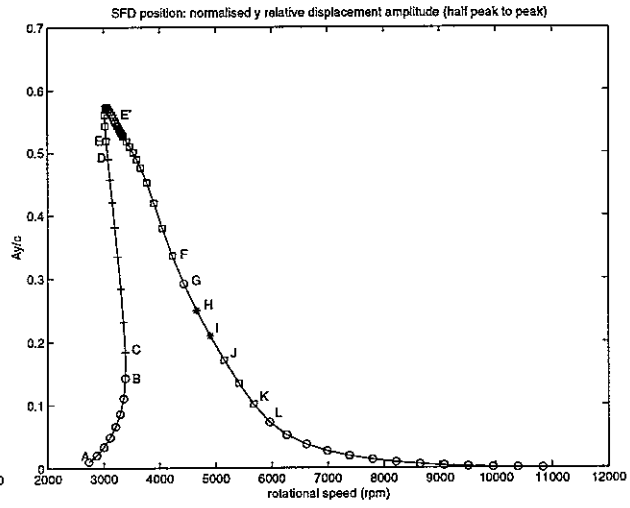

(a2) *y direction, half peak to peak*

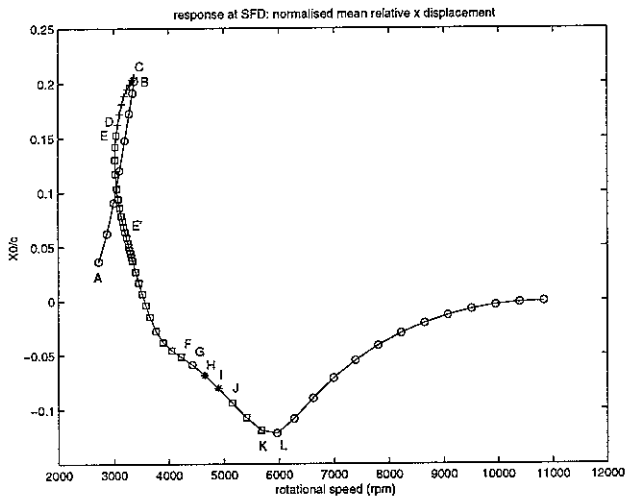

(b1) *x direction, mean relative displacement*

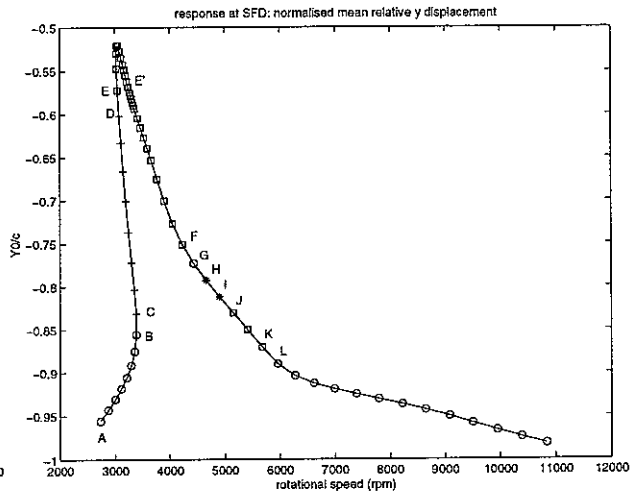

(b2) *y direction, mean relative displacement (lift)*

Figure 9: ***Predicted relative displacement response for configuration B with*** $u = 0.229$, $p_S = 34.5\,kPa$.

HB, $N = 1$, $m = 5$, ***absolute zero cavitation.***

Stable solutions: ' o '; unstable, same period instability: ' + '; unstable, period-doubling instability: ' □ ', unstable, quasi-periodic instability: ' * '.

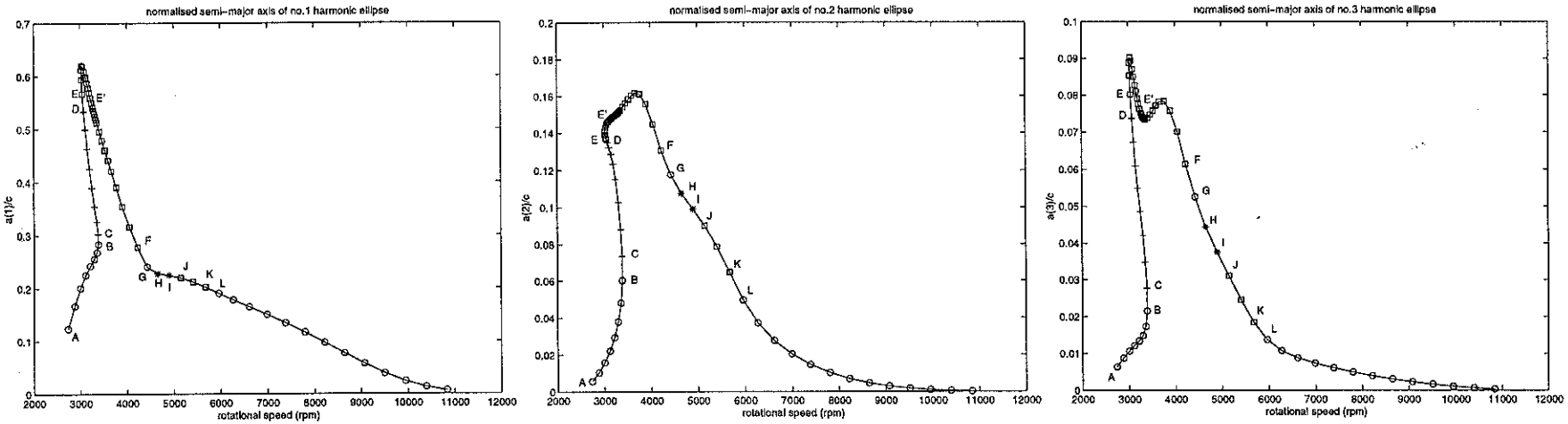

(a) *1st harmonic ellipse* (b) *2nd harmonic ellipse* (c) *3rd harmonic ellipse*

Figure 10: *Variation of semi-major axes of harmonic ellipses of predicted relative displacement with rotational speed for configuration B.* [1]

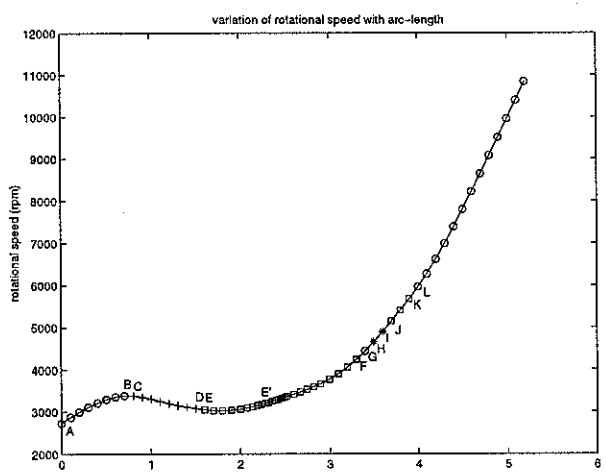

Figure 11: *Variation of rotational speed with the arc-length control parameter* σ. [1]

[1] *In above Figures : Stable solutions: ' o ';*
*unstable, same period instability: ' + '; unstable, period-doubling instability: ' □ ', unstable, quasi-periodic instability: ' * '.*

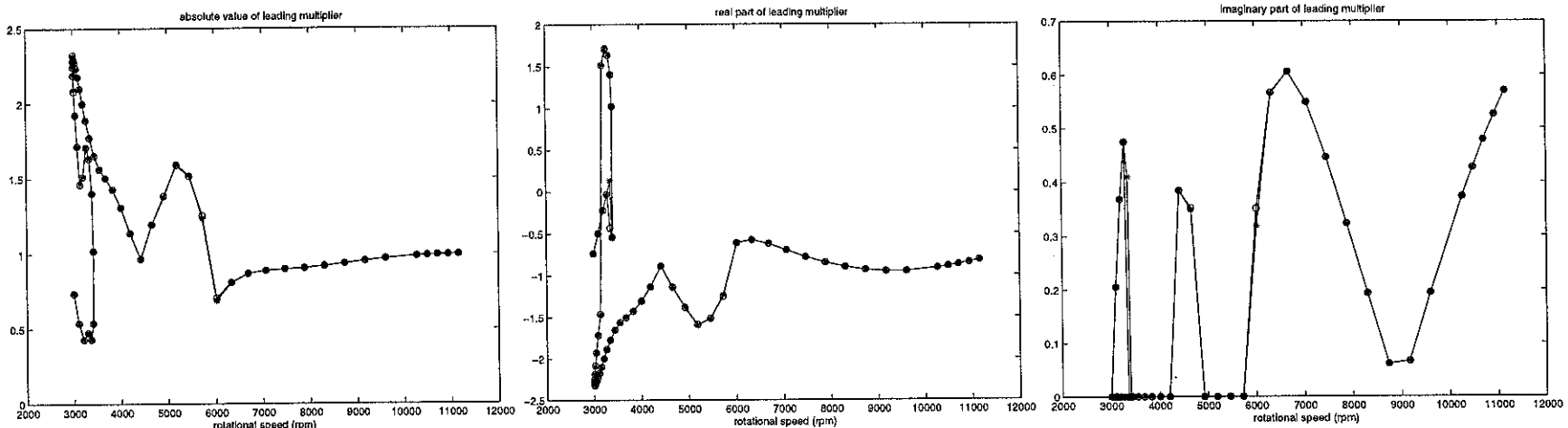

(a) *Absolute value of leading multiplier* (b) *Real part of leading multiplier* (c) *Imaginary part of leading multiplier*

Figure 12: *Comparison of stability curves of HB solutions for configuration B using Method IIa (—*—) and IIb (—O—).*

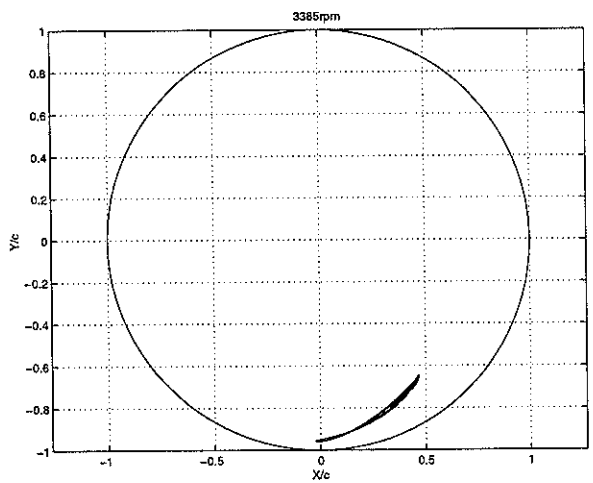

Figure 13: *Stability check by Method I: predicted relative orbits at point B (3383 rpm) on Figure 10(a) (stable). HB, $N = 1$, $m = 5$ (– – –), time domain integration (——) (over 10 revolutions, initial conditions derived from HB solution).*

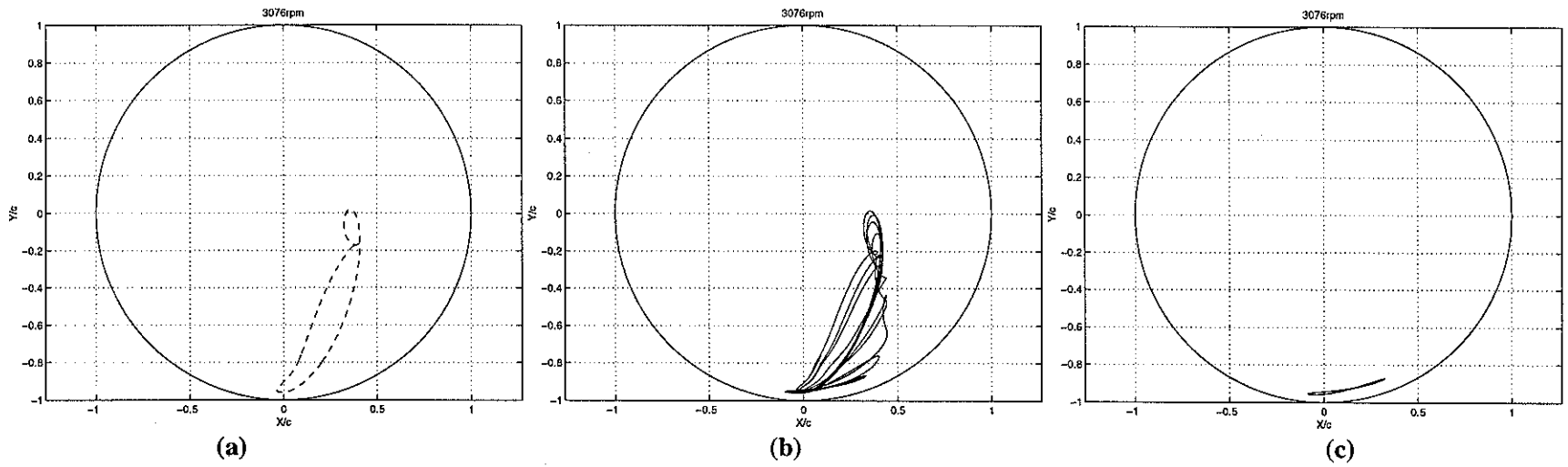

Figure 14: ***Stability check by Method I: predicted relative orbits at point D (3076 rpm) on Figure 10(a) (same period instability).***
(a) ***HB, $N = 1$, $m = 5$.*** **(b)** ***Time domain integration over 10 revolutions, initial conditions from HB solution.***
(c) ***Time domain integration over a further 5 revolutions.***

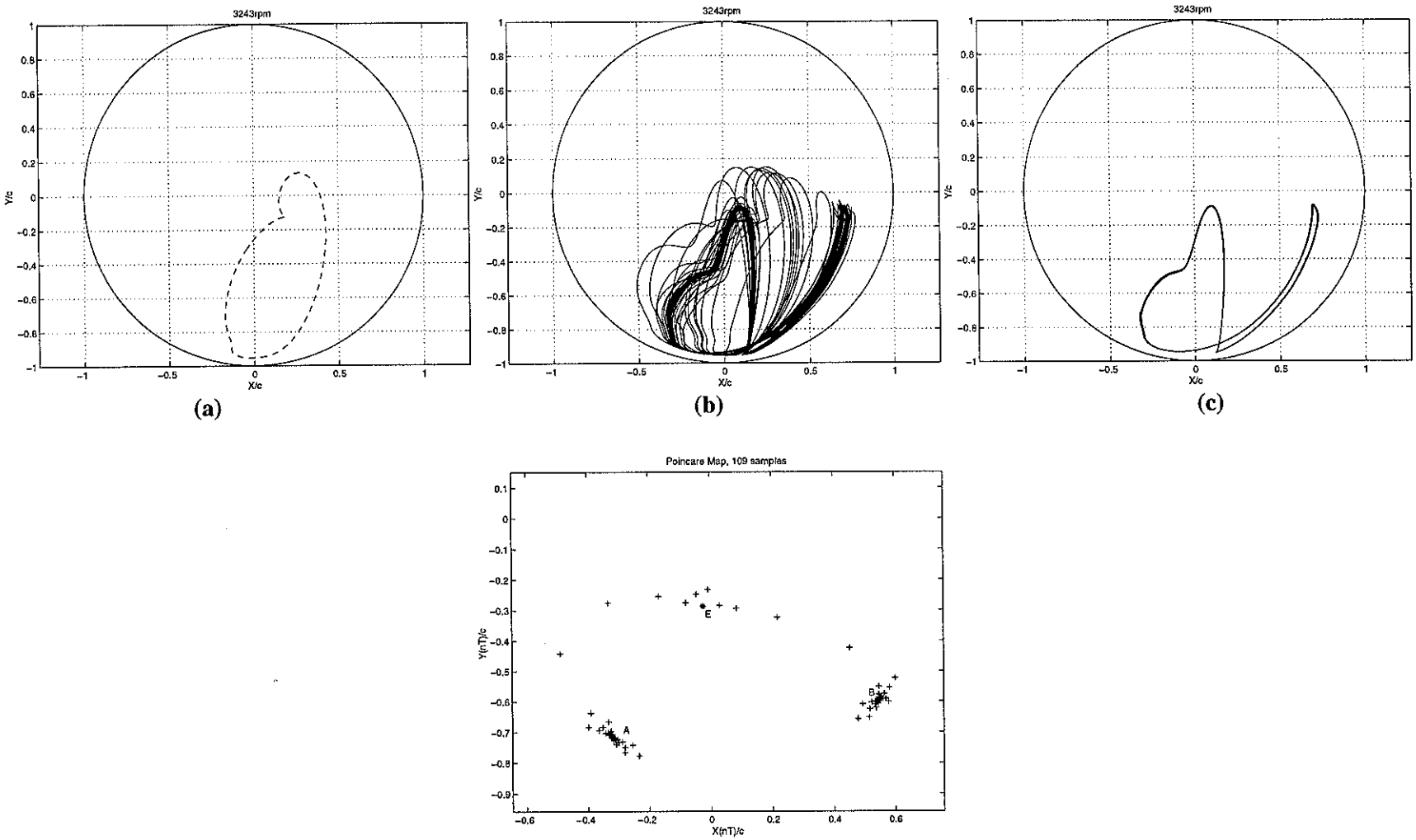

Figure 15: ***Stability check by Method I: predicted relative orbits at point E' (3243 rpm) on Figure 10(a) (period-doubling instability).***
(a) ***HB, $N = 1$, $m = 5$.*** **(b)** ***Time domain integration over 60 revolutions, initial conditions from HB solution.***
(c) ***Time domain integration over a further 50 revolutions.***
(d) ***Poincare map, sampling rate once per shaft revolution, 109 samples (unstable equilibrium point is E, indicated by ' * ').***

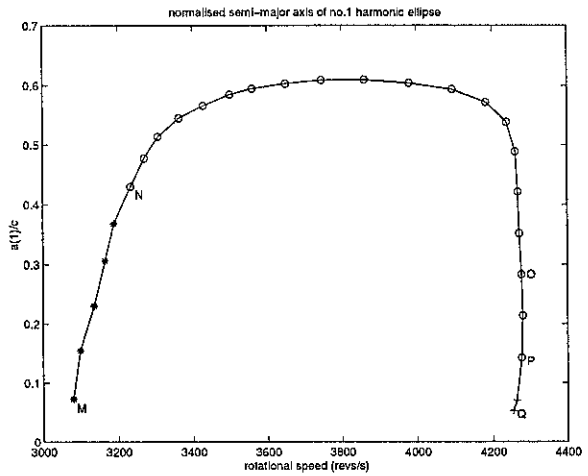

(a) ***Variation of semi-major axis first harmonic ellipse of subharmonic HB solutions (stable solutions: ' o ', unstable, same period: ' + ', unstable, quasi-periodic: ' * ').***

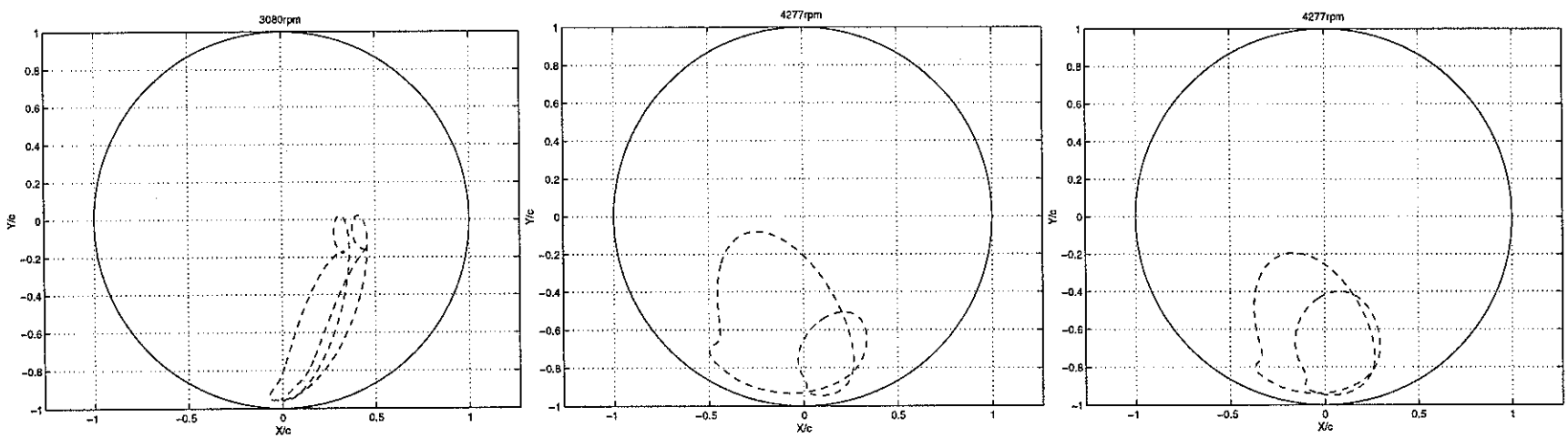

(b1) ***unstable relative orbit at M (3080 rpm) (see* (a))**

(b2) ***stable relative orbit at O (4277 rpm) (see* (a))**

(b3) ***stable relative orbit at P (4277 rpm) (see* (a))**

Figure 16: ***Subharmonic HB solutions, $N = 2$, $m = 10$ between points D (3076 rpm) and F (4277 rpm) on Figure 10(a).***

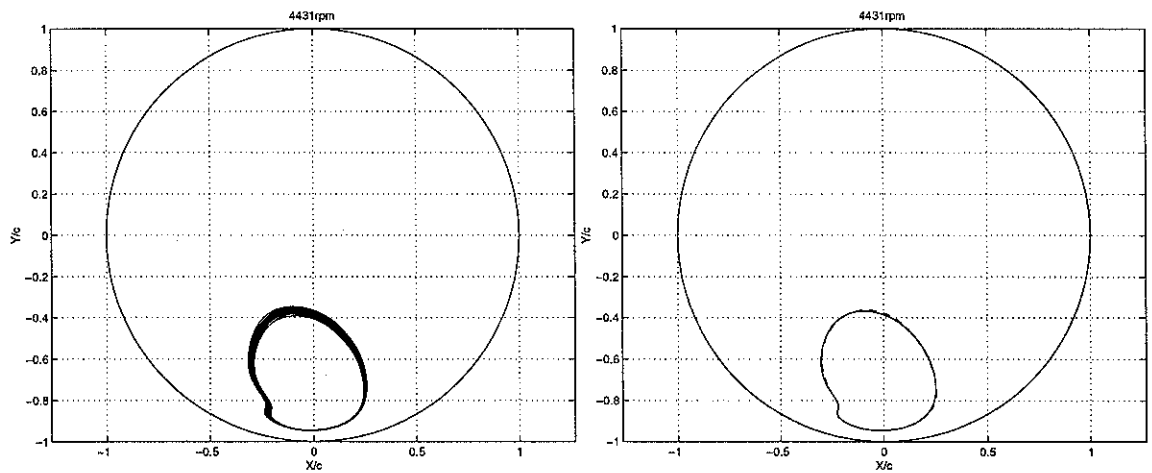

Figure 17: ***Stability check by Method I: predicted relative orbits at point G (4431 rpm) on Figure 10(a) (stable).***
(a) ***HB, $N = 1$, $m = 5$ (– – –), time domain integration (———) (over 50 revolutions, initial conditions derived from HB solution).***
(b) ***HB, $N = 1$, $m = 5$ (– – –), time domain integration (———) (over a further 5 revolutions).***

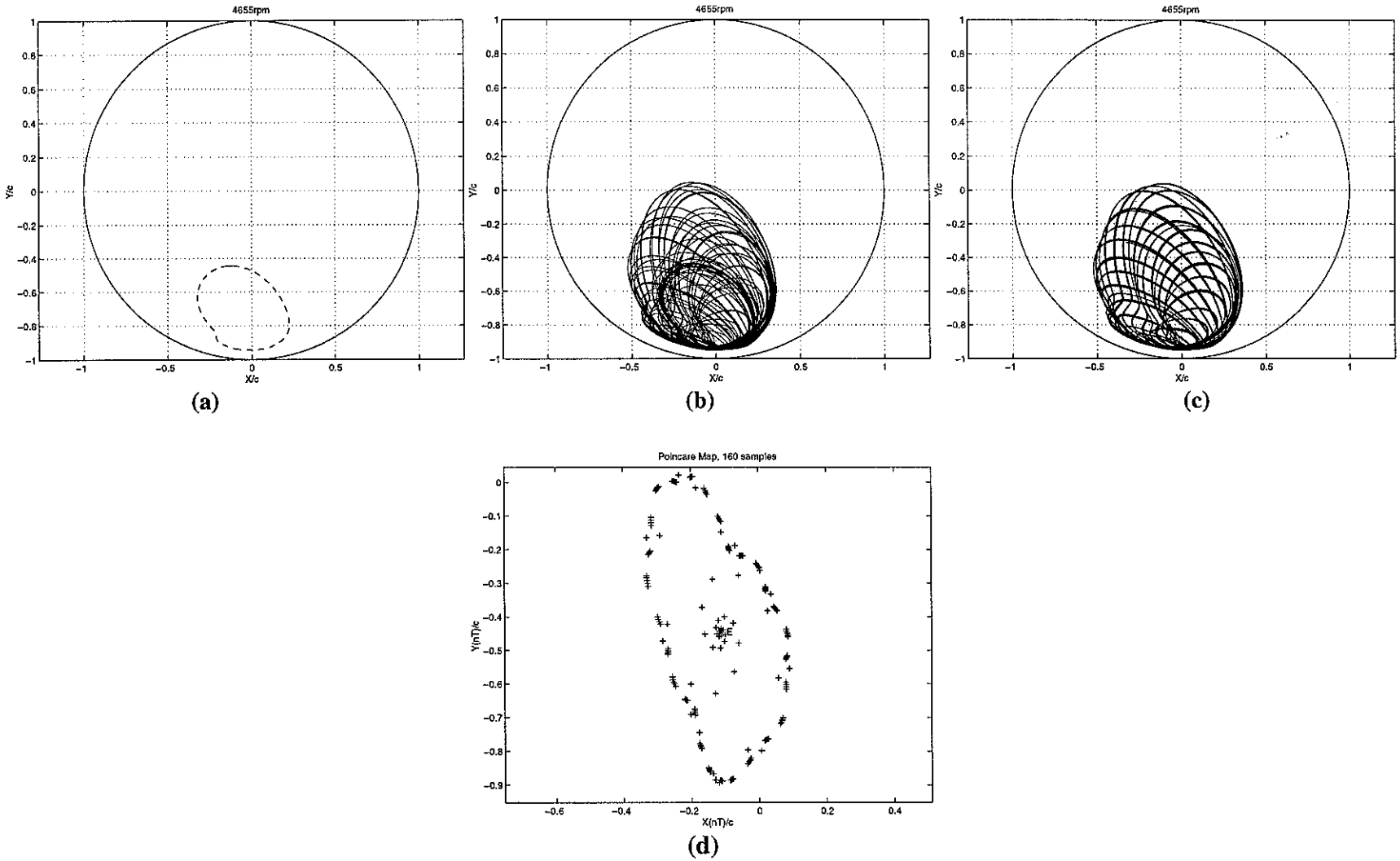

Figure 18: ***Stability check by Method I: predicted relative orbits at point H (4655 rpm) on Figure 10(a) (quasi-periodic instability).***
(a) ***HB, $N = 1$, $m = 5$.*** **(b)** ***Time domain integration over 80 revolutions, initial conditions from HB solution.***
(c) ***Time domain integration over a further 80 revolutions (steady state).***
(d) ***Poincare map, sampling rate once per shaft revolution, 160 samples (unstable equilibrium point is E, indicated by ' * ').***

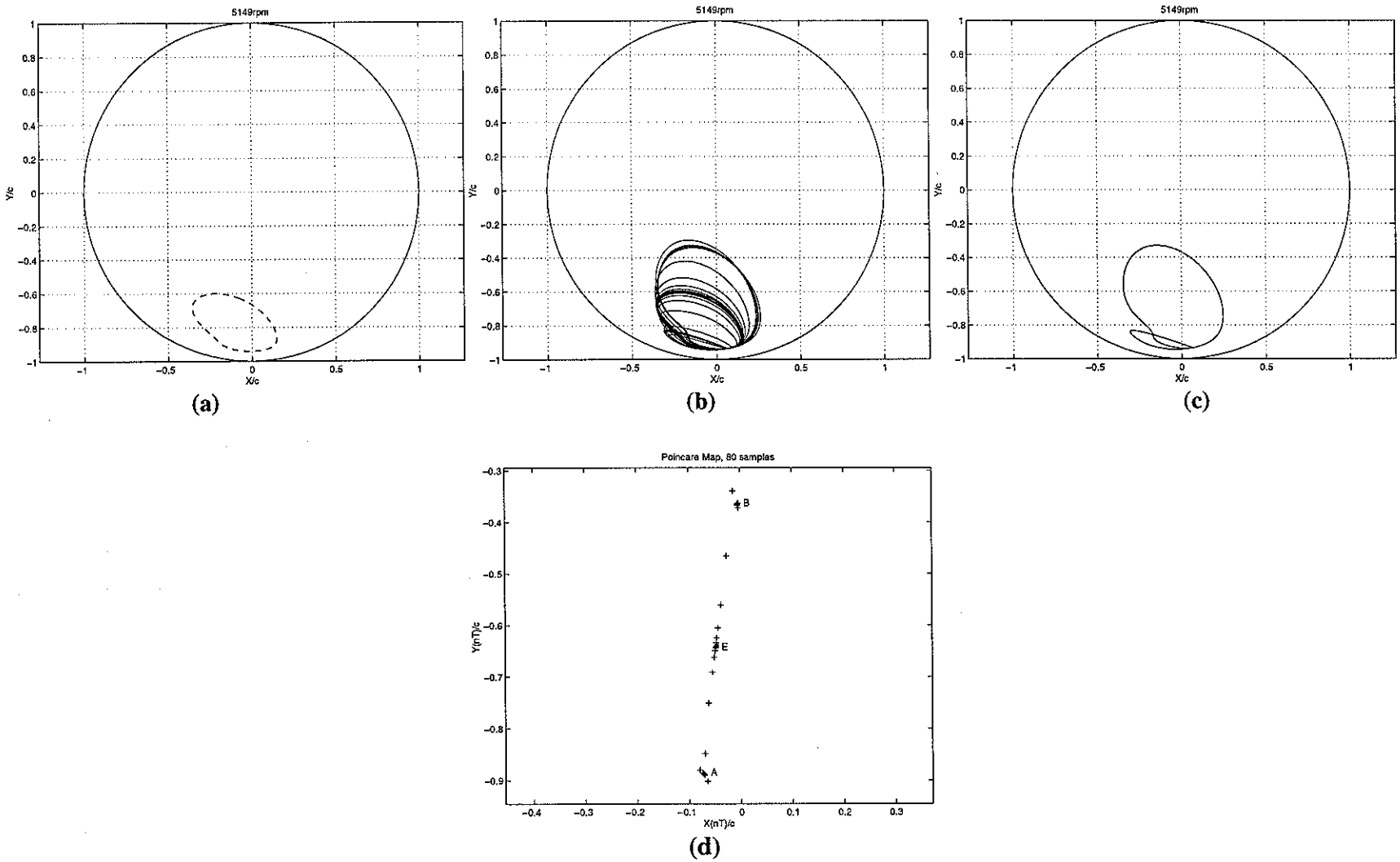

Figure 19: *Stability check by Method I: predicted relative orbits at point J (5149 rpm) on Figure 10(a) (period doubling instability).*
(a) *HB, $N = 1$, $m = 5$.* (b) *Time domain integration over 30 revolutions, initial conditions from HB solution.*
(c) *Time domain integration over a further 50 revolutions.*
(d) *Poincare map, sampling rate once per shaft revolution, 80 samples (unstable equilibrium point is E, indicated by ' * ').*

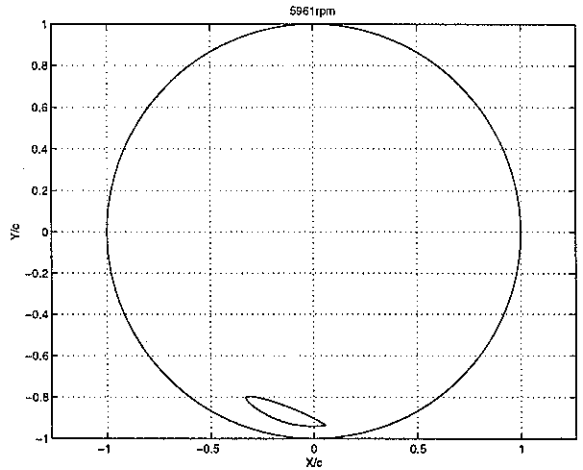

Figure 20: ***Stability check by Method I: predicted relative orbits at point L (5961 rpm) on Figure 10(a) (stable). HB, $N = 1$, $m = 5$ (– – –), time domain integration (——) (over 10 revolutions, initial conditions derived from HB solution).***

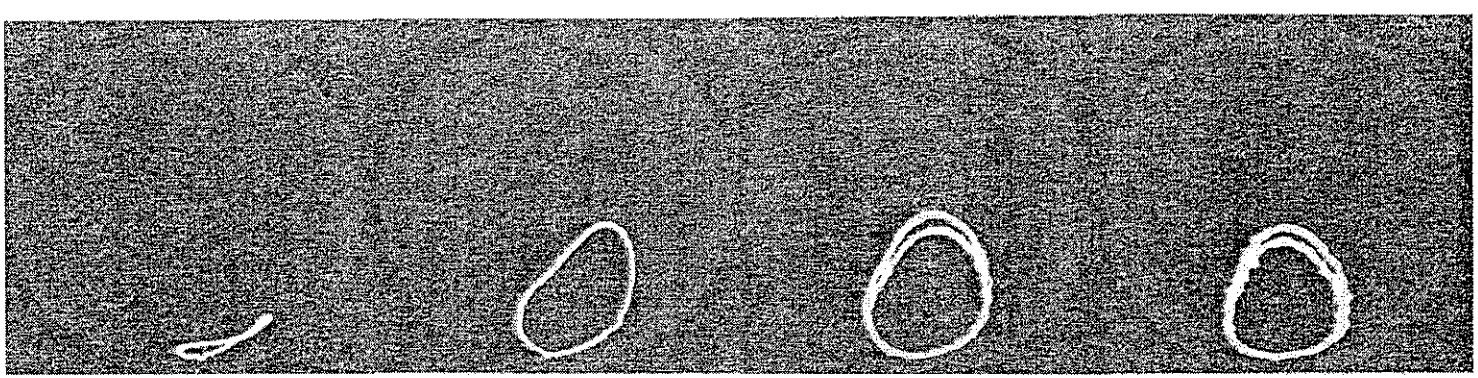

Figure 21: ***Measured relative orbits for dynamic load parameter $u = 0.229$, $p_S = 34.5\,kPa$, obtained from [27], [34].***

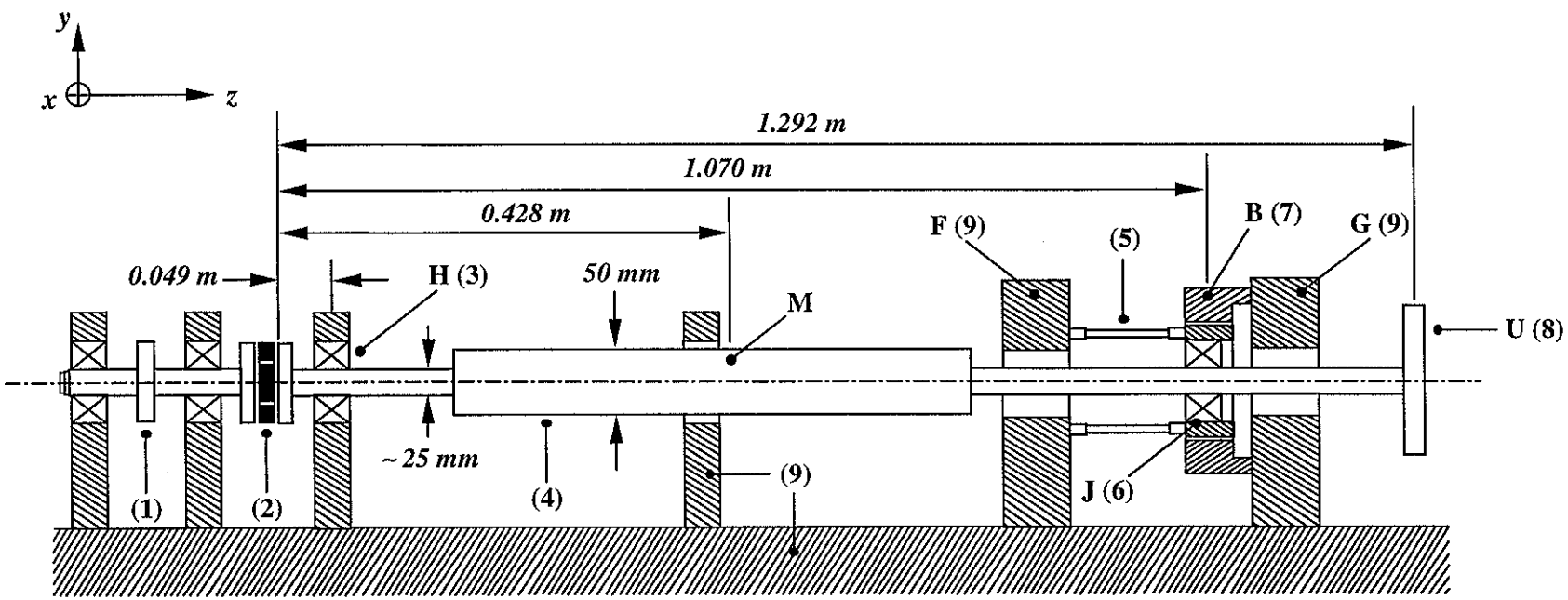

(1) Motor driven pulley
(2) Flexible coupling
(3) Self-aligning bearing (H)
(4) Flexible shaft
(5) Flexible bar ×4 (retainer spring)
(6) Self aligning bearing and squeeze ring (J)
(7) Bearing housing (B)
(8) Overhung unbalance disc (U)
(9) Frame and bedplate

Figure 22: *Test rig used for experimental validation of simulations for configuration A.*

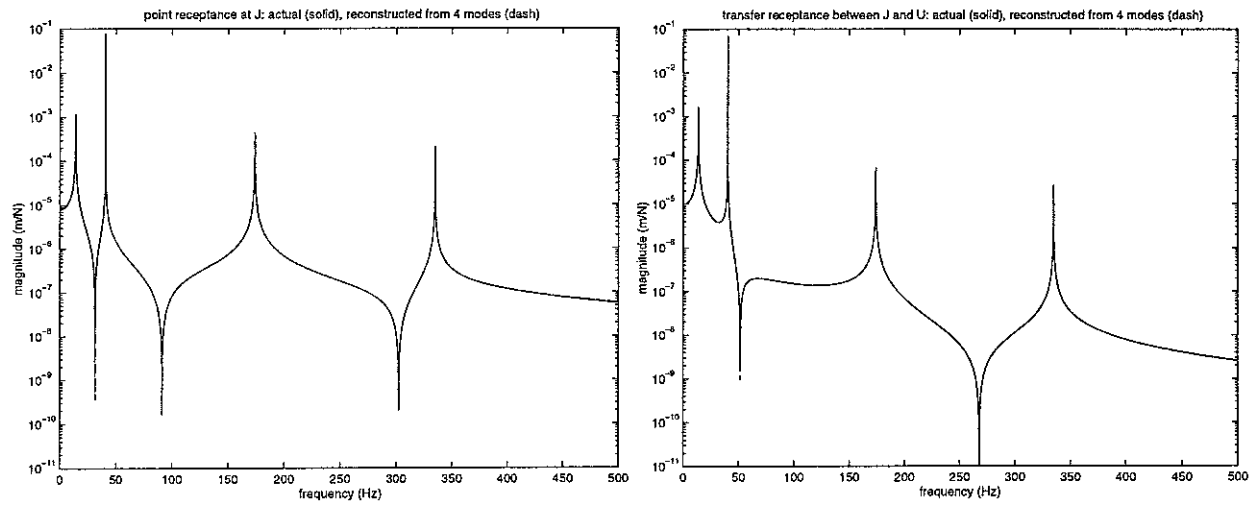

(a) *Point receptance at J,* α_{JJ} (b) *Transfer receptance between J and U,* α_{JU}

Figure 23: *Receptances for configuration A1.*
Exact: ——— *, reconstructed from 4 modes:* – – –.

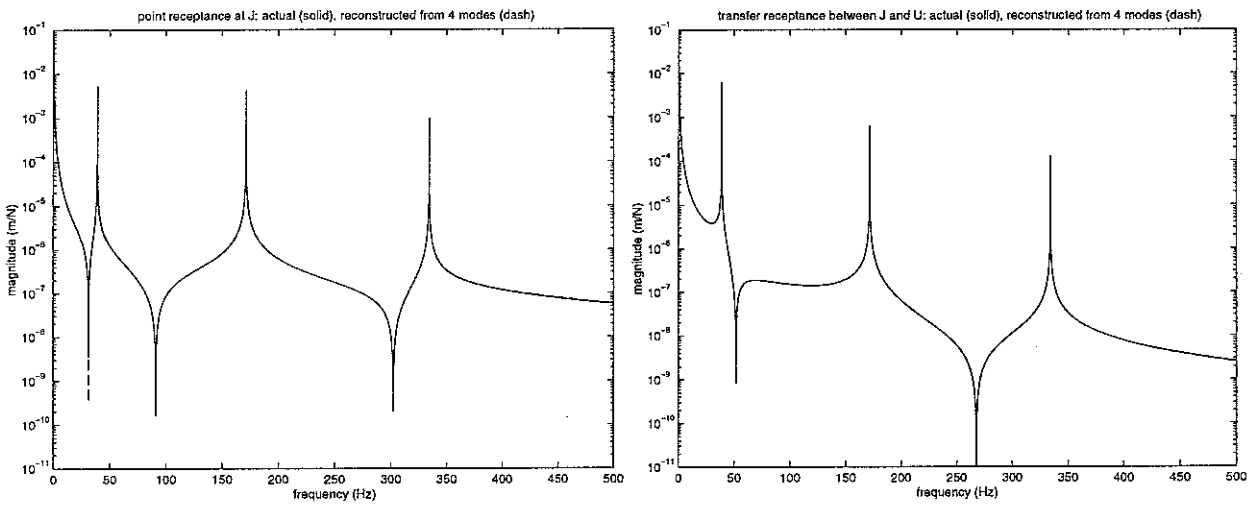

(a) *Point receptance at J,* α_{JJ} (b) *Transfer receptance between J and U,* α_{JU}

Figure 24: *Receptances for configuration A2.*
Exact: ——— *, reconstructed from 4 modes:* – – –.

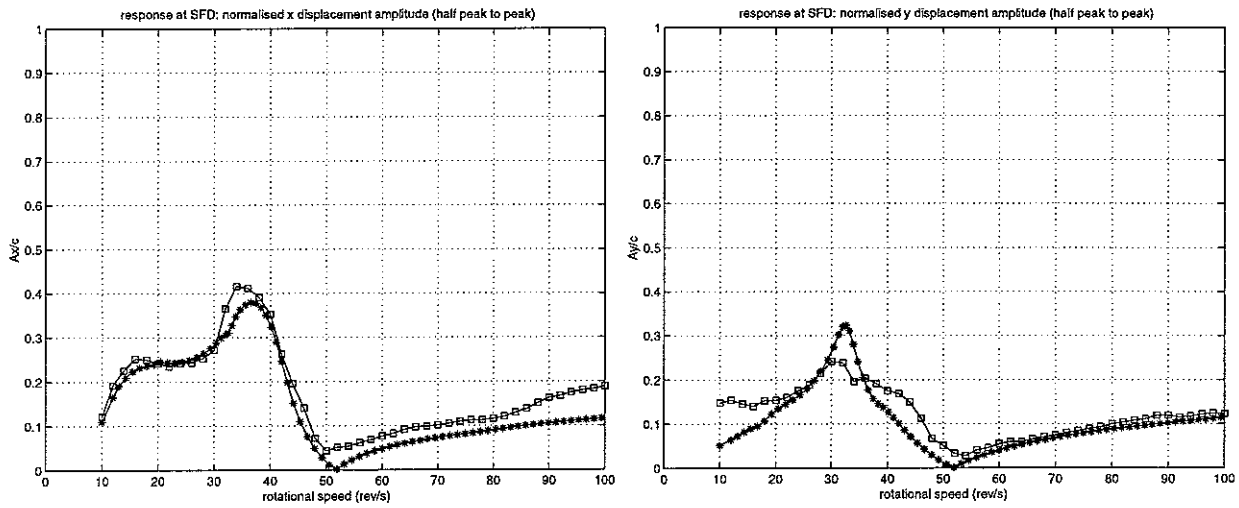

(a) *SFD (J), x direction*

(b) *SFD (J), y direction*

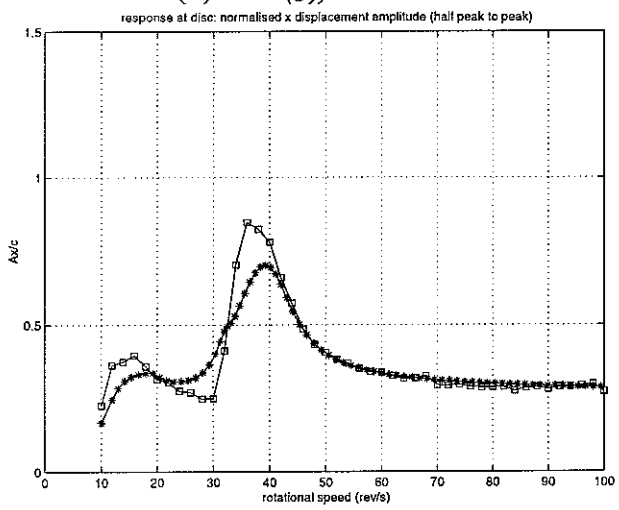

(c) *Disc (U), x direction*

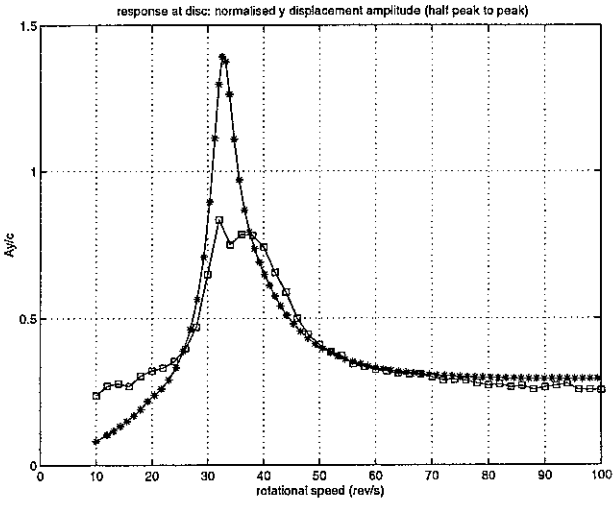

(d) *Disc (U), y direction*

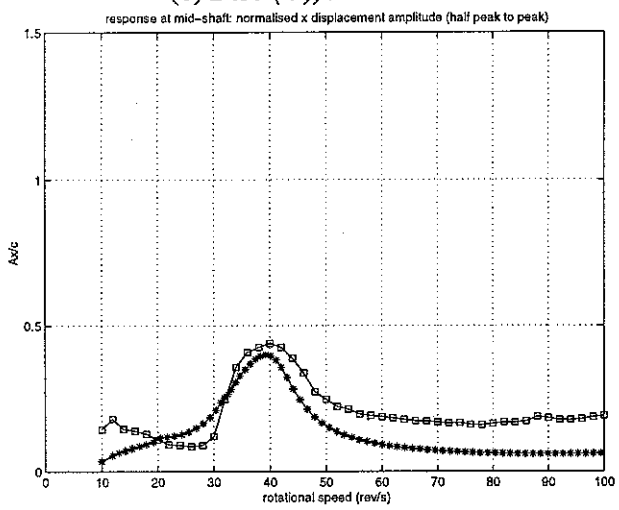

(e) *Mid-shaft (M), x direction*

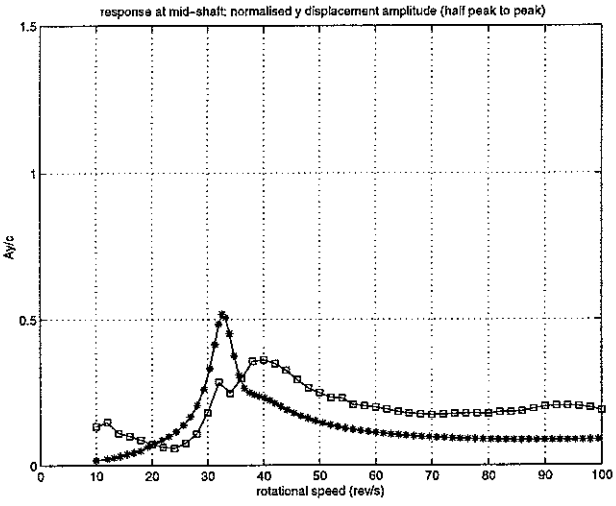

(f) *Mid-shaft (M), y direction*

Figure 25: *Unbalance response (normalised half peak-to-peak) for A1 with* $\varepsilon_{0yJ} = -0.6$ *,* $U = 2.59 \times 10^{-4}\,kgm$, $p_S = 1\,bar$.

Measurements: —□— . *Predictions, HB,* $N = 1$, $m = 5$ *: full film* —*— .

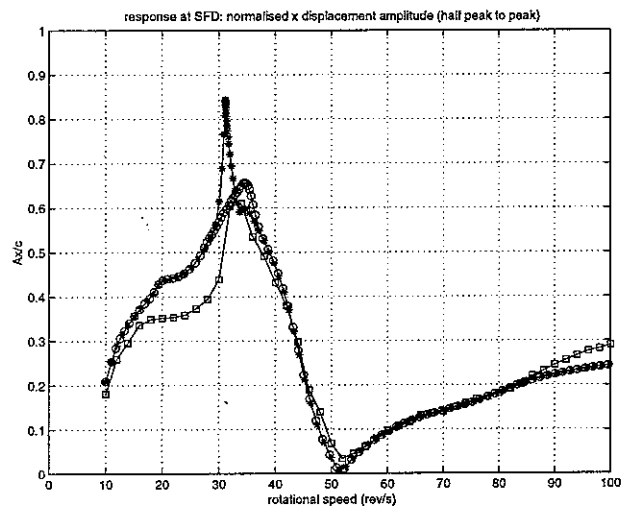

(a) *SFD (J), x direction*

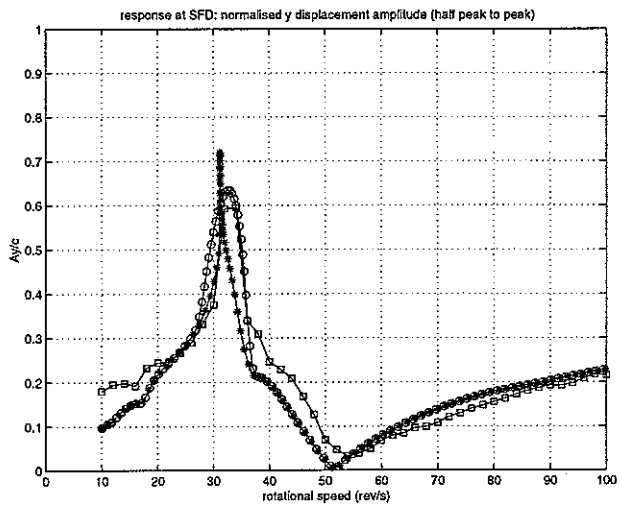

(b) *SFD (J), y direction*

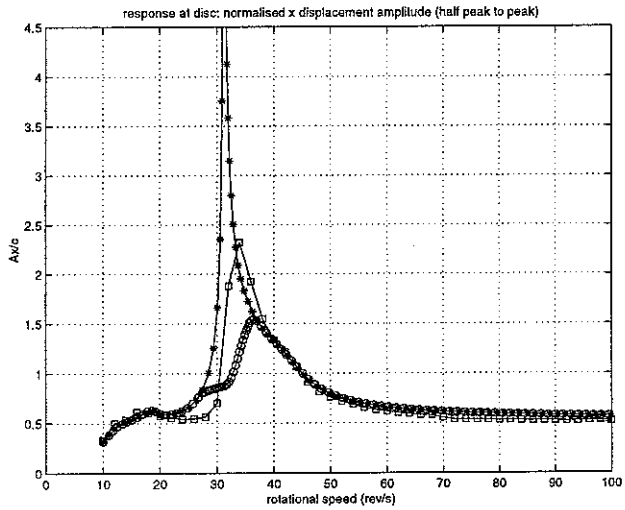

(c) *Disc (U), x direction*

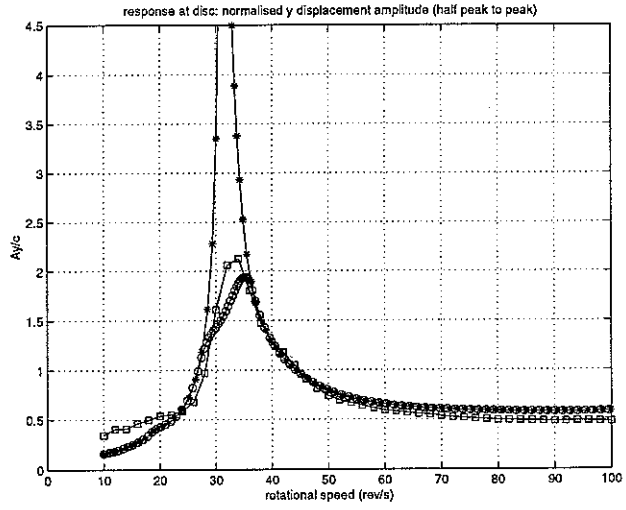

(d) *Disc (U), y direction*

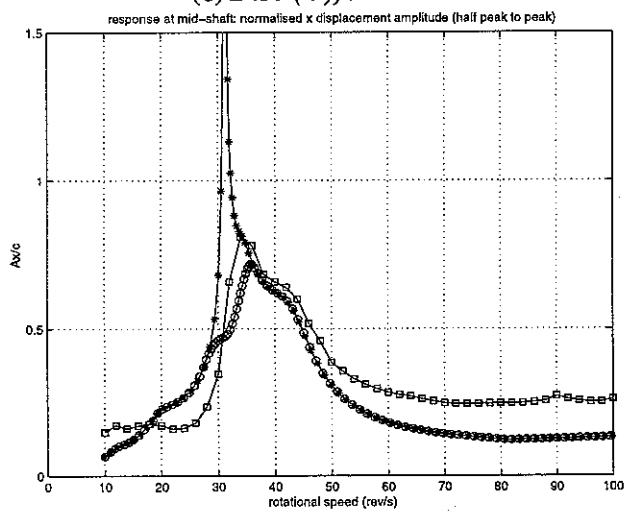

(e) *Mid-shaft (M), x direction*

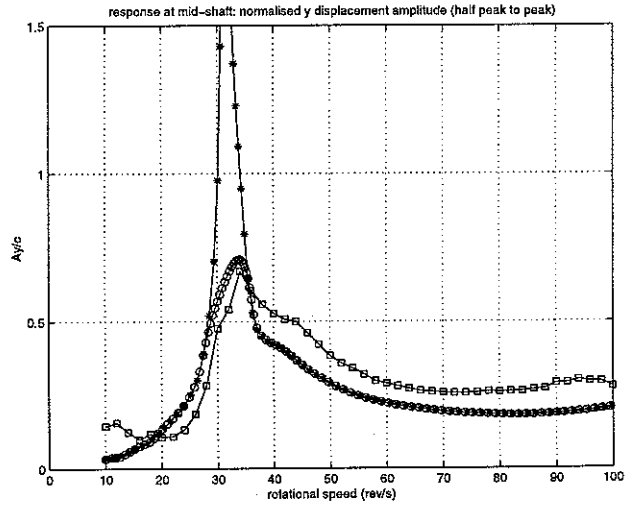

(f) *Mid-shaft (M), y direction*

Figure 25: *Unbalance response (normalised half peak-to-peak) for A1 with* $\varepsilon_{0yJ} = -0.6$ *,* $U = 5.1\times10^{-4}\,kgm$, $p_S = 1\,bar$. *Measurements:* —□—. *Predictions, HB,* $N = 1$, $m = 5$ *: full film* —*—, *absolute zero cavitation* —○—.

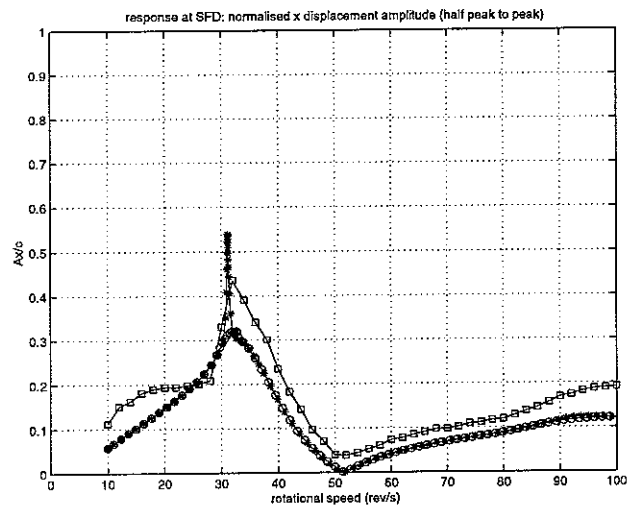

(a) *SFD (J), x direction*

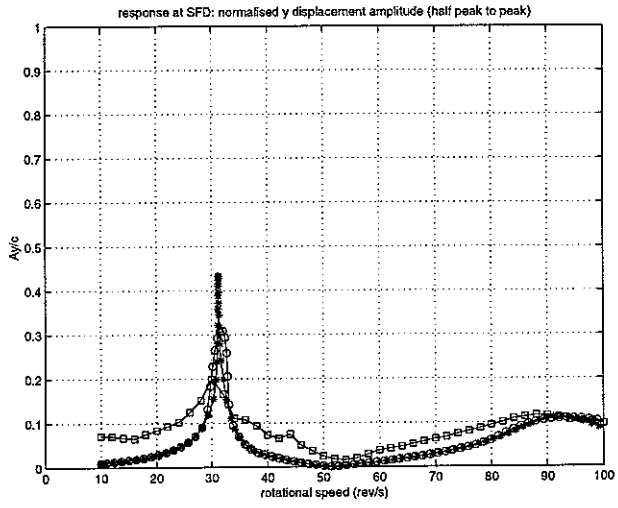

(b) *SFD (J), y direction*

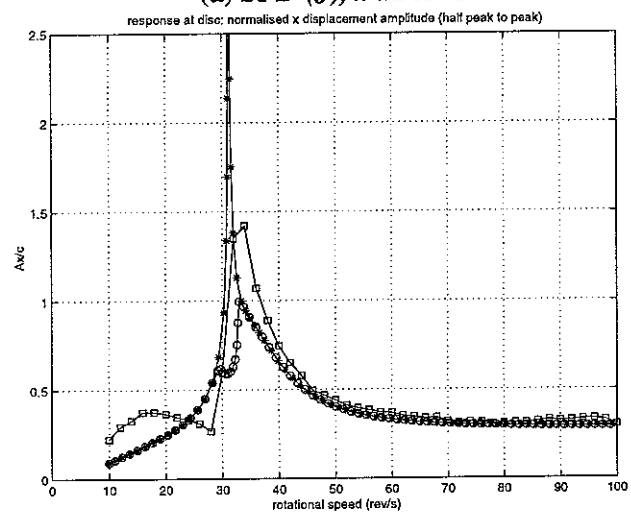

(c) *Disc (U), x direction*

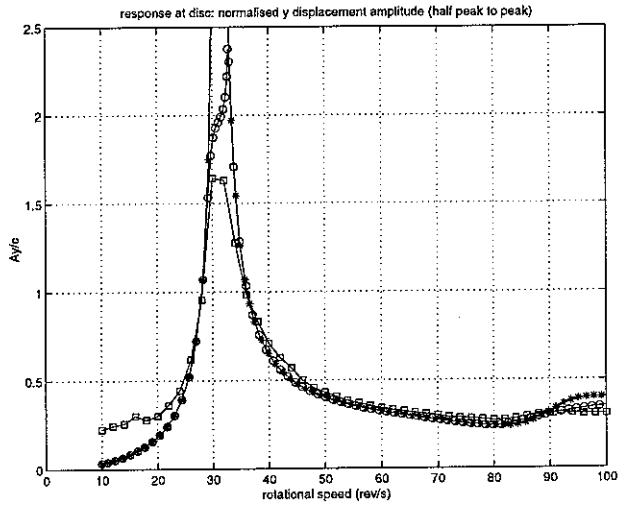

(d) *Disc (U), y direction*

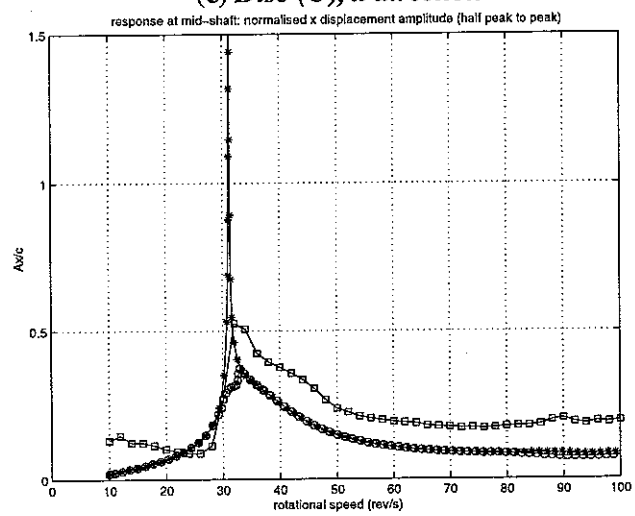

(e) *Mid-shaft (M), x direction*

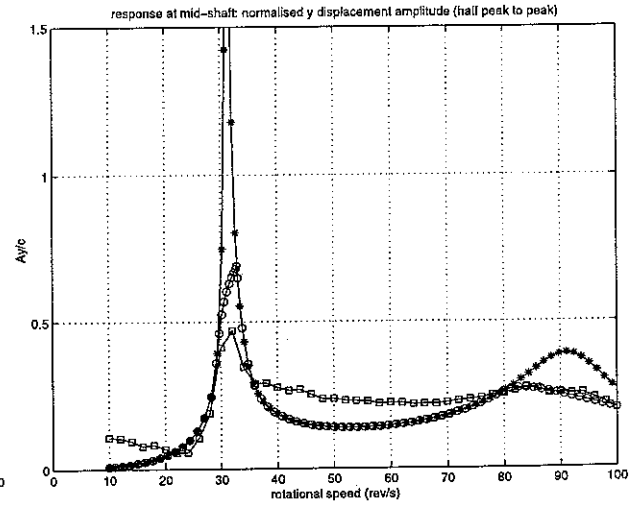

(f) *Mid-shaft (M), y direction*

Figure 27: *Unbalance response (normalised half peak-to-peak) for A1 with* $\varepsilon_{0yJ} = -0.8$ *,* $U = 2.59 \times 10^{-4}\ kgm$*,* $p_S = 1\ bar$*. Measurements:* —□—*.*
Predictions, HB, $N = 1$*,* $m = 5$*: full film* —*—*, absolute zero cavitation* —○—*.*

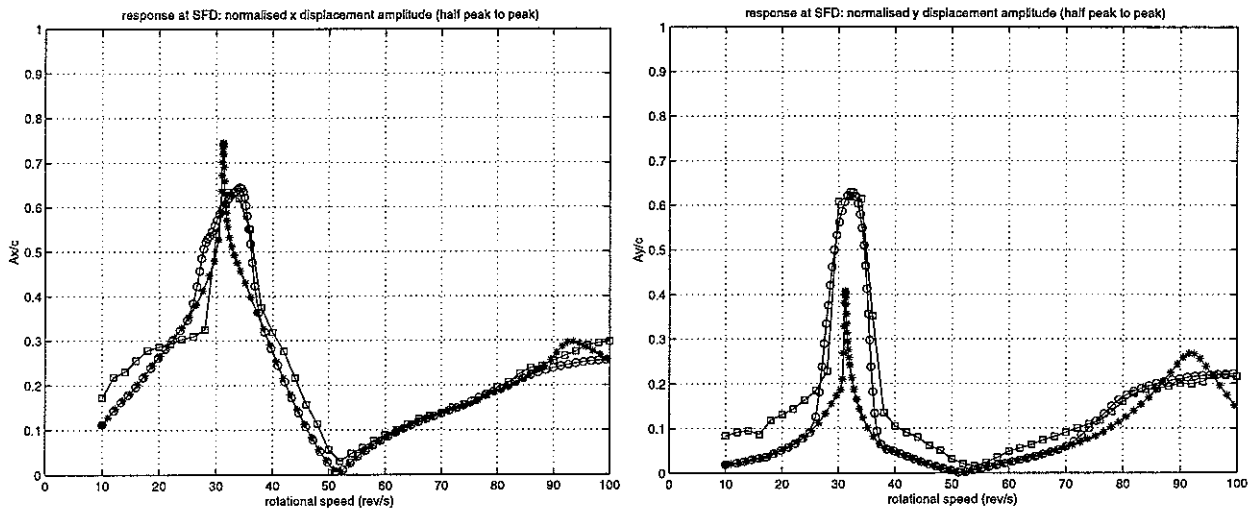

(a) *SFD (J), x direction*

(b) *SFD (J), y direction*

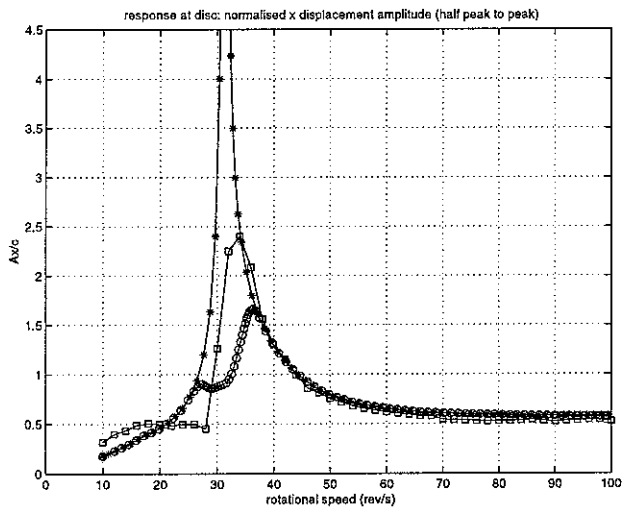

(c) *Disc (U), x direction*

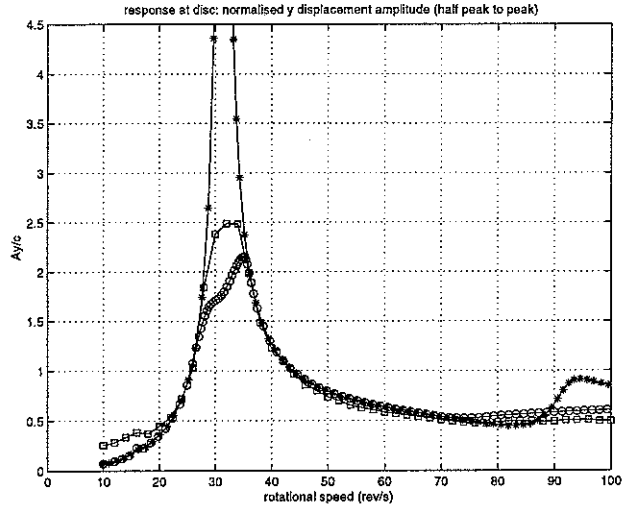

(d) *Disc (U), y direction*

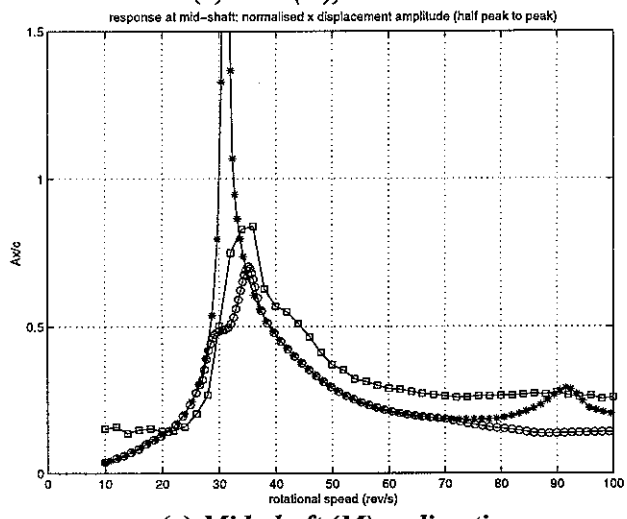

(e) *Mid-shaft (M), x direction*

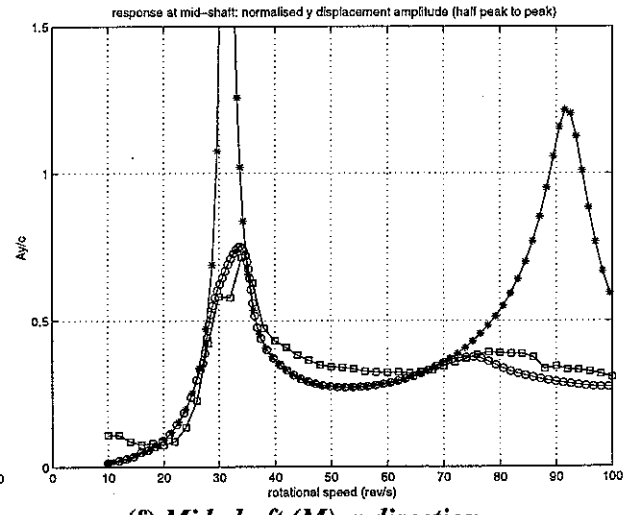

(f) *Mid-shaft (M), y direction*

Figure 28: *Unbalance response (normalised half peak-to-peak) for A1 with* $\varepsilon_{0yJ} = -0.8$ *,* $U = 5.1 \times 10^{-4}$ *kgm,* $p_S = 1$ *bar. Measurements:* —□— *.*

Predictions, HB, $N = 1$*,* $m = 5$*: full film* —*— *, absolute zero cavitation* —○— *.*

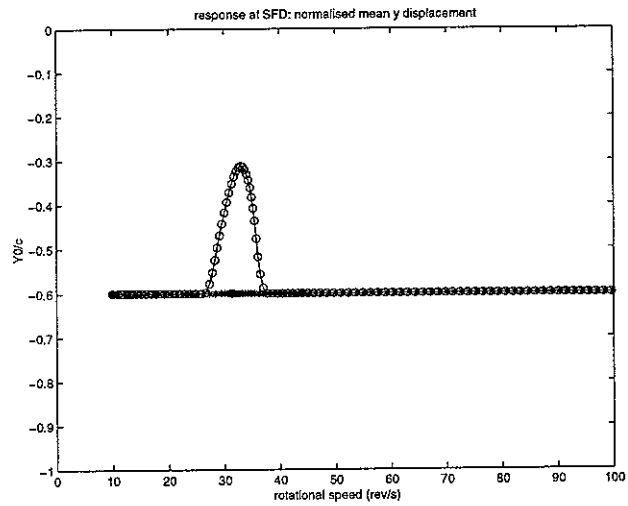

Figure 29: *Normalised HB predicted mean y displacement (lift) for A1 with* $\varepsilon_{0yJ} = -0.6$, $U = 5.1\times10^{-4}\,kgm$, $p_S = 1\,bar$. *Full film* —*—, absolute zero cavitation* —O—.

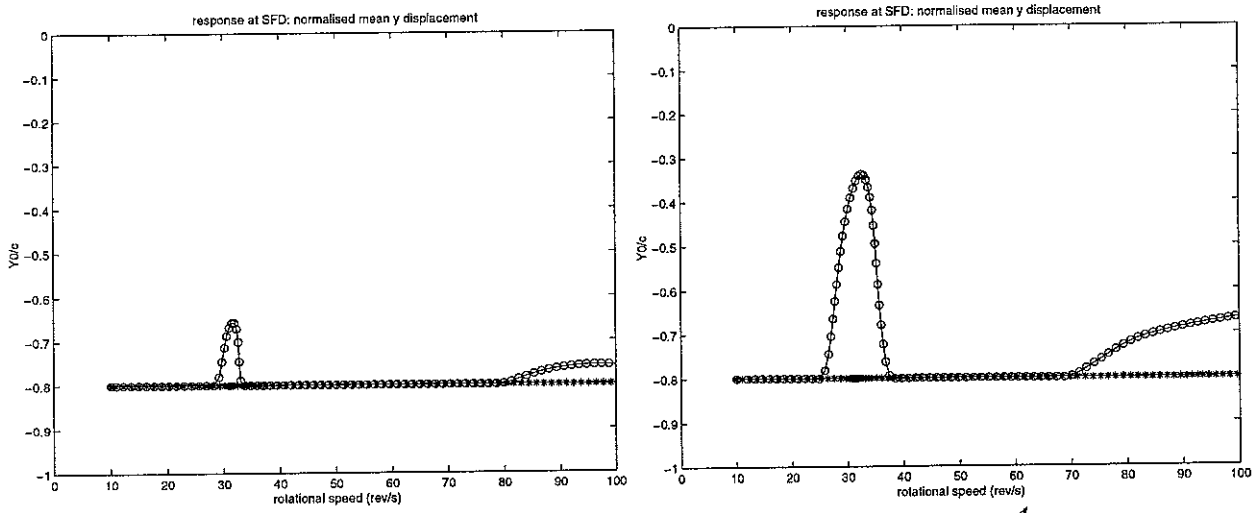

(a) $U = 2.59\times10^{-4}\,kgm$ (b) $U = 5.1\times10^{-4}\,kgm$

Figure 30: *Normalised HB predicted mean y displacement (lift) for A1 with* $\varepsilon_{0yJ} = -0.8$, $p_S = 1\,bar$. *Full film* —*—, *absolute zero cavitation* —O—.

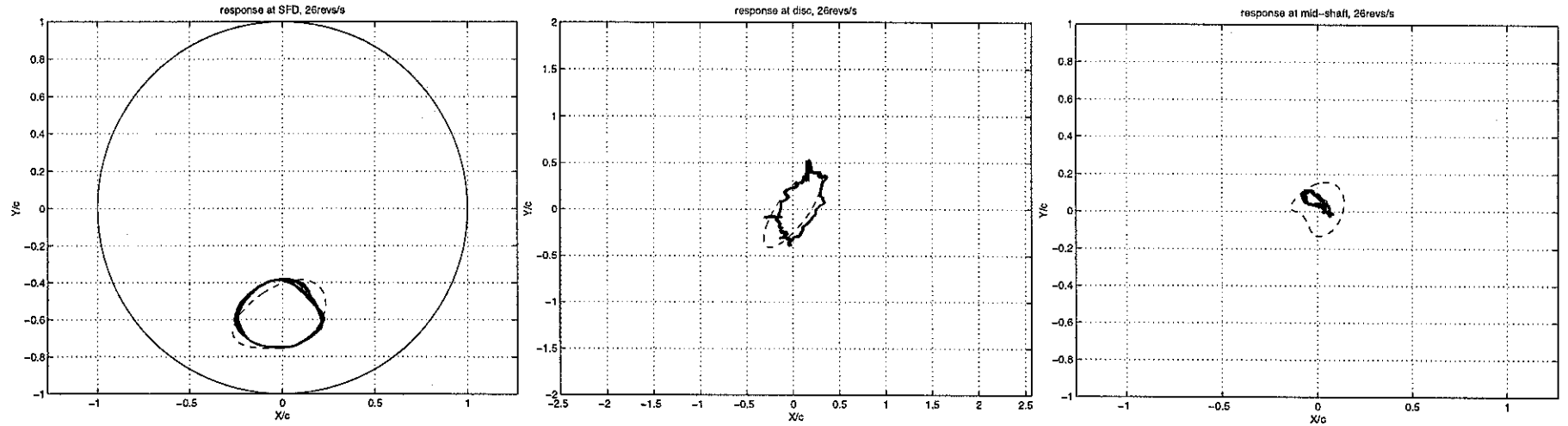

(a1) *SFD (J) 26 rev/s* (a2) *Disc (U) 26 rev/s* (a3) *Mid-shaft (M) 26 rev/s*

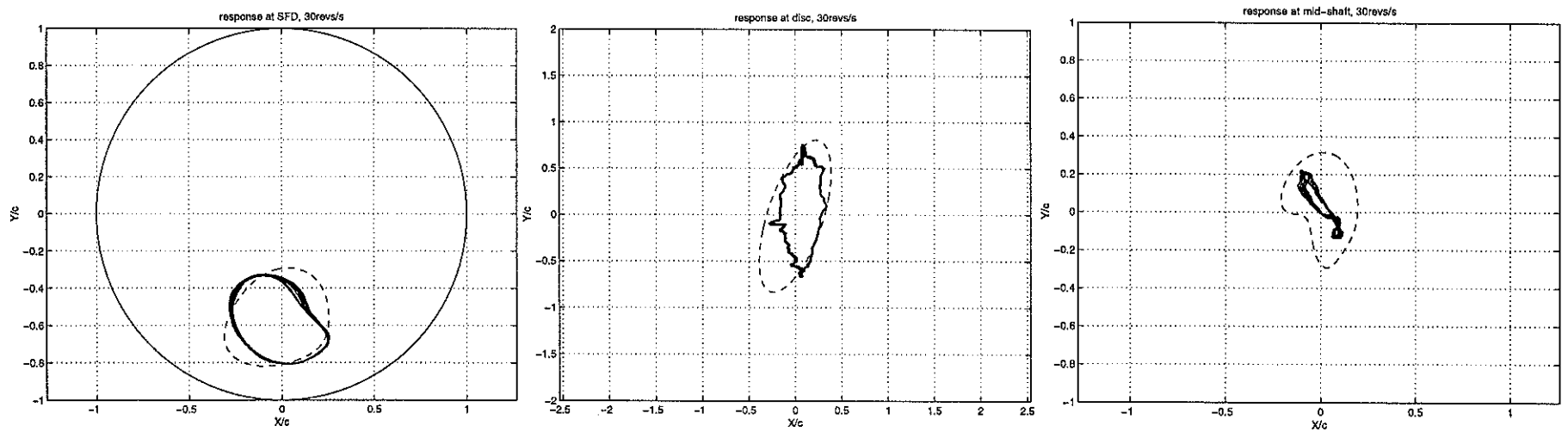

(b1) *SFD (J) 30 rev/s* (b2) *Disc (U) 30 rev/s* (b3) *Mid-shaft (M) 30 rev/s*

Figure 31: *Comparison of predicted and measured orbits for* $\varepsilon_{0yJ} = -0.6$, $U = 2.59\times10^{-4}$ *kgm,* $p_S = 1$ *bar. Prediction: full film, HB,* $N = 1$, $m = 5$ (– – –). *Measurement (0.5s)* (——).

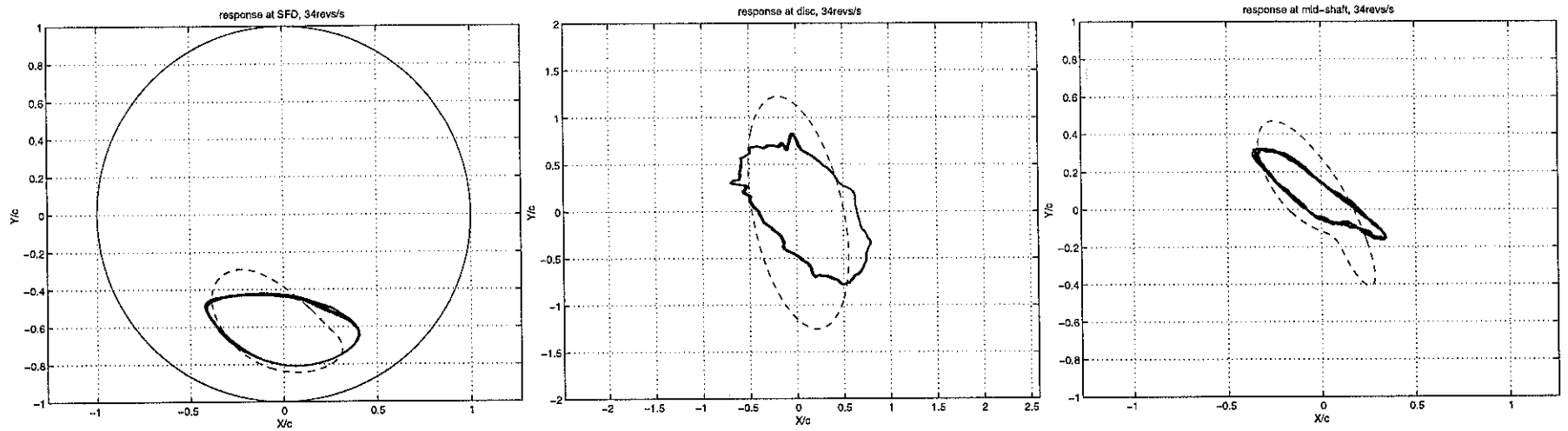

(c1) *SFD (J) 34 rev/s* (c2) *Disc (U) 34 rev/s* (c3) *Mid-shaft (M) 34 rev/s*

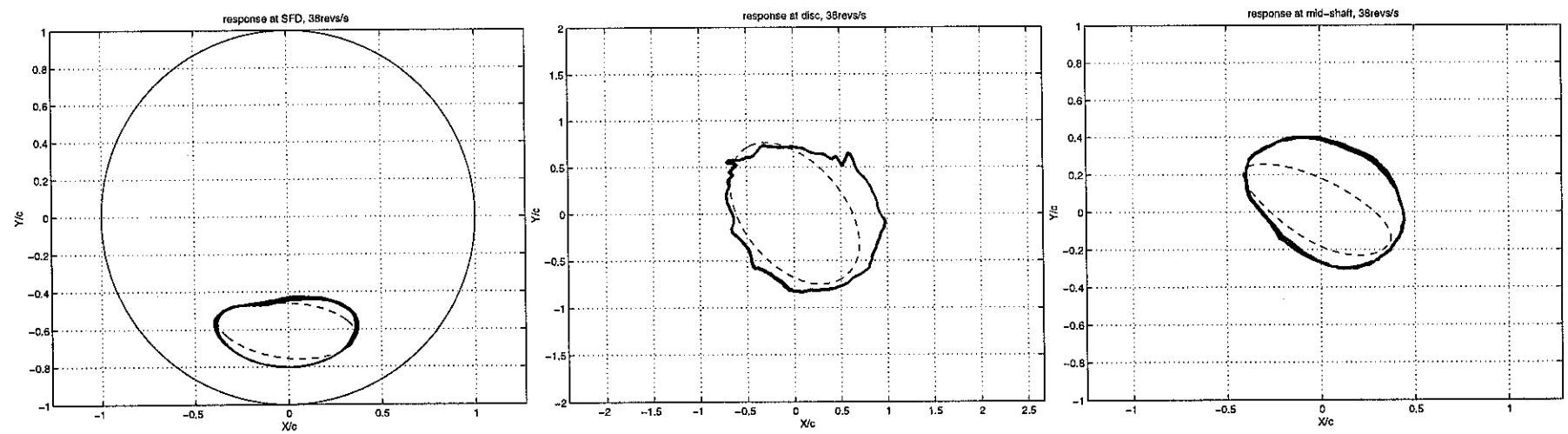

(d1) *SFD (J) 38 rev/s* (d2) *Disc (U) 38 rev/s* (d3) *Mid-shaft (M) 38 rev/s*

Figure 31 (continued): *Comparison of predicted and measured orbits for* $\varepsilon_{0yJ} = -0.6$, $U = 2.59 \times 10^{-4}$ *kgm,* $p_S = 1$ *bar. Prediction: full film, HB,* $N = 1$, $m = 5$ (– – –). *Measurement (0.5s)* (——).

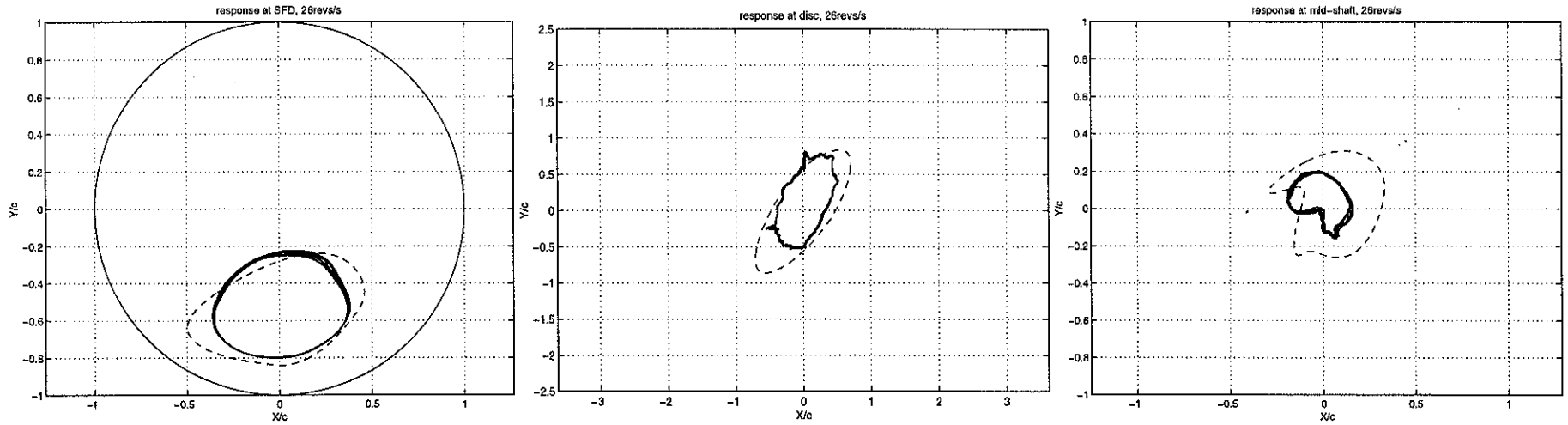

(a1) *SFD (J) 26 rev/s* (a2) *Disc (U) 26 rev/s* (a3) *Mid-shaft (M) 26 rev/s*

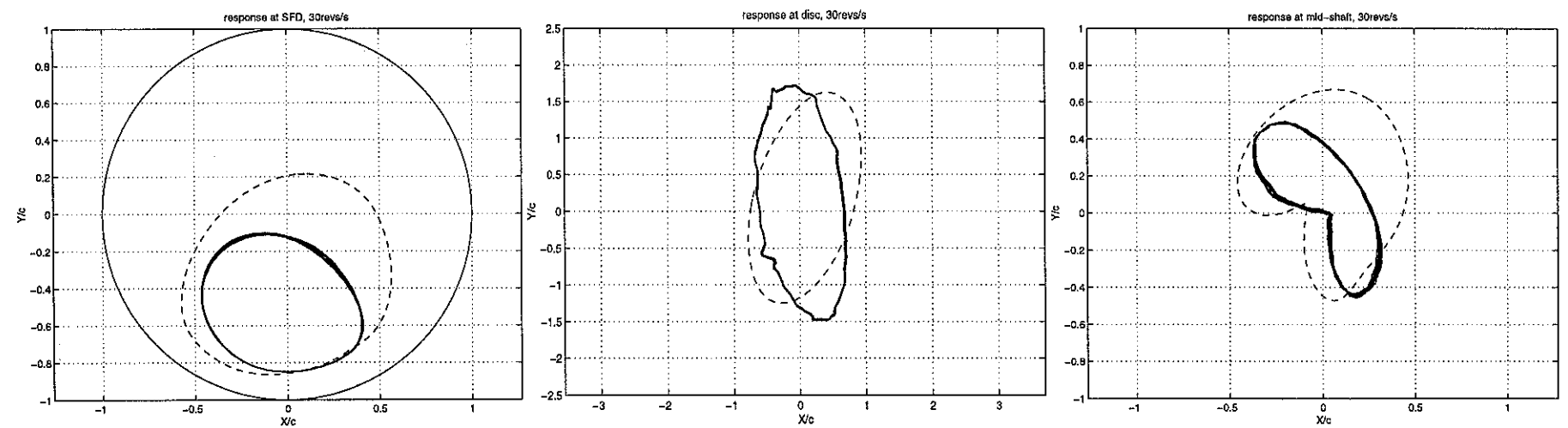

(b1) *SFD (J) 30 rev/s* (b2) *Disc (U) 30 rev/s* (b3) *Mid-shaft (M) 30 rev/s*

Figure 32: *Comparison of predicted and measured orbits for* $\varepsilon_{0yJ} = -0.6$, $U = 5.1 \times 10^{-4}$ *kgm,* $p_S = 1$ *bar. Prediction: absolute zero cavitation, HB,* $N = 1$, $m = 5$ (– – –). *Measurement (0.5s)* (——).

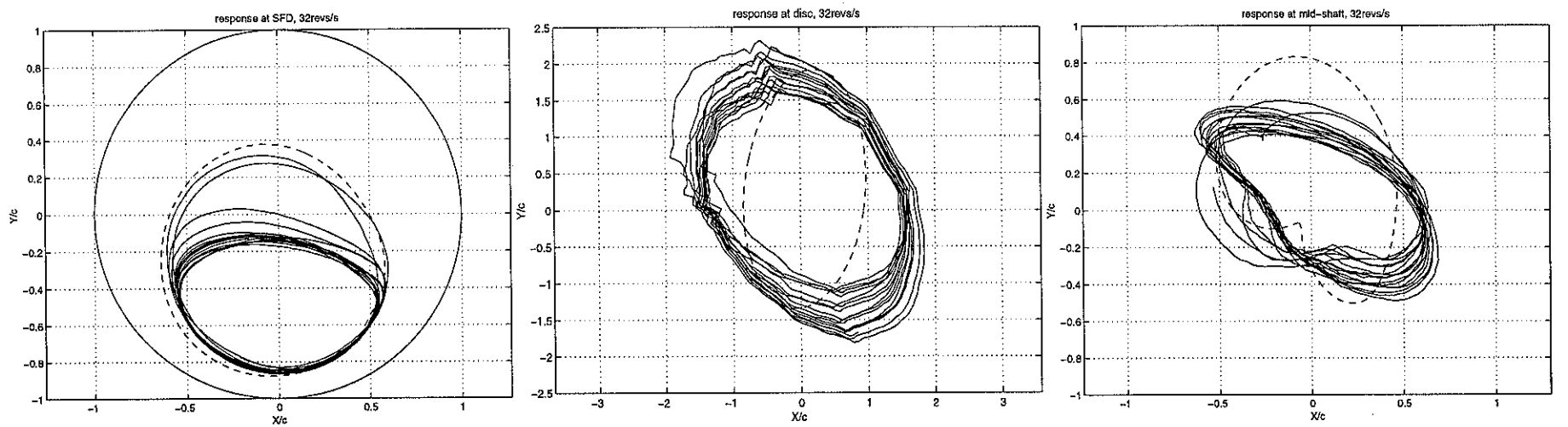

(c1) *SFD (J) 32 rev/s* (c2) *Disc (U) 32 rev/s* (c3) *Mid-shaft (M) 32 rev/s*

(d1) *SFD (J) 34 rev/s* (d2) *Disc (U) 34 rev/s* (d3) *Mid-shaft (M) 34 rev/s*

Figure 32 (continued): *Comparison of predicted and measured orbits for* $\varepsilon_{0yJ} = -0.6$, $U = 5.1\times10^{-4}$ *kgm,* $p_S = 1$ *bar. Prediction: absolute zero cavitation, HB,* $N = 1$, $m = 5$ (– – –). *Measurement (0.5s)* (——).

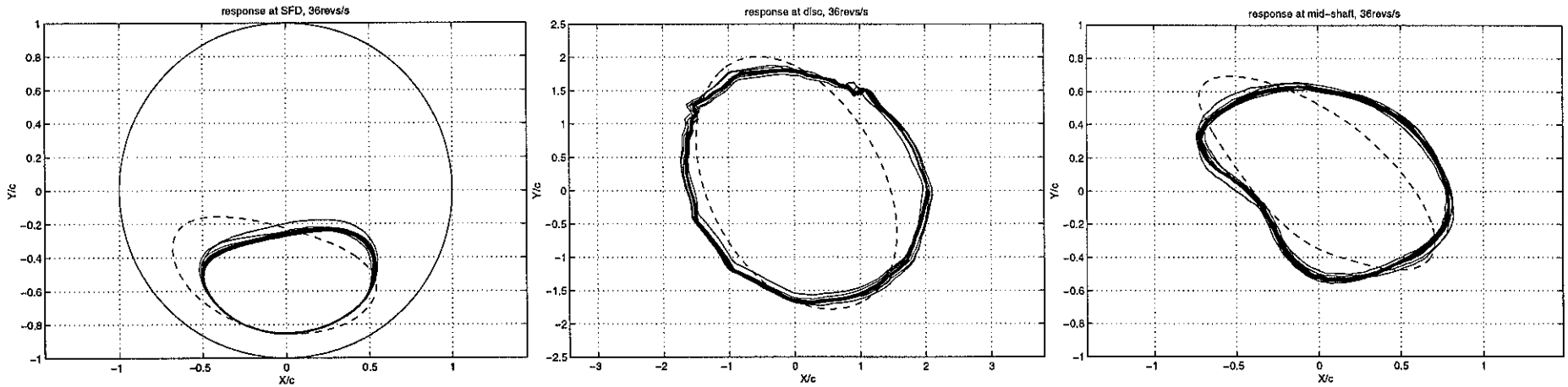

(e1) *SFD (J) 36 rev/s* (e2) *Disc (U) 36 rev/s* (e3) *Mid-shaft (M) 36 rev/s*

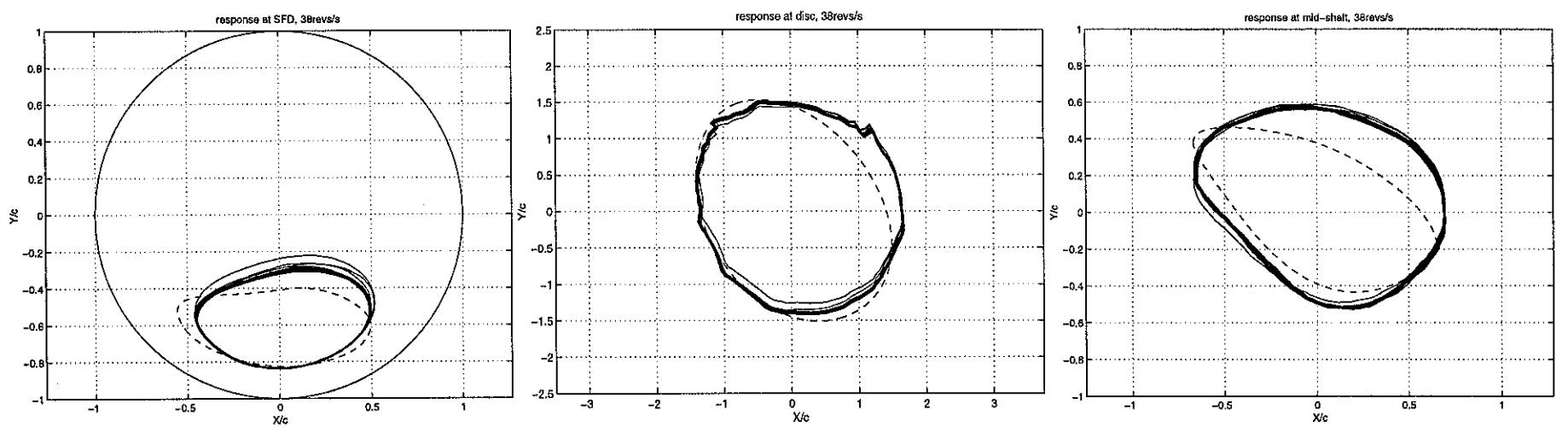

(f1) *SFD (J) 38 rev/s* (f2) *Disc (U) 38 rev/s* (f3) *Mid-shaft (M) 38 rev/s*

Figure 32 (continued): *Comparison of predicted and measured orbits for* $\varepsilon_{0yJ} = -0.6$, $U = 5.1\times10^{-4}$ *kgm,* $p_S = 1$ *bar. Prediction: absolute zero cavitation, HB,* $N = 1$, $m = 5$ (– – –). *Measurement (0.5s)* (——).

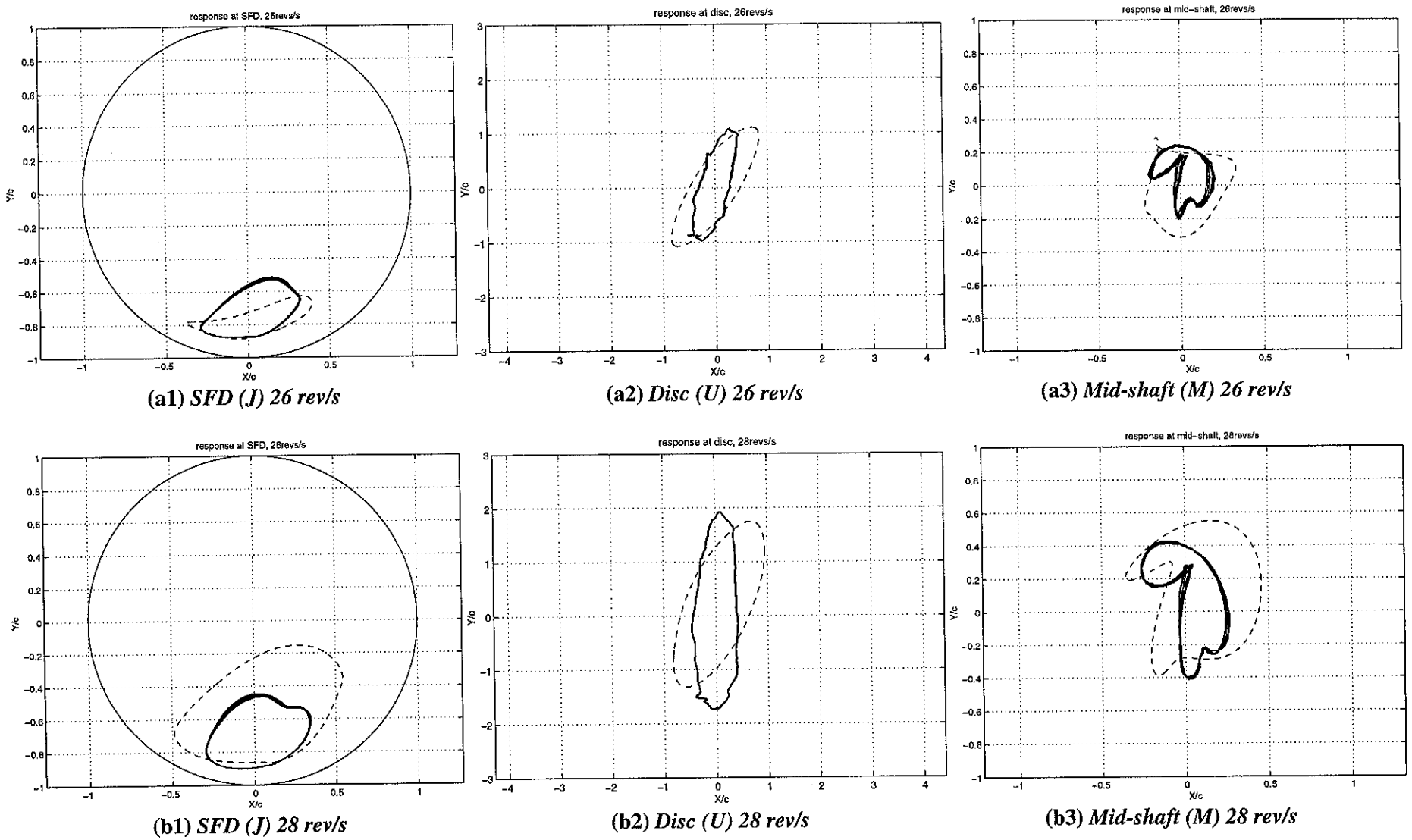

(a1) *SFD (J) 26 rev/s* (a2) *Disc (U) 26 rev/s* (a3) *Mid-shaft (M) 26 rev/s*

(b1) *SFD (J) 28 rev/s* (b2) *Disc (U) 28 rev/s* (b3) *Mid-shaft (M) 28 rev/s*

Figure 33: *Comparison of predicted and measured orbits for* $\varepsilon_{0yJ} = -0.8$, $U = 5.1\times10^{-4}$ *kgm,* $p_S = 1$ *bar. Prediction: absolute zero cavitation, HB,* $N = 1$, $m = 5$ (– – –). *Measurement (0.5s)* (——).

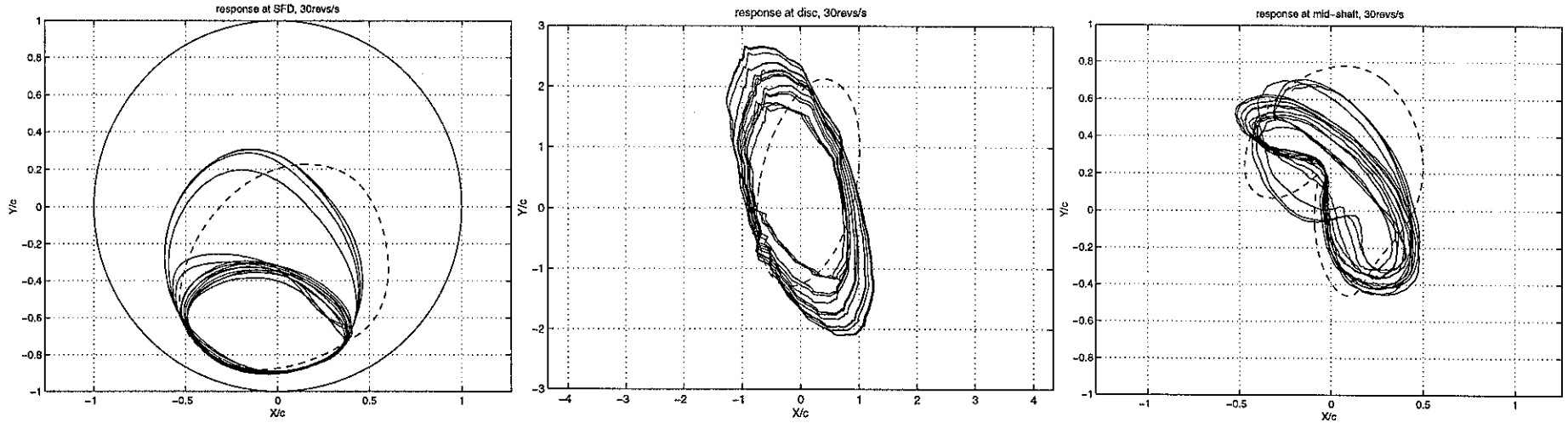

(c1) *SFD (J) 30 rev/s* (c2) *Disc (U) 30 rev/s* (c3) *Mid-shaft (M) 30 rev/s*

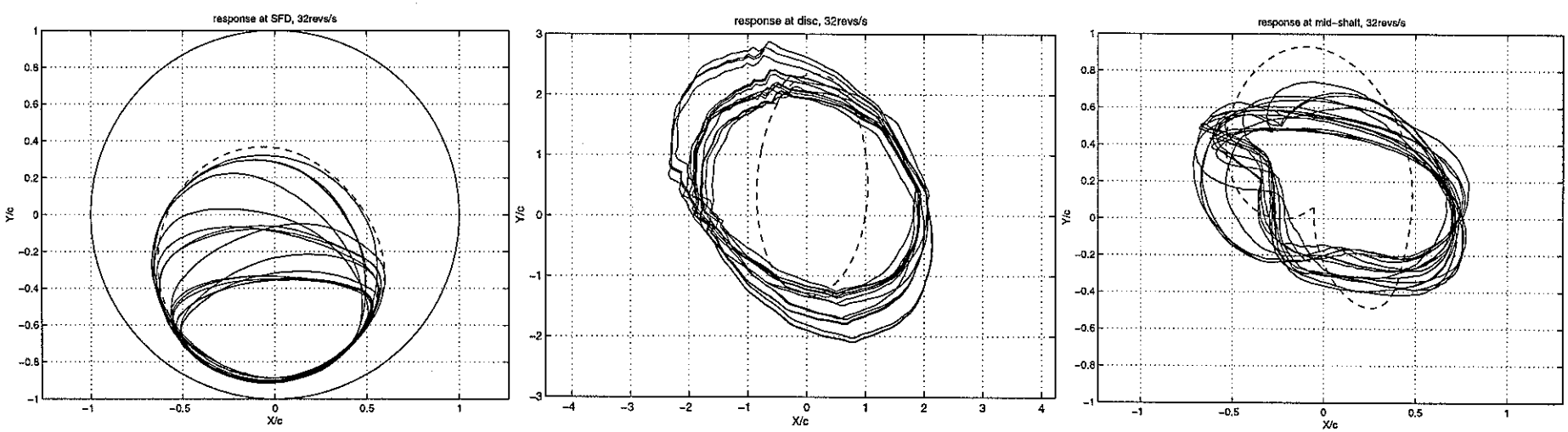

(d1) *SFD (J) 32 rev/s* (d2) *Disc (U) 32 rev/s* (d3) *Mid-shaft (M) 32 rev/s*

Figure 33 (continued): *Comparison of predicted and measured orbits for* $\varepsilon_{0yJ} = -0.8$, $U = 5.1\times10^{-4}$ *kgm,* $p_S = 1$*bar. Prediction: absolute zero cavitation, HB,* $N = 1$, $m = 5$ (– – –). *Measurement (0.5s)* (——).

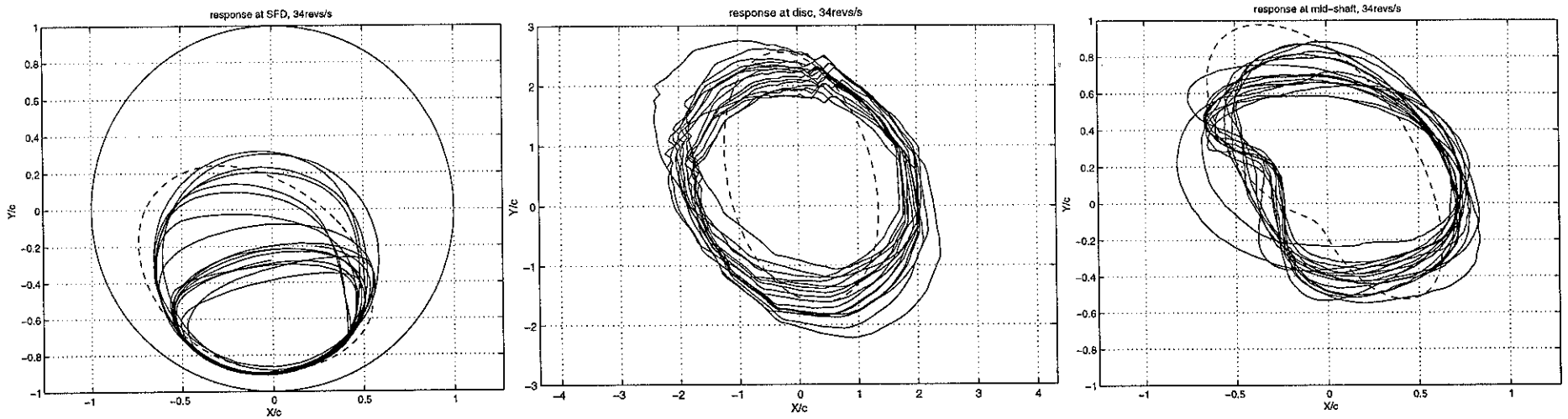

(e1) *SFD (J) 34 rev/s* (e2) *Disc (U) 34 rev/s* (e3) *Mid-shaft (M) 34 rev/s*

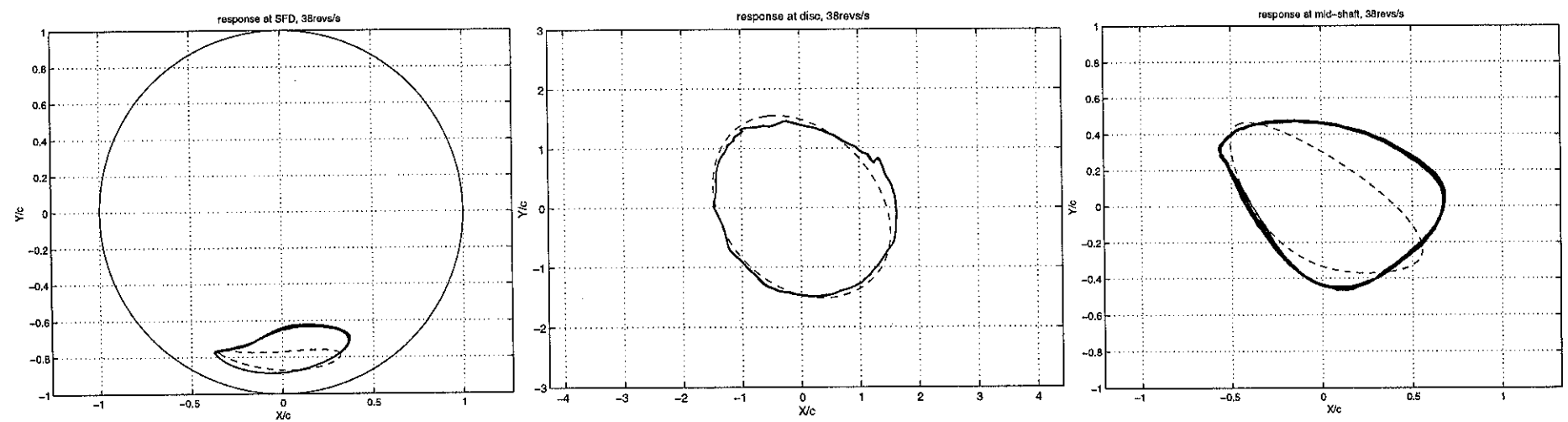

(f1) *SFD (J) 38 rev/s* (f2) *Disc (U) 38 rev/s* (f3) *Mid-shaft (M) 38 rev/s*

Figure 33 (continued): *Comparison of predicted and measured orbits for* $\varepsilon_{0yJ} = -0.8$, $U = 5.1\times10^{-4}$ *kgm,* $p_S = 1$*bar. Prediction: absolute zero cavitation, HB,* $N = 1$, $m = 5$ (– – –). *Measurement (0.5s)* (——).

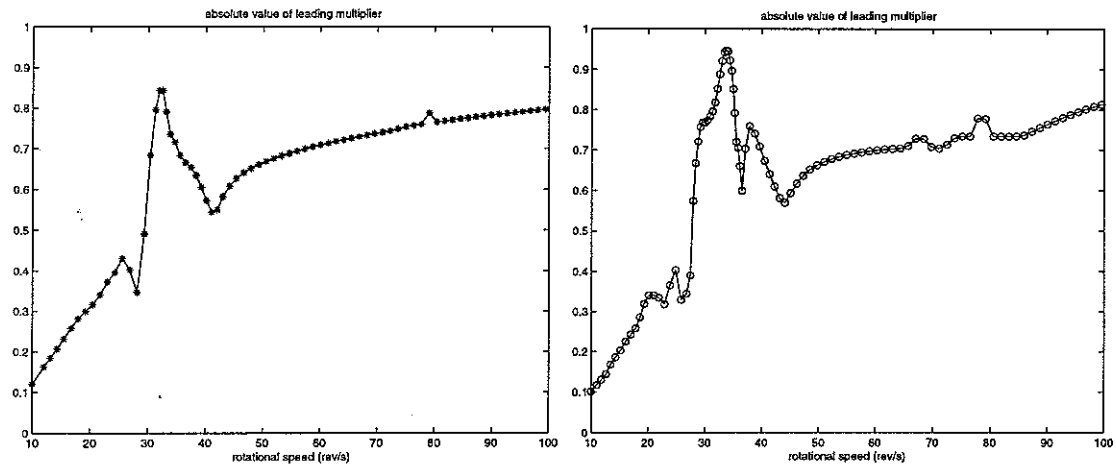

(a) $U = 2.59\times10^{-4}$ *kgm, full film theory* (b) $U = 5.1\times10^{-4}$ *kgm, absolute zero theory*

Figure 34: ***Fast stabilty check (Method IIb) for harmonic balance solutions*** $N = 1,\ m = 5,$ ***for*** $\varepsilon_{0yJ} = -0.6$ ***: variation of magnitude of leading multiplier.***

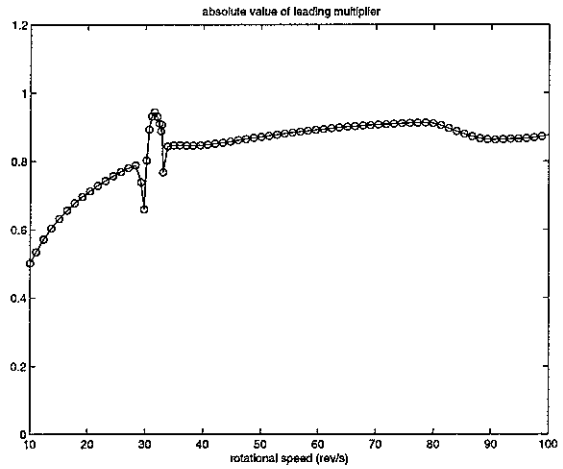

(a) *magnitude of leading multiplier*

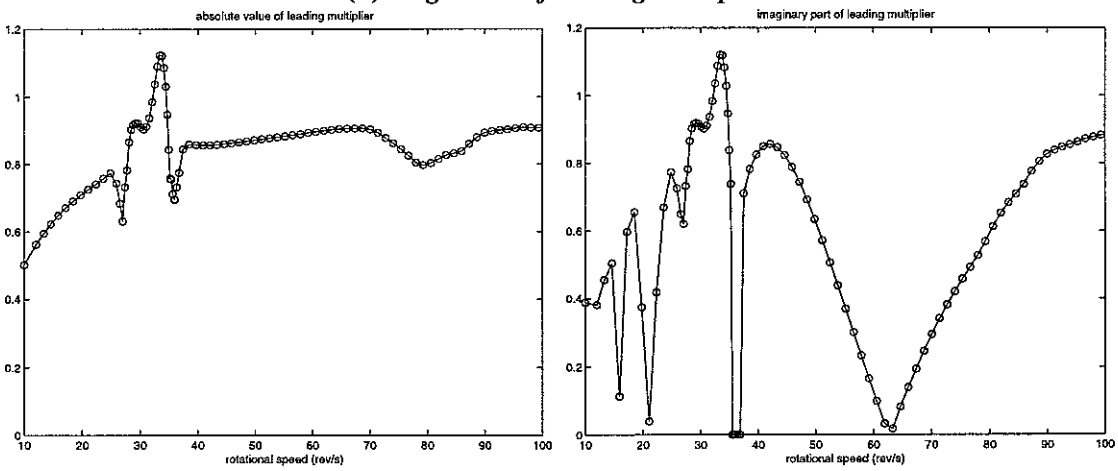

(b1) *magnitude of leading multiplier* (b2) *imaginary part of leading multiplier*

Figure 35: ***Fast stabilty check (Method IIb) for harmonic balance solutions*** $N = 1,\ m = 5,$ ***for*** $\varepsilon_{0yJ} = -0.8$ ***:***

(a): $U = 2.59\times10^{-4}$ *kgm, absolute zero theory.* **(b1), (b2):** $U = 5.1\times10^{-4}$ *kgm, absolute zero theory.*

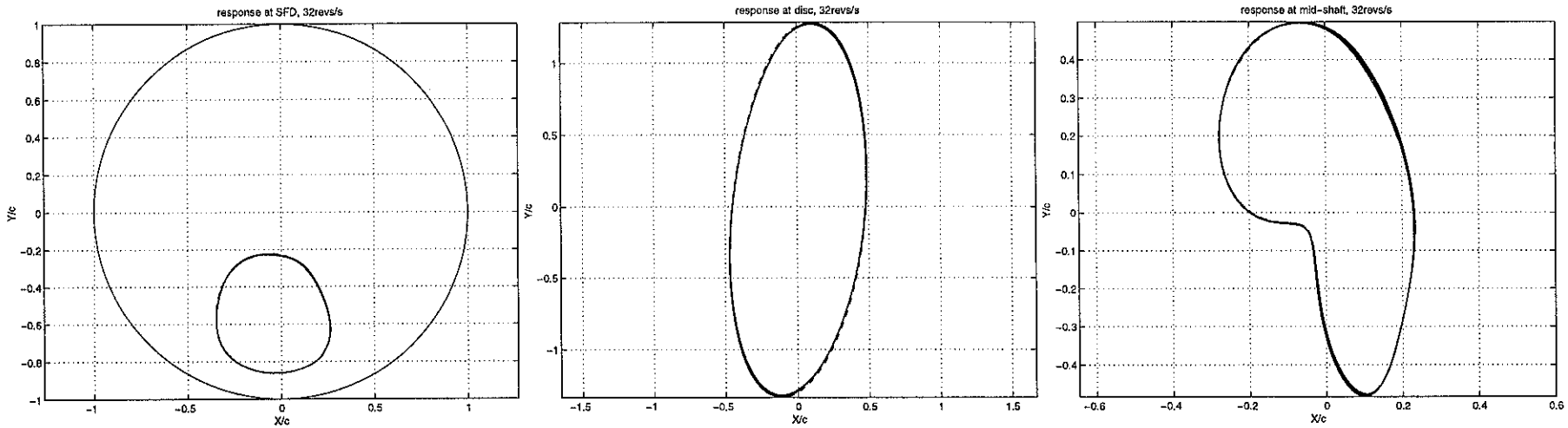

(a) *SFD (J) 26 rev/s* (b) *Disc (U) 26 rev/s* (c) *Mid-shaft (M) 26 rev/s*

Figure 36: *Stability check by Method I: predicted orbits at 26 rev/s for* $\varepsilon_{0yJ} = -0.6$, $U = 2.59 \times 10^{-4}$ *kgm, full film theory. HB,* $N = 1$, $m = 5$ (– – –), *time domain integration* (——) *(over 10 revolutions with* $q = 4$, *initial conditions derived from HB solution).*

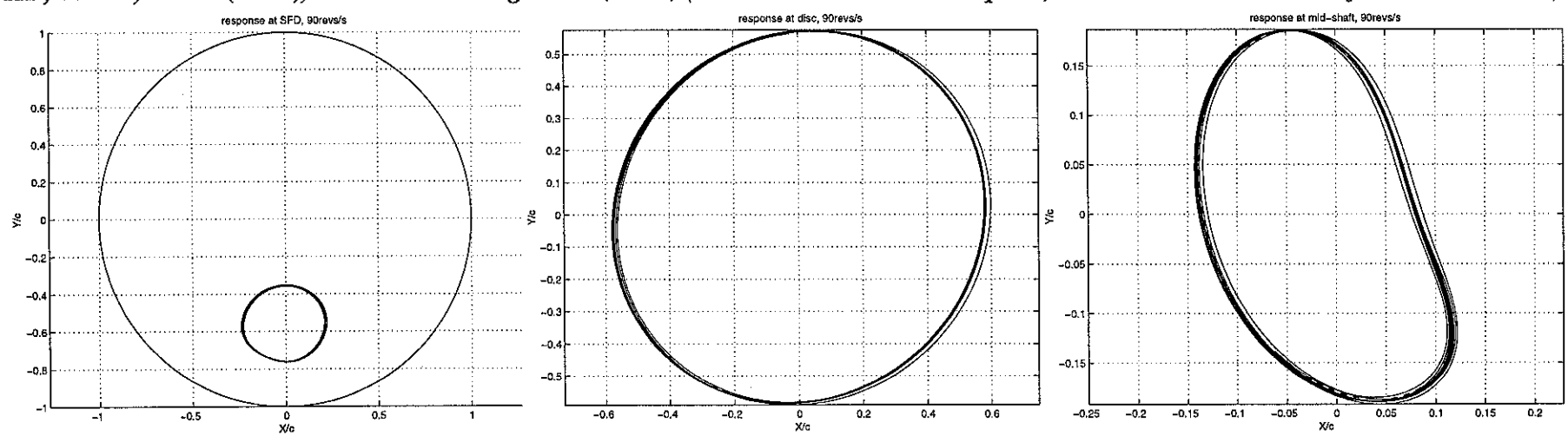

(a) *SFD (J) 90 rev/s* (b) *Disc (U) 90 rev/s* (c) *Mid-shaft (M) 90 rev/s*

Figure 37: *Stability check by Method I: orbits at 90 rev/s for* $\varepsilon_{0yJ} = -0.6$, $U = 5.1 \times 10^{-4}$ *kgm, absolute zero theory,* $p_S = 1$ *bar. HB,* $N = 1$, $m = 5$ (– – –), *time domain integration* (——) *(over 10 revolutions with* $q = 4$, *initial conditions derived from HB solution).*

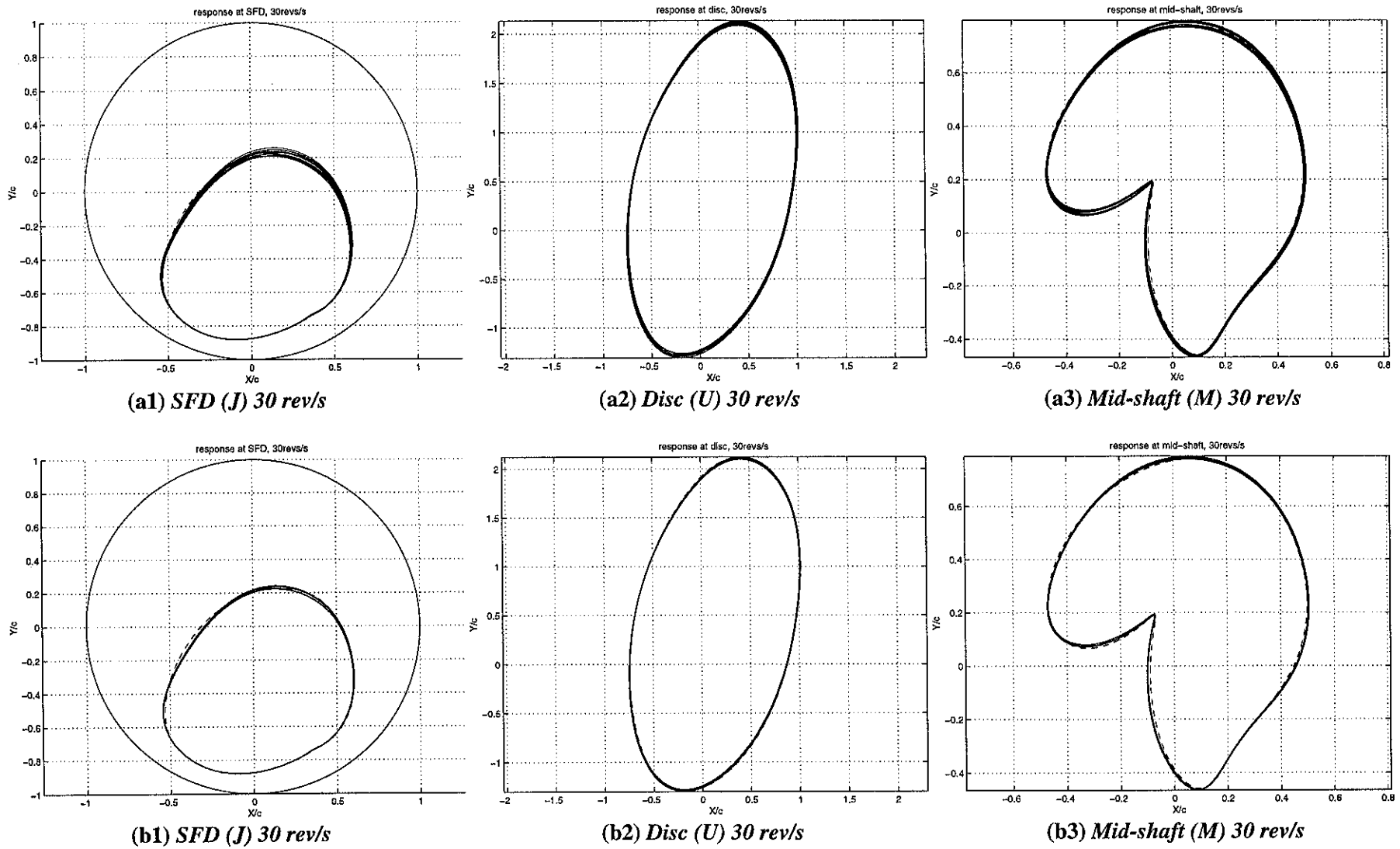

(a1) *SFD (J) 30 rev/s* (a2) *Disc (U) 30 rev/s* (a3) *Mid-shaft (M) 30 rev/s*

(b1) *SFD (J) 30 rev/s* (b2) *Disc (U) 30 rev/s* (b3) *Mid-shaft (M) 30 rev/s*

Figure 38: *Stability check by Method I: predicted orbits at 30 rev/s for* $\varepsilon_{0yJ} = -0.8$, $U = 5.1\times10^{-4}$ *kgm, absolute zero theory,* $p_S = 1$ *bar.* **(a1)-(a3):** *HB,* $N = 1$, $m = 5$ (– – –), *time domain integration* (——) *(over 10 revolutions with* $q = 4$, *initial conditions derived from HB solution).* **(b1)-(b3):** *HB* (– – –), *time domain integration* (——) *(over a further 5 revolutions).*

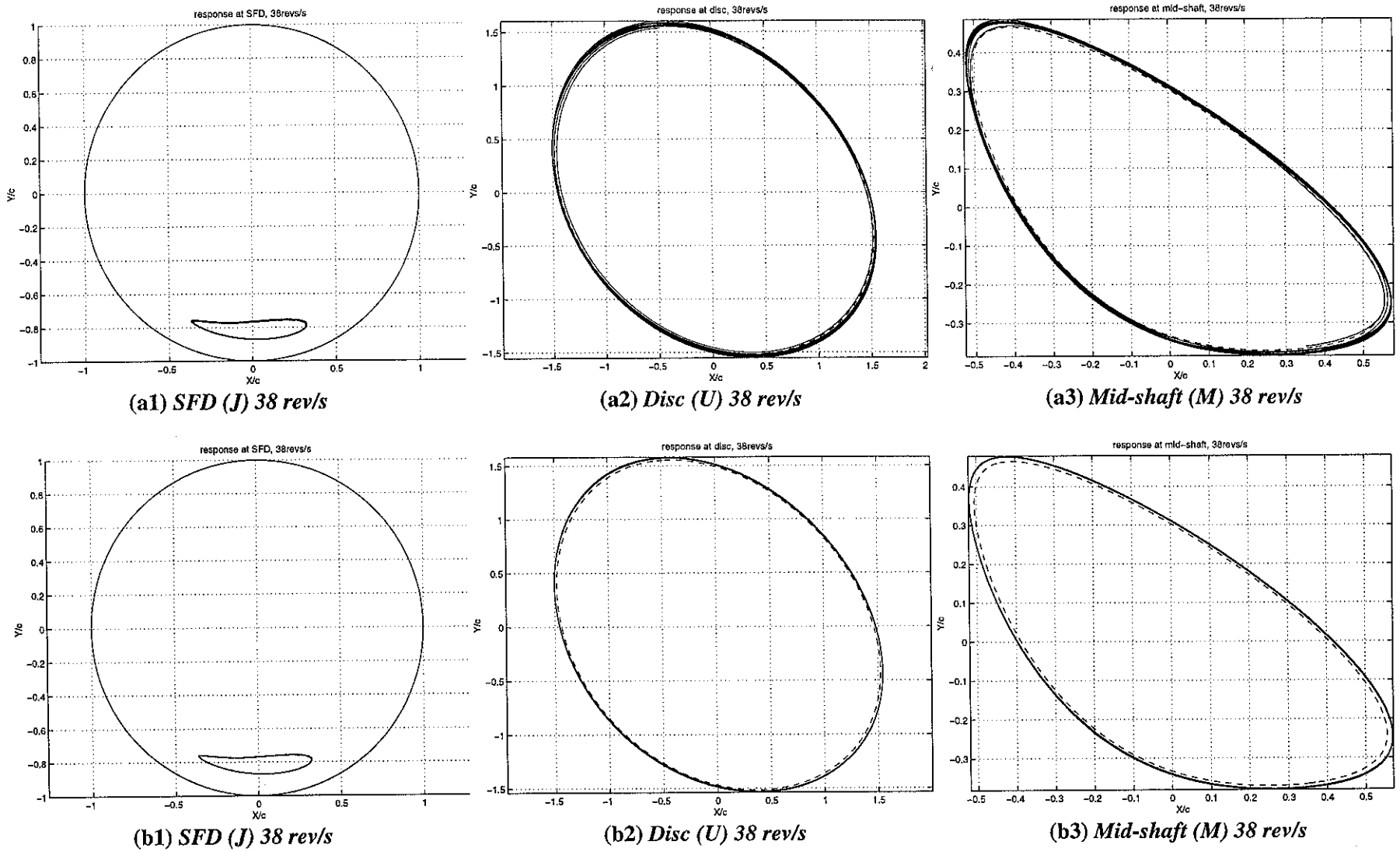

(a1) *SFD (J) 38 rev/s* (a2) *Disc (U) 38 rev/s* (a3) *Mid-shaft (M) 38 rev/s*

(b1) *SFD (J) 38 rev/s* (b2) *Disc (U) 38 rev/s* (b3) *Mid-shaft (M) 38 rev/s*

Figure 39: *Stability check by Method I: predicted orbits at 38 rev/s for* $\varepsilon_{0yJ} = -0.8$, $U = 5.1\times10^{-4}$ *kgm, absolute zero theory,* $p_S = 1$ *bar.* **(a1)-(a3):** *HB,* $N = 1$, $m = 5$ (– – –), *time domain integration* (——) *(over 10 revolutions with* $q = 4$, *initial conditions derived from HB solution).* **(b1)-(b3):** *HB* (– – –), *time domain integration* (——) *(over a further 5 revolutions).*

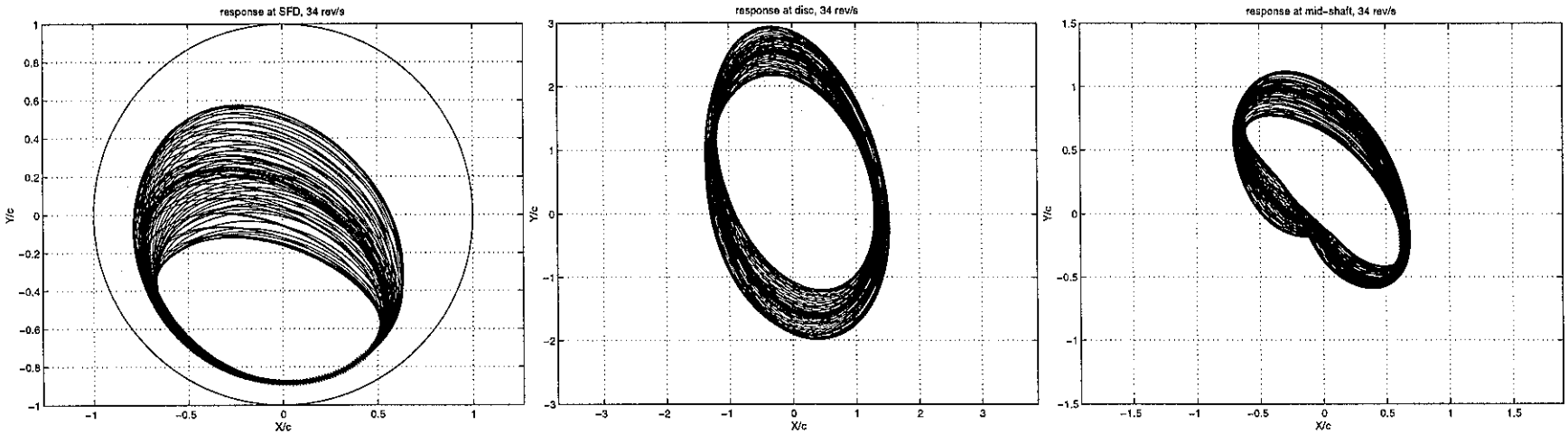

(a) *SFD (J) 34 rev/s* (b) *Disc (U) 34 rev/s* (c) *Mid-shaft (M) 34 rev/s*

Figure 40: *Stability check by Method I: predicted orbits at 34 rev/s for* $\varepsilon_{0yJ} = -0.8$, $U = 5.1\times10^{-4}$ *kgm, absolute zero theory,* $p_S = 1$ *bar. HB,* $N = 1$, $m = 5$ (****), *time domain integration* (——) *(over 80 revolutions with* $q = 4$, *initial conditions derived from HB solution).*

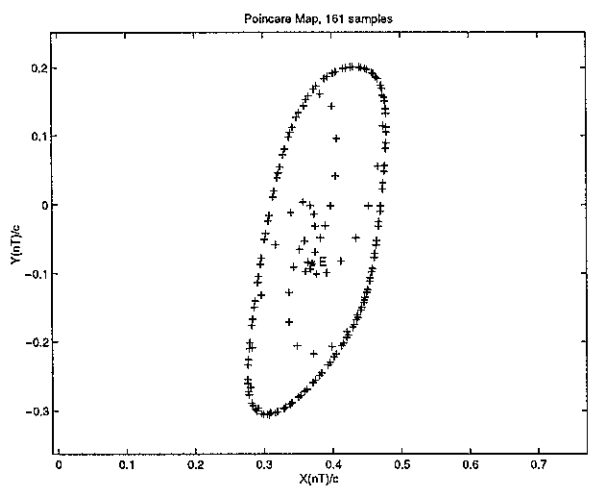

Figure 41: *Poincare map of SFD orbit in Figure 40(a)*
(unstable equilibrium point is E, indicated by ""; sampling rate: once per shaft revolution, no. of samples: 160).*

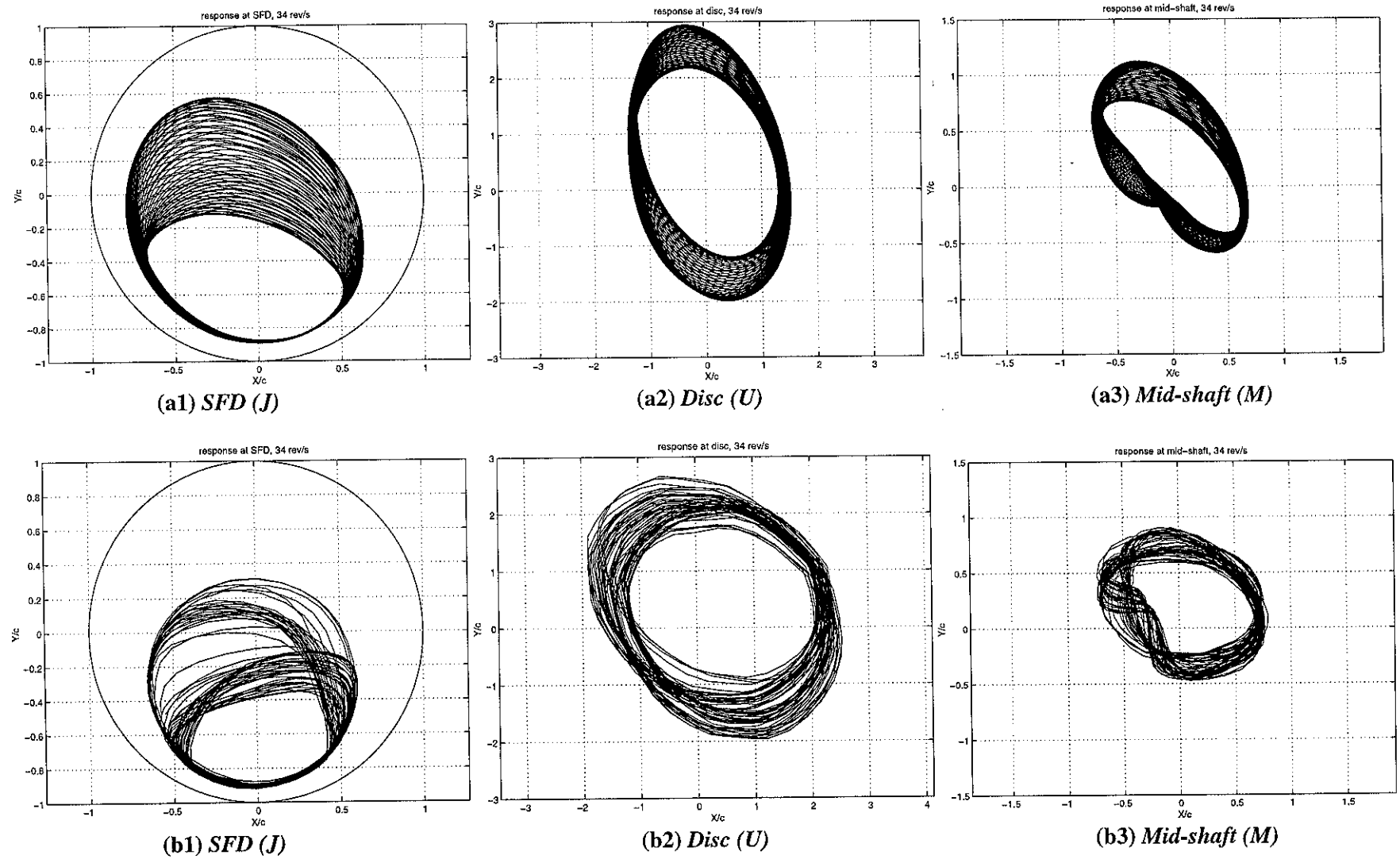

Figure 42: *Orbits at 34 rev/s for* $\varepsilon_{0yJ} = -0.8$, $U = 5.1\times10^{-4}$ *kgm,* $p_S = 1$ *bar.* **(a1)-(a3):** *time domain integration with* $q = 4$, *absolute zero theory (steady state solution, last 80 revolutions out of a total of 160).* **(b1)-(b3):** *measurement over 2s.*

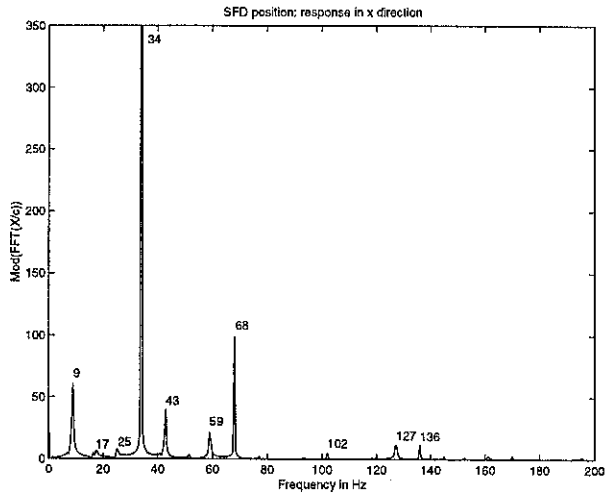

(a1) *SFD, x direction*

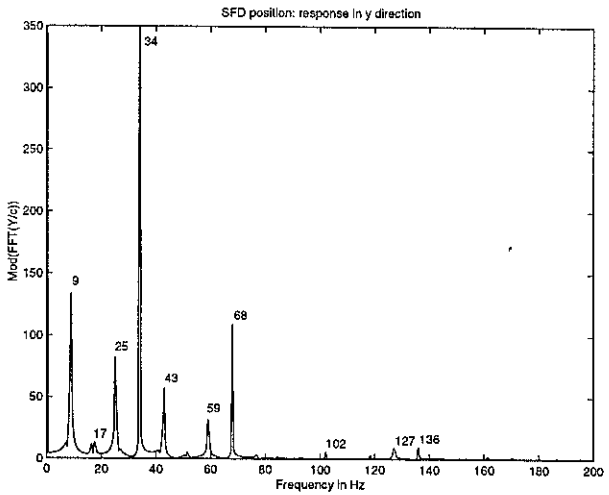

(a2) *SFD, y direction*

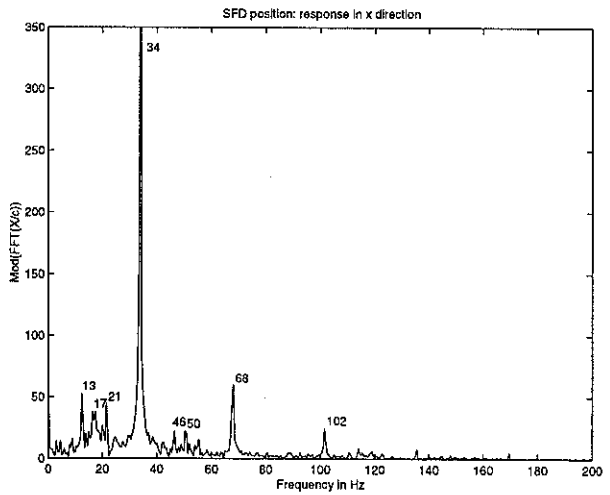

(b1) *SFD, x direction*

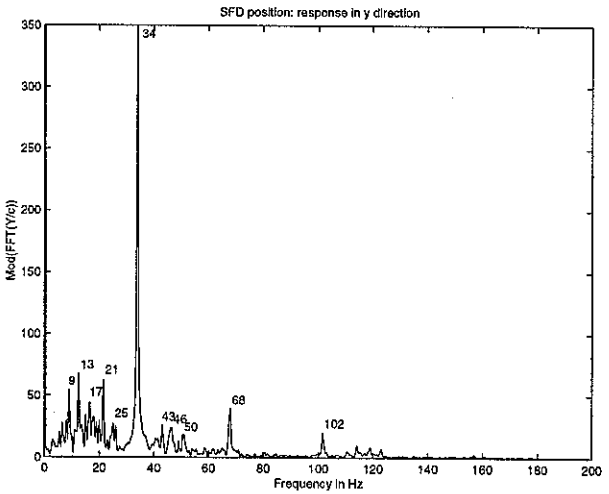

(b2) *SFD, y direction*

Figure 43: *Frequency spectra of SFD orbit at 34 rev/s for* $\varepsilon_{0yJ} = -0.8$, $U = 5.1 \times 10^{-4}$ *kgm,* $p_S = 1$ *bar.*
(a1), (a2): *predicted (absolute zero theory).* **(b1), (b2):** *measured.*

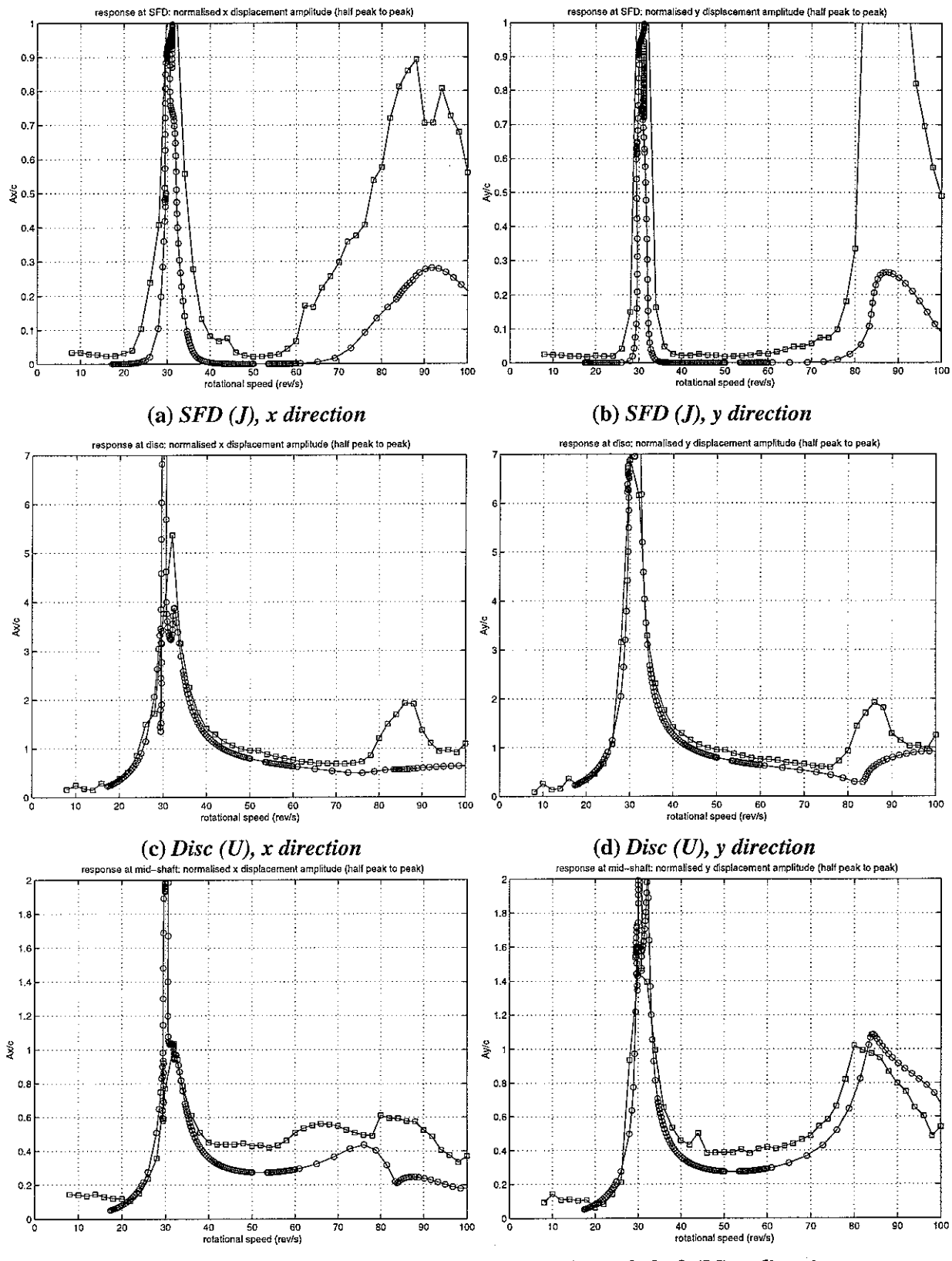

(a) *SFD (J), x direction*

(b) *SFD (J), y direction*

(c) *Disc (U), x direction*

(d) *Disc (U), y direction*

(e) *Mid-shaft (M), x direction*

(f) *Mid-shaft (M), y direction*

Figure 44: *Unbalance response (normalised half peak-to-peak) for A2 with* $U = 5.1 \times 10^{-4}\,kgm$, $p_S = 1.2\,bar$. *Measurements:* —□—. *Predictions, HB,* $N = 1$, $m = 5$ *: absolute zero cavitation* —○—.

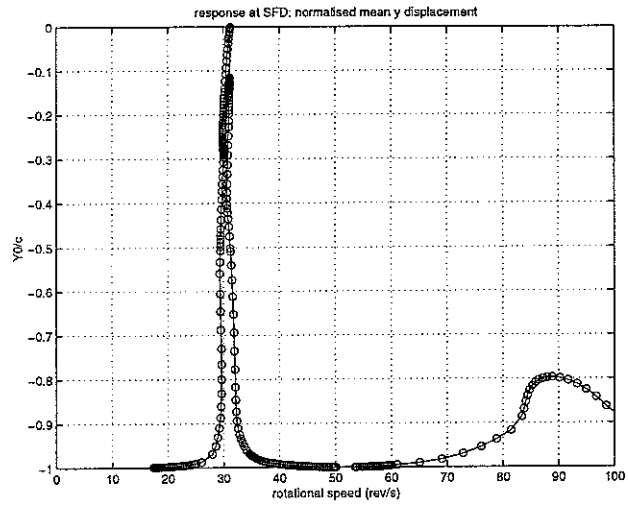

Figure 45: *Normalised HB predicted mean y displacement (lift) for A2 with* $U = 5.1\times10^{-4}\,kgm,\ p_S = 1.2\,bar,$ *absolute zero cavitation.*

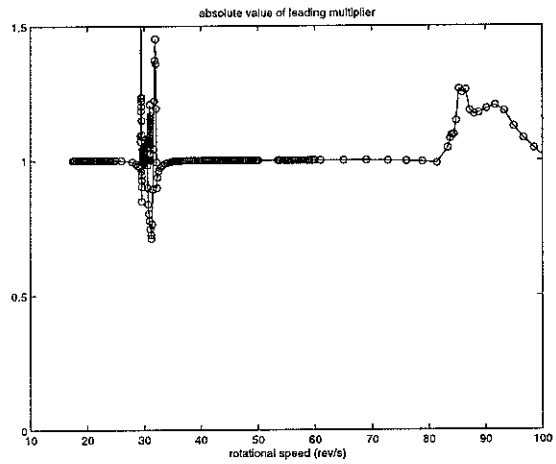

(a) *magnitude of leading multiplier*

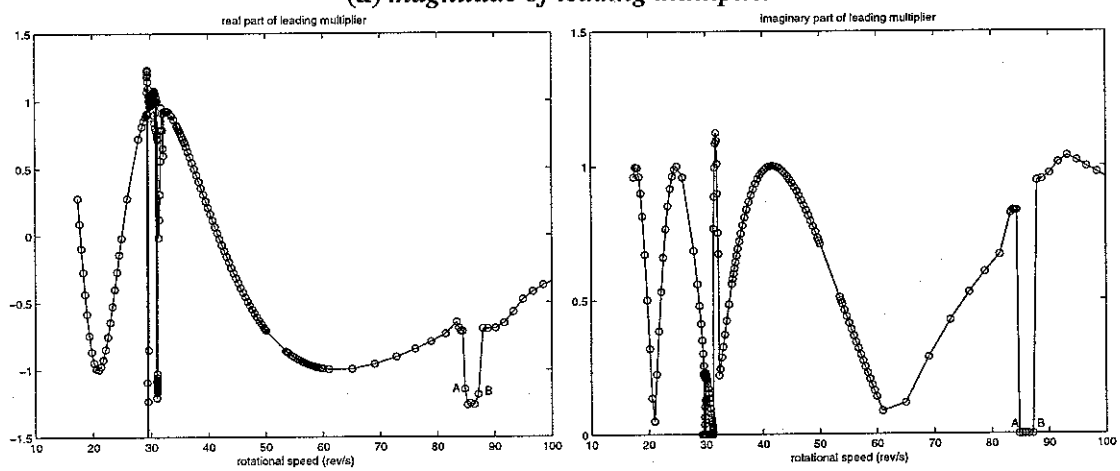

(b1) *real part of leading multiplier* **(b2)** *imaginary part of leading multiplier*

Figure 46: *Fast stabilty check (Method IIb) for harmonic balance solutions* $N = 1,\ m = 5$ *for A2 with* $U = 5.1\times10^{-4}$ *kgm, absolute zero theory.*

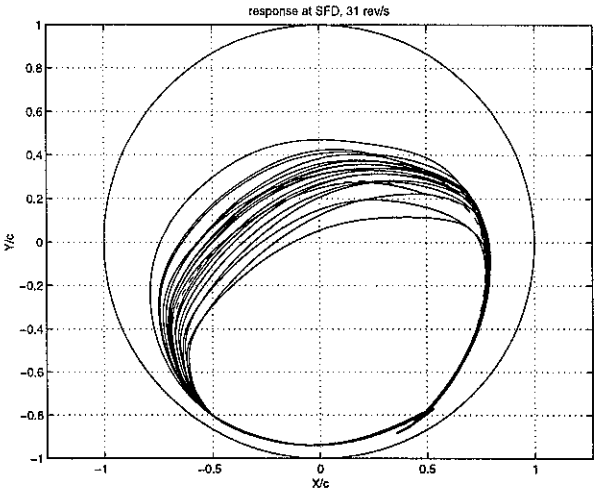

(a) *SFD (J) 31 rev/s*

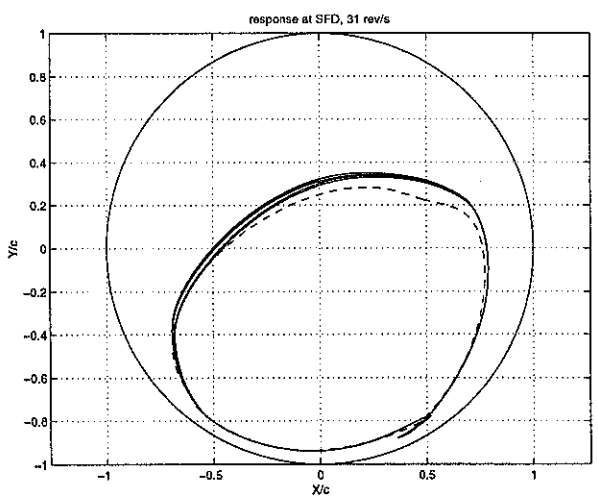

(b1) *SFD (J) 31 rev/s*

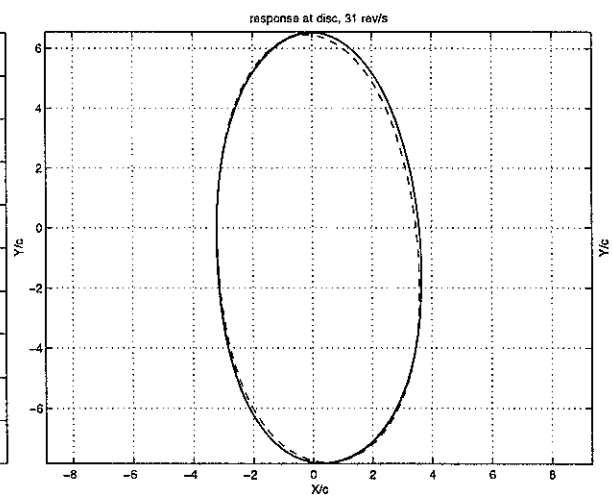

(b2) *Disc (U) 31 rev/s*

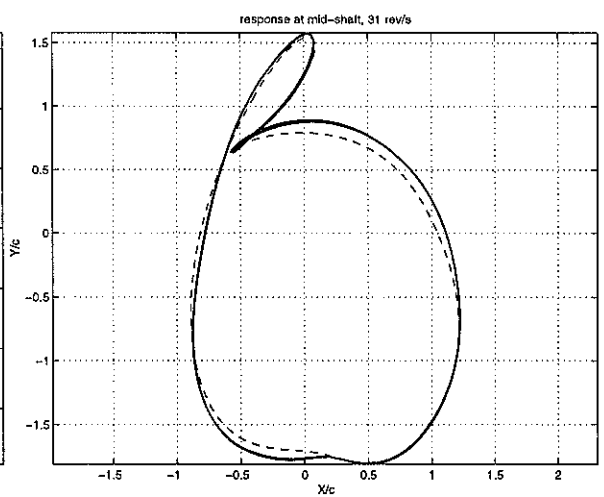

(b3) *Mid-shaft (M) 31 rev/s*

Figure 47: ***Stability check by Method I: predicted orbits at 31 rev/s for A2, $U = 5.1\times10^{-4}$ kgm, absolute zero theory, $p_S = 1.2$ bar.*** **(a):** ***HB, $N = 1$, $m = 5$ (– – –), time domain integration (——) (over 20 revolutions with $q = 4$, initial conditions derived from HB solution).*** **(b1)-(b3):** ***HB (– – –), time domain integration (——) (over a further 5 revolutions).***

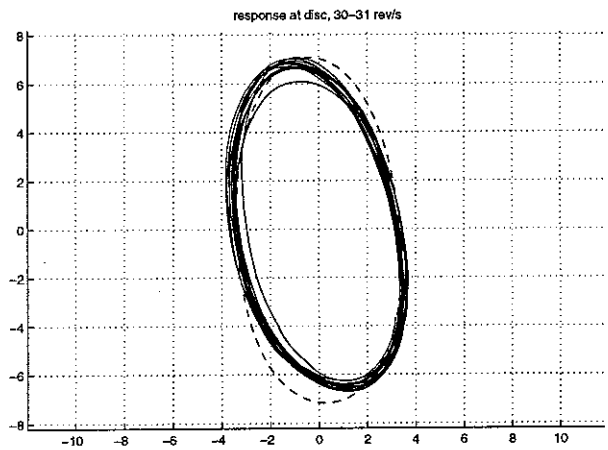

(a1) *Disc (U) 30-31 rev/s*

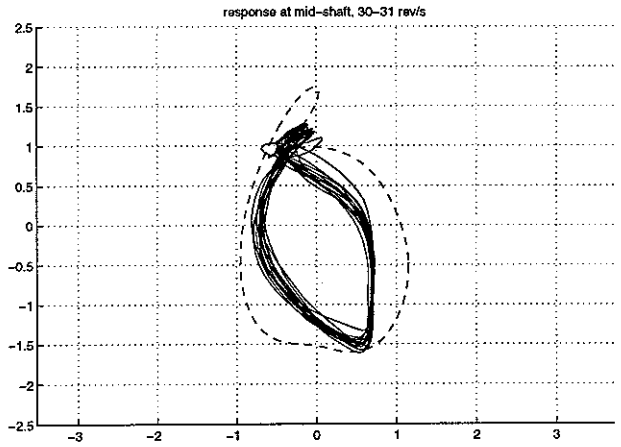

(a2) *Mid-shaft (M) 30-31 rev/s*

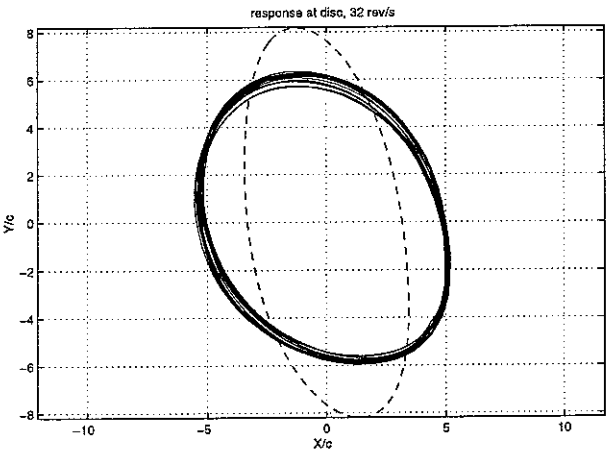

(b1) *Disc (U) 32 rev/s*

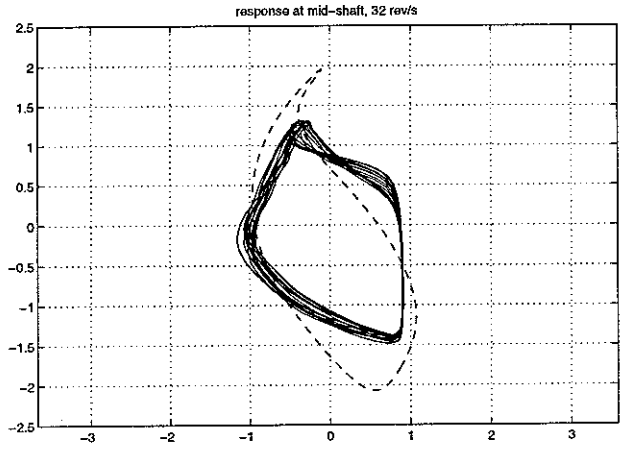

(b2) *Mid-shaft (M) 32 rev/s*

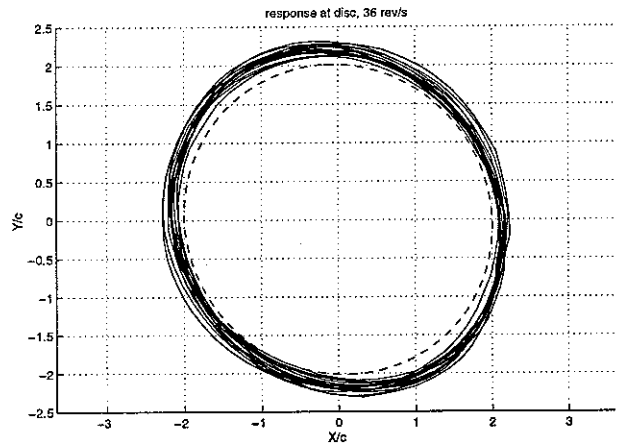

(c1) *Disc (U) 36 rev/s*

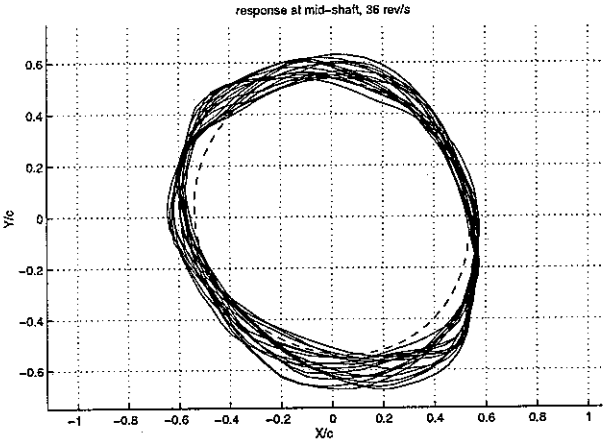

(c2) *Mid-shaft (M) 36 rev/s*

Figure 48: *Predicted and measured "a.c" orbits for A2 near the first critical speed (31 rev/s) with* $U = 5.1 \times 10^{-4}$ *kgm,* $p_S = 1.2$ *bar.*

Prediction: HB, $N = 1$, $m = 8$, *absolute zero theory* (– – –). *Measurement (0.5s)* (——). *In* (a1), (a2) *prediction at 31 rev/s, measurement at 30 rev/s. Scaling of axes in* (c1), (c2) *enlarged for clarity.*

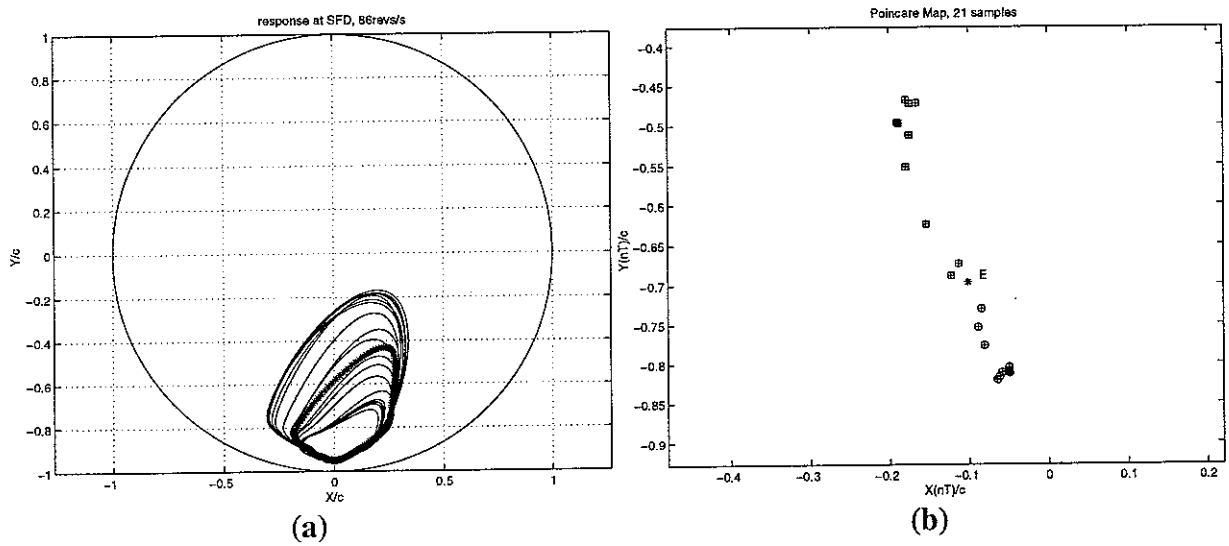

(a) (b)

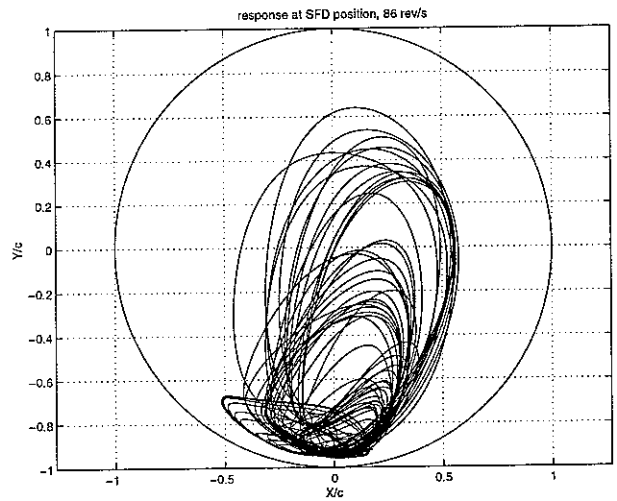

(c)

Figure 49: ***Stability check by Method I: predicted SFD orbits at 86 rev/s for A2, $U = 5.1 \times 10^{-4}$ kgm, absolute zero theory, $p_S = 1.2$ bar.***

(a) ***HB, $N = 1$, $m = 5$ (****), time domain integration (——) (over 20 revolutions with $q = 4$, initial conditions derived from HB solution).***

(b) ***Poincare map of (a) (sampling rate: once per shaft revolution, no. of samples: 21; unstable equilibrium point is E, indicated by "*", consecutive return points enclosed in circles and squares).***

(c) ***Time domain integration over a further 80 shaft revolutions.***

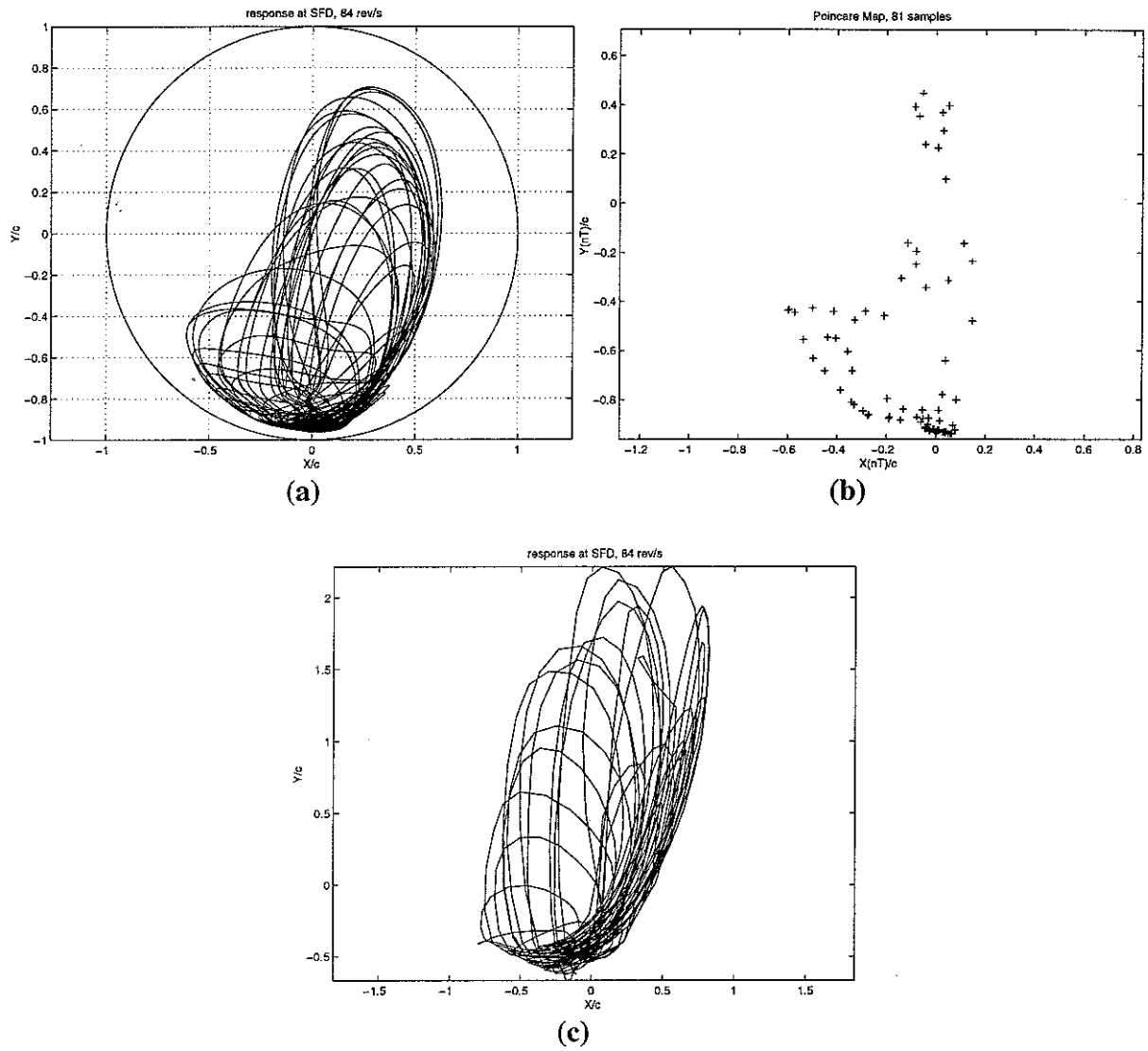

Figure 50: ***Aperiodic motion at 84 rev/s at SFD for A2, $U = 5.1\times10^{-4}$ kgm, $p_S = 1.2$ bar.***

(a) ***Time domain integration (with $q = 4$, last 80 out of 180 revolutions, absolute zero theory).***

(b) ***Poincare map of (a) (sampling rate: once per shaft revolution, no. of samples: 81)***

(c) ***Measured orbit ("a.c." component only)***

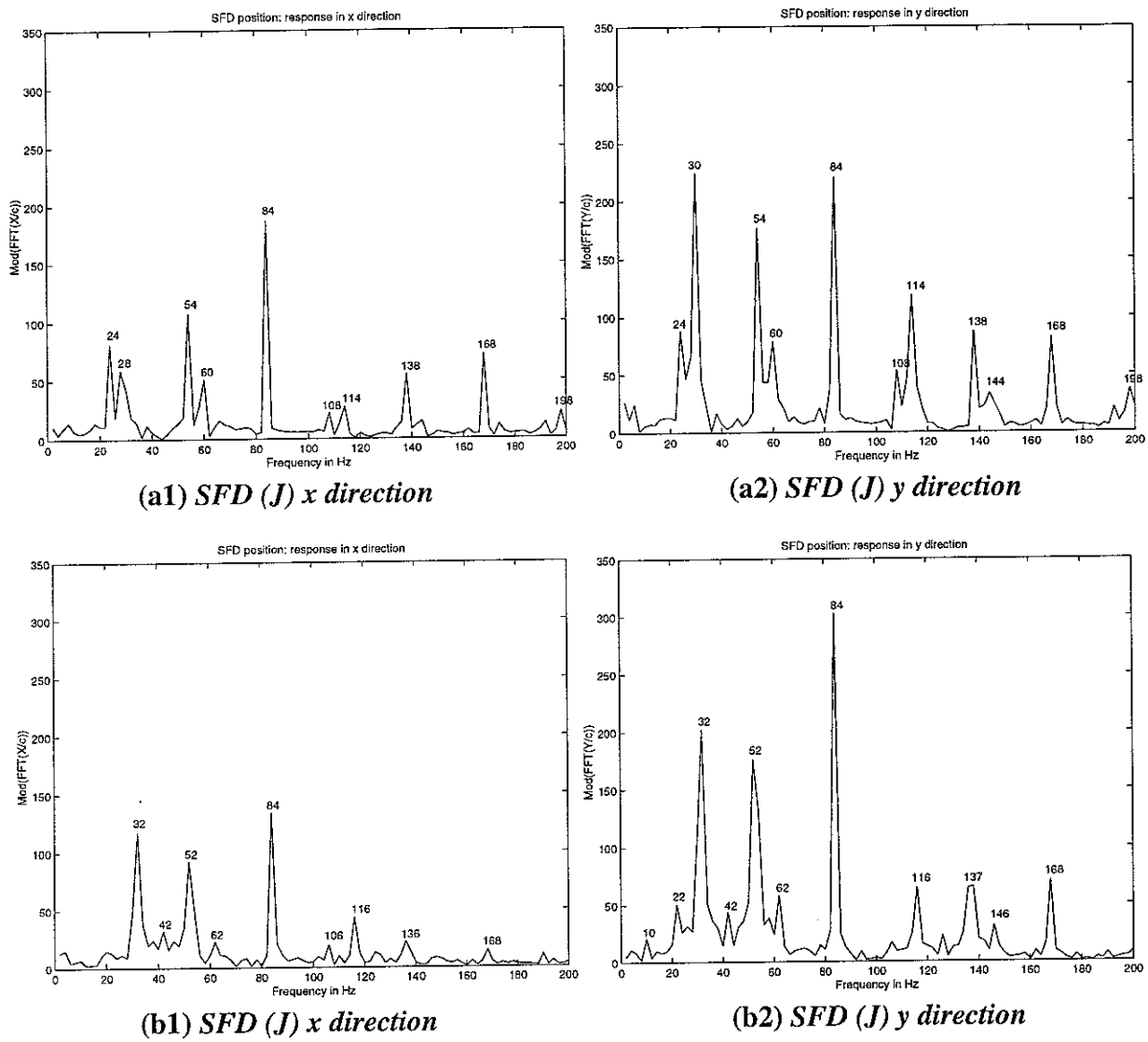

(a1) *SFD (J) x direction*

(a2) *SFD (J) y direction*

(b1) *SFD (J) x direction*

(b2) *SFD (J) y direction*

Figure 51: *Frequency spectra of SFD orbit at 84 rev/s for A2, $U = 5.1\times10^{-4}$ kgm, $p_S = 1.2$ bar.*

(a1), (a2): *predicted (absolute zero theory).* **(b1), (b2):** *measured.*

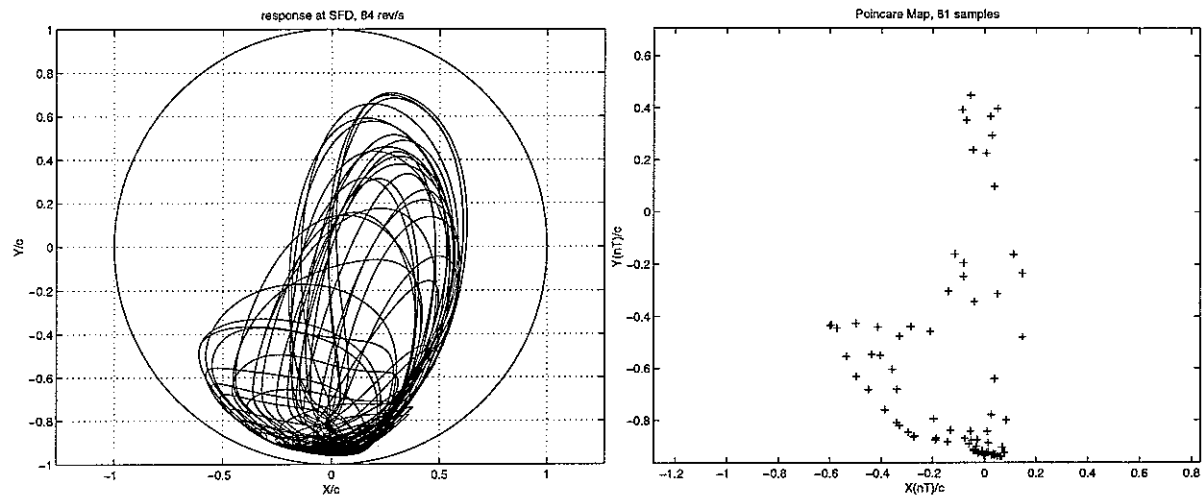

(a1) *SFD Orbit* (a2) *Poincare Map of (a1)*

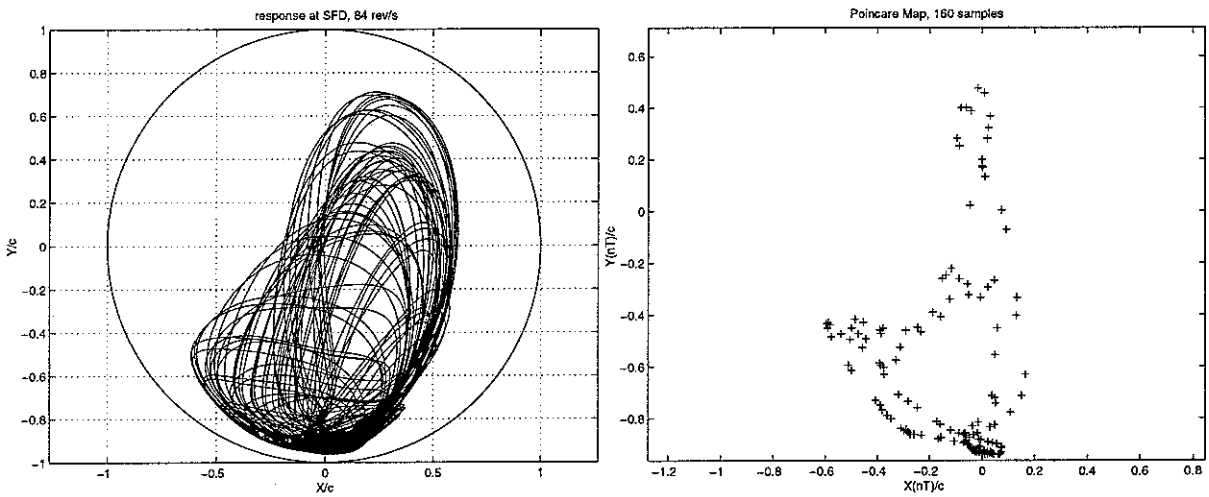

(b1) *SFD Orbit* (b2) *Poincare Map of (b1)*

Figure 52: *Predicted aperiodic motion at 84 rev/s at SFD for A2, $U = 5.1\times10^{-4}$ kgm, absolute zero theory, $p_S = 1.2$ bar*

(a1), (a2): *Last 80 out of 180 shaft revolutions (as in Figure 50(a),(b)).*
(b1), (b2): *Further 160 shaft revolutions.*

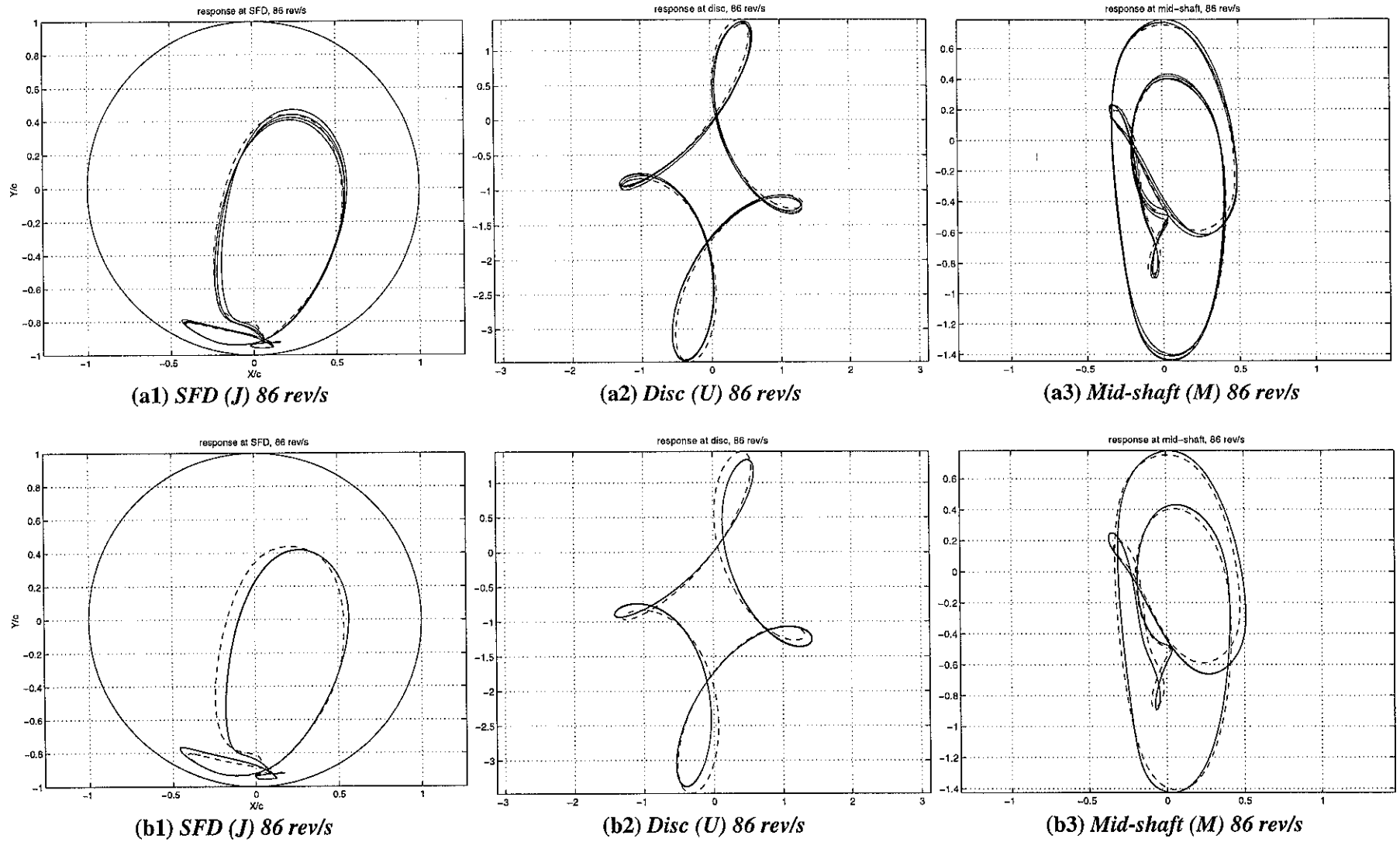

Figure 53: *Stability check of 3T- periodic motion by Method I at 86 rev/s for A2, $U = 5.1\times10^{-4}$ kgm, absolute zero theory, $p_S = 1.2$ bar.* **(a1)-(a3):** *HB, $N = 3$, $m = 20$ (– – –), time domain integration (——) (over 10 revolutions with $q = 4$, initial conditions derived from HB solution).* **(b1)-(b3):** *HB (– – –), steady state time domain integration solution over 30 revolutions (——).*

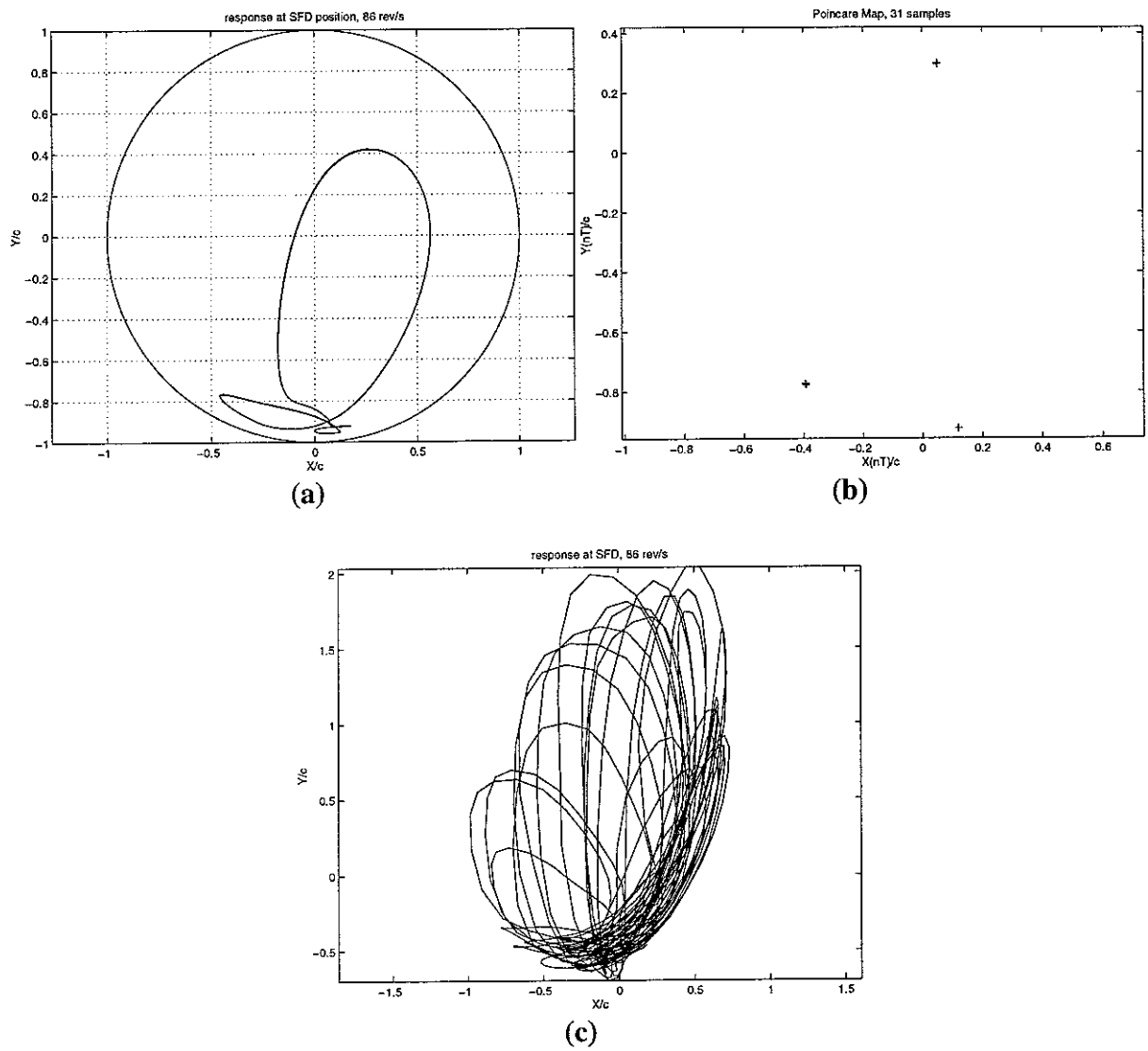

Figure 54: *Motion at 86 rev/s at SFD for A2, $U = 5.1\times10^{-4}$ kgm, $p_S = 1.2$ bar.*

(a) *Time domain integration (with $q = 4$, over 30 revolutions, absolute zero theory).*

(b) *Poincare map of (a) (sampling rate: once per shaft revolution, no. of samples: 31)*

(c) *Measured orbit ("a.c." component only)*

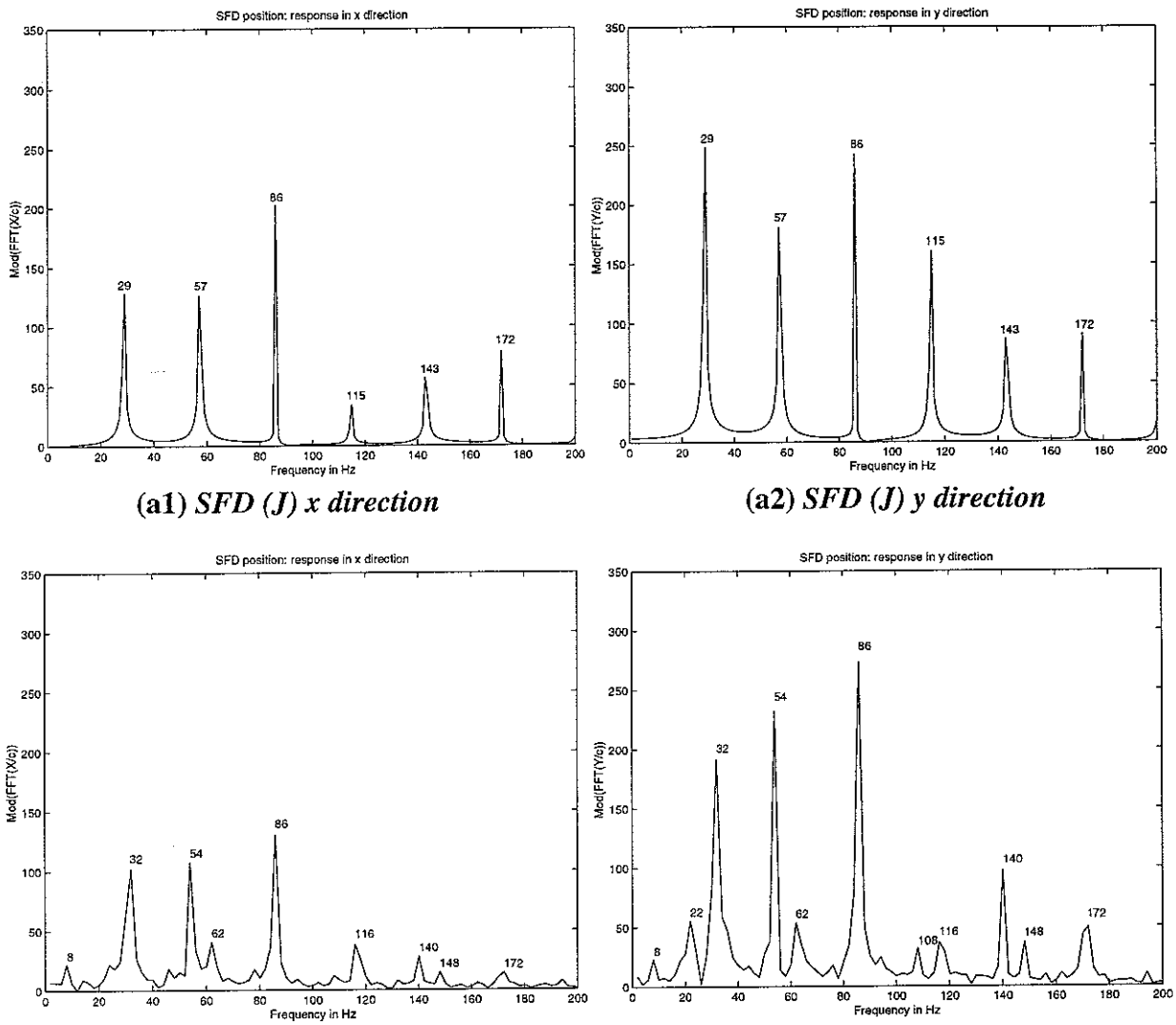

(a1) ***SFD (J) x direction*** **(a2)** ***SFD (J) y direction***

(b1) ***SFD (J) x direction*** **(b2)** ***SFD (J) y direction***

Figure 55: ***Frequency spectra of SFD orbit at 86 rev/s for A2, $U = 5.1 \times 10^{-4}$ kgm, $p_S = 1.2$ bar.***

(a1), (a2): ***predicted (absolute zero theory) (Figure 54(a)).***

(b1), (b2): ***measured.***

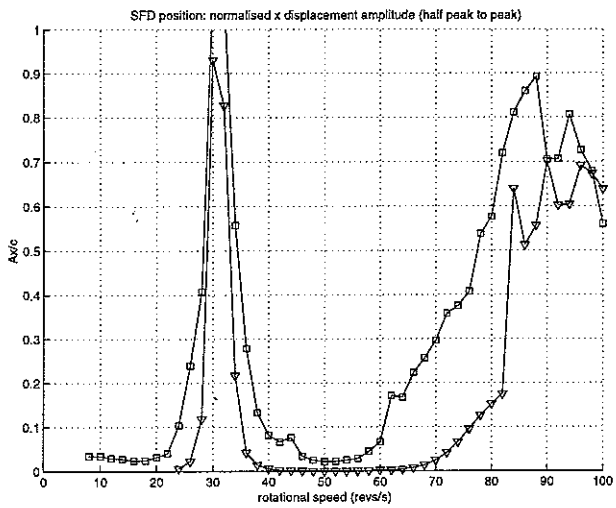

(a) *SFD (J), x direction*

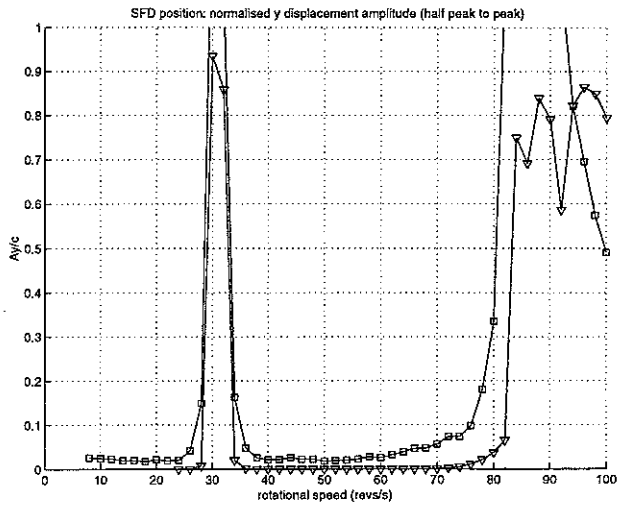

(b) *SFD (J), y direction*

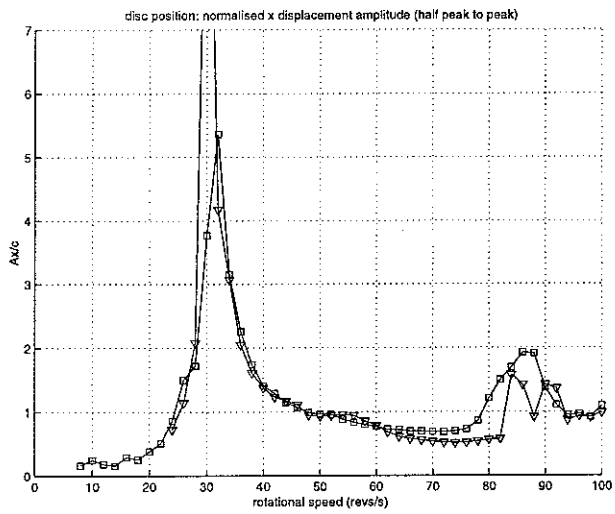

(c) *Disc (U), x direction*

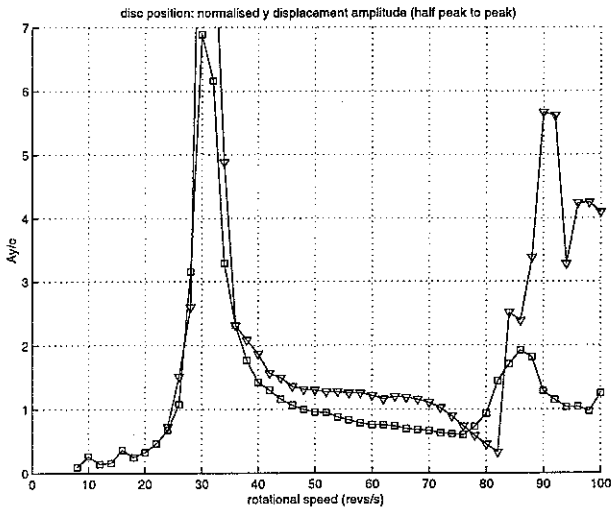

(d) *Disc (U), y direction*

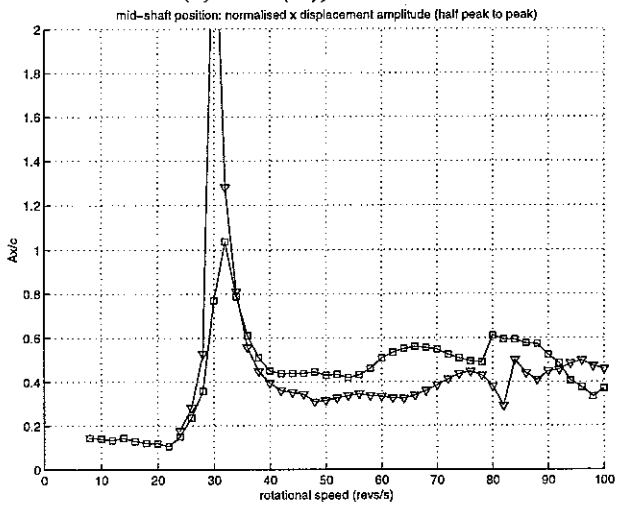

(e) *Mid-shaft (M), x direction*

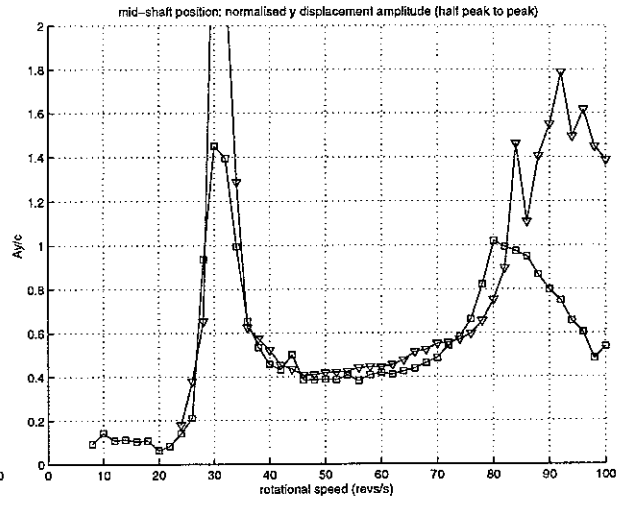

(f) *Mid-shaft (M), y direction*

Figure 56: *Unbalance response (normalised half peak-to-peak) for A2 with* $U = 5.1 \times 10^{-4}\,kgm$, $p_S = 1.2\,bar$. *Measurements:* —□—. *Predictions: time domain integration,* $q = 4$, *absolute zero cavitation* —▽—.

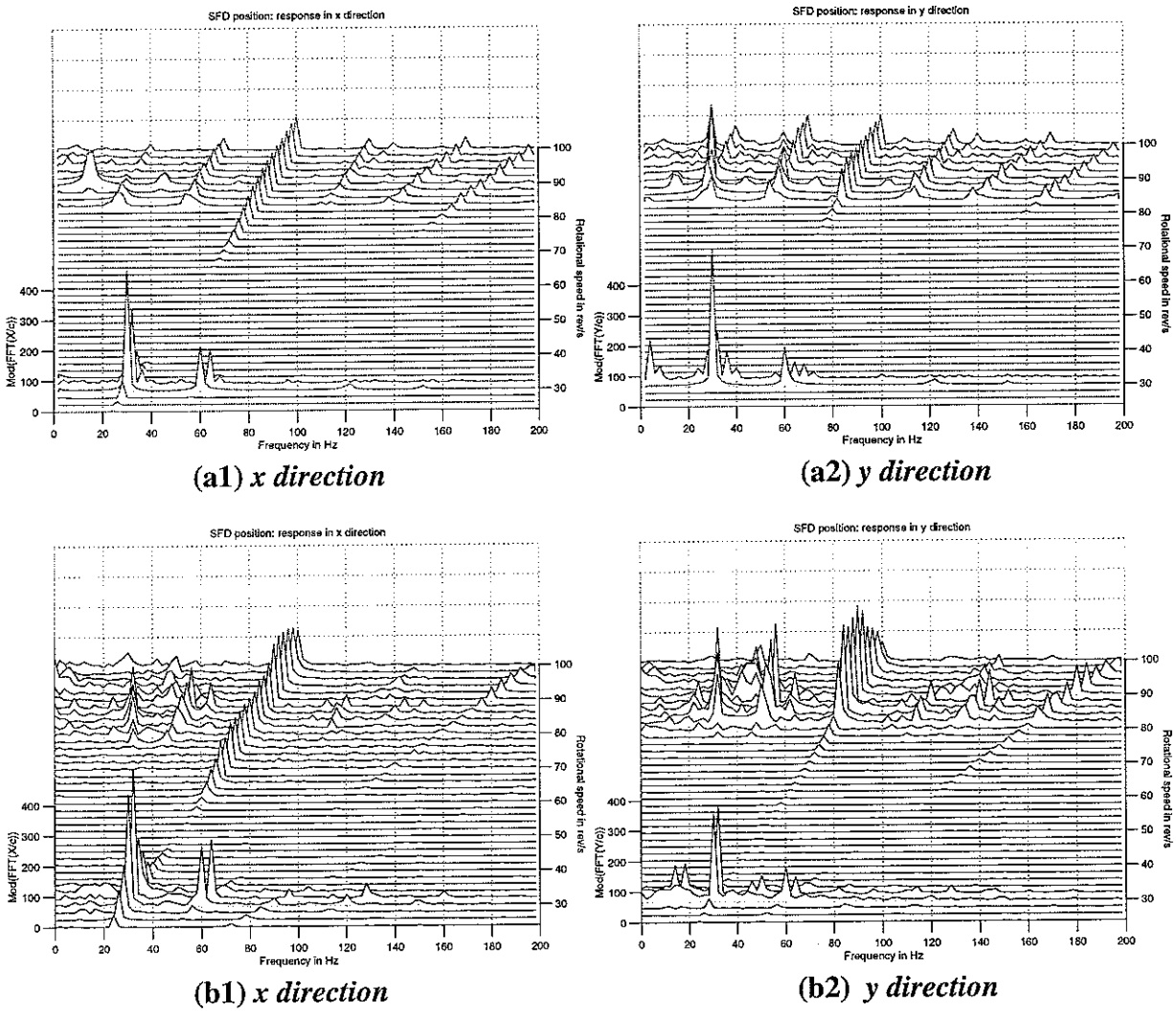

(a1) *x direction* (a2) *y direction*

(b1) *x direction* (b2) *y direction*

Figure 57: *Waterfall diagrams of vibration at SFD (J) for A2,* $U = 5.1 \times 10^{-4}$ *kgm,* $p_S = 1.2$ *bar.*

(a1), (a2): *predicted (absolute zero theory).* **(b1), (b2):** *measured.*

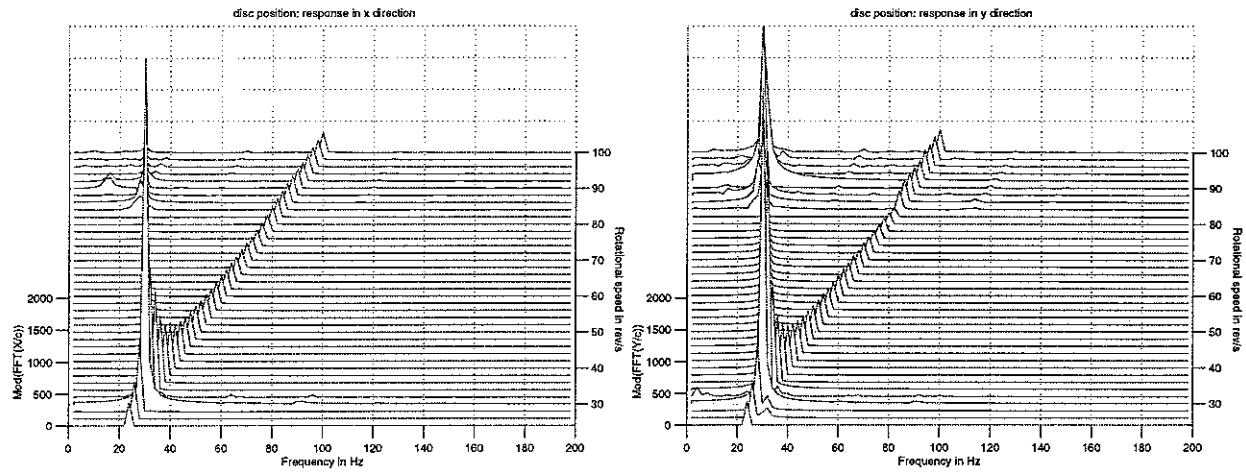

(a1) *x direction*

(a2) *y direction*

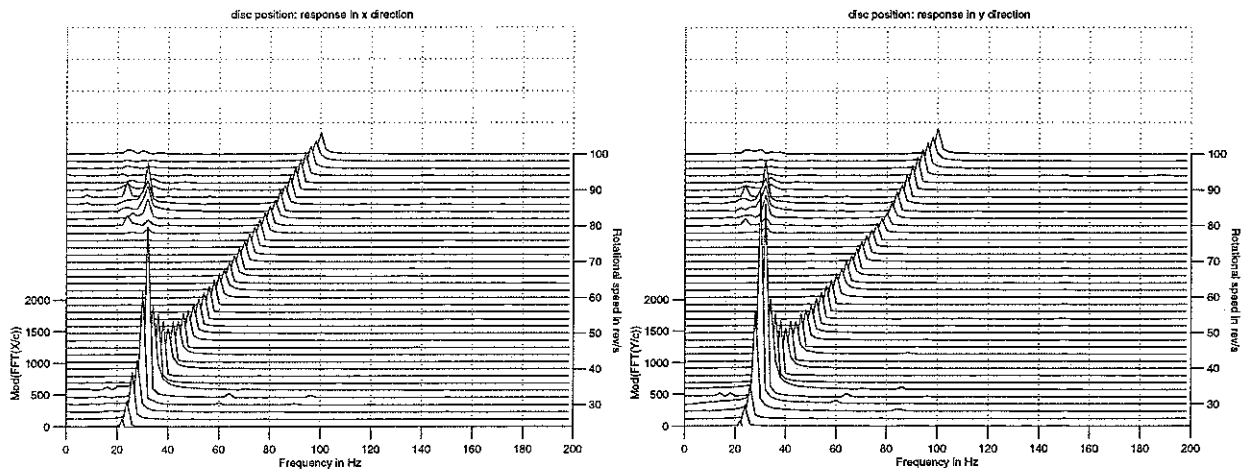

(b1) *x direction*

(b2) *y direction*

Figure 58: ***Waterfall diagrams of vibration at disc (U) for A2, $U = 5.1\times10^{-4}$ kgm, $p_S = 1.2$ bar.***

(a1), (a2): ***predicted (absolute zero theory).*** **(b1), (b2):** ***measured.***

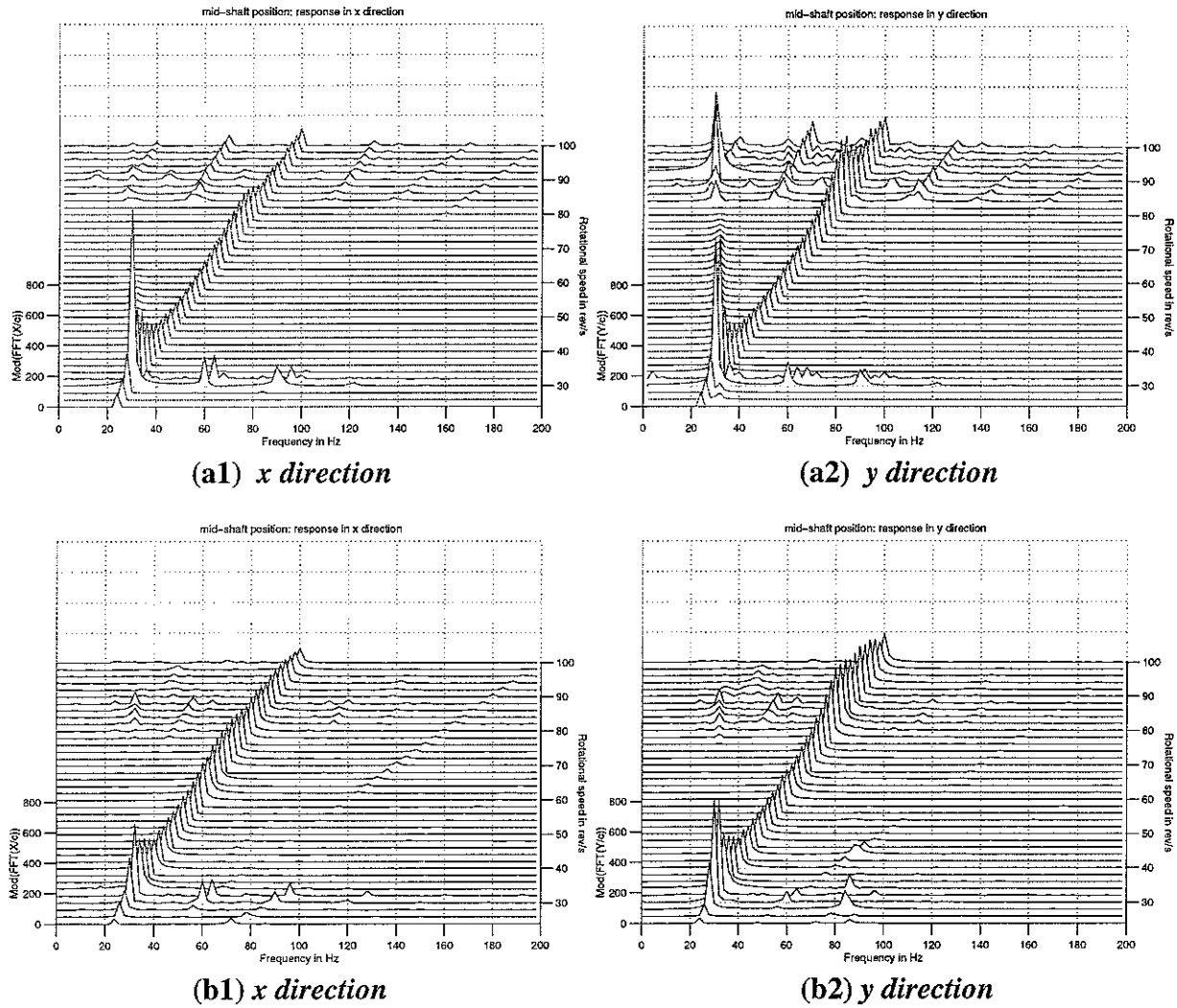

(a1) ***x direction*** **(a2)** ***y direction***

(b1) ***x direction*** **(b2)** ***y direction***

Figure 59: ***Waterfall diagrams of vibration at mid-shaft (M) for A2, $U = 5.1\times10^{-4}$ kgm, $p_S = 1.2$ bar.***

(a1), (a2): ***predicted (absolute zero theory).*** **(b1), (b2):** ***measured.***

APPENDIX A

HARMONIC BALANCE MATRICES

Substitute for $\overline{Q}_{xj}$, p^s_{xj}, q^s_{xj}, $\overline{Q}_{yj}$, p^s_{yj}, q^s_{yj} from equations (33a,b) into equations (38)-(41).

Equations (38) become:

$$X_{0Ji} - e_{0xJi} = \sum_{j=1}^{n}\left[\alpha\alpha_{JiJj}(0) - \alpha\alpha_{JiBj}(0)\right]\left(Q_{x0j} + k_{xxj}X_{0j}\right) + \sum_{j=1}^{n}\left[\alpha\beta_{JiJj}(0) - \alpha\beta_{JiBj}(0)\right]\left(Q_{y0j} + k_{yyj}Y_{0j}\right) \tag{A1a}$$

$$\begin{aligned}
a^s_{XJi} = {} & \sum_{j=1}^{n}\left[\alpha\alpha^{\mathrm{R}}_{JiJj}(s\omega) - \alpha\alpha^{\mathrm{R}}_{JiBj}(s\omega)\right]\left[k_{xxj}\left(a^s_{XJj} - a^s_{XBj}\right) + s\omega c_{xxj}\left(b^s_{XJj} - b^s_{XBj}\right) + A^s_{xj}\right] \\
& + \sum_{j=1}^{n}\left[\alpha\alpha^{\mathrm{I}}_{JiJj}(s\omega) - \alpha\alpha^{\mathrm{I}}_{JiBj}(s\omega)\right]\left[-s\omega c_{xxj}\left(a^s_{XJj} - a^s_{XBj}\right) + k_{xxj}\left(b^s_{XJj} - b^s_{XBj}\right) + B^s_{xj}\right] \\
& + \sum_{j=1}^{n}\left[\alpha\beta^{\mathrm{R}}_{JiJj}(s\omega) - \alpha\beta^{\mathrm{R}}_{JiBj}(s\omega)\right]\left[k_{yyj}\left(a^s_{YJj} - a^s_{YBj}\right) + s\omega c_{yyj}\left(b^s_{YJj} - b^s_{YBj}\right) + A^s_{yj}\right] \\
& + \sum_{j=1}^{n}\left[\alpha\beta^{\mathrm{I}}_{JiJj}(s\omega) - \alpha\beta^{\mathrm{I}}_{JiBj}(s\omega)\right]\left[-s\omega c_{yyj}\left(a^s_{YJj} - a^s_{YBj}\right) + k_{yyj}\left(b^s_{YJj} - b^s_{YBj}\right) + B^s_{yj}\right] \\
& + \delta_{Ns}\sum_{k=1}^{p}\alpha\alpha^{\mathrm{R}}_{JiUk}(s\omega)U_k\Omega^2\sin\phi_k + \delta_{Ns}\sum_{k=1}^{p}\alpha\alpha^{\mathrm{I}}_{JiUk}(s\omega)U_k\Omega^2\cos\phi_k \\
& + \delta_{Ns}\sum_{k=1}^{p}-\alpha\beta^{\mathrm{R}}_{JiUk}(s\omega)U_k\Omega^2\cos\phi_k + \delta_{Ns}\sum_{k=1}^{p}\alpha\beta^{\mathrm{I}}_{JiUk}(s\omega)U_k\Omega^2\sin\phi_k
\end{aligned} \tag{A2a}$$

$$\begin{aligned}
b^s_{XJi} = {} & \sum_{j=1}^{n}\left[\alpha\alpha^{\mathrm{R}}_{JiJj}(s\omega) - \alpha\alpha^{\mathrm{R}}_{JiBj}(s\omega)\right]\left[-s\omega c_{xxj}\left(a^s_{XJj} - a^s_{XBj}\right) + k_{xxj}\left(b^s_{XJj} - b^s_{XBj}\right) + B^s_{xj}\right] \\
& - \sum_{j=1}^{n}\left[\alpha\alpha^{\mathrm{I}}_{JiJj}(s\omega) - \alpha\alpha^{\mathrm{I}}_{JiBj}(s\omega)\right]\left[k_{xxj}\left(a^s_{XJj} - a^s_{XBj}\right) + s\omega c_{xxj}\left(b^s_{XJj} - b^s_{XBj}\right) + A^s_{xj}\right] \\
& + \sum_{j=1}^{n}\left[\alpha\beta^{\mathrm{R}}_{JiJj}(s\omega) - \alpha\beta^{\mathrm{R}}_{JiBj}(s\omega)\right]\left[-s\omega c_{yyj}\left(a^s_{YJj} - a^s_{YBj}\right) + k_{yyj}\left(b^s_{YJj} - b^s_{YBj}\right) + B^s_{yj}\right] \\
& - \sum_{j=1}^{n}\left[\alpha\beta^{\mathrm{I}}_{JiJj}(s\omega) - \alpha\beta^{\mathrm{I}}_{JiBj}(s\omega)\right]\left[k_{yyj}\left(a^s_{YJj} - a^s_{YBj}\right) + s\omega c_{yyj}\left(b^s_{YJj} - b^s_{YBj}\right) + A^s_{yj}\right] \\
& + \delta_{Ns}\sum_{k=1}^{p}\alpha\alpha^{\mathrm{R}}_{JiUk}(s\omega)U_k\Omega^2\cos\phi_k - \delta_{Ns}\sum_{k=1}^{p}\alpha\alpha^{\mathrm{I}}_{JiUk}(s\omega)U_k\Omega^2\sin\phi_k \\
& + \delta_{Ns}\sum_{k=1}^{p}\alpha\beta^{\mathrm{R}}_{JiUk}(s\omega)U_k\Omega^2\sin\phi_k - \delta_{Ns}\sum_{k=1}^{p}-\alpha\beta^{\mathrm{I}}_{JiUk}(s\omega)U_k\Omega^2\cos\phi_k
\end{aligned} \tag{A1c}$$

Equations (39) become:

$$X_{0Bi} = \sum_{j=1}^{n}\left[\alpha\alpha_{BiJj}(0) - \alpha\alpha_{BiBj}(0)\right]\left(Q_{x0j} + k_{xxj}X_{0j}\right) + \sum_{j=1}^{n}\left[\alpha\beta_{BiJj}(0) - \alpha\beta_{BiBj}(0)\right]\left(Q_{y0j} + k_{yyj}Y_{0j}\right) \tag{A2a}$$

$$\begin{aligned}
a^s_{XBi} = &\sum_{j=1}^{n}\left[\alpha\alpha^{\mathrm{R}}_{BiJj}(s\omega) - \alpha\alpha^{\mathrm{R}}_{BiBj}(s\omega)\right]\left[k_{xxj}\left(a^s_{XJj} - a^s_{XBj}\right) + s\omega c_{xxj}\left(b^s_{XJj} - b^s_{XBj}\right) + A^s_{xj}\right] \\
&+ \sum_{j=1}^{n}\left[\alpha\alpha^{\mathrm{I}}_{BiJj}(s\omega) - \alpha\alpha^{\mathrm{I}}_{BiBj}(s\omega)\right]\left[-s\omega c_{xxj}\left(a^s_{XJj} - a^s_{XBj}\right) + k_{xxj}\left(b^s_{XJj} - b^s_{XBj}\right) + B^s_{xj}\right] \\
&+ \sum_{j=1}^{n}\left[\alpha\beta^{\mathrm{R}}_{BiJj}(s\omega) - \alpha\beta^{\mathrm{R}}_{BiBj}(s\omega)\right]\left[k_{yyj}\left(a^s_{YJj} - a^s_{YBj}\right) + s\omega c_{yyj}\left(b^s_{YJj} - b^s_{YBj}\right) + A^s_{yj}\right] \\
&+ \sum_{j=1}^{n}\left[\alpha\beta^{\mathrm{I}}_{BiJj}(s\omega) - \alpha\beta^{\mathrm{I}}_{BiBj}(s\omega)\right]\left[-s\omega c_{yyj}\left(a^s_{YJj} - a^s_{YBj}\right) + k_{yyj}\left(b^s_{YJj} - b^s_{YBj}\right) + B^s_{yj}\right] \\
&+ \delta_{Ns}\sum_{k=1}^{p}\alpha\alpha^{\mathrm{R}}_{BiUk}(s\omega)U_k\Omega^2\sin\phi_k + \delta_{Ns}\sum_{k=1}^{p}\alpha\alpha^{\mathrm{I}}_{BiUk}(s\omega)U_k\Omega^2\cos\phi_k \\
&+ \delta_{Ns}\sum_{k=1}^{p} -\alpha\beta^{\mathrm{R}}_{BiUk}(s\omega)U_k\Omega^2\cos\phi_k + \delta_{Ns}\sum_{k=1}^{p}\alpha\beta^{\mathrm{I}}_{BiUk}(s\omega)U_k\Omega^2\sin\phi_k
\end{aligned} \tag{A2b}$$

$$\begin{aligned}
b^s_{XBi} = &\sum_{j=1}^{n}\left[\alpha\alpha^{\mathrm{R}}_{BiJj}(s\omega) - \alpha\alpha^{\mathrm{R}}_{BiBj}(s\omega)\right]\left[-s\omega c_{xxj}\left(a^s_{XJj} - a^s_{XBj}\right) + k_{xxj}\left(b^s_{XJj} - b^s_{XBj}\right) + B^s_{xj}\right] \\
&- \sum_{j=1}^{n}\left[\alpha\alpha^{\mathrm{I}}_{BiJj}(s\omega) - \alpha\alpha^{\mathrm{I}}_{BiBj}(s\omega)\right]\left[k_{xxj}\left(a^s_{XJj} - a^s_{XBj}\right) + s\omega c_{xxj}\left(b^s_{XJj} - b^s_{XBj}\right) + A^s_{xj}\right] \\
&+ \sum_{j=1}^{n}\left[\alpha\beta^{\mathrm{R}}_{BiJj}(s\omega) - \alpha\beta^{\mathrm{R}}_{BiBj}(s\omega)\right]\left[-s\omega c_{yyj}\left(a^s_{YJj} - a^s_{YBj}\right) + k_{yyj}\left(b^s_{YJj} - b^s_{YBj}\right) + B^s_{yj}\right] \\
&- \sum_{j=1}^{n}\left[\alpha\beta^{\mathrm{I}}_{BiJj}(s\omega) - \alpha\beta^{\mathrm{I}}_{BiBj}(s\omega)\right]\left[k_{yyj}\left(a^s_{YJj} - a^s_{YBj}\right) + s\omega c_{yyj}\left(b^s_{YJj} - b^s_{YBj}\right) + A^s_{yj}\right] \\
&+ \delta_{Ns}\sum_{k=1}^{p}\alpha\alpha^{\mathrm{R}}_{BiUk}(s\omega)U_k\Omega^2\cos\phi_k - \delta_{Ns}\sum_{k=1}^{p}\alpha\alpha^{\mathrm{I}}_{BiUk}(s\omega)U_k\Omega^2\sin\phi_k \\
&+ \delta_{Ns}\sum_{k=1}^{p}\alpha\beta^{\mathrm{R}}_{BiUk}(s\omega)U_k\Omega^2\sin\phi_k - \delta_{Ns}\sum_{k=1}^{p} -\alpha\beta^{\mathrm{I}}_{BiUk}(s\omega)U_k\Omega^2\cos\phi_k
\end{aligned} \tag{A2c}$$

Equations (40) become:

$$Y_{0Ji} - e_{0yJi} = \sum_{j=1}^{n} \left[\beta\beta_{JiJj}(0) - \beta\beta_{JiBj}(0)\right]\left(Q_{y0j} + k_{yyj} Y_{0j}\right) + \sum_{j=1}^{n} \left[\beta\alpha_{JiJj}(0) - \beta\alpha_{JiBj}(0)\right]\left(Q_{x0j} + k_{xxj} X_{0j}\right)$$

(A3a)

$$\begin{aligned}
a^s_{YJi} = & \sum_{j=1}^{n} \left[\beta\beta^{\mathrm{R}}_{JiJj}(s\omega) - \beta\beta^{\mathrm{R}}_{JiBj}(s\omega)\right]\left[k_{yyj}\left(a^s_{YJj} - a^s_{YBj}\right) + s\omega c_{yyj}\left(b^s_{YJj} - b^s_{YBj}\right) + A^s_{yj}\right] \\
& + \sum_{j=1}^{n} \left[\beta\beta^{\mathrm{I}}_{JiJj}(s\omega) - \beta\beta^{\mathrm{I}}_{JiBj}(s\omega)\right]\left[-s\omega c_{yyj}\left(a^s_{YJj} - a^s_{YBj}\right) + k_{yyj}\left(b^s_{YJj} - b^s_{YBj}\right) + B^s_{yj}\right] \\
& + \sum_{j=1}^{n} \left[\beta\alpha^{\mathrm{R}}_{JiJj}(s\omega) - \beta\alpha^{\mathrm{R}}_{JiBj}(s\omega)\right]\left[k_{xxj}\left(a^s_{XJj} - a^s_{XBj}\right) + s\omega c_{xxj}\left(b^s_{XJj} - b^s_{XBj}\right) + A^s_{xj}\right] \\
& + \sum_{j=1}^{n} \left[\beta\alpha^{\mathrm{I}}_{JiJj}(s\omega) - \beta\alpha^{\mathrm{I}}_{JiBj}(s\omega)\right]\left[-s\omega c_{xxj}\left(a^s_{XJj} - a^s_{XBj}\right) + k_{xxj}\left(b^s_{XJj} - b^s_{XBj}\right) + B^s_{xj}\right] \\
& + \delta_{Ns} \sum_{k=1}^{p} -\beta\beta^{\mathrm{R}}_{JiUk}(s\omega) U_k \Omega^2 \cos\phi_k + \delta_{Ns} \sum_{k=1}^{p} \beta\beta^{\mathrm{I}}_{JiUk}(s\omega) U_k \Omega^2 \sin\phi_k \\
& + \delta_{Ns} \sum_{k=1}^{p} \beta\alpha^{\mathrm{R}}_{JiUk}(s\omega) U_k \Omega^2 \sin\phi_k + \delta_{Ns} \sum_{k=1}^{p} \beta\alpha^{\mathrm{I}}_{JiUk}(s\omega) U_k \Omega^2 \cos\phi_k
\end{aligned}$$

(A3b)

$$\begin{aligned}
b^s_{YJi} = & \sum_{j=1}^{n} \left[\beta\beta^{\mathrm{R}}_{JiJj}(s\omega) - \beta\beta^{\mathrm{R}}_{JiBj}(s\omega)\right]\left[-s\omega c_{yyj}\left(a^s_{YJj} - a^s_{YBj}\right) + k_{yyj}\left(b^s_{YJj} - b^s_{YBj}\right) + B^s_{yj}\right] \\
& - \sum_{j=1}^{n} \left[\beta\beta^{\mathrm{I}}_{JiJj}(s\omega) - \beta\beta^{\mathrm{I}}_{JiBj}(s\omega)\right]\left[k_{yyj}\left(a^s_{YJj} - a^s_{YBj}\right) + s\omega c_{yyj}\left(b^s_{YJj} - b^s_{YBj}\right) + A^s_{yj}\right] \\
& + \sum_{j=1}^{n} \left[\beta\alpha^{\mathrm{R}}_{JiJj}(s\omega) - \beta\alpha^{\mathrm{R}}_{JiBj}(s\omega)\right]\left[-s\omega c_{xxj}\left(a^s_{XJj} - a^s_{XBj}\right) + k_{xxj}\left(b^s_{XJj} - b^s_{XBj}\right) + B^s_{xj}\right] \\
& - \sum_{j=1}^{n} \left[\beta\alpha^{\mathrm{I}}_{JiJj}(s\omega) - \beta\alpha^{\mathrm{I}}_{JiBj}(s\omega)\right]\left[k_{xxj}\left(a^s_{XJj} - a^s_{XBj}\right) + s\omega c_{xxj}\left(b^s_{XJj} - b^s_{XBj}\right) + A^s_{xj}\right] \\
& + \delta_{Ns} \sum_{k=1}^{p} \beta\beta^{\mathrm{R}}_{JiUk}(s\omega) U_k \Omega^2 \sin\phi_k - \delta_{Ns} \sum_{k=1}^{p} -\beta\beta^{\mathrm{I}}_{JiUk}(s\omega) U_k \Omega^2 \cos\phi_k \\
& + \delta_{Ns} \sum_{k=1}^{p} \beta\alpha^{\mathrm{R}}_{JiUk}(s\omega) U_k \Omega^2 \cos\phi_k - \delta_{Ns} \sum_{k=1}^{p} \beta\alpha^{\mathrm{I}}_{JiUk}(s\omega) U_k \Omega^2 \sin\phi_k
\end{aligned}$$

(A3c)

Equations (41) become:

$$Y_{0Bi} = \sum_{j=1}^{n} \left[\beta\beta_{BiJj}(0) - \beta\beta_{BiBj}(0)\right]\left(Q_{y0j} + k_{yyj} Y_{0j}\right) + \sum_{j=1}^{n} \left[\beta\alpha_{BiJj}(0) - \beta\alpha_{BiBj}(0)\right]\left(Q_{x0j} + k_{xxj} X_{0j}\right) \tag{A4a}$$

$$\begin{aligned}
a^s_{YBi} = & \sum_{j=1}^{n} \left[\beta\beta^{\mathrm{R}}_{BiJj}(s\omega) - \beta\beta^{\mathrm{R}}_{BiBj}(s\omega)\right]\left[k_{yyj}\left(a^s_{YJj} - a^s_{YBj}\right) + s\omega c_{yyj}\left(b^s_{YJj} - b^s_{YBj}\right) + A^s_{yj}\right] \\
& + \sum_{j=1}^{n} \left[\beta\beta^{\mathrm{I}}_{BiJj}(s\omega) - \beta\beta^{\mathrm{I}}_{BiBj}(s\omega)\right]\left[-s\omega c_{yyj}\left(a^s_{YJj} - a^s_{YBj}\right) + k_{yyj}\left(b^s_{YJj} - b^s_{YBj}\right) + B^s_{yj}\right] \\
& + \sum_{j=1}^{n} \left[\beta\alpha^{\mathrm{R}}_{BiJj}(s\omega) - \beta\alpha^{\mathrm{R}}_{BiBj}(s\omega)\right]\left[k_{xxj}\left(a^s_{XJj} - a^s_{XBj}\right) + s\omega c_{xxj}\left(b^s_{XJj} - b^s_{XBj}\right) + A^s_{xj}\right] \\
& + \sum_{j=1}^{n} \left[\beta\alpha^{\mathrm{I}}_{BiJj}(s\omega) - \beta\alpha^{\mathrm{I}}_{BiBj}(s\omega)\right]\left[-s\omega c_{xxj}\left(a^s_{XJj} - a^s_{XBj}\right) + k_{xxj}\left(b^s_{XJj} - b^s_{XBj}\right) + B^s_{xj}\right] \\
& + \delta_{Ns} \sum_{k=1}^{p} -\beta\beta^{\mathrm{R}}_{BiUk}(s\omega) U_k \Omega^2 \cos\phi_k + \delta_{Ns} \sum_{k=1}^{p} \beta\beta^{\mathrm{I}}_{BiUk}(s\omega) U_k \Omega^2 \sin\phi_k \\
& + \delta_{Ns} \sum_{k=1}^{p} \beta\alpha^{\mathrm{R}}_{BiUk}(s\omega) U_k \Omega^2 \sin\phi_k + \delta_{Ns} \sum_{k=1}^{p} \beta\alpha^{\mathrm{I}}_{BiUk}(s\omega) U_k \Omega^2 \cos\phi_k
\end{aligned} \tag{A4b}$$

$$\begin{aligned}
b^s_{YBi} = & \sum_{j=1}^{n} \left[\beta\beta^{\mathrm{R}}_{BiJj}(s\omega) - \beta\beta^{\mathrm{R}}_{BiBj}(s\omega)\right]\left[-s\omega c_{yyj}\left(a^s_{YJj} - a^s_{YBj}\right) + k_{yyj}\left(b^s_{YJj} - b^s_{YBj}\right) + B^s_{yj}\right] \\
& - \sum_{j=1}^{n} \left[\beta\beta^{\mathrm{I}}_{BiJj}(s\omega) - \beta\beta^{\mathrm{I}}_{BiBj}(s\omega)\right]\left[k_{yyj}\left(a^s_{YJj} - a^s_{YBj}\right) + s\omega c_{yyj}\left(b^s_{YJj} - b^s_{YBj}\right) + A^s_{yj}\right] \\
& + \sum_{j=1}^{n} \left[\beta\alpha^{\mathrm{R}}_{BiJj}(s\omega) - \beta\alpha^{\mathrm{R}}_{BiBj}(s\omega)\right]\left[-s\omega c_{xxj}\left(a^s_{XJj} - a^s_{XBj}\right) + k_{xxj}\left(b^s_{XJj} - b^s_{XBj}\right) + B^s_{xj}\right] \\
& - \sum_{j=1}^{n} \left[\beta\alpha^{\mathrm{I}}_{BiJj}(s\omega) - \beta\alpha^{\mathrm{I}}_{BiBj}(s\omega)\right]\left[k_{xxj}\left(a^s_{XJj} - a^s_{XBj}\right) + s\omega c_{xxj}\left(b^s_{XJj} - b^s_{XBj}\right) + A^s_{xj}\right] \\
& + \delta_{Ns} \sum_{k=1}^{p} \beta\beta^{\mathrm{R}}_{BiUk}(s\omega) U_k \Omega^2 \sin\phi_k - \delta_{Ns} \sum_{k=1}^{p} -\beta\beta^{\mathrm{I}}_{BiUk}(s\omega) U_k \Omega^2 \cos\phi_k \\
& + \delta_{Ns} \sum_{k=1}^{p} \beta\alpha^{\mathrm{R}}_{BiUk}(s\omega) U_k \Omega^2 \cos\phi_k - \delta_{Ns} \sum_{k=1}^{p} \beta\alpha^{\mathrm{I}}_{BiUk}(s\omega) U_k \Omega^2 \sin\phi_k
\end{aligned} \tag{A4c}$$

Defining

$$\mathbf{v}_x = \begin{bmatrix} \mathbf{v}_{xJ} \\ \mathbf{v}_{xB} \end{bmatrix} \qquad \mathbf{v}_{xJ} = \begin{bmatrix} \mathbf{v}_{xJ1} \\ \vdots \\ \mathbf{v}_{xJn} \end{bmatrix} \quad \mathbf{v}_{xB} = \begin{bmatrix} \mathbf{v}_{xB1} \\ \vdots \\ \mathbf{v}_{xBn} \end{bmatrix}$$

$$\mathbf{v}_{xJi} = \begin{bmatrix} X_{0Ji} & a^1_{XJi} & b^1_{XJi} & \cdots & a^m_{XJi} & b^m_{XJi} \end{bmatrix}^T$$

$$\mathbf{v}_{xBi} = \begin{bmatrix} X_{0Bi} & a^1_{XBi} & b^1_{XBi} & \cdots & a^m_{XBi} & b^m_{XBi} \end{bmatrix}^T$$

Similarly,

$$\mathbf{v}_y = \begin{bmatrix} \mathbf{v}_{yJ} \\ \mathbf{v}_{yB} \end{bmatrix} \qquad \mathbf{v}_{yJ} = \begin{bmatrix} \mathbf{v}_{yJ1} \\ \vdots \\ \mathbf{v}_{yJn} \end{bmatrix} \quad \mathbf{v}_{yB} = \begin{bmatrix} \mathbf{v}_{yB1} \\ \vdots \\ \mathbf{v}_{yBn} \end{bmatrix}$$

$$\mathbf{v}_{yJi} = \begin{bmatrix} Y_{0Ji} & a^1_{YJi} & b^1_{YJi} & \cdots & a^m_{YJi} & b^m_{YJi} \end{bmatrix}^T$$

$$\mathbf{v}_{yBi} = \begin{bmatrix} Y_{0Bi} & a^1_{YBi} & b^1_{YBi} & \cdots & a^m_{YBi} & b^m_{YBi} \end{bmatrix}^T$$

Equations (A1)-(A4) can collected into the following system

$$\left\{ \begin{bmatrix} \mathbf{M}_{xx} & \mathbf{M}_{xy} \\ \mathbf{M}_{yx} & \mathbf{M}_{yy} \end{bmatrix} - \mathbf{I}_{4n(2m+1)} \right\} \begin{bmatrix} \mathbf{v}_x \\ \mathbf{v}_y \end{bmatrix} = \begin{bmatrix} \mathbf{f}_{xx} + \mathbf{f}_{xy} \\ \mathbf{f}_{yx} + \mathbf{f}_{yy} \end{bmatrix} \tag{A5}$$

where:

$$\mathbf{M}_{xx} = \begin{bmatrix} \mathbf{M}_{xxJ} & -\mathbf{M}_{xxJ} \\ \mathbf{M}_{xxB} & -\mathbf{M}_{xxB} \end{bmatrix}, \quad \mathbf{M}_{xy} = \begin{bmatrix} \mathbf{M}_{xyJ} & -\mathbf{M}_{xyJ} \\ \mathbf{M}_{xyB} & -\mathbf{M}_{xyB} \end{bmatrix} \tag{A6),(A7}$$

$$\mathbf{M}_{yx} = \begin{bmatrix} \mathbf{M}_{yxJ} & -\mathbf{M}_{yxJ} \\ \mathbf{M}_{yxB} & -\mathbf{M}_{yxB} \end{bmatrix}, \quad \mathbf{M}_{yy} = \begin{bmatrix} \mathbf{M}_{yyJ} & -\mathbf{M}_{yyJ} \\ \mathbf{M}_{yyB} & -\mathbf{M}_{yyB} \end{bmatrix} \tag{A8), (A9}$$

$$\mathbf{M}_{xxJ} = \left\{ \mathbf{M}^{\mathbf{R}}_{xxJij} \right\} + \left\{ \mathbf{M}^{\mathbf{I}}_{xxJij} \right\} = \begin{bmatrix} \mathbf{M}^{\mathbf{R}}_{xxJ11} & \cdots & \mathbf{M}^{\mathbf{R}}_{xxJ1n} \\ \vdots & \vdots & \vdots \\ \mathbf{M}^{\mathbf{R}}_{xxJn1} & \cdots & \mathbf{M}^{\mathbf{R}}_{xxJnn} \end{bmatrix} + \begin{bmatrix} \mathbf{M}^{\mathbf{I}}_{xxJ11} & \cdots & \mathbf{M}^{\mathbf{I}}_{xxJ1n} \\ \vdots & \vdots & \vdots \\ \mathbf{M}^{\mathbf{I}}_{xxJn1} & \cdots & \mathbf{M}^{\mathbf{I}}_{xxJnn} \end{bmatrix} \tag{A10a}$$

$$\mathbf{M}_{xxB} = \left\{\mathbf{M}^{R}_{xxBij}\right\} + \left\{\mathbf{M}^{I}_{xxBij}\right\} = \begin{bmatrix} \mathbf{M}^{R}_{xxB11} & \cdots & \mathbf{M}^{R}_{xxB1n} \\ \vdots & \vdots & \vdots \\ \mathbf{M}^{R}_{xxBn1} & \cdots & \mathbf{M}^{R}_{xxBnn} \end{bmatrix} + \begin{bmatrix} \mathbf{M}^{I}_{xxB11} & \cdots & \mathbf{M}^{I}_{xxB1n} \\ \vdots & \vdots & \vdots \\ \mathbf{M}^{I}_{xxBn1} & \cdots & \mathbf{M}^{I}_{xxBnn} \end{bmatrix} \qquad \text{(A10b)}$$

$$\mathbf{M}_{xyJ} = \left\{\mathbf{M}^{R}_{xyJij}\right\} + \left\{\mathbf{M}^{I}_{xyJij}\right\}, \quad \mathbf{M}_{xyB} = \left\{\mathbf{M}^{R}_{xyBij}\right\} + \left\{\mathbf{M}^{I}_{xyBij}\right\} \qquad \text{(A11a,b)}$$

$$\mathbf{M}_{yxJ} = \left\{\mathbf{M}^{R}_{yxJij}\right\} + \left\{\mathbf{M}^{I}_{yxJij}\right\}, \quad \mathbf{M}_{yxB} = \left\{\mathbf{M}^{R}_{yxBij}\right\} + \left\{\mathbf{M}^{I}_{yxBij}\right\} \qquad \text{(A12a,b)}$$

$$\mathbf{M}_{yyJ} = \left\{\mathbf{M}^{R}_{yyJij}\right\} + \left\{\mathbf{M}^{I}_{yyJij}\right\}, \quad \mathbf{M}_{yyB} = \left\{\mathbf{M}^{R}_{yyBij}\right\} + \left\{\mathbf{M}^{I}_{yyBij}\right\} \qquad \text{(A13a,b)}$$

$$\mathbf{M}^{\mathbf{R}}_{\mathbf{xxJij}} =$$

$$\begin{bmatrix} k_{xxj}\left[\alpha\alpha_{JiJj}(0)-\alpha\alpha_{JiBj}(0)\right] & 0 & & & \\ 0 & k_{xxj}\left[\alpha\alpha^{R}_{JiJj}(\omega)-\alpha\alpha^{R}_{JiBj}(\omega)\right] & \omega c_{xxj}\left[\alpha\alpha^{R}_{JiJj}(\omega)-\alpha\alpha^{R}_{JiBj}(\omega)\right] & & \\ & -\omega c_{xxj}\left[\alpha\alpha^{R}_{JiJj}(\omega)-\alpha\alpha^{R}_{JiBj}(\omega)\right] & k_{xxj}\left[\alpha\alpha^{R}_{JiJj}(\omega)-\alpha\alpha^{R}_{JiBj}(\omega)\right] & & \\ & & & \ddots & \\ & & & & k_{xxj}\left[\alpha\alpha^{R}_{JiJj}(m\omega)-\alpha\alpha^{R}_{JiBj}(m\omega)\right] \quad m\omega c_{xxj}\left[\alpha\alpha^{R}_{JiJj}(m\omega)-\alpha\alpha^{R}_{JiBj}(m\omega)\right] \\ & & & & -m\omega c_{xxj}\left[\alpha\alpha^{R}_{JiJj}(m\omega)-\alpha\alpha^{R}_{JiBj}(m\omega)\right] \quad k_{xxj}\left[\alpha\alpha^{R}_{JiJj}(m\omega)-\alpha\alpha^{R}_{JiBj}(m\omega)\right] \end{bmatrix}$$

(A14a)

$$\mathbf{M}^{\mathbf{R}}_{\mathbf{xxBij}} =$$

$$\begin{bmatrix} k_{xxj}\left[\alpha\alpha_{BiJj}(0)-\alpha\alpha_{BiBj}(0)\right] & 0 & & & \\ 0 & k_{xxj}\left[\alpha\alpha^{R}_{BiJj}(\omega)-\alpha\alpha^{R}_{BiBj}(\omega)\right] & \omega c_{xxj}\left[\alpha\alpha^{R}_{BiJj}(\omega)-\alpha\alpha^{R}_{BiBj}(\omega)\right] & & \\ & -\omega c_{xxj}\left[\alpha\alpha^{R}_{BiJj}(\omega)-\alpha\alpha^{R}_{BiBj}(\omega)\right] & k_{xxj}\left[\alpha\alpha^{R}_{BiJj}(\omega)-\alpha\alpha^{R}_{BiBj}(\omega)\right] & & \\ & & & \ddots & \\ & & & & k_{xxj}\left[\alpha\alpha^{R}_{BiJj}(m\omega)-\alpha\alpha^{R}_{BiBj}(m\omega)\right] \quad m\omega c_{xxj}\left[\alpha\alpha^{R}_{BiJj}(m\omega)-\alpha\alpha^{R}_{BiBj}(m\omega)\right] \\ & & & & -m\omega c_{xxj}\left[\alpha\alpha^{R}_{BiJj}(m\omega)-\alpha\alpha^{R}_{BiBj}(m\omega)\right] \quad k_{xxj}\left[\alpha\alpha^{R}_{BiJj}(m\omega)-\alpha\alpha^{R}_{BiBj}(m\omega)\right] \end{bmatrix}$$

(A14b)

$$\mathbf{M}^{\mathbf{I}}_{\mathbf{xxJij}} =$$

$$\begin{bmatrix} 0 & 0 & & \\ 0 & -\omega c_{xxj}\left[\alpha\alpha^{\mathrm{I}}_{JiIj}(\omega)-\alpha\alpha^{\mathrm{I}}_{JiBj}(\omega)\right] & k_{xxj}\left[\alpha\alpha^{\mathrm{I}}_{JiIj}(\omega)-\alpha\alpha^{\mathrm{I}}_{JiBj}(\omega)\right] & \\ & -k_{xxj}\left[\alpha\alpha^{\mathrm{I}}_{JiIj}(\omega)-\alpha\alpha^{\mathrm{I}}_{JiBj}(\omega)\right] & -\omega c_{xxj}\left[\alpha\alpha^{\mathrm{I}}_{JiIj}(\omega)-\alpha\alpha^{\mathrm{I}}_{JiBj}(\omega)\right] & \ddots \\ & & \ddots & \ddots \\ & & & -m\omega c_{xxj}\left[\alpha\alpha^{\mathrm{I}}_{JiIj}(m\omega)-\alpha\alpha^{\mathrm{I}}_{JiBj}(m\omega)\right] \quad k_{xxj}\left[\alpha\alpha^{\mathrm{I}}_{JiIj}(m\omega)-\alpha\alpha^{\mathrm{I}}_{JiBj}(m\omega)\right] \\ & & & -k_{xxj}\left[\alpha\alpha^{\mathrm{I}}_{JiIj}(m\omega)-\alpha\alpha^{\mathrm{I}}_{JiBj}(m\omega)\right] \quad -m\omega c_{xxj}\left[\alpha\alpha^{\mathrm{I}}_{JiIj}(m\omega)-\alpha\alpha^{\mathrm{I}}_{JiBj}(m\omega)\right] \end{bmatrix}$$

(A14c)

$$\mathbf{M}^{\mathbf{I}}_{\mathbf{xxBij}} =$$

$$\begin{bmatrix} 0 & 0 & & \\ 0 & -\omega c_{xxj}\left[\alpha\alpha^{\mathrm{I}}_{BiIj}(\omega)-\alpha\alpha^{\mathrm{I}}_{BJiBj}(\omega)\right] & k_{xxj}\left[\alpha\alpha^{\mathrm{I}}_{BiIj}(\omega)-\alpha\alpha^{\mathrm{I}}_{BiBj}(\omega)\right] & \\ & -k_{xxj}\left[\alpha\alpha^{\mathrm{I}}_{BiIj}(\omega)-\alpha\alpha^{\mathrm{I}}_{BiBj}(\omega)\right] & -\omega c_{xxj}\left[\alpha\alpha^{\mathrm{I}}_{BiIj}(\omega)-\alpha\alpha^{\mathrm{I}}_{BiBj}(\omega)\right] & \ddots \\ & & \ddots & \ddots \\ & & & -m\omega c_{xxj}\left[\alpha\alpha^{\mathrm{I}}_{BiIj}(m\omega)-\alpha\alpha^{\mathrm{I}}_{BiBj}(m\omega)\right] \quad k_{xxj}\left[\alpha\alpha^{\mathrm{I}}_{BiIj}(m\omega)-\alpha\alpha^{\mathrm{I}}_{BiBj}(m\omega)\right] \\ & & & -k_{xxj}\left[\alpha\alpha^{\mathrm{I}}_{BiIj}(m\omega)-\alpha\alpha^{\mathrm{I}}_{BiBj}(m\omega)\right] \quad -m\omega c_{xxj}\left[\alpha\alpha^{\mathrm{I}}_{BiIj}(m\omega)-\alpha\alpha^{\mathrm{I}}_{BiBj}(m\omega)\right] \end{bmatrix}$$

(A14d)

$\mathbf{M}^{\mathbf{R}}_{\mathbf{yxJij}}$, $\mathbf{M}^{\mathbf{R}}_{\mathbf{yxBij}}$, $\mathbf{M}^{\mathbf{I}}_{\mathbf{yxJij}}$, $\mathbf{M}^{\mathbf{I}}_{\mathbf{yxBij}}$ are obtained from $\mathbf{M}^{\mathbf{R}}_{\mathbf{xxJij}}$, $\mathbf{M}^{\mathbf{R}}_{\mathbf{xxBij}}$, $\mathbf{M}^{\mathbf{I}}_{\mathbf{xxJij}}$, $\mathbf{M}^{\mathbf{I}}_{\mathbf{xxBij}}$ respectively, equations (A14), by replacing the receptances $\alpha\alpha$ by $\beta\alpha$.

$$\mathbf{M}^{\mathbf{R}}_{\mathbf{yyJij}} =$$

$$\begin{bmatrix} k_{yyj}\left[\beta\beta_{JiJj}(0)-\beta\beta_{JiBj}(0)\right] & 0 & & \\ 0 & k_{yyj}\left[\beta\beta^{R}_{JiJj}(\omega)-\beta\beta^{R}_{JiBj}(\omega)\right] & \omega c_{yyj}\left[\beta\beta^{R}_{JiJj}(\omega)-\beta\beta^{R}_{JiBj}(\omega)\right] & \\ & -\omega c_{yyj}\left[\beta\beta^{R}_{JiJj}(\omega)-\beta\beta^{R}_{JiBj}(\omega)\right] & k_{yyj}\left[\beta\beta^{R}_{JiJj}(\omega)-\beta\beta^{R}_{JiBj}(\omega)\right] & \\ & & & \ddots \\ & & & k_{yyj}\left[\beta\beta^{R}_{JiJj}(m\omega)-\beta\beta^{R}_{JiBj}(m\omega)\right] \quad m\omega c_{yyj}\left[\beta\beta^{R}_{JiJj}(m\omega)-\beta\beta^{R}_{JiBj}(m\omega)\right] \\ & & & -m\omega c_{yyj}\left[\beta\beta^{R}_{JiJj}(m\omega)-\beta\beta^{R}_{JiBj}(m\omega)\right] \quad k_{yyj}\left[\beta\beta^{R}_{JiJj}(m\omega)-\beta\beta^{R}_{JiBj}(m\omega)\right] \end{bmatrix}$$

(A15a)

$$\mathbf{M}^{\mathbf{R}}_{\mathbf{yyBij}} =$$

$$\begin{bmatrix} k_{yyj}\left[\beta\beta_{BiJj}(0)-\beta\beta_{BiBj}(0)\right] & 0 & & \\ 0 & k_{yyj}\left[\beta\beta^{R}_{BiJj}(\omega)-\beta\beta^{R}_{BiBj}(\omega)\right] & \omega c_{yyj}\left[\beta\beta^{R}_{BiJj}(\omega)-\beta\beta^{R}_{BiBj}(\omega)\right] & \\ & -\omega c_{yyj}\left[\beta\beta^{R}_{BiJj}(\omega)-\beta\beta^{R}_{BiBj}(\omega)\right] & k_{yyj}\left[\beta\beta^{R}_{BiJj}(\omega)-\beta\beta^{R}_{BiBj}(\omega)\right] & \\ & & & \ddots \\ & & & k_{yyj}\left[\beta\beta^{R}_{BiJj}(m\omega)-\beta\beta^{R}_{BiBj}(m\omega)\right] \quad m\omega c_{yyj}\left[\beta\beta^{R}_{BiJj}(m\omega)-\beta\beta^{R}_{BiBj}(m\omega)\right] \\ & & & -m\omega c_{yyj}\left[\beta\beta^{R}_{BiJj}(m\omega)-\beta\beta^{R}_{BiBj}(m\omega)\right] \quad k_{yyj}\left[\beta\beta^{R}_{BiJj}(m\omega)-\beta\beta^{R}_{BiBj}(m\omega)\right] \end{bmatrix}$$

(A15b)

$$\mathbf{M}^{\mathbf{I}}_{\mathbf{yyJij}} =$$

$$\begin{bmatrix} 0 & 0 & & \\ 0 & -\omega c_{yyj}\left[\beta\beta^{\mathrm{I}}_{JiIj}(\omega)-\beta\beta^{\mathrm{I}}_{JiBj}(\omega)\right] & k_{yyj}\left[\beta\beta^{\mathrm{I}}_{JiIj}(\omega)-\beta\beta^{\mathrm{I}}_{JiBj}(\omega)\right] & \\ & -k_{yyj}\left[\beta\beta^{\mathrm{I}}_{JiIj}(\omega)-\beta\beta^{\mathrm{I}}_{JiBj}(\omega)\right] & -\omega c_{yyj}\left[\beta\beta^{\mathrm{I}}_{JiIj}(\omega)-\beta\beta^{\mathrm{I}}_{JiBj}(\omega)\right] & \ddots \\ & & \ddots & \ddots \\ & & & -m\omega c_{yyj}\left[\beta\beta^{\mathrm{I}}_{JiIj}(m\omega)-\beta\beta^{\mathrm{I}}_{JiBj}(m\omega)\right] \quad k_{yyj}\left[\beta\beta^{\mathrm{I}}_{JiIj}(m\omega)-\beta\beta^{\mathrm{I}}_{JiBj}(m\omega)\right] \\ & & & -k_{yyj}\left[\beta\beta^{\mathrm{I}}_{JiIj}(m\omega)-\beta\beta^{\mathrm{I}}_{JiBj}(m\omega)\right] \quad -m\omega c_{yyj}\left[\beta\beta^{\mathrm{I}}_{JiIj}(m\omega)-\beta\beta^{\mathrm{I}}_{JiBj}(m\omega)\right] \end{bmatrix}$$

(A15c)

$$\mathbf{M}^{\mathbf{I}}_{\mathbf{yyBij}} =$$

$$\begin{bmatrix} 0 & 0 & & \\ 0 & -\omega c_{yyj}\left[\beta\beta^{\mathrm{I}}_{BiIj}(\omega)-\beta\beta^{\mathrm{I}}_{BiBj}(\omega)\right] & k_{yyj}\left[\beta\beta^{\mathrm{I}}_{BiIj}(\omega)-\beta\beta^{\mathrm{I}}_{BiBj}(\omega)\right] & \\ & -k_{yyj}\left[\beta\beta^{\mathrm{I}}_{BiIj}(\omega)-\beta\beta^{\mathrm{I}}_{BiBj}(\omega)\right] & -\omega c_{yyj}\left[\beta\beta^{\mathrm{I}}_{BiIj}(\omega)-\beta\beta^{\mathrm{I}}_{BiBj}(\omega)\right] & \ddots \\ & & \ddots & \ddots \\ & & & -m\omega c_{yyj}\left[\beta\beta^{\mathrm{I}}_{BiIj}(m\omega)-\beta\beta^{\mathrm{I}}_{BiBj}(m\omega)\right] \quad k_{yyj}\left[\beta\beta^{\mathrm{I}}_{BiIj}(m\omega)-\beta\beta^{\mathrm{I}}_{BiBj}(m\omega)\right] \\ & & & -k_{yyj}\left[\beta\beta^{\mathrm{I}}_{BiIj}(m\omega)-\beta\beta^{\mathrm{I}}_{BiBj}(m\omega)\right] \quad -m\omega c_{yyj}\left[\beta\beta^{\mathrm{I}}_{BiIj}(m\omega)-\beta\beta^{\mathrm{I}}_{BiBj}(m\omega)\right] \end{bmatrix}$$

(A15d)

$\mathbf{M}^{\mathbf{R}}_{\mathbf{xyJij}}$, $\mathbf{M}^{\mathbf{R}}_{\mathbf{xyBij}}$, $\mathbf{M}^{\mathbf{I}}_{\mathbf{xyJij}}$, $\mathbf{M}^{\mathbf{I}}_{\mathbf{xyBij}}$ are obtained from $\mathbf{M}^{\mathbf{R}}_{\mathbf{yyJij}}$, $\mathbf{M}^{\mathbf{R}}_{\mathbf{yyBij}}$, $\mathbf{M}^{\mathbf{I}}_{\mathbf{yyJij}}$, $\mathbf{M}^{\mathbf{I}}_{\mathbf{yyBij}}$ respectively, equations (A15), by replacing the receptances $\beta\beta$ by $\alpha\beta$.

$$\mathbf{f}_{xx} = \begin{bmatrix} \mathbf{f}_{xxJ} \\ \mathbf{f}_{xxB} \end{bmatrix}, \quad \mathbf{f}_{xy} = \begin{bmatrix} \mathbf{f}_{xyJ} \\ \mathbf{f}_{xyB} \end{bmatrix} \qquad \text{(A16),(A17)}$$

$$\mathbf{f}_{yx} = \begin{bmatrix} \mathbf{f}_{yxJ} \\ \mathbf{f}_{yxB} \end{bmatrix}, \quad \mathbf{f}_{yy} = \begin{bmatrix} \mathbf{f}_{yyJ} \\ \mathbf{f}_{yyB} \end{bmatrix} \qquad \text{(A18),(A19)}$$

$$\mathbf{f}_{xxJ} = \begin{bmatrix} \mathbf{f}^{R}_{xxJ1} \\ \vdots \\ \mathbf{f}^{R}_{xxJn} \end{bmatrix} + \begin{bmatrix} \mathbf{f}^{I}_{xxJ1} \\ \vdots \\ \mathbf{f}^{I}_{xxJn} \end{bmatrix}, \quad \mathbf{f}_{xxB} = \begin{bmatrix} \mathbf{f}^{R}_{xxB1} \\ \vdots \\ \mathbf{f}^{R}_{xxBn} \end{bmatrix} + \begin{bmatrix} \mathbf{f}^{I}_{xxB1} \\ \vdots \\ \mathbf{f}^{I}_{xxBn} \end{bmatrix} \qquad \text{(A20a,b)}$$

$$\mathbf{f}_{xyJ} = \begin{bmatrix} \mathbf{f}^{R}_{xyJ1} \\ \vdots \\ \mathbf{f}^{R}_{xyJn} \end{bmatrix} + \begin{bmatrix} \mathbf{f}^{I}_{xyJ1} \\ \vdots \\ \mathbf{f}^{I}_{xyJn} \end{bmatrix}, \quad \mathbf{f}_{xyB} = \begin{bmatrix} \mathbf{f}^{R}_{xyB1} \\ \vdots \\ \mathbf{f}^{R}_{xyBn} \end{bmatrix} + \begin{bmatrix} \mathbf{f}^{I}_{xyB1} \\ \vdots \\ \mathbf{f}^{I}_{xyBn} \end{bmatrix} \qquad \text{(A21a,b)}$$

$$\mathbf{f}_{yxJ} = \begin{bmatrix} \mathbf{f}^{R}_{yxJ1} \\ \vdots \\ \mathbf{f}^{R}_{yxJn} \end{bmatrix} + \begin{bmatrix} \mathbf{f}^{I}_{yxJ1} \\ \vdots \\ \mathbf{f}^{I}_{yxJn} \end{bmatrix}, \quad \mathbf{f}_{yxB} = \begin{bmatrix} \mathbf{f}^{R}_{yxB1} \\ \vdots \\ \mathbf{f}^{R}_{yxBn} \end{bmatrix} + \begin{bmatrix} \mathbf{f}^{I}_{yxB1} \\ \vdots \\ \mathbf{f}^{I}_{yxBn} \end{bmatrix} \qquad \text{(A22a,b)}$$

$$\mathbf{f}_{yyJ} = \begin{bmatrix} \mathbf{f}^{R}_{yyJ1} \\ \vdots \\ \mathbf{f}^{R}_{yyJn} \end{bmatrix} + \begin{bmatrix} \mathbf{f}^{I}_{yyJ1} \\ \vdots \\ \mathbf{f}^{I}_{yyJn} \end{bmatrix}, \quad \mathbf{f}_{yyB} = \begin{bmatrix} \mathbf{f}^{R}_{yyB1} \\ \vdots \\ \mathbf{f}^{R}_{yyBn} \end{bmatrix} + \begin{bmatrix} \mathbf{f}^{I}_{yyB1} \\ \vdots \\ \mathbf{f}^{I}_{yyBn} \end{bmatrix} \qquad \text{(A23a,b)}$$

$$\mathbf{f}^{\mathbf{R}}_{\mathbf{xxJi}} = -\begin{bmatrix} e_{oxJi} + \sum_{j=1}^{n}\left[\alpha\alpha^{\mathrm{R}}_{JiJj}(0) - \alpha\alpha^{\mathrm{R}}_{JiBj}(0)\right]Q_{x0\,j} \\ \sum_{j=1}^{n}\left[\alpha\alpha^{\mathrm{R}}_{JiJj}(\omega) - \alpha\alpha^{\mathrm{R}}_{JiBj}(\omega)\right]A^{1}_{xj} + \delta_{N1}\sum_{k=1}^{p}\alpha\alpha^{\mathrm{R}}_{JiUk}(\omega)U_k\Omega^2\sin\phi_k \\ \sum_{j=1}^{n}\left[\alpha\alpha^{\mathrm{R}}_{JiJj}(\omega) - \alpha\alpha^{\mathrm{R}}_{JiBj}(\omega)\right]B^{1}_{xj} + \delta_{N1}\sum_{k=1}^{p}\alpha\alpha^{\mathrm{R}}_{JiUk}(\omega)U_k\Omega^2\cos\phi_k \\ \vdots \\ \vdots \\ \sum_{j=1}^{n}\left[\alpha\alpha^{\mathrm{R}}_{JiJj}(m\omega) - \alpha\alpha^{\mathrm{R}}_{JiBj}(m\omega)\right]A^{m}_{xj} + \delta_{Nm}\sum_{k=1}^{p}\alpha\alpha^{\mathrm{R}}_{JiUk}(m\omega)U_k\Omega^2\sin\phi_k \\ \sum_{j=1}^{n}\left[\alpha\alpha^{\mathrm{R}}_{JiJj}(m\omega) - \alpha\alpha^{\mathrm{R}}_{JiBj}(m\omega)\right]B^{m}_{xj} + \delta_{Nm}\sum_{k=1}^{p}\alpha\alpha^{\mathrm{R}}_{JiUk}(m\omega)U_k\Omega^2\cos\phi_k \end{bmatrix}, \quad \mathbf{f}^{\mathbf{R}}_{\mathbf{xxBi}} = -\begin{bmatrix} \sum_{j=1}^{n}\left[\alpha\alpha^{\mathrm{R}}_{BiJj}(0) - \alpha\alpha^{\mathrm{R}}_{BiBj}(0)\right]Q_{x0\,j} \\ \sum_{j=1}^{n}\left[\alpha\alpha^{\mathrm{R}}_{BiJj}(\omega) - \alpha\alpha^{\mathrm{R}}_{BiBj}(\omega)\right]A^{1}_{xj} + \delta_{N1}\sum_{k=1}^{p}\alpha\alpha^{\mathrm{R}}_{BiUk}(\omega)U_k\Omega^2\sin\phi_k \\ \sum_{j=1}^{n}\left[\alpha\alpha^{\mathrm{R}}_{BiJj}(\omega) - \alpha\alpha^{\mathrm{R}}_{BiBj}(\omega)\right]B^{1}_{xj} + \delta_{N1}\sum_{k=1}^{p}\alpha\alpha^{\mathrm{R}}_{BiUk}(\omega)U_k\Omega^2\cos\phi_k \\ \vdots \\ \vdots \\ \sum_{j=1}^{n}\left[\alpha\alpha^{\mathrm{R}}_{BiJj}(m\omega) - \alpha\alpha^{\mathrm{R}}_{BiBj}(m\omega)\right]A^{m}_{xj} + \delta_{Nm}\sum_{k=1}^{p}\alpha\alpha^{\mathrm{R}}_{BiUk}(m\omega)U_k\Omega^2\sin\phi_k \\ \sum_{j=1}^{n}\left[\alpha\alpha^{\mathrm{R}}_{BiJj}(m\omega) - \alpha^{\mathrm{R}}_{BiBj}(m\omega)\right]B^{m}_{xj} + \delta_{Nm}\sum_{k=1}^{p}\alpha\alpha^{\mathrm{R}}_{BiUk}(m\omega)U_k\Omega^2\cos\phi_k \end{bmatrix}$$

(A24a,b)

$$\mathbf{f}^{\mathbf{I}}_{\mathbf{xxJi}} = -\begin{bmatrix} 0 \\ \sum_{j=1}^{n}\left[\alpha\alpha^{\mathrm{I}}_{JiJj}(\omega) - \alpha\alpha^{\mathrm{I}}_{JiBj}(\omega)\right]B^{1}_{xj} + \delta_{N1}\sum_{k=1}^{p}\alpha\alpha^{\mathrm{I}}_{JiUk}(\omega)U_k\Omega^2\cos\phi_k \\ -\sum_{j=1}^{n}\left[\alpha\alpha^{\mathrm{I}}_{JiJj}(\omega) - \alpha\alpha^{\mathrm{I}}_{JiBj}(\omega)\right]A^{1}_{xj} - \delta_{N1}\sum_{k=1}^{p}\alpha\alpha^{\mathrm{I}}_{JiUk}(\omega)U_k\Omega^2\sin\phi_k \\ \vdots \\ \vdots \\ \sum_{j=1}^{n}\left[\alpha\alpha^{\mathrm{I}}_{JiJj}(m\omega) - \alpha\alpha^{\mathrm{I}}_{JiBj}(m\omega)\right]B^{m}_{xj} + \delta_{Nm}\sum_{k=1}^{p}\alpha\alpha^{\mathrm{I}}_{JiUk}(m\omega)U_k\Omega^2\cos\phi_k \\ -\sum_{j=1}^{n}\left[\alpha\alpha^{\mathrm{I}}_{JiJj}(m\omega) - \alpha\alpha^{\mathrm{I}}_{JiBj}(m\omega)\right]A^{m}_{xj} - \delta_{Nm}\sum_{k=1}^{p}\alpha\alpha^{\mathrm{I}}_{JiUk}(m\omega)U_k\Omega^2\sin\phi_k \end{bmatrix}, \quad \mathbf{f}^{\mathbf{I}}_{\mathbf{xxBi}} = -\begin{bmatrix} 0 \\ \sum_{j=1}^{n}\left[\alpha\alpha^{\mathrm{I}}_{BiJj}(\omega) - \alpha\alpha^{\mathrm{I}}_{BiBj}(\omega)\right]B^{1}_{xj} + \delta_{N1}\sum_{k=1}^{p}\alpha\alpha^{\mathrm{I}}_{BiUk}(\omega)U_k\Omega^2\cos\phi_k \\ -\sum_{j=1}^{n}\left[\alpha\alpha^{\mathrm{I}}_{BiJj}(\omega) - \alpha\alpha^{\mathrm{I}}_{BiBj}(\omega)\right]A^{1}_{xj} - \delta_{N1}\sum_{k=1}^{p}\alpha\alpha^{\mathrm{I}}_{BiUk}(\omega)U_k\Omega^2\sin\phi_k \\ \vdots \\ \vdots \\ \sum_{j=1}^{n}\left[\alpha\alpha^{\mathrm{I}}_{BiJj}(m\omega) - \alpha\alpha^{\mathrm{I}}_{BiBj}(m\omega)\right]B^{m}_{xj} + \delta_{Nm}\sum_{k=1}^{p}\alpha\alpha^{\mathrm{I}}_{BiUk}(m\omega)U_k\Omega^2\cos\phi_k \\ -\sum_{j=1}^{n}\left[\alpha\alpha^{\mathrm{I}}_{BiJj}(m\omega) - \alpha\alpha^{\mathrm{I}}_{BiBj}(m\omega)\right]A^{m}_{xj} - \delta_{Nm}\sum_{k=1}^{p}\alpha\alpha^{\mathrm{I}}_{BiUk}(m\omega)U_k\Omega^2\sin\phi_k \end{bmatrix}$$

(A24c,d)

$\mathbf{f}^{\mathbf{R}}_{\mathbf{yxJij}}$, $\mathbf{f}^{\mathbf{R}}_{\mathbf{yxBij}}$, $\mathbf{f}^{\mathbf{I}}_{\mathbf{yxJij}}$, $\mathbf{f}^{\mathbf{I}}_{\mathbf{yxBij}}$ are obtained from $\mathbf{f}^{\mathbf{R}}_{\mathbf{xxJij}}$, $\mathbf{f}^{\mathbf{R}}_{\mathbf{xxBij}}$, $\mathbf{f}^{\mathbf{I}}_{\mathbf{xxJij}}$, $\mathbf{f}^{\mathbf{I}}_{\mathbf{xxBij}}$ respectively, equations (A24), by replacing the receptances $\alpha\alpha$ by $\beta\alpha$.

$$\mathbf{f}^{\mathbf{R}}_{\mathbf{yyJi}} = -\begin{bmatrix} e_{oyJi} + \sum_{j=1}^{n}\left[\beta\beta^{\mathrm{R}}_{JiJj}(0) - \beta\beta^{\mathrm{R}}_{JiBj}(0)\right]Q_{y0j} \\ \sum_{j=1}^{n}\left[\beta\beta^{\mathrm{R}}_{JiJj}(\omega) - \beta\beta^{\mathrm{R}}_{JiBj}(\omega)\right]A^{1}_{yj} - \delta_{N1}\sum_{k=1}^{p}\beta\beta^{\mathrm{R}}_{JiUk}(\omega)U_k\Omega^2\cos\phi_k \\ \sum_{j=1}^{n}\left[\beta\beta^{\mathrm{R}}_{JiJj}(\omega) - \beta\beta^{\mathrm{R}}_{JiBj}(\omega)\right]B^{1}_{yj} + \delta_{N1}\sum_{k=1}^{p}\beta\beta^{\mathrm{R}}_{JiUk}(\omega)U_k\Omega^2\sin\phi_k \\ \vdots \\ \vdots \\ \sum_{j=1}^{n}\left[\beta\beta^{\mathrm{R}}_{JiJj}(m\omega) - \beta\beta^{\mathrm{R}}_{JiBj}(m\omega)\right]A^{m}_{yj} - \delta_{Nm}\sum_{k=1}^{p}\beta\beta^{\mathrm{R}}_{JiUk}(m\omega)U_k\Omega^2\cos\phi_k \\ \sum_{j=1}^{n}\left[\beta\beta^{\mathrm{R}}_{JiJj}(m\omega) - \beta\beta^{\mathrm{R}}_{JiBj}(m\omega)\right]B^{m}_{yj} + \delta_{Nm}\sum_{k=1}^{p}\beta\beta^{\mathrm{R}}_{JiUk}(m\omega)U_k\Omega^2\sin\phi_k \end{bmatrix}, \quad \mathbf{f}^{\mathbf{R}}_{\mathbf{yyBi}} = -\begin{bmatrix} \sum_{j=1}^{n}\left[\beta\beta^{\mathrm{R}}_{BiJj}(0) - \beta\beta^{\mathrm{R}}_{BiBj}(0)\right]Q_{y0j} \\ \sum_{j=1}^{n}\left[\beta\beta^{\mathrm{R}}_{BiJj}(\omega) - \beta\beta^{\mathrm{R}}_{BiBj}(\omega)\right]A^{1}_{yj} - \delta_{N1}\sum_{k=1}^{p}\beta\beta^{\mathrm{R}}_{BiUk}(\omega)U_k\Omega^2\cos\phi_k \\ \sum_{j=1}^{n}\left[\beta\beta^{\mathrm{R}}_{BiJj}(\omega) - \beta\beta^{\mathrm{R}}_{BiBj}(\omega)\right]B^{1}_{yj} + \delta_{N1}\sum_{k=1}^{p}\beta\beta^{\mathrm{R}}_{BiUk}(\omega)U_k\Omega^2\sin\phi_k \\ \vdots \\ \vdots \\ \sum_{j=1}^{n}\left[\beta\beta^{\mathrm{R}}_{BiJj}(m\omega) - \beta\beta^{\mathrm{R}}_{BiBj}(m\omega)\right]A^{m}_{yj} - \delta_{Nm}\sum_{k=1}^{p}\beta\beta^{\mathrm{R}}_{BiUk}(m\omega)U_k\Omega^2\cos\phi_k \\ \sum_{j=1}^{n}\left[\beta\beta^{\mathrm{R}}_{BiJj}(m\omega) - \beta\beta^{\mathrm{R}}_{BiBj}(m\omega)\right]B^{m}_{yj} + \delta_{Nm}\sum_{k=1}^{p}\beta\beta^{\mathrm{R}}_{BiUk}(m\omega)U_k\Omega^2\sin\phi_k \end{bmatrix}$$

(A25a,b)

$$\mathbf{f}^{\mathbf{I}}_{\mathbf{yyJi}} = -\begin{bmatrix} 0 \\ \sum_{j=1}^{n}\left[\beta\beta^{\mathrm{I}}_{JiJj}(\omega) - \beta\beta^{\mathrm{I}}_{JiBj}(\omega)\right]B^{1}_{yj} + \delta_{N1}\sum_{k=1}^{p}\beta\beta^{\mathrm{I}}_{JiUk}(\omega)U_k\Omega^2\sin\phi_k \\ -\sum_{j=1}^{n}\left[\beta\beta^{\mathrm{I}}_{JiJj}(\omega) - \beta\beta^{\mathrm{I}}_{JiBj}(\omega)\right]A^{1}_{yj} + \delta_{N1}\sum_{k=1}^{p}\beta\beta^{\mathrm{I}}_{JiUk}(\omega)U_k\Omega^2\cos\phi_k \\ \vdots \\ \vdots \\ \sum_{j=1}^{n}\left[\beta\beta^{\mathrm{I}}_{JiJj}(m\omega) - \beta\beta^{\mathrm{I}}_{JiBj}(m\omega)\right]B^{m}_{yj} + \delta_{Nm}\sum_{k=1}^{p}\beta\beta^{\mathrm{I}}_{JiUk}(m\omega)U_k\Omega^2\sin\phi_k \\ -\sum_{j=1}^{n}\left[\beta\beta^{\mathrm{I}}_{JiJj}(m\omega) - \beta\beta^{\mathrm{I}}_{JiBj}(m\omega)\right]A^{m}_{yj} + \delta_{Nm}\sum_{k=1}^{p}\beta\beta^{\mathrm{I}}_{JiUk}(m\omega)U_k\Omega^2\cos\phi_k \end{bmatrix}, \quad \mathbf{f}^{\mathbf{I}}_{\mathbf{yyBi}} = -\begin{bmatrix} 0 \\ \sum_{j=1}^{n}\left[\beta\beta^{\mathrm{I}}_{BiJj}(\omega) - \beta\beta^{\mathrm{I}}_{BiBj}(\omega)\right]B^{1}_{yj} + \delta_{N1}\sum_{k=1}^{p}\beta\beta^{\mathrm{I}}_{BiUk}(\omega)U_k\Omega^2\sin\phi_k \\ -\sum_{j=1}^{n}\left[\beta\beta^{\mathrm{I}}_{BiJj}(\omega) - \beta\beta^{\mathrm{I}}_{BiBj}(\omega)\right]A^{1}_{yj} + \delta_{N1}\sum_{k=1}^{p}\beta\beta^{\mathrm{I}}_{BiUk}(\omega)U_k\Omega^2\cos\phi_k \\ \vdots \\ \vdots \\ \sum_{j=1}^{n}\left[\beta\beta^{\mathrm{I}}_{BiJj}(m\omega) - \beta\beta^{\mathrm{I}}_{BiBj}(m\omega)\right]B^{m}_{yj} + \delta_{Nm}\sum_{k=1}^{p}\beta\beta^{\mathrm{I}}_{BiUk}(m\omega)U_k\Omega^2\sin\phi_k \\ -\sum_{j=1}^{n}\left[\beta\beta^{\mathrm{I}}_{BiJj}(m\omega) - \beta\beta^{\mathrm{I}}_{BiBj}(m\omega)\right]A^{m}_{yj} + \delta_{Nm}\sum_{k=1}^{p}\beta\beta^{\mathrm{I}}_{BiUk}(m\omega)U_k\Omega^2\cos\phi_k \end{bmatrix}$$

(A25c,d)

$\mathbf{f}^{\mathbf{R}}_{\mathbf{xyJij}}$, $\mathbf{f}^{\mathbf{R}}_{\mathbf{xyBij}}$, $\mathbf{f}^{\mathbf{I}}_{\mathbf{xyJij}}$, $\mathbf{f}^{\mathbf{I}}_{\mathbf{xyBij}}$ are obtained from $\mathbf{f}^{\mathbf{R}}_{\mathbf{yyJij}}$, $\mathbf{f}^{\mathbf{R}}_{\mathbf{yyBij}}$, $\mathbf{f}^{\mathbf{I}}_{\mathbf{yyJij}}$, $\mathbf{f}^{\mathbf{I}}_{\mathbf{yyBij}}$ respectively, equations (A25), by replacing the receptances $\beta\beta$ by $\alpha\beta$.

APPENDIX B

EXPERIMENTAL PROCEDURE DATA

DISPLACEMENT TRANSDUCER CALIBRATION

All probes were "bench" calibrated using a micrometer screw gauge calibrator and a digital voltmeter. Additionally, the calibration of the SFD probes (at J) was rechecked "on the job" *i.e.* when in position on the rig, using a digital voltmeter and a dial test indicator at J. The reason for this was that the lateral clearance of the SFD probes from the bearing housing face was within the limits of tolerance recommended by the manufacturer. The change in sensitivity over the bench test value was found to be $-1.0\,\%$ for the x probe and $-2.7\,\%$ for the y probe. The calibration curves and sensitivities are given in Figures B1(a),(b)-B4(a),(b). A least squares fit was used to determine the sensitivities.

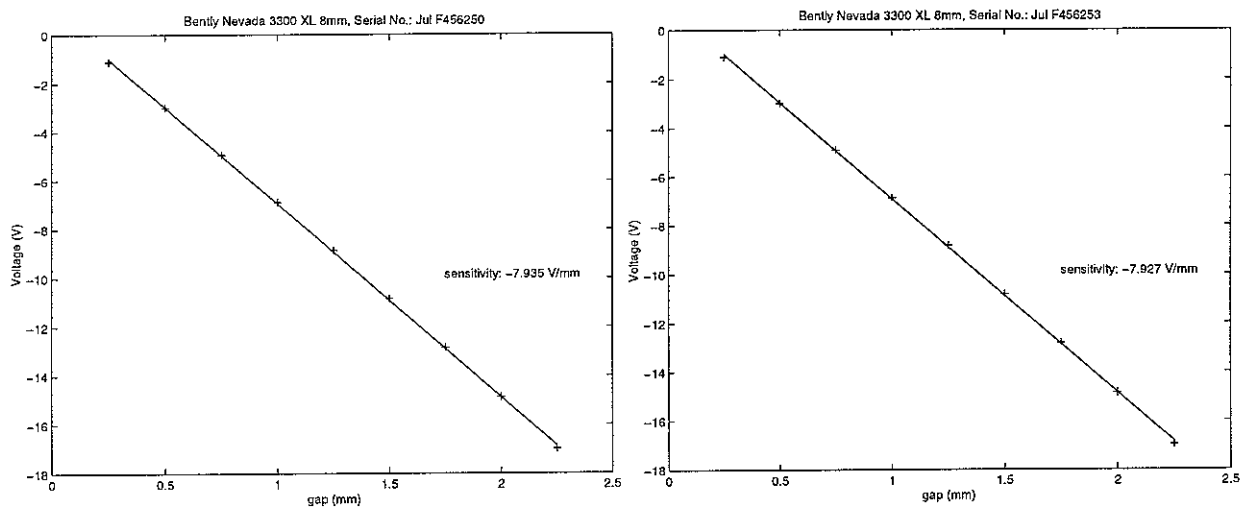

(a) *x probe* (b) *y probe*

Figure B1: ***SFD position transducers: bench test calibration.***

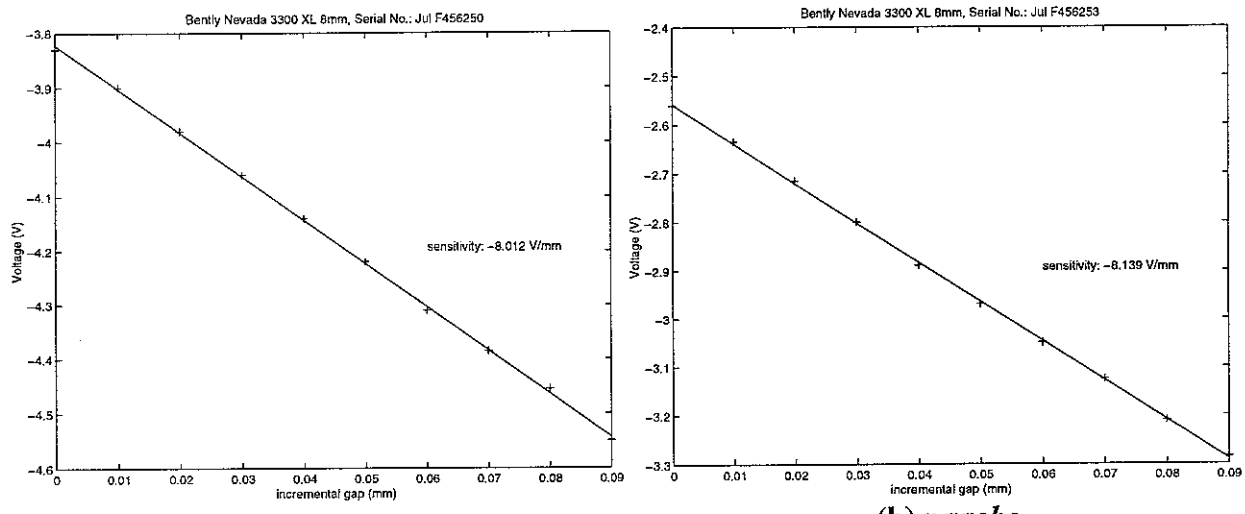

(a) *x probe* (b) *y probe*

Figure B2: ***SFD position transducers: calibration "on the job".***

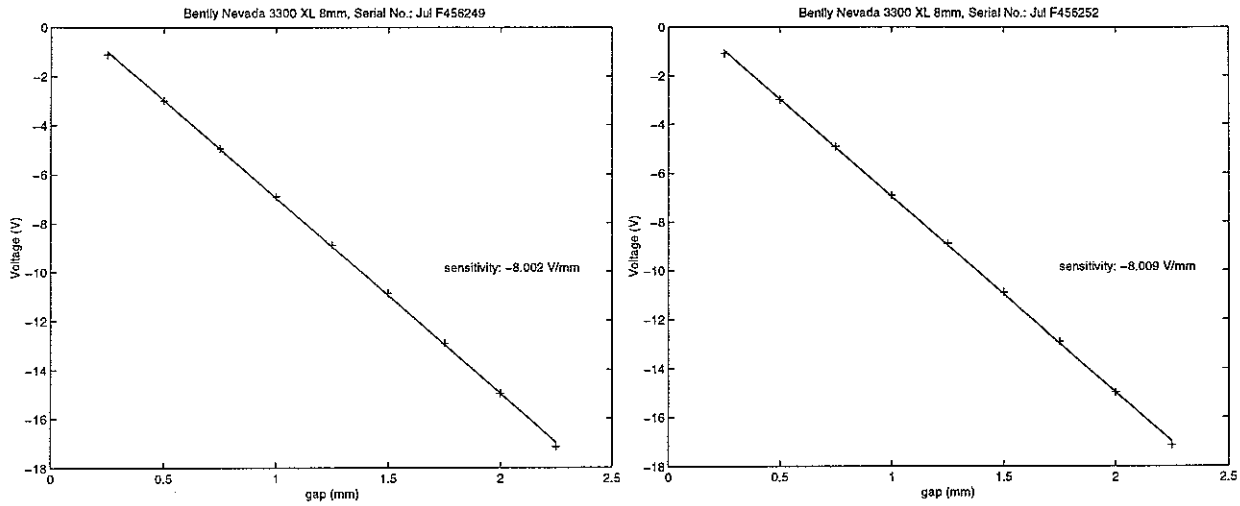

(a) *x probe* (b) *y probe*

Figure B3: ***Disc position transducers: bench test calibration.***

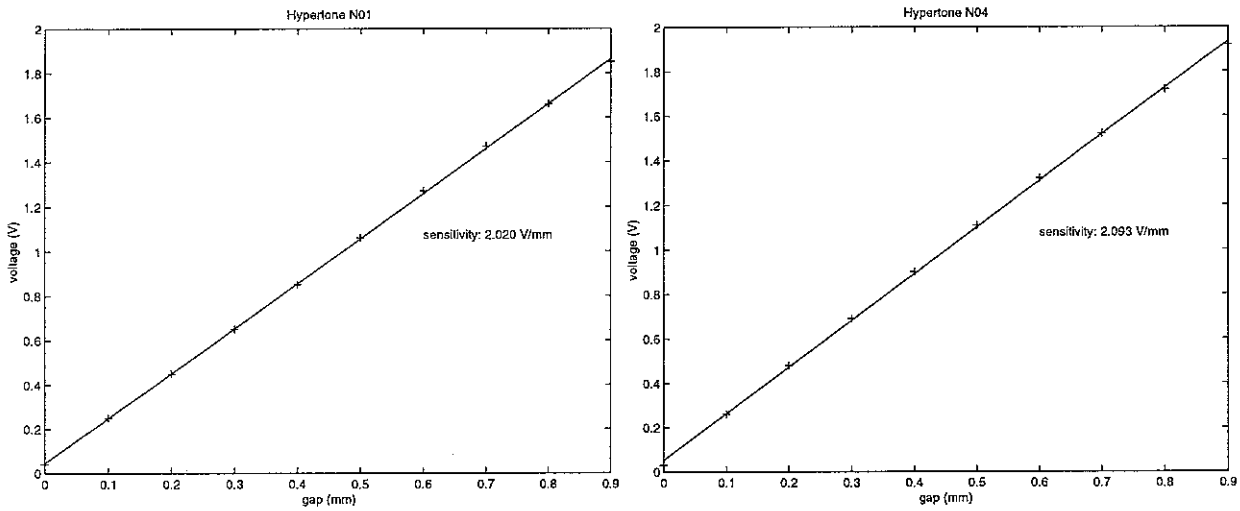

(a) *x probe* (b) *y probe*

Figure B4: ***Mid-shaft position transducers: bench test calibration.***

STATIC MISALIGNMENT ADJUSTMENT

The cold (25°C) and hot (33°C) static misalignment conditions for the two chosen settings are shown in Tables B1, B2. In Table B1, the grand means, to one decimal place, are $\varepsilon_{0xJ} = 0.0$, $\varepsilon_{0yJ} = -0.6$. In Table B2, the grand means, to one decimal place, are $\varepsilon_{0xJ} = 0.0$, $\varepsilon_{0yJ} = -0.8$. These values where used in the simulations.

θ (°)	ε_{0xJ}
0	0.03
90	0.08
180	0.01
270	0.00
$\bar{\varepsilon}_{0xJ}$	0.03

(a1) ***x direction, 25°C***

θ (°)	ε_{0yJ}
0	-0.39
90	-0.64
180	-0.78
270	-0.55
$\bar{\varepsilon}_{0yJ}$	-0.59

(a2) ***y direction, 25°C***

θ (°)	ε_{0xJ}
0	0.08
90	0.10
180	0.06
270	0.01
$\bar{\varepsilon}_{0xJ}$	0.06

(b1) ***x direction, 33°C***

θ (°)	ε_{0yJ}
0	-0.39
90	-0.66
180	-0.79
270	-0.60
$\bar{\varepsilon}_{0yJ}$	-0.61

(b2) ***y direction, 33°C***

Table B1: *Static eccentricity adjustment for* $\varepsilon_{0xJ} = 0.0$, $\varepsilon_{0yJ} = -0.6$

θ (°)	ε_{0xJ}
0	-0.03
90	0.03
180	-0.03
270	-0.07
$\bar{\varepsilon}_{0xJ}$	-0.03

(a1) ***x direction, 25°C***

θ (°)	ε_{0yJ}
0	-0.63
90	-0.84
180	-0.96
270	-0.77
$\bar{\varepsilon}_{0yJ}$	-0.80

(a2) ***y direction, 25°C***

θ (°)	ε_{0xJ}
0	0.02
90	0.05
180	0.07
270	-0.05
$\bar{\varepsilon}_{0xJ}$	0.02

(b1) ***x direction, 33°C***

θ (°)	ε_{0yJ}
0	-0.66
90	-0.91
180	-1.00
270	-0.86
$\bar{\varepsilon}_{0yJ}$	-0.86

(b2) ***y direction, 33°C***

Table B2: *Static eccentricity adjustment for* $\varepsilon_{0xJ} = 0.0$, $\varepsilon_{0yJ} = -0.8$

MEASUREMENT OF "DC" COMPONENTS

A data acquisition with the rig stationary had to be performed. This was done after the rig had been run for about 30 minutes for the oil temperature to reach 25°C. With the rig stationary, the voltages $\{V_{0xJ\theta}, V_{0yJ\theta}\}$, $\{V_{0xU\theta}, V_{0yU\theta}\}$, $\{V_{0xM\theta}, V_{0yM\theta}\}$ at the locations J, U and M respectively were acquired with the analyser for the four angular positions of the shaft θ = 0°, 90°, 180°, 270°. This allows for the run-out of the shaft. The average static dc voltages in the x and y directions at locations J, U and M were then obtained as:

$$\overline{V}_{0xJ} = \frac{V_{0xJ0^\circ} + V_{0xJ90^\circ} + V_{0xJ180^\circ} + V_{0xJ270^\circ}}{4}, \quad \overline{V}_{0yJ} = \frac{V_{0yJ0^\circ} + V_{0yJ90^\circ} + V_{0yJ180^\circ} + V_{0yJ270^\circ}}{4} \tag{B1a,b}$$

$$\overline{V}_{0xU} = \frac{V_{0xU0^\circ} + V_{0xU90^\circ} + V_{0xU180^\circ} + V_{0xU270^\circ}}{4}, \quad \overline{V}_{0yU} = \frac{V_{0yU0^\circ} + V_{0yU90^\circ} + V_{0yU180^\circ} + V_{0yU270^\circ}}{4} \tag{B2a,b}$$

$$\overline{V}_{0xM} = \frac{V_{0xM0^\circ} + V_{0xM90^\circ} + V_{0xM180^\circ} + V_{0xM270^\circ}}{4}, \quad \overline{V}_{0yM} = \frac{V_{0yM0^\circ} + V_{0yM90^\circ} + V_{0yM180^\circ} + V_{0yM270^\circ}}{4} \tag{B3a,b}$$

The rig was then run and the x, y voltage measurements $\{V_{0xJ}(t), V_{0yJ}(t)\}$, $\{V_{0xU}(t), V_{0yU}(t)\}$, $\{V_{0xM}(t), V_{0yM}(t)\}$ at J, U, M respectively were then taken at each speed. Let $\{\gamma_{xJ}, \gamma_{yJ}\}$, $\{\gamma_{xU}, \gamma_{yU}\}$, $\{\gamma_{xM}, \gamma_{yM}\}$ be the sensitivities of the x, y probes at J, U, M respectively. Let x_J, y_J be the non-dimensional displacements of J from B. Let (x_U, y_U), (x_M, y_M) be the non-dimensional displacements of U and M from their respective static equilibrium positions. Then

$$x_J = \varepsilon_{0xJ} + \frac{V_{xJ}(t) - \overline{V}_{0xJ}}{\gamma_{xJ} c}, \qquad y_J = \varepsilon_{0yJ} + \frac{V_{yJ}(t) - \overline{V}_{0yJ}}{\gamma_{yJ} c} \tag{B4a,b}$$

$$x_U = \frac{V_{xU}(t) - \overline{V}_{0xU}}{\gamma_{xU} c}, \qquad y_U = \frac{V_{yU}(t) - \overline{V}_{0yU}}{\gamma_{yU} c} \tag{B5a,b}$$

$$x_M = \frac{V_{xM}(t) - \overline{V}_{0xM}}{\gamma_{xM} c}, \qquad y_M = \frac{V_{yM}(t) - \overline{V}_{0yM}}{\gamma_{yM} c} \tag{B6a,b}$$

The above displacements are hence directly comparable with the predictions. For added precision the static voltage acquisition was repeated at the end of each experiment with the rig hot. The static voltages used in equations (B4)-(B6) where in fact the averages of the cold and hot values.